

University of Windsor

Scholarship at UWindor

Electronic Theses and Dissertations

Theses, Dissertations, and Major Papers

1-1-1980

An analytical investigation of developing flows through concentric annuli and pipes.

Seeraj Mattai
University of Windsor

Follow this and additional works at: <https://scholar.uwindsor.ca/etd>

Recommended Citation

Mattai, Seeraj, "An analytical investigation of developing flows through concentric annuli and pipes." (1980). *Electronic Theses and Dissertations*. 6118.
<https://scholar.uwindsor.ca/etd/6118>

This online database contains the full-text of PhD dissertations and Masters' theses of University of Windsor students from 1954 forward. These documents are made available for personal study and research purposes only, in accordance with the Canadian Copyright Act and the Creative Commons license—CC BY-NC-ND (Attribution, Non-Commercial, No Derivative Works). Under this license, works must always be attributed to the copyright holder (original author), cannot be used for any commercial purposes, and may not be altered. Any other use would require the permission of the copyright holder. Students may inquire about withdrawing their dissertation and/or thesis from this database. For additional inquiries, please contact the repository administrator via email (scholarship@uwindsor.ca) or by telephone at 519-253-3000ext. 3208.

AN ANALYTICAL INVESTIGATION OF
DEVELOPING FLOWS THROUGH CONCENTRIC
ANNULI AND PIPES

by

Seeraj Mattai

A Dissertation
submitted to the Faculty of Graduate Studies
through the Department of Mechanical Engineering
in partial fulfillment of the requirements for
the Degree of Doctor of Philosophy at
The University of Windsor.

Windsor, Ontario, Canada
1980

UMI Number: DC53209

INFORMATION TO USERS

The quality of this reproduction is dependent upon the quality of the copy submitted. Broken or indistinct print, colored or poor quality illustrations and photographs, print bleed-through, substandard margins, and improper alignment can adversely affect reproduction.

In the unlikely event that the author did not send a complete manuscript and there are missing pages, these will be noted. Also, if unauthorized copyright material had to be removed, a note will indicate the deletion.

UMI[®]

UMI Microform DC53209
Copyright 2009 by ProQuest LLC
All rights reserved. This microform edition is protected against
unauthorized copying under Title 17, United States Code.

ProQuest LLC
789 East Eisenhower Parkway
P.O. Box 1346
Ann Arbor, MI 48106-1346

AR 8264

© Seeraj Mattai 1980
All Rights Reserved.

747987

ABSTRACT

Developing laminar annular, entry-region turbulent annular and entry-region turbulent pipe flows were analytically studied employing integral methods of solution.

Both the laminar and turbulent annular flow problems were solved by two methods, a Simplified Model and a General Model. In the Simplified Model, the ratio of inner to outer wall layer thickness was assumed to be constant at all axial positions and equal to the fully developed value. The General Model was solved relaxing the constant ratio of wall layer growth assumption. The assumed velocity distribution in the developing region was based on fully developed flow.

In developing laminar annular flows, it was found from inspection of the velocity profile plots that only near the inner wall, predictions of the two models differ appreciably. In addition, both model predictions of mean flow characteristics, such a core velocity, $f_{app} Re$ and incremental pressure drop, are in good agreement with each other. Further, comparison of results obtained from the General Model is consistent with previous studies and the only experimental data available.

For entry-region turbulent annular flows, predictions of velocity profiles (except near the walls), core velocity and pressure gradient from both the Simplified and the General Models are in reasonable agreement with available experimental data. Disagreement near the walls may be due to the inherent problems associated with the measurement of

low velocities and to the unsuitability of applying power law mean velocity profiles near wall areas. In fact, the scatter of existing experimental values is indicative of the difficulty involved with obtaining reliable experimental data in the entire flow area of entry-region turbulent annular flows.

For entry-region turbulent pipe flows, the eddy viscosity model of Reichardt was used together with a linear shear stress assumption in the wall layer. The purpose of the study was to compare the results of using the Bernoulli's equation in the core region only with that obtained by using a macroscopic mechanical energy balance over the whole flow area. The analysis using the macroscopic energy balance predicts a much smaller pressure gradient distribution than that using the Bernoulli's equation. The non-linearity of the shear stress profile near the edge of the wall layer was taken into account separately. The aforementioned procedure was repeated using the Van Driest eddy viscosity model.

To: My wife, Nan
Our son, Anand
My mother and
The memory of my father.

ACKNOWLEDGEMENTS

The author wishes to express his deep and sincere gratitude to Professor K. Sridhar for his unceasing encouragement and excellent guidance which he furnished and who in many ways has made this work a reality.

The author is indebted to Professor W.G. Colborne for providing the opportunity to pursue this investigation and Professor T.W. McDonald who contributed in solidifying his concepts of fluid flow fundamentals. Also, he acknowledges their continuous support and help.

The enthusiastic counsel and many valuable suggestions provided by Professor P.N. Kaloni (Mathematics Department) and Dr. H.J. Tucker are deeply appreciated.

My final thanks go to Gary Rankin for his willing help and cooperation; Mrs. Marion Campeau who has typed the Dissertation and the Natural Sciences and Engineering Research Council of Canada for providing financial support (through Grant Number A-2190).

TABLE OF CONTENTS

	Page
ABSTRACT	iv
DEDICATION	vi
ACKNOWLEDGEMENTS	vii
TABLE OF CONTENTS	viii
LIST OF FIGURES	x
LIST OF TABLES	xiv
NOMENCLATURE	xv
CHAPTER I INTRODUCTION	1
1.1 Characteristics of Developing Flows	1
1.2 Flow Geometry	2
1.3 Purpose of Present Research	4
CHAPTER II LITERATURE SURVEY	6
2.1 General	6
2.2 Developing Annular Flows	6
2.2.1 Laminar Studies	6
2.2.2 Turbulent Studies	10
2.3 Developing Turbulent Pipe Flows	13
2.4 Closure	17
CHAPTER III ANALYSIS OF DEVELOPING FLOWS	18
3.1 General	18
3.2 Method of Approach	19
3.2.1 Developing Laminar Annular Flows	19
3.2.2 Entry-Region Turbulent Annular Flows	20
3.2.3 Entry-Region Turbulent Pipe Flows	21
3.3 Mathematical Analysis	21
3.3.1 Developing Laminar Annular Flows	21
3.3.2 Entry-Region Turbulent Annular Flows	31
3.3.3 Entry-Region Turbulent Pipe Flows	39

	Page
CHAPTER IV DISCUSSION	45
4.1 Discussion of Assumptions	45
4.1.1 Velocity Profile	45
4.1.2 Wall Layer Growth	47
4.1.3 Shear Stress Variation	48
4.1.4 Radius of Maximum Velocity Location	48
4.2 Discussion of Results	50
4.2.1 Developing Laminar Annular Flows	50
4.2.2 Entry-Region Turbulent Annular Flows	57
4.2.3 Entry-Region Turbulent Pipe Flows	66
4.3 Discussion of Numerical Method	67
4.3.1 General	67
4.3.2 Simplified Model	67
4.3.3 General Model	68
4.3.4 Pipe-Flow Analysis	69
 CHAPTER V CONCLUSIONS AND RECOMMENDATIONS	 70
 REFERENCES	 73
 FIGURES	 79
 APPENDICES	 133
A Details of Formulations	133
B Computer Programs	165
 VITA AUCTORIS	 180

LIST OF FIGURES

FIGURE		Page
3.1	Schematic of Flow in Inlet Region of Annulus	79
4.1	Velocity Profiles in Fully Developed Turbulent Annular Flows	80
4.2	Non-Dimensional Velocity Variation ($\alpha = 0.05$: $\phi = 0.1, 0.2, 0.3$)	81
4.3	Non-Dimensional Velocity Variation ($\alpha = 0.05$: $\phi = 0.4, 0.5, 0.6$)	82
4.4	Non-Dimensional Velocity Variation ($\alpha = 0.05$: $\phi = 0.7, 0.8, 0.9$)	83
4.5	Non-Dimensional Velocity Variation ($\alpha = 0.1$: $\phi = 0.1, 0.2, 0.3$)	84
4.6	Non-Dimensional Velocity Variation ($\alpha = 0.1$: $\phi = 0.1, 0.2, 0.3$)	85
4.7	Non-Dimensional Velocity Variation ($\alpha = 0.1$: $\phi = 0.4, 0.6, 0.8$)	86
4.8	Non-Dimensional Velocity Variation ($\alpha = 0.1$: $\phi = 0.5, 0.7, 0.9$)	87
4.9	Non-Dimensional Velocity Variation ($\alpha = 0.5$: $\phi = 0.1, 0.2, 0.3$)	88
4.10	Non-Dimensional Velocity Variation ($\alpha = 0.5$: $\phi = 0.4, 0.5, 0.6$)	89
4.11	Non-Dimensional Velocity Variation ($\alpha = 0.5$: $\phi = 0.7, 0.8, 0.9$)	90
4.12	Non-Dimensional Velocity Variation ($\alpha = 0.75$: $\phi = 0.1, 0.2, 0.3$)	91
4.13	Non-Dimensional Velocity Variation ($\alpha = 0.75$: $\phi = 0.4, 0.5, 0.6$)	92

(x)

FIGURE		Page
4.14	Non-Dimensional Velocity Variation ($\alpha = 0.75$: $\phi = 0.7, 0.8, 0.9$)	93
4.15	Comparison with Experimental Results ($\alpha = 0.732$)	94
4.16	Predicted Wall Layer Growth ($\alpha = 0.05$)	95
4.17	Predicted Wall Layer Growth ($\alpha = 0.10$)	96
4.18	Predicted Wall Layer Growth ($\alpha = 0.50$)	97
4.19	Predicted Wall Layer Growth ($\alpha = 0.75$)	98
4.20	Core Velocity Variation ($\alpha = 0.05$)	99
4.21	Core Velocity Variation ($\alpha = 0.1$)	100
4.22	Core Velocity Variation ($\alpha = 0.50$)	101
4.23	Core Velocity Variation ($\alpha = 0.75$)	102
4.24	Incremental Pressure Drop Number Variation ($\alpha = 0.05$)	103
4.25	Incremental Pressure Drop Number Variation ($\alpha = 0.10$)	104
4.26	Incremental Pressure Drop Number Variation ($\alpha = 0.50$)	105
4.27	Incremental Pressure Drop Number Variation ($\alpha = 0.75$)	106
4.28	f_{app} Re Variation ($\alpha = 0.05$)	107

FIGURE		Page
4.29	f_{app} Re Variation ($\alpha = 0.1$)	108
4.30	f_{app} Re Variation ($\alpha = 0.5$)	109
4.31	f_{app} Re Variation ($\alpha = 0.75$)	110
4.32	Comparison with Experimental Results with Suction ($\alpha = 0.732$)	111
4.33	$\ln(u/U)$ vs. $\ln(y/\delta)$	112
4.34	Non-Dimensional Velocity Profiles ($\alpha = 0.344$ (Re = 78800); X = 3.81)	113
4.35	Non-Dimensional Velocity Profiles ($\alpha = 0.344$ (Re = 78800); X = 10.9)	114
4.36	Non-Dimensional Velocity Profiles ($\alpha = 0.531$ (Re = 142000); X = 5.33)	115
4.37	Non-Dimensional Velocity Profiles ($\alpha = 0$ (Re = 388000); $R/R_0 = 0$ and 0.499)	116
4.38	Non-Dimensional Velocity Profiles ($\alpha = 0$ (Re = 388000); $R/R_0 = 0.749$ and 0.936)	117
4.39	Comparison with Predicted Shear Stress Variation ($\alpha = 0$ (pipe); Re = 388000)	118
4.40	Non-Dimensional Velocity Profiles ($\alpha = 0.1002$ (Re = 320000))	119
4.41	Non-Dimensional Velocity Profiles ($\alpha = 0.1002$ (Re = 451000))	120
4.42	Non-Dimensional Velocity Profiles ($\alpha = 0.0239$ (Re = 531000))	121

FIGURE		Page
4.43	Predicted Wall Layer Growth ($\alpha = 0.344$ (Re = 78800))	122
4.44	Predicted Wall Layer Growth ($\alpha = 0$ (Re = 388000))	123
4.45	Predicted Wall Layer Growth ($\alpha = 0.531$ (Re = 142000))	124
4.46	Predicted Outer Wall Layer Growth	125
4.47	Predicted Inner Wall Layer Growth	126
4.48	Comparison with Predicted Core Velocity Variation	127
4.49	Predicted Core Velocity Variation	128
4.50	Predicted Core Velocity Variation	129
4.51	Comparison with Predicted Pressure Gradient Variation	130
4.52	Comparison with Predicted Core Velocity Variation ($\alpha = 0$ (Re = 388000))	131
4.53	Pressure Variation ($\alpha = 0$ (Re = 388000))	132

LIST OF TABLES

Table		Page
4.1	Axial locations when $\delta_1 = \delta_{1\max}$ and $\tau_1 = \tau_{1\min}$ in laminar annular developing flows.	53
4.2	C values for Equation (4.1)	57
4.3	Experimental values of power-law exponents. ($\alpha=0.344$; (Re = 78800) and $\alpha=0.531$ (Re = 142000)).	59
4.4	Experimental values of power-law exponents taken from Paranjpe [2].	59

NOMENCLATURE

a_1	constant in Equation (3.61)
A	total flow cross-sectional area
A_1, A_2, \dots, A_{57}	defined in Appendix A
A^+	damping constant
B_1, B_2	defined by Equation (3.15)
c_1, c_2	defined by Equations (3.11a) & (3.34a) respectively
C	defined by Equation (4.6)
C_1, C_2, \dots, C_5	defined in Appendix A
D_h	hydraulic or equivalent diameter = $2(R_2 - R_1)$; $D_h = D$ for pipes
E_0, E_1, \dots, E_{17}	defined in Appendix A
f	perimeter average 'Fanning' friction factor for fully developed flow = $[(p_i - p) / (\rho V^2 / 2) - k(x)] / (4ReX)$
f_{app}	apparent 'Fanning' friction factor = $[(p_i - p) / (\rho V^2 / 2)] / (4ReX)$
f_x	local 'Fanning' friction factor in hydrodynamic entry length = $\tau_w / (\rho V^2 / 2)$
F_1, F_2, \dots, F_9	defined by Equations (3.25a) & (3.25b)
G_1, G_2, \dots, G_6	defined by Equation (3.48)
h	step size in Runge-Kutta integration routine
H	shape factor = δ^* / δ^{**}
I_1, I_2	defined by Equation (3.17)
$k(x)$	incremental pressure drop number
$k(\infty)$	incremental pressure drop number for fully developed flow

m_1, m_2, m_3	constants in Equation (3.1)
n	power law constant
p	static pressure
P	dimensionless static pressure = $(p_i - p) / (\rho V^2 / 2)$
r	defined by Equation (2.4)
R	radial distance
R_0	pipe radius
R^+	dimensionless radial distance = Ru^* / ν
Re	Reynolds number = VD_h / ν
S_1, S_2	defined by Equation (3.38)
T_1, T_2, T_3	defined by Equation (3.40)
u	velocity component in axial direction for laminar flows; mean value of velocity component in axial direction for turbulent flows
u^*	friction velocity = $(\tau_w / \rho)^{0.5}$
u^+	dimensionless velocity = u / u^*
U	core velocity
v	velocity component in radial direction
V	bulk or average velocity
x	axial distance
X	dimensionless axial distance (= $x / (D_h Re)$ for laminar flows; = x / D_h for turbulent flows)

y	radial distance measured from wall
y^+	dimensionless radial distance = yu^*/ν
α	radius (or diameter) ratio = R_1/R_2
α_k	kinetic energy correction factor = $\frac{1}{A} \int_A \left(\frac{u}{V}\right)^3 dA$
β	momentum correction factor = $\frac{1}{A} \int_A \left(\frac{u}{V}\right)^2 dA$
δ	thickness of wall layer
δ^+	dimensionless wall layer thickness = $\delta u^*/\nu$
δ^*	displacement thickness of wall layer
δ^{**}	momentum thickness of wall layer
ϵ	eddy diffusivity
η	defined in Equation (2.1)
θ	defined in Equation (2.1)
κ	constant in Equation (2.4)
μ	dynamic viscosity
ν	kinematic viscosity = μ/ρ
ϕ	dimensionless radial distance = $2(R_2 - R)/D_h$
χ	dimensionless radial distance = $(1 - \phi)$
τ	shear stress
ρ	density

Subscripts

1	inner wall or inner wall layer of annulus
2	outer wall or outer wall layer of annulus

fd	fully developed
i	condition at inlet plane
M	condition at maximum velocity location in fully developed flows
max	condition at maximum inner wall layer thickness location
min	condition at minimum inner wall shear stress variation
x	condition at wall
x	at a location which is at an axial distance x from inlet plane
δ	edge of wall layer

NOTE: Exceptions for subscripts 1 and 2 are defined in the first part of the Nomenclature.

CHAPTER I
INTRODUCTION

1.1 Characteristics of Developing Flows

When a fluid enters a duct, a velocity profile develops (along the duct) until the fully developed profile is reached some distance from the entrance of the duct. This flow development occurs in a flow regime referred usually as the developing (or inlet) region. The developing (entrance, inlet or settling) length is the axial length of the developing region.

The velocity adjustment is due to the presence of boundary layers (denoted as wall layers in this Dissertation) associated with the inner and outer walls which increase in thickness as the distance along the flow increases. This results in a decrease in the size of the potential flow region.

The velocity changes from zero at the wall (no-slip condition) to core velocity at the edge of the wall layer. Since the mass flow rate must remain constant, the flow in the central potential core region must accelerate to compensate for retardation of flow in the wall layers. As a consequence of wall layer and velocity development, very large pressure gradients and wall shear stresses exist in the developing region.

In laminar annular flows, the end of the developing region is marked by the meeting of the inner and outer wall layers. All flow parameters attain their fully developed values at the end of the hydrodynamic developing region. In turbulent annular flows, however, the situation is somewhat different in that the inner and outer wall layers meet initially at an axial location before the end of the developing region. The velocity profile at this location, still not fully developed, further readjusts itself in the axial direction until the fully developed velocity distribution is attained. Most flow parameters, for example, pressure gradient, wall shear stress, turbulence intensity reach their fully developed values before the end of the developing region and generally at different axial positions along the duct.

In this Dissertation, for the turbulent flow analysis, the developing region is divided into two sub-regions, i.e, entry-region and adjustment region (within which the wall layers initially meet and the velocity profile further adjusts itself to the fully developed profile respectively). The experimental evidence of Okiishi and Serovy [1] and Paranjpe [2] attest to the existence of two such flow regimes for turbulent annular flows.

1.2 Flow Geometry

The basic geometry studied is the concentric constant cross-sectional area annulus. The annular configuration finds itself in various industrial applications, for example, heat exchangers, axial flow

turbomachinery and atomic reactors. For short annular sections, the developing region has a considerable effect on pressure drop and heat transfer rates.

The shape of the entrance to an annular passage will influence the development of both the thermal and hydrodynamic wall layer growths. The experimental studies of Okiishi and Serovy [1] and Sridhar et al. [3] indicated that for a given annulus developing lengths were shorter using a square-edged entrance than for a rounded entrance. This may be attributed to the fact that, provided there is no intentional tripping of a wall layer at the start, a laminar wall layer usually precedes a turbulent wall layer for a rounded entrance while the wall layer is turbulent from the inlet plane for a square-edged entrance annulus.

In the present analysis, a well rounded entrance is considered as it provides a convenient mathematical condition of a relatively flat inlet velocity profile to the annulus. In addition, the hydrodynamic wall layers are assumed to initiate from the inlet plane. The small length of laminar wall layer which precedes a turbulent wall layer in turbulent flows decreases with increase in Reynolds number. As relatively high Reynolds number will be considered, in the present study, the effect on the flow of this small laminar length will be neglected.

Pipes and parallel plates are extreme cases of the annulus, that is, radius ratio zero and one respectively. Entrance-region pipe flow

studies are of special importance for the design of closed-jet working sections for wind and water tunnels, as well as for the design of tubular heat exchangers and hydraulic-pipe systems.

While the velocity distribution for the above cases are symmetrical, that for the annulus is asymmetrical. This aspect of the velocity distribution represents a fundamental difference between these related flow problems. Also, it has been recognized (Sparrow and Lin [4], for example) that the flow situation in which the radius ratio tends to zero does not represent the pipe flow solution. This is due to the presence of the different physical boundary conditions of zero velocity and maximum velocity at the centre for very small and zero diameter ratio respectively.

1.3 Purpose of Present Research

The present study is directed towards the prediction of flow characteristics in developing flows through annuli and pipes using an integral viewpoint. The method of analysis involves writing the relation between the change in momentum, the pressure drop and the friction force acting on an element of a wall layer.

In the annular flow study, the main objective is to provide simple, but realistic, solutions unlike those currently available. Laminar and turbulent annular flows are investigated. For both of these flows, two models (a Simplified Model and a General Model) will be considered in order to check the validity of an assumption used.

Also, for turbulent annular flows, the proposed analysis will focus itself onto flow within the entry region only. Very little information, if any, is presently available on local flow characteristics in the adjustment region. As in most previous works, the analysis can only be used up to the end of the entry region since the Bernoulli's equation ceases to apply after this axial location due to the disappearance of potential core flow.

In the turbulent pipe flow study, a comparison will be made between the results using the Bernoulli's equation and that using a macroscopic energy balance.

For both of the above mentioned flow geometries, the fully developed situation has extensively been studied analytically and experimentally and consequently (fully developed flows) will not be discussed to any great extent in this paper.

Unless otherwise specified, developing steady and isothermal flow of an incompressible Newtonian fluid through a constant cross-sectional flow area is considered.

CHAPTER II

LITERATURE SURVEY

2.1 General

There are three basic types of developing duct flows, i.e., hydrodynamically, thermal and simultaneously developing flows. Hydrodynamically developing flow refers to flow within a region in which the thickness of the velocity wall layer is growing. Thermal developing is related to flow in which the temperature wall layer is developing. The velocity profile in this region could be either developing or developed. A combination of thermal and hydrodynamic developing flow is referred to as simultaneously developing flow.

The present study will be concerned only with hydrodynamically developing flows. Many approximate solutions have appeared in the literature. These will now be discussed.

2.2 Hydrodynamic Developing Annular Flows

2.2.1 Laminar Studies

One of the first solutions to the hydrodynamic entry length problem for the annulus was undertaken, by Murakawa [6], in 1960. He employed a series solution approach and the results which involved an infinite series of Bessel functions satisfy the physical boundary conditions only in part.

The first and only experimental study to date known to the author of developing laminar annular flows was presented, in 1961, by Astill [5] who considered entrance region flows with the inner cylinder rotating for a radius ratio of 0.732. It was found that for axial flow with the inner cylinder rotating, four modes of flow could exist, i.e., laminar flow, laminar flow plus vortices, turbulent flow and turbulent flow plus vortices. Lines of demarcation of the four modes were established as functions of axial velocity, rotational speed of the cylinder, distance from the entrance and the radial distance across the annulus. He applied various amount of suction at the inner wall and measured radial and axial velocity profiles for different angular velocity of rotation.

Techniques of accurate solutions fall into three general groupings: solutions of linearized momentum equations, solutions by finite difference methods, and solution by stream-tube approach. These will be considered separately.

(a) Solutions of linearized momentum equations:

Sugino [7], in 1962, adopted the Langhaar approach [8] and used:

$$\left. \begin{aligned} \frac{u \partial u}{\partial x} + v \frac{\partial u}{\partial R} &= v \theta^2 u \\ g_x - \frac{1}{\rho} \frac{dp}{dx} &= -v \eta \end{aligned} \right\} (2.1)$$

where θ and η were functions of x only. He solved the resulting

equations and obtained a closed form solution in terms of modified Bessel functions. He tabulated ΔP vs $4X$, and $k(\infty)$, fRe , and $4X_{fd}$ for $\alpha = 0.2, 0.5$ and 0.833 . While his $f_{app} Re$ factors agree with other researchers, his X_{fd} value of 0.005 obtained for all the above radius ratios is in disagreement with other studies and appears to be in error.

In 1962, Chang and Atabek [9] used the linearization technique suggested by Targ [10], i.e.,

$$\frac{u\partial u}{\partial x} + v \frac{\partial u}{\partial R} = U \frac{\partial u}{\partial x} \quad (2.2)$$

and obtained closed-form relations for the axial velocity and pressure gradient in the entrance region. They also presented X_{fd} vs α and found that X_{fd} decreases with increase in radius ratio.

Heaton et al. [11], similar to Sugino [7], used the Langhaar method of linearization in 1964. Instead of the Bernoulli's equation in the potential core region they used the momentum equation as boundary condition to eliminate the pressure gradient term. Shumway and McEligot [12] further showed that the pressure drop of Heaton et al. [11] obtained by using the momentum integral equation, differed from the results based on the mechanical energy equation by 20% for $X \leq 10^{-3}$. They concluded that the velocity profiles and ΔP values of Heaton et al. [11] are not reliable in this region.

Sparrow and Lin [4], in 1964, used the method of stretched coordinates (to

'stretch' the axial coordinate) and in this way were able to linearize the momentum equation. Velocity variation and plots of $k(x)$ vs $4X$ were presented for radius ratios of 0.001, 0.01, 0.05, 0.1, 0.2, 0.4, 0.8. The $f_{app} Re$ factors calculated from $k(x)$ of Sparrow and Lin [4] are between 0 and 2% lower than those of Liu [13].

The technique of Targ [10] was also applied by Roy [14], in 1965, who similar to Chang and Atabek [9] obtained closed-form relations for the axial velocity and pressure gradient in the entrance region. In fact, the results of Chang and Atabek [9] and Roy [14] are identical.

(b) Solutions by finite difference methods

The first finite difference approach to the entrance-region annular flow problem was undertaken by Manohar [15], in 1965, who solved the momentum equation for $\alpha = 0.1, 0.3, 0.5$ and 0.7 . He presented graphically the velocity profiles, pressure distribution and hydrodynamic entrance lengths.

Shah and Farnia [16], in 1974, used the finite difference method of Patankar and Spalding [17] for concentric annuli. (Basically, in this method the axial coordinate x and dimensionless stream function are used as independent variables and these are used to transform the momentum and energy equations into finite difference form). They presented $f_x Re$ and $f_{app} Re$ as a function of $1/X$ for $\alpha = 0, 0.005, 0.1$, and 1 .

A modified implicit finite difference method was used by Coney and El-Shaarawi [18], in 1975, to analyze the hydrodynamic entrance problem

for concentric annuli. They presented both radial and axial developing velocity profiles and hydrodynamic entry lengths for fifteen different concentric annular ducts. Their developing axial velocity profiles are in good agreement with those of Sparrow and Lin [4].

(c) Solution by stream-tube approach

The complete set of Navier-Stokes equations, without the boundary layer type assumptions were analyzed, in 1971, by Fuller and Samuels [19]. They used a stream tube approach and included the effect of axial vorticity diffusion. They obtained the velocity profiles for various x/R_2 and Re for $\alpha = 0.5$.

2.2.2 Turbulent Studies

Rothfus et al. [20] in 1955, were among the first researchers on turbulent developing annular flows. They found that the outer wall shear stress was still approaching its asymptotic value at 250 equivalent diameters from the entrance. For $5000 < Re < 45000$, they reported that the effect of the level of turbulence at the inlet on downstream flow was negligible.

The work of Olson and Sparrow [21] in 1963, was based on static pressure measurements. They reported that the entrance length, based on 95% of fully developed pressure gradient, was within 20 to 25 equivalent diameters.

In 1967 velocity profiles at different axial locations along the annulus were measured for rounded and square-edged entrances by

Okiiski and Serovy [1]. It was found that flow separation caused by the abrupt change in area of the square-edged entrance resulted in skewed velocity profiles near the inlet. Also for the rounded entrance, transition from laminar to turbulent flow occurring near the entrance appreciably affected velocity profiles, shape factors, displacement thickness and local friction factors. The developing length for a square-edged entrance was found to be less than that for a rounded entrance.

Nicol et al. [22] in 1967, investigated developing flow through square-edged entrance annuli only. They measured velocity profiles and presented correlating equations for the settling length over the annulus Reynolds number range, 5000 - 50000, relating the equivalent diameter, Reynolds number and diameter ratio. Quarmby [23], in 1967, from his experimental investigation reported that the settling length is of the order of 30 to 40 hydraulic diameters. The inside surface of the tube was honed and the Reynolds number ranged from 10,000 to 90,000.

In 1970 Sridhar et al. [3] measured developing velocity profiles for turbulent flows in smooth concentric annuli with square-edged and bellmouth entrances. Settling length correlations proposed (similar to Nicol et al. [22]) for both entrances for $7000 < Re < 47500$ suggested an inverse radius ratio effect. They observed, as did Okiishi and Serovy [1], that the settling length with a square-edged entrance was less than with a bellmouth entrance.

Wilson and Medwell [24], in 1970, used a modified form of Reichardt [25] momentum eddy diffusivity equation and solved for the

developing turbulent hydrodynamic and thermal wall layers for internally heated annuli. Satisfactory agreement was obtained with the experimental data of Okiishi and Serovy [1]. Their analysis predicted hydrodynamically fully developed flow was obtained within 10 equivalent diameters.

Also in 1970, Okiishi and Bathie [26] developed an analytical model for turbulent flow in the developing region of an annulus. Their integral approach utilized the empirical wall shear stress correlation of Ludwig and Tillman [27] and the assumption of constant shape factors for both the inner and outer wall layers. Predictions of displacement and momentum thickness were not unreasonable when comparison was made with the experimental data of Okiishi and Serovy [1].

In 1971, Lee and Park [28] made an analytical and experimental study of developing turbulent flow through concentric annuli. Their analytical work was based, similar to Wilson and Medwell [24] on a modified form of Reichardt's expression for eddy diffusivity of momentum. Comparison of experimental and predicted eddy diffusivity in the developing region was not too good.

Developing and developed isothermal annular flow was studied analytically and experimentally in 1973, by Paranjpe [2]. Unlike previous researchers who used the universal logarithmic mean velocity profile, he suggested and experimentally verified the use of power law profiles for fully developed flow (for $92800 < Re < 531000$).

His analytical work in the developing region was also based on power law profiles and the wall shear stresses were expressed in terms of the power law constants based on the fully developed flow. Entrance lengths from the prediction was 15% lower than values found experimentally and increase with annulus Reynolds number.

2.3 Hydrodynamically Developing Turbulent Pipe Flows

One of the earliest investigations of developing pipe flows was done by Latzko [29] in 1921. He analyzed the development of turbulent velocity profile in a pipe by a method analogous to Schiller [30]. The velocity distribution followed the one-seventh power-law. For a total inlet length of a purely turbulent flow, he found

$$X_{fd} / D_h = 0.69 \text{ Re}^{0.25}, \quad (2.3)$$

Schiller and Kirsten [31] in 1929, investigated the velocity profile development in pipes for both rounded and sharp-edged entrances. For $10,000 < \text{Re} < 50,000$ they found that the fully developed velocity profile is attained in 50 to 100 equivalent diameters. They also observed that while for a rounded entrance, the settling length decreased as Reynolds number increased, for a sharp-edged entrance the opposite appeared to be the case. They may be due to the possible existence of a small length of laminar wall layer near the inlet for the rounded entrance.

Deissler [32] measured velocity profiles at various distances for rounded and right-angle-edged entrances for the flow of air in a tube

over a range $48000 < Re < 580000$. His results indicated that the flow development was more rapid for a right-angle entrance than for a rounded entrance as the length to reach fully developed flow was about 45 and 100 tube diameters respectively.

In 1955, Deissler [33], in addition to the usual boundary layer approximations, assumed in the developing flow that the eddy diffusivity, ϵ , is given by

$$\epsilon = r^2 u y (1 - \exp \{ -r^2 u y / \nu \}) \text{ for } y^+ < 26 \quad (2.4)$$

$$\text{and } \epsilon = \kappa^2 \frac{(\frac{du}{dy})^3}{(\frac{d^2u}{dy^2})^2} \text{ for } y^+ > 26$$

where r and κ are experimental constants. The eddy diffusivities for momentum and heat transfer were assumed to be equal. The results indicate that approximately fully developed heat transfer and friction are, in general, attained in less than 10 equivalent diameters.

Ross [34], in 1956, used an integral approach and presented an approximate analytical solution for the turbulent wall-layer flow within ten diameters of the entrance. Formulae for momentum thickness, pressure drop and head loss were obtained. Comparison of the theoretical expressions with the few available raw data showed good agreement.

Under the assumption of a logarithmic law rather than a one-seventh power law, as suggested by Latzko [29] for the velocity profile,

Filippov [35], in 1958, calculated turbulent flow development in the entrance length of a straight tube. Good agreement with experiment was obtained not only near the wall but also at the outer edge of the wall layer.

Perhaps the first reliable experimental data on turbulent inlet flow was provided in 1963, by Barbin and Jones [36]. They measured mean velocities, turbulence intensities, and turbulence stresses in the first 40 diameters of pipe length for Reynolds number of 388,000. While fully developed flow was not attained in this length, the wall shear stress and static pressure gradient attained their fully developed values within the first 15 diameters. They also experimentally showed that velocity profiles in the inlet region were not similar.

Bowlus and Brighton [37], in 1968, used a one-seventh power law velocity distribution coupled with an expression for the wall shear stress based on the Schultz-Grunow [27] relation for flat plates, that is,

$$\frac{\tau_w}{\rho U^2} = 0.185 \left[\log_{10} \left(\text{Re} \frac{UX}{V} \right) \right]^{-2.584} \quad (2.5)$$

and obtained reasonable agreement with experimental data for the core velocity development within the first 25 pipe diameters.

A numerical study based on finite-difference techniques and an experimental investigation of developing turbulent pipe flows were done by, in 1973, Richman and Azad [38]. They solved simultaneously the vorticity transport and stream function equations using a modified

form of Van Driest [39] eddy viscosity model. Very good agreement was obtained between the analytical prediction and experimental results.

In 1973, Na and Lu [40] used an integral approach and based their assumed velocity profile on the general power law mean velocity profile. The wall shear stress correlation of Ludwig and Tillman [27] was used and the variation of the shape factor (and hence the power law exponent) was considered by utilizing the entrainment equation of Von Doenhoff and Tetervin [27]. Good agreement was obtained with the experimental results of Barbin and Jones [36].

Wang and Tullis [41] in 1973 studied both analytically and experimentally turbulent flow development through rough pipes. Their analysis which was based on the logarithmic velocity profile predicted that the wall shear stress and velocity profile becomes fully developed in about 15 and 50 diameters respectively. Also predictions of wall layer growth, core velocity and pressure coefficient development agree reasonably well with the experimental data for the first 12 diameters.

Measurement and prediction of turbulence kinetic energy, Reynolds stress, velocity profiles and heat transfer were made in the flow development region of a pipe by Walklate et al. [42] in 1976. The experimental results indicated an approximately linear shear stress variation within the wall layer similar to the case for fully developed flows. Reasonable agreement was obtained between the measured and predicted velocity profiles.

Also, in 1976, Reichart and Azad [43], from measurements of the mean velocity profiles in the first 70 diameters of the pipe, showed a non-asymptotic development for turbulent pipe flows for $56000 < Re < 153000$. They also found that within the inlet region the mean velocity along the pipe centre-line "overshoots" the fully developed value.

2.4 Closure

From the literature survey presented, we may conclude that

- (i) for laminar annular flows no simple solution of hydrodynamic development is available. Further, no prediction of the growth of the wall layers exists.
- (ii) for turbulent flows in annuli no complete study of the entry region using simple expressions for velocity profiles in the wall layers can be found.
- (iii) for developing turbulent flows in pipes and annuli, there has been no known attempt other than using Bernoulli's equation for the purpose of eliminating the pressure gradient term in the analysis.

The present study primarily directs itself to the problems mentioned above in items (i) and (ii). An attempt will be made to provide some preliminary information on item (iii) by using a form of the macroscopic mechanical energy balance equation over the entire flow area of a pipe.

CHAPTER III

ANALYSIS OF DEVELOPING FLOWS

3.1 General

For most flow geometries, less attention has been given in the past to hydrodynamically developing flows than fully developed flows. The reason is, for most part, while both problems are difficult to handle, analysis of developing flows basically involves two independent variables (R and x) compared to one in the fully developed case. This fundamental difference between the nature of these two types of flow has created additional gross non-linearity in the inertia terms in the Navier-Stokes equation for the hydrodynamic developing flow analysis which resulted in complex analytical and numerical procedures being used in order to obtain solutions.

When we analyze developing flows through annuli, further algebraic complications arise due to the asymmetrical nature of the velocity distribution unlike the cases of pipe and parallel plates, limiting forms of the annular geometry.

For developing flows through annuli, most of the analytical works in the literature have used the differential approach for the laminar case. On the other hand, it appears that all of the few theoretical solutions available for developing turbulent annular flows are based on integral methods presumably because they are more manageable than

differential methods. The present study is based on integral methods of solution.

3.2 Method of Approach

3.2.1 Hydrodynamic Developing Laminar Annular Flows

Basically, there are eight dependent variables involved in developing laminar annular flows. They are u_1 , u_2 , U , δ_1 , δ_2 , τ_{1w} , τ_{2w} , p . As a result, a maximum number of eight independent equations are needed in order to solve the problem.

As in most integral methods, an assumed velocity distribution (which will be checked out in Chapter 4) will be specified. Two flow models were investigated, a Simplified Model and a General Model.

Equations common to both models are:

the assumed velocity distribution for u_1 and u_2

Newton's Law of Viscosity for τ_1 and τ_2

Continuity Equation

an equation resulting from application of
Macroscopic Mechanical Energy Balance

(A)

For the Simplified Model, we have:

(i) Equations of (A)

(ii) The integral momentum equation applied to entire flow area.

(iii) an assumption of constant ratio of wall layer thickness, $(\delta_1/\delta_2) = c_1 = (\delta_1/\delta_2)_{fd}$.

In the case of the General Model we have:

- (i) Equations of (A)
- (ii) Momentum equation applied to inner wall layer
- (iii) Momentum equation applied to outer wall layer.

In both models, there are eight equations present.

3.2.2 Hydrodynamic Entry-Region Turbulent Annular Flows

As in the laminar flow situation, eight dependent variables are present and so a minimum number of eight equations is required in order to obtain a solution. Similar to the laminar flow case, also, two flow models were investigated, i.e., a Simplified Model and a General Model. Common to both were:

- two equations from assumed velocity distribution
 - two equations from assumed wall shear stress variation
 - one equation from Conservation of mass
 - Bernoulli's equation
- } (B)

For the Simplified Model we write:

- (i) Equations of (B)
- (ii) Momentum equation applied to entire flow cross-sectional area
- (iii) One equation from assumption of constant ratio of wall layer thickness

We have for the General Model:

- (i) Equations of (B)
- (ii) Momentum equation applied to inner wall layer
- (iii) Momentum equation applied to outer wall layer.

There are eight equations present in both models.

3.2.3 Entry-Region Turbulent Pipe Flows

There are five dependent variables present in the analysis of entry-region turbulent pipe flows, namely, u , U , δ , τ and p . At least five equations are therefore required in order to solve the problem. These equations are obtained as follows:

- (i) One equation from assumption of linear shear stress variation in wall layer
- (ii) One equation from the assumed eddy viscosity model
- (iii) Continuity equation
- (iv) Momentum equation applied to the wall layer
- (v) An equation resulting from application of the macroscopic energy balance or the Bernoulli's equation.

We, therefore, have the minimum number of equations required for a solution, i.e., 5.

3.3 Mathematical Analysis

3.3.1 Developing Laminar Annular Flows

For fully developed laminar annular flows, we may write

$$u_{fd} = m_1 R^2 + m_2 \ln R + m_3 \quad (3.1)$$

where m_1, m_2 and m_3 are functions of the annulus radius ratio and hence constants for a given annulus. Equation (3.1) is obtained by integrating the Navier-Stokes equation in the axial direction for fully developed flows. Using the following boundary conditions in Equation (3.1),

$$u_{fd} = 0 \text{ at } R = R_1$$

$$u_{fd} = 0 \text{ at } R = R_2$$

by direct substitution it may be shown that

$$\left(\frac{u}{U}\right)_{fd} = \frac{[R^2 - R_1^2 - 2R_M^2 \ln(R/R_1)]}{[R_M^2 - R_1^2 - 2R_M^2 \ln(R_M/R_1)]} \quad (3.2)$$

or

$$\left(\frac{u}{U}\right)_{fd} = \frac{[R^2 - R_2^2 - 2R_M^2 \ln(R/R_2)]}{[R_M^2 - R_2^2 - 2R_M^2 \ln(R_M/R_2)]} \quad (3.3)$$

Analogous to Equation (3.2) and Equation (3.3), we assume the velocity profile in the developing region is, by replacing R_M by $R_{\delta 1}$ and $R_{\delta 2}$ respectively,

$$\frac{u_1}{U} = \frac{[R^2 - R_1^2 - 2R_{\delta 1}^2 \ln(R/R_1)]}{[R_{\delta 1}^2 - R_1^2 - 2R_{\delta 1}^2 \ln(R_{\delta 1}/R_1)]} \quad (3.4)$$

for the inner wall layer and

$$\frac{u_2}{U} = \frac{[R^2 - R_2^2 - 2R_{\delta_2}^2 \ln(R/R_2)]}{[R_{\delta_2}^2 - R_2^2 - 2R_{\delta_2}^2 \ln(R_{\delta_2}/R_2)]} \quad (3.5)$$

for the outer wall layer.

Equation (3.4) and Equation (3.5) satisfy all the physical boundary conditions, i.e.,

$$\left. \begin{aligned} u_1 &= u_1(x, R_1) = 0 \\ u_1 &= u_1(x, R_{\delta_1}) = U \\ \frac{\partial u_1}{\partial R} \Big|_{R=R_{\delta_1}} &= 0 \\ u_2 &= u_2(x, R_2) = 0 \\ u_2 &= u_2(x, R_{\delta_2}) = U \\ \frac{\partial u_2}{\partial R} \Big|_{R=R_{\delta_2}} &= 0 \end{aligned} \right\} \quad (3.6)$$

A short-hand notation will now be used where $j = 1, 2$ refer to parameters associated with the inner and outer wall layer respectively.

The assumed velocity distribution may then be written as

$$\frac{u_j}{U} = \frac{[R^2 - R_j^2 - 2R_{\delta_j}^2 \ln(R/R_j)]}{[R_{\delta_j}^2 - R_j^2 - 2R_{\delta_j}^2 \ln(R_{\delta_j}/R_j)]} \quad (3.7)$$

Newton's Law of Viscosity is

$$\tau_j = \mu \frac{\partial u_j}{\partial R} \quad (3.8)$$

The Continuity equation can be expressed as

$$\int_{R_1}^{R_2} u \, 2\pi R \, dR = AV \quad (3.9)$$

Writing a macroscopic mechanical energy balance between the entrance and some distance x from the entrance of the duct, and then differentiating with respect to x yields

$$\begin{aligned} -AV \, dp = 2 \mu \pi \left[\int_{R_1}^{R_2} \left(\frac{\partial u}{\partial R} \right)^2 R \, dR \right] dx \\ + \pi \rho d \left[\int_{R_1}^{R_2} (u^3 - V^3) R \, dR \right] \end{aligned} \quad (3.10)$$

Equation (3.7) to Equation (3.10) are common to both the Simplified and the General Model].

For the Simplified Model, one can write

(i) Equation (3.7) to Equation (3.10)

$$(ii) -\tau_{1W} \, 2\pi R_1 \, dx + \tau_{2W} \, 2\pi R_2 \, dx - dpA = \rho d \left[\int_{R_1}^{R_2} u^2 \, 2\pi R \, dR \right] \quad (3.11)$$

$$(iii) \delta_1 = \delta_1 (\delta_2) = c_1 \delta_2 \text{ for all } x \text{ where } c_1 = (\delta_1/\delta_2)_{fd} \quad (3.11a)$$

Similarly, for the General Model, we can write

(i) Equation (3.7) to Equation (3.10)

$$\begin{aligned}
 \text{(ii)} \quad & -\tau_{1W} 2\pi R_1 dx - \pi (R_{\delta_1}^2 - R_1^2) dp = -\rho d \left[\int_{R_1}^{R_{\delta_1}} u_1^2 2\pi R dR \right] U \\
 & + \rho d \left[\int_{R_1}^{R_{\delta_1}} u_1^2 2\pi R dR \right]
 \end{aligned} \tag{3.12}$$

$$\begin{aligned}
 \text{(iii)} \quad & +\tau_{2W} 2\pi R_2 dx - \pi (R_2^2 - R_{\delta_2}^2) dp = -\rho d \left[\int_{R_{\delta_2}}^{R_2} u_2^2 2\pi R dR \right] U \\
 & + \rho d \left[\int_{R_{\delta_2}}^{R_2} u_2^2 2\pi R dR \right]
 \end{aligned} \tag{3.13}$$

The analysis for the two models will now be considered separately.

(a) Simplified Model:

Eliminating the pressure term between Equation (3.10) and Equation (3.11) the following expression is obtained.

$$\begin{aligned}
 V \{ & \tau_{1W} 2\pi R_1 dx - \tau_{2W} 2\pi R_2 dx + \rho d \left[\int_{R_1}^{R_2} u^2 2\pi R dR \right] \} \\
 = & 2\mu\pi \left[\int_{R_1}^{R_{\delta_1}} \left(\frac{\partial u_1}{\partial R} \right)^2 R dR + \int_{R_{\delta_2}}^{R_2} \left(\frac{\partial u_2}{\partial R} \right)^2 R dR \right] dx \\
 & + \pi \rho d \left[\int_{R_1}^{R_2} (u^3 - v^3) R dR \right]
 \end{aligned} \tag{3.14}$$

We define

$$\left. \begin{aligned}
 B_1 &= \frac{R_1^2}{R_{\delta_1}^2} \\
 B_2 &= \frac{R_2^2}{R_{\delta_2}^2}
 \end{aligned} \right\} \tag{3.15}$$

It may be shown that

$$\tau_{1w} = \mu \left. \frac{\partial u_1}{\partial R} \right|_{R=R_1} = 2\mu \frac{U}{R_1} \frac{(B_1 - 1)}{(1 - B_1 + \epsilon \ln B_1)}$$

$$\tau_{2w} = \mu \left. \frac{\partial u_2}{\partial R} \right|_{R=R_2} = 2\mu \frac{U}{R_2} \frac{(B_2 - 1)}{(1 - B_2 + \epsilon \ln B_2)}$$

$$\int_{R_1}^{R_2} u^2 2\pi R dR = \pi \rho U^2 \left[\frac{R_1^2}{B_1} \frac{\left\{ \frac{11}{6} - 3B_1 + \frac{3}{2} B_1^2 - \frac{B_1^3}{3} + \epsilon \ln B_1 \right\}}{(1 - B_1 + \epsilon \ln B_1)^2} \right. \\ \left. - \frac{R_2^2}{B_2} \frac{\left\{ \frac{11}{6} - 3B_2 + \frac{3}{2} B_2^2 - \frac{B_2^3}{3} + \epsilon \ln B_2 \right\}}{(1 - B_2 + \epsilon \ln B_2)^2} \right]$$

(3.16)

$$\int_{R_1}^{R_2} \left(\frac{\partial u}{\partial R} \right)^2 R dR = U^2 \left[\frac{\left\{ (1-B_1^2) + 4(B_1-1) - 2\epsilon \ln B_1 \right\}}{(1 - B_1 + \epsilon \ln B_1)^2} \right. \\ \left. - \frac{\left\{ (1-B_2^2) + 4(B_2-1) - 2\epsilon \ln B_2 \right\}}{(1 - B_2 + \epsilon \ln B_2)^2} \right]$$

$$\int_{R_1}^{R_2} u^3 R dR = \frac{U^3 R_1^2}{2 B_1} \left[-B_1 + \frac{3 \left(\frac{1}{2} - \frac{1}{2} B_1^2 + B_1 \epsilon \ln B_1 \right)}{(1 - B_1 + \epsilon \ln B_1)} \right. \\ \left. + \frac{3 \left(\frac{5}{6} - B_1 + \frac{B_1^2}{2} - \frac{B_1^3}{3} + B_1^2 \epsilon \ln B_1 - B_1 \epsilon \ln^2 B_1 \right)}{(1 - B_1 + \epsilon \ln B_1)^2} \right]$$

$$\begin{aligned}
& + \frac{\left(\frac{7}{3} - 2B_1 - \frac{3}{4}B_1^2 + \frac{2}{3}B_1^3 - \frac{B_1^4}{4} + (3B_1 - \frac{3}{2}B_1^2 + B_1^3)\ln B_1 - \frac{3}{2}B_1^2 \ln^2 B_1 + B_1 \ln^3 B_1\right)}{(1 - B_1 + \ln B_1)^3} \\
& - \frac{U^3 R_2^2}{2B_2} \left[-B_2 + 3 \frac{\left(\frac{1}{2} - \frac{B_2^2}{2} + B_2 \ln B_2\right)}{(1 - B_2 + \ln B_2)} \right. \\
& + \frac{3 \left(\frac{5}{6} - B_2 + \frac{B_2^2}{2} - \frac{B_2^3}{2} + B_2^2 \ln B_2 - B_2 \ln^2 B_2\right)}{(1 - B_2 + \ln B_2)^2} \\
& \left. + \frac{\left(\frac{7}{3} - 2B_2 - \frac{3}{4}B_2^2 + \frac{2}{3}B_2^3 - \frac{B_2^4}{4} + (3B_2 - \frac{3}{2}B_2^2 + B_2^3)\ln B_2 - \frac{3}{2}B_2^2 \ln^2 B_2 + B_2 \ln^3 B_2\right)}{(1 - B_2 + \ln B_2)^3} \right]
\end{aligned}$$

Using Equation (3.15) and Equation (3.16) in Equation (3.14) we obtain after extensive algebraic manipulation,

$$8(1 - \alpha)^2 dX = I_1 dB_1 + I_2 dB_2 \quad (3.17)$$

where I_1 and I_2 are functions of A_1, A_2, \dots, A_{26} defined in Appendix A.

From the assumption of a constant ratio of wall layer growth, i.e.,

$$\left. \frac{\delta_1}{\delta_2} \right|_x = \left. \frac{\delta_1}{\delta_2} \right|_{fd} \quad (3.18)$$

it may be shown that

$$\frac{dB_1}{dX} = \frac{-\left[\left\{\frac{(1-\alpha^2)}{-2\ln \alpha}\right\}^{1/2} - \alpha\right]}{\left[1 - \left\{\frac{(1-\alpha^2)}{-2\ln \alpha}\right\}^{1/2}\right]} \frac{1}{\alpha} \left(\frac{B_1}{B_2}\right)^{3/2} \frac{dB_2}{dX} \quad (3.19)$$

Finally substituting Equation (3.19) in Equation (3.17), we obtain

$$\frac{8(1-\alpha)^2}{ReD_h} = \left[-I_1 \frac{\left[\left\{\frac{(1-\alpha^2)}{-2\ln \alpha}\right\}^{1/2} - \alpha\right]}{\left[1 - \left\{\frac{(1-\alpha^2)}{-2\ln \alpha}\right\}^{1/2}\right]} \frac{1}{\alpha} \left(\frac{B_1}{B_2}\right)^{3/2} + I_2 \right] \frac{dB_2}{dx} \quad (3.20)$$

The term B_1 can be expressed in terms of B_2 , using Equation (3.18) as

$$\left. \frac{\left(\frac{1}{B_1}\right)^{1/2} - 1}{\left(1 - \left(\frac{1}{B_2}\right)^{1/2}\right)} \right|_x = \left. \frac{\left(\frac{1}{B_1}\right)^{1/2} - 1}{\left(1 - \left(\frac{1}{B_2}\right)^{1/2}\right)} \right|_{fd} \quad (3.21)$$

The right hand side of Equation (3.21) is a function of radius ratio only and hence can be obtained for a given annulus. Thus Equation (3.20) is reduced to a non-linear first order ordinary differential equation which was numerically solved using Simpson's rule. Having obtained B_2 , B_1 can be found from Equation (3.21) and hence we can determine the non-dimensional wall layer thickness δ_1/D_h and δ_2/D_h from Equation (3.15). The boundary condition is:

$$\text{at } X = 0, \quad B_2 = 1.$$

(b) General Model:

For simplicity, the pressure term in Equation (3.12) and Equation (3.13) was eliminated using Equation (3.10) and we obtain

$$\begin{aligned}
& -\tau_{1w} 2\pi R_1 dx + \pi(R_{\delta_1}^2 - R_1^2) \frac{1}{AV} \{2\mu\pi \left[\int_{R_1}^{R_2} \left(\frac{\partial u}{\partial R}\right)^2 R dR \right] dx \\
& + \pi \rho d \left[\int_{R_1}^{R_2} (u^3 - v^3) R dR \right] \} \\
& = -\rho U d \left[\int_{R_1}^{R_{\delta_1}} u_1^2 2\pi R dR \right] + \rho d \left[\int_{R_1}^{R_{\delta_1}} u_1^2 2\pi R dR \right] \quad (3.22)
\end{aligned}$$

for the inner wall layer and

$$\begin{aligned}
& +\tau_{2w} 2\pi R_2 dx + \pi(R_2^2 - R_{\delta_2}^2) \frac{1}{AV} \{2\mu\pi \left[\int_{R_1}^{R_2} \left(\frac{\partial u}{\partial R}\right)^2 R dR \right] dx \\
& + \pi \rho d \left[\int_{R_1}^{R_2} (u^3 - v^3) R dR \right] \} \\
& = \rho U d \left[\int_{R_{\delta_2}}^{R_2} u_2^2 2\pi R dR \right] + \rho d \left[\int_{R_{\delta_2}}^{R_2} u_2^2 2\pi R dR \right] \quad (3.23)
\end{aligned}$$

for the outer wall layer.

It may be shown that

$$\int_{R_1}^{R_{\delta_1}} u_1^2 2\pi R dR = \pi U \frac{R_1^2}{B_1} \left[1 + \frac{(1 - B_1)^2}{2(1 - B_1 + \ln B_1)} \right]$$

$$\int_{R_{\delta_2}}^{R_2} u_2^2 2\pi R dR = -\pi U \frac{R_2^2}{B_2} \left[1 + \frac{(1 - B_2)^2}{2(1 - B_2 + \ln B_2)} \right] \quad (3.24)$$

$$\int_{R_1}^{R_{\delta_1}} u_1^2 2\pi R dR = \pi U^2 \frac{R_1^2}{B_1} \left[1 + \frac{\left\{ \frac{11}{6} - 3B_1 + \frac{3}{2} B_1^2 - \frac{B_1^3}{3} + \ln B_1 \right\}}{(1 - B_1 + \ln B_1)^2} \right]$$

$$\int_{R_{\delta_2}}^{R_2} u_2^2 2\pi R dR = -\pi U^2 \frac{R_2^2}{B_2} \left[1 + \frac{\left\{ \frac{11}{6} - 3B_2 + \frac{3}{2} B_2^2 - \frac{B_2^3}{3} + \ln B_2 \right\}}{(1 - B_2 + \ln B_2)^2} \right]$$

Substituting Equation (3.24) in Equation (3.22) and Equation (3.23) using Equation (3.15) and Equation (3.16), we get after extensive mathematical calculations (see Appendix A),

$$F_1 \frac{d(\delta_1/D_h)}{dX} + F_2 \frac{d(\delta_2/D_h)}{dX} = F_3 \quad (3.25a)$$

$$F_4 \frac{d(\delta_1/D_h)}{dX} + F_5 \frac{d(\delta_2/D_h)}{dX} = F_6$$

where F_1, F_2, \dots, F_6 are functions of B_1 and B_2 (and hence δ_1/D_h and δ_2/D_h) and are defined in Appendix A.

Also, an equation for the pressure can be obtained by using Equation (3.10). This equation may be written in the form

$$\frac{dP}{dX} = F_7 \frac{d(\delta_1/D_h)}{dX} + F_8 \frac{d(\delta_2/D_h)}{dX} + F_9 \quad (3.25b)$$

where F_7 , F_8 and F_9 are similar to F_1, F_2, \dots, F_6 , functions of B_1 and B_2 and are defined in Appendix A.

Equations (3.25a) and (3.25b) form a system of non-linear first order ordinary differential equations which was solved using the fifth order Runge-Kutta integration routine. It is worth mentioning that Equation (3.25a) may be solved independent of Equation (3.25b). The boundary conditions are:

$$\text{at } X = 0, \delta_1/D_h = 0, \delta_2/D_h = 0, P = 0.$$

3.3.2 Entry-Region Turbulent Annular Flows

Most of the few analytical solutions to developing turbulent annular flows presently available have used one basic assumption, i.e., the shear stress variation in the wall layers is linear. Coupled with this and an appropriate eddy viscosity model, velocity profiles non-dimensionalized with respect to the wall shear stress could be obtained. The linear shear stress variation will now be checked.

For fully developed flows, writing a force balance between $R = R_M$ and $R = R$ and $R = R_2$ respectively, we have

$$\left. \begin{aligned} dp\pi (R_2^2 - R_M^2) &= \tau_{2w} 2\pi R_2 dx \\ dp\pi (R^2 - R_M^2) &= \tau_2 2\pi R dx \end{aligned} \right\} \quad (3.26)$$

From Equation (3.26),

$$\tau_2 = \tau_{2w} \frac{R_2}{R} \frac{(R^2 - R_M^2)}{(R_2^2 - R_M^2)} = \tau_{2w} \frac{R_2}{(R_2^2 - R_M^2)} \left(R - \frac{R_M^2}{R} \right) . \quad (3.27)$$

Similarly, writing a force balance for the inner wall

layer between $R = R_M$ and $R = R$ and $R = R_1$ respectively, we obtain

$$\left. \begin{aligned} dp\pi (R_M^2 - R_1^2) &= \tau_{1w} 2\pi R_1 dx \\ dp\pi (R_M^2 - R^2) &= \tau_1 2\pi R dx \end{aligned} \right\} . \quad (3.28)$$

From Equation (3.28),

$$\tau_1 = \tau_{1w} \frac{R_1}{R} \frac{(R_M^2 - R^2)}{(R_M^2 - R_1^2)} = \frac{\tau_{1w} R_1}{(R_M^2 - R_1^2)} \left(\frac{R_M^2}{R} - R \right) \quad (3.29)$$

It can be seen from Equation (3.27) and Equation (3.29) that for fully developed flows, while the assumption of linear shear stress variation in the outer wall layer may be acceptable (corresponds to large values of R), it is not reasonable in the case for the inner wall layer (corresponds to small values of R). It is unlikely that a linear shear stress distribution would exist in the developing region (at least the entry-region) if such a distribution is not present in the fully developed case. This observation may be the reason for the discrepancy between the experimental results of Okiishi and Serovy [1]

and the analytical study of Wilson and Medwell [24] near the inner wall region.

In the present study, the velocity distribution is assumed to be represented by a general power-law mean velocity profile, that is,

$$\frac{u_j}{U} = \left(\frac{y_j}{\delta_j} \right)^{1/n_j} \quad (3.30)$$

where, as in the laminar flow situation, $j = 1, 2$ corresponds to quantities associated with the inner and outer wall layers respectively. The radial coordinate y_j is measured from the wall and n_j takes different values for the inner and outer wall layer. The velocities are time-averaged quantities.

For the present turbulent wall layer flow with a pressure gradient, the shear stress at the wall will be approximated by the empirical correlation of Ludwig and Tillman [27]. We may, thus, write for the inner and outer walls

$$\frac{\tau_{jw}}{\rho U^2} = 0.123 * 10^{-0.678 H_j} \left(\frac{U \delta_j^{**}}{\nu} \right)^{-0.268} \quad (3.31)$$

The Continuity equation is

$$\int_{R_1}^{R_2} u \, 2\pi R dR = AV \quad (3.32)$$

Bernoulli's equation applied to the central potential core region may be written as

$$dp = - \rho U dU \quad (3.33)$$

Equations (3.30) to (3.33) are common to both flow models analyzed.

For the Simplified Model we can write

(i) Equation (3.30) to Equation (3.33)

$$(ii) -\tau_{1w} 2\pi R_1 dx - \tau_{2w} 2\pi R_2 dx - dpA = \rho d \left[\int_{R_1}^{R_2} u^2 2\pi R dR \right] \quad (3.34)$$

$$(iii) \delta_1 = \delta_1(\delta_2) = c_2 \delta_2 \text{ for all } x \text{ where } c_2 = (\delta_1/\delta_2)_{fd} \quad (3.34a)$$

and for the General Model

(i) Equation (3.30) to Equation (3.33)

$$(ii) -\tau_{1w} 2\pi R_1 dx - \pi(R_{\delta_1}^2 - R_1^2) dp = - \rho d \left[\int_{R_1}^{R_{\delta_1}} u_1 2\pi R \right] U \\ + \rho d \left[\int_{R_1}^{R_{\delta_1}} u_1^2 2\pi R dR \right] \quad (3.35)$$

$$(iii) -\tau_{2w} 2\pi R_2 dx - \pi(R_2^2 - R_{\delta_2}^2) dp = - \rho d \left[\int_{R_{\delta_2}}^{R_2} u_2 2\pi R dR \right] U \\ + \rho d \left[\int_{R_{\delta_2}}^{R_2} u_2^2 2\pi R dR \right] \quad (3.36)$$

At this point the analysis for both models will be discussed separately.

(a) Simplified Model:

Using Equation (3.31) and Equation (3.33) in Equation (3.34)

we get,

$$\begin{aligned}
 & -0.123 * 10^{-0.678H_1} \left(\frac{U\delta_1^{**}}{\nu} \right)^{-0.268} \rho U^2 2\pi R_1 dx \\
 & -0.123 * 10^{-0.678H_2} \left(\frac{U\delta_2^{**}}{\nu} \right)^{-0.268} \rho U^2 2\pi R_2 dx \\
 & + \rho U dUA = \rho d \left[\int_{R_1}^{R_2} u^2 2\pi R dR \right] \quad . \quad (3.37)
 \end{aligned}$$

We define

$$\begin{aligned}
 S_1 &= \frac{R_1}{R_{\delta_1}} \\
 S_2 &= \frac{R_2}{R_{\delta_2}}
 \end{aligned} \quad \left. \vphantom{\begin{aligned} S_1 \\ S_2 \end{aligned}} \right\} \quad (3.38)$$

It may be shown that

$$\begin{aligned}
 \int_{R_1}^{R_2} u^2 2\pi R dR &= 2\pi \frac{R_1^2}{S_1^2} U^2 \frac{(1 - S_1)}{\left(\frac{2}{n_1} + 1\right)} \left[1 - \frac{(1 - S_1)}{\left(\frac{2}{n_1} + 2\right)} \right] \\
 &+ \pi U^2 \left(\frac{R_2^2}{S_2^2} - \frac{R_1^2}{S_1^2} \right) \\
 &+ 2\pi \frac{R_2^2}{S_2^2} U^2 \frac{(S_2 - 1)}{\left(\frac{2}{n_2} + 1\right)} \left[1 - \frac{(1 - S_2)}{\left(\frac{2}{n_2} + 2\right)} \right] \quad . \quad (3.39)
 \end{aligned}$$

Substituting Equation (3.39) in Equation (3.37) using Equation (3.30) and Equation (3.38) we obtain after extensive calculations.

$$T_1 dS_1 + T_2 dS_2 = T_3 dX \quad (3.40)$$

where T_1 , T_2 and T_3 are functions of E_0, E_1, \dots, E_9 defined in Appendix A.

From the simple assumption of constant ratio of wall layer growth, i.e.,

$$\frac{\delta_1}{\delta_2} \Big|_x = \frac{\delta_1}{\delta_2} \Big|_{fd} \quad (3.41)$$

it can be shown that

$$dS_1 = \frac{[\alpha(1-S_1) - c_2 S_1]}{[\alpha S_2 + c_2(S_2-1)]} dS_2 \quad (3.42)$$

The term S_1 can be expressed in terms of S_2 using Equation (3.41) as

$$\frac{(\frac{1}{S_1} - \alpha)}{(1 - \frac{1}{S_2})} = \frac{(\frac{1}{S_1} - \alpha)}{(1 - \frac{1}{S_2})} \Big|_{fd} \quad (3.43)$$

The right hand side of Equation (3.43) is a function of radius ratio only and thus can be determined for a given annulus.

Using Equation (3.42) in Equation (3.40) yields:

$$dX = \left\{ T_1 \frac{[\alpha (1-S_1) - c_2 S_1]}{(\alpha S_2 + c_2 (S_2-1))} + T_2 \right\} \frac{1}{T_3} dS_2 \quad (3.44)$$

Finally, combining Equation (3.43) with Equation (3.44) results in a first order non-linear ordinary differential equation which is solved numerically using Simpson's rule. From the values obtained for S_2 (and X), S_1 can be determined from Equation (3.43) and δ_1/D_h and δ_2/D_h can be obtained from Equation (3.38). The boundary condition is:

$$\text{at } X = 0, \quad S_2 = 1.$$

(b) General Model:

Introducing Equation (3.31) and Equation (3.33) in Equation (3.35) and Equation (3.36) produces

$$\begin{aligned} & -0.123 * 10^{-0.678H_1} \left(\frac{U\delta_1^{**}}{\nu} \right)^{-0.268} \rho U^2 2\pi R_1 dx \\ & + \pi(R_{\delta_1}^2 - R_1^2) \rho U dU = - \rho d \left[\int_{R_1}^{R_{\delta_1}} u_1 2\pi R dR \right] U \\ & \quad + \rho d \left[\int_{R_1}^{R_{\delta_1}} u_1^2 2\pi R dR \right] \end{aligned} \quad (3.45)$$

and

$$\begin{aligned} & -0.123 * 10^{-0.678H_2} \left(\frac{U\delta_2^{**}}{\nu} \right)^{-0.268} \rho U^2 2\pi R_2 dx \\ & + \pi(R_2^2 - R_{\delta_2}^2) \rho U dU = - \rho d \left[\int_{R_{\delta_2}}^{R_2} u_2 2\pi R dR \right] U \end{aligned}$$

$$+ \rho d \left[\int_{R_{\delta_2}}^{R_2} u_2^2 2\pi R dR \right] \quad (3.46)$$

for the inner and outer wall layer respectively. It can be shown that

$$\left. \begin{aligned} \int_{R_1}^{R_{\delta_1}} u_1^2 2\pi R dR &= 2\pi U \frac{R_1^2}{S_1^2} \frac{(1-S_1)}{\left(\frac{1}{n_1} + 1\right)} \left[1 - \frac{(1-S_1)}{\left(\frac{1}{n_1} + 2\right)} \right] \\ \int_{R_{\delta_2}}^{R_2} u_2^2 2\pi R dR &= 2\pi U \frac{R_2^2}{S_2^2} \frac{(S_2-1)}{\left(\frac{1}{n_2} + 1\right)} \left[1 - \frac{(1-S_2)}{\left(\frac{1}{n_2} + 2\right)} \right] \\ \int_{R_1}^{R_{\delta_1}} u_1^2 2\pi R dR &= 2\pi U \frac{R_1^2}{S_1^2} \frac{(1-S_1)}{\left(\frac{2}{n_1} + 1\right)} \left[1 - \frac{(1-S_1)}{\left(\frac{2}{n_1} + 2\right)} \right] \\ \int_{R_{\delta_2}}^{R_2} u_2^2 2\pi R dR &= 2\pi U \frac{R_2^2}{S_2^2} \frac{(S_2-1)}{\left(\frac{2}{n_2} + 1\right)} \left[1 - \frac{(1-S_2)}{\left(\frac{2}{n_2} + 2\right)} \right] \end{aligned} \right\} \quad (3.47)$$

Employing Equation (3.47) in Equation (3.45) and Equation (3.46) yields (see Appendix A),

$$\left. \begin{aligned} G_1 \frac{d(\delta_1/D_h)}{dX} + G_2 \frac{d(\delta_2/D_h)}{dX} &= G_3 \\ G_4 \frac{d(\delta_1/D_h)}{dX} + G_5 \frac{d(\delta_2/D_h)}{dX} &= G_6 \end{aligned} \right\} \quad (3.48)$$

where G_1, G_2, \dots, G_6 are functions of S_1 and S_2 (and hence δ_1/D_h and δ_2/D_h) defined in Appendix A.

An equation relating the pressure may be obtained from Equation (3.33) (Bernoulli's equation).

$$P = \left(\frac{U^2}{V^2} - 1 \right) \quad (3.49)$$

The pair of first order non-linear ordinary differential equations represented by Equation (3.48) was solved numerically using a fifth-order Runge-Kutta integration routine. The boundary conditions are:

$$\text{at } X = 0, \quad \delta_1/D_h = 0, \quad \delta_2/D_h = 0.$$

3.3.3 Entry-Region Turbulent Pipe Flows

We may write the shear stress distribution in the wall layer as

$$\tau = \rho(\nu + \epsilon) \frac{du}{dy} \quad (3.50)$$

Defining dimensionless quantities,

$$y^+ = \frac{yu^*}{\nu} \quad ; \quad u^+ = \frac{u}{u^*} \quad (3.51)$$

where $u^* = (\tau_w / \rho)^{0.5}$

Equation (3.50) becomes:

$$\tau = \rho\nu \left(1 + \frac{\varepsilon}{\nu}\right) u^{*2} \frac{du^+}{dy^+}$$

$$\frac{\tau}{\tau_w} = \left(1 + \frac{\varepsilon}{\nu}\right) \frac{du^+}{dy^+} \quad (3.52)$$

The experimental results of Walklate et al. [42] indicate an approximately linear shear stress variation in the wall layer. Using this linear shear stress assumption and combining with Equation (3.52), we obtain

$$\frac{\tau}{\tau_w} = \left(1 - \frac{y}{\delta}\right) = \left(1 + \frac{\varepsilon}{\nu}\right) \frac{du^+}{dy^+} \quad (3.53)$$

Consequently, in order to obtain the velocity distribution a suitable eddy viscosity model has to be selected. This approach is to some extent different from the annular flow cases studied in this dissertation as a velocity profile is not initially specified.

The continuity equation is

$$\int_0^R u \, 2\pi R dR = AV \quad (3.54)$$

The momentum equation applied to the wall layer may be written as

$$\delta(2R_0 - \delta) dp + 2R_0 \tau_w dx = 2\rho U d \left[\int_0^\delta u(R_0 - y) dy \right] - 2\rho d \left[\int_0^\delta u^2(R_0 - y) dy \right] \quad (3.55)$$

All previous analytical solutions have used the Bernoulli's equation (in the core region) to eliminate the pressure term in the momentum equation (Equation 3.55).

A different approach was used to eliminate the pressure term in Equation (3.55). The macroscopic energy balance was used and may be written in the form

$$dp \frac{Q}{2\pi} = - \frac{1}{2} \rho d \left[\int_0^{R_0} u^3 R dR \right] - dx \int_0^{R_0} \tau \frac{\partial u}{\partial R} dR \quad (3.56)$$

Combining Equation (3.53), Equation (3.55) and Equation (3.56),

$$\delta(2R_0 - \delta) \frac{2\pi}{Q} \left[- \frac{1}{2} \rho d \left\{ \int_0^{R_0} u^3 R dR \right\} - dx \int_0^{R_0} \left(1 - \frac{y}{\delta}\right)^a \tau_w \frac{\partial u}{\partial R} dR \right] + 2R_0 \tau_w dx = 2\rho U d \left[\int_0^\delta u(R_0 - y) dy \right] - 2\rho d \left[\int_0^\delta u^2(R_0 - y) dy \right] \quad (3.57)$$

Non-dimensionalizing all velocities and all radial distances with the shear velocity, $u^* = (\tau_w/\rho)^{0.5}$, the continuity and momentum equation can be written, after numerous algebraic calculations (see Appendix A), as

$$\int_{\delta^+}^0 \left(1 - \frac{y^+}{R_0^+}\right) u^+ dy^+ = -\frac{Re}{4} - U^+ \left[\delta^+ \left(1 - \frac{\delta^+}{2R_0^+}\right) - \frac{R_0^+}{2} \right]$$

and

$$\begin{aligned} 2R_0^{+2} d\left(\frac{x}{D}\right) & \left[-\frac{2}{Re} \delta^+ \left(2 - \frac{\delta^+}{R_0^+}\right) \left\{ \int_{\delta^+}^0 \left(1 - \frac{y^+}{\delta^+}\right)^a \left(1 - \frac{y^+}{R_0^+}\right) \frac{du^+}{dy^+} dy^+ + 1 \right\} \right. \\ & = U^+ R_0^+ d \left[\int_0^{\delta^+} u^+ \left(1 - \frac{y^+}{R_0^+}\right) dy^+ \right] - d \left[R_0^+ \int_0^{\delta^+} u^{+2} \left(1 - \frac{y^+}{R_0^+}\right) dy^+ \right] \quad (3.58) \\ & - \frac{1}{Re} \frac{\delta^+}{R_0^+} \left(2 - \frac{\delta^+}{R_0^+}\right) d \left[R_0^{+2} \left\{ U^{+3} \left(\delta^+ \left(1 - \frac{\delta^+}{2R_0^+}\right) - \frac{R_0^+}{2} \right) \right. \right. \\ & \left. \left. + \int_{\delta^+}^0 u^{+3} \left(1 - \frac{y^+}{R_0^+}\right) dy^+ \right\} \right] \end{aligned}$$

Equation (3.58) cannot be solved as yet until an eddy viscosity distribution is specified. Two models were tested:

(1) Van Driest wall model:

$$\frac{\varepsilon}{\nu} = \frac{0.16y^2}{\nu} \left[1 - \exp\left(\frac{-y^+}{26}\right) \right]^2 \frac{du^+}{dy^+} \quad (3.59)$$

Using Equation (3.59) in Equation (3.53), it can be shown that

$$\frac{du^+}{dy^+} = \frac{-1 + \sqrt{\left\{ 1 + 0.64y^{+2} \left[1 - \exp\left(\frac{-y^+}{26}\right) \right]^2 \left(1 - \frac{y^+}{\delta^+}\right)^a \right\}}}{0.32y^{+2} \left[1 - \exp\left(\frac{-y^+}{26}\right) \right]^2} \quad (3.60)$$

(2) Reichardt Model:

$$\frac{\varepsilon}{\nu} = \frac{\kappa}{6} \delta^+ \left[1 - \left(\frac{y^+ - \delta^+}{\delta^+} \right)^2 \right] \left[1 + 2.5 \left(\frac{y^+ - \delta^+}{\delta^+} \right)^2 \right] \quad (3.61)$$

$$* \left[1 - \exp \left\{ - \frac{y^+}{A^+} \right\} \right]$$

giving

$$\frac{du^+}{dy^+} = \frac{\left(1 - \frac{y^+}{\delta^+} \right)^{a_1}}{\left\{ 1 + \frac{\kappa}{6} \delta^+ \left[1 - \left(\frac{y^+ - \delta^+}{\delta^+} \right)^2 \right] \left[1 + 2.5 \left(\frac{y^+ - \delta^+}{\delta^+} \right)^2 \right] \left[1 - \exp \left(- \frac{y^+}{A^+} \right) \right] \right\}} \quad (3.62)$$

The boundary condition on Equation (3.60) and Equation (3.62) is:
at $y^+ = 0$, $u^+ = 0$.

Equations (3.60) and Equation (3.62) were solved by the fifth-order Runge-Kutta integration technique to obtain u^+ and y^+ for a given δ^+ and these values were then substituted in Equation (3.58). Using integration methods R_0^+ and X were obtained. This technique was repeated for different values of δ^+ .

Finally, to account for the non-linear shear stress variation in the wall layer and the fact that the shear stress should blend in smoothly to zero value in the potential core region, a novel technique was adopted. Writing

$$\frac{\tau}{\tau_w} = \left(1 - \frac{y}{\delta} \right)^{a_1} \quad (3.63)$$

and differentiating Equation (3.63) with respect to y , we obtain noting that a_1 is a constant value

$$\frac{d\tau}{dy} \frac{1}{\tau_w} = a_1 \left(1 - \frac{y}{\delta}\right)^{a_1-1} \left(-\frac{1}{\delta}\right) \quad (3.64)$$

It can be seen from Equation (3.64) that for a_1 greater than unity,

$$\left. \frac{d\tau}{dy} \right|_{y=\delta} = 0$$

and hence the shear stress would merge smoothly to zero value at the edge of the wall layer.

Also, choosing values of a_1 close to unity, the shear stress profile can be made approximately linear (to be consistent with experimental data).

CHAPTER IV

DISCUSSION

4.1 Discussion of Assumptions

4.1.1 Velocity Profile

For hydrodynamically developing annular flows, velocity profiles were assumed. In both the laminar and turbulent cases, the assumed velocity distribution was based on fully developed flows, information of which is well established. Unlike previous approaches, this method simplified mathematical analysis and resulting numerical work for these problems considerably. Using the assumed velocity profile, expressions obtained for momentum and continuity in terms of δ_1 , δ_2 and U can be integrated without resorting to any numerical procedure.

In the laminar flow problem, the velocity distribution satisfied all the physical boundary conditions:

- (i) requirement of no-slip at a wall
- (ii) attaining core velocity at edge of a wall layer
- (iii) existence of frictionless flow in potential core region.

In addition, the profile converges to the fully developed profile at the initial meeting point of the inner and outer wall layers, thereafter remaining invariant in shape.

For the developing turbulent annular case, the assumed velocity distribution did not satisfy all the physical boundary conditions as

it had imposed upon it, some basic limitations associated with the use of power-law mean velocity profiles, i.e.,

- (i) wall shear stress cannot be obtained from velocity profile
- (ii) velocity distribution does not blend in smoothly with the core velocity
- (iii) agreement with experimental data near the walls is not too good.

Despite these restrictions, however, predictions of mean velocity profiles and pressure variation for turbulent entry-region pipe flow were reasonable (Na and Lu [40], Bowlus and Brighton [37]). The present study attempts to extend the use of power law distributions to annular flows.

It is worth mentioning that most previous analytical studies in developing turbulent annular flows have used indirect means of obtaining the velocity distribution. For example, from an assumed eddy viscosity model and a linear shear stress variation in the wall layer assumption, the velocity profile may be obtained. In all of these cases, the resulting expression for velocity is rather long and mathematically inconvenient to handle.

For entrance region flows, the power law exponents are dependent on axial distance and Reynolds number and for the annulus, they also depend on radius ratio and radius of inner pipe as found by Paranjpe [2]. In the case of pipes, the exponents vary between $1/7$ and $1/8$ in the entry region (Na and Lu [40]). As this variation is not appreciable, the exponent may be approximated to be a constant value of $1/7$. Consequently,

the exponents for annular flows were taken constant and equal to the values for fully developed flow.

Figure 4.1 shows the variation of $\log u^+$ vs $\log y^+$ for different radius ratios and annulus Reynolds numbers for the experimental investigations of Brighton and Jones [44], Rehme [45] and Lee and Park [28]. It can be seen that the relationship in all these cases is linear for most of the range, (except near the inner and outer walls) thereby justifying to some extent the use of a power law mean velocity distribution. In fact, it is unlikely to expect a power-law velocity distribution in the entry-region flow if such a distribution is not present in the fully developed flow.

A non-dimensional velocity profile for developing pipe flow was obtained using an eddy viscosity model and a linear shear stress distribution assumption in the wall layer (discussed in section 4.2.3).

4.1.2 Wall Layer Growth

For the Simplified Models in both the laminar and turbulent developing annular flow problems, in order to obtain (the minimum number of) eight equations, an additional relationship had to be used. For mathematical convenience, this relationship was obtained by assuming the ratio of wall layer thicknesses is constant for all axial positions along the duct, i.e., $(\delta_1/\delta_2)_x = (\delta_1/\delta_2)_{fd}$. For flows through pipes and parallel plates, the constant ratio assumption is valid since $\delta_1/\delta_2 = 0$ and $\delta_1/\delta_2 = 1$ respectively for all axial locations. Consequently, this idea was

carried over to the annulus where $0 < \alpha < 1$. In addition, while it appears that this assumption has not been used before in laminar flow theory, for turbulent annular flows Lee and Park [28] assumed a constant ratio of wall layer growth in order to simplify their resulting numerical work.

4.1.3 Shear Stress Variation

Unlike laminar flows, the wall shear stress in turbulent flows cannot be determined from an assumed velocity distribution. For developing turbulent annular flows, the semi-empirical correlation of Ludwig and Tillman [27], valid for turbulent wall layer flow with a pressure gradient, was adopted for the wall shear stress. Okiishi and Bathie [26] used this wall shear stress model in predicting inlet turbulent flow development characteristics. The effect of transverse curvature on the Ludwig and Tillman [27] friction formula was neglected.

A linear shear stress distribution in the wall layer for developing turbulent pipe flow was assumed on the basis of the experimental (and analytical) study of Walklate, Heikal and Hatton [42] who measured and predicted turbulence properties and heat transfer characteristics in the entrance region of a pipe. A modification to the linear shear stress distribution was made to account for the fact that the shear stress profile should blend in smoothly to zero value (in the potential core region).

4.1.4 Radius of Maximum Velocity

While in laminar annular fully developed flows an exact expression for the radius of maximum velocity location could be derived, in turbulent

annular fully developed flows this is not the case. Consequently, many researchers have proposed correlations for the radius of maximum velocity position for turbulent annular flows.

Kays and Leung [46] proposed the following empirical expression:

$$\frac{R_M}{R_2} = \frac{[\alpha + \alpha^{0.343}]}{[1 + \alpha^{0.343}]} \quad (4.1)$$

Rothfus et al. [47] employed the following correlation:

$$\frac{R_M}{R_2} = \frac{1}{2} \alpha^{0.2} (1 - \alpha) + \alpha \quad (4.2)$$

Clump and Kwasnoski [48] used standard polynomial curve-fitting techniques to the data of Brighton and Jones [44] and obtained

$$\left. \begin{array}{l} \frac{R_M}{R_2} = \alpha + \frac{(1-\alpha)}{2} [1.08 \alpha^3 - 2.2 \alpha^2 + 1.65 \alpha + 0.48] \\ \text{for } 0.0625 \leq \alpha \leq 1 \text{ and} \\ \frac{R_M}{R_2} = [1 + 18.1 (1-\alpha)] \alpha \\ \text{for } 0 < \alpha < 0.0625 \end{array} \right\} (4.3)$$

Doshi and Gill [49] obtained an approximate relationship for R_M given by

$$\frac{R_M}{R_2} = \left[\alpha \frac{(1+\alpha)}{2} \right]^{1/3} \quad (4.4)$$

Also, many researchers have assumed or found experimentally that R_M can be approximated by its laminar value (for example, Rothfus et al. [50]), i.e.,

$$\frac{R_M}{R_2} = \left[\frac{(1-\alpha^2)}{-2 \ln \alpha} \right]^{1/2} \quad (4.5)$$

Equation (4.1) to Equation (4.5) were each used to determine R_M . The wall layers were assumed to meet when $R_{\delta_1} = R_{\delta_2} = R_M$ (i.e., at the end of the entry-region). (This information was needed in order to terminate the numerical calculations for the Simplified Model in the case of the turbulent annular flow analysis.) It was found that there was no significant difference in the results using any one of the above relations for the R_M value. For convenience, only results using Equation (4.5) is presented for entry-region turbulent annular flows using the Simplified Model.

4.2 Discussion of Results

4.2.1 Developing Laminar Annular Flows

(a) Velocity Profiles

Velocity profiles at non-dimensional radial distances $\phi = 0.1$ to 0.9 are presented in Figure 4.2 to Figure 4.14. Results obtained from the Simplified Model and General Model analysis are compared with those of Sparrow and Lin [4] and wherever possible Chang and Atabek [9]. Agreement between the findings of Sparrow and Lin [4] and the present study at all radial locations is quite good, the maximum difference occurring

near the entrance being approximately 3 percent. It is worth mentioning that Sparrow and Lin [4] used the method of stretched coordinates to solve the developing annular flow problem.

The results of Chang and Atabek [9] agree well with both the present study and Sparrow and Lin [4] some distance downstream from the entrance. Their results in the immediate vicinity of the entrance plane, however, appear to be questionable.

Two general trends may be seen from the figures plotted. Firstly, at positions near the bounding surface, i.e., for values of ϕ close to unity and zero, the flow decelerates with increasing downstream distance. This is due to retarding effects of wall friction. Secondly, at radial positions away from the walls, the flow accelerates with downstream distance to compensate for the deficit in mass flow resulting from the aforementioned retardation near the wall.

From an inspection of the velocity profile plots, it can also be seen that as the radius ratio increases, the flow tends more and more to the symmetrical situation, i.e., the curve of $\phi = 0.1$ and 0.9 ($\phi = 0.2$ and 0.8 , etc.) fall approximately upon each other. The same curves, expectedly, separate out as the radius ratio decreases.

For small radius ratios ($\alpha = 0.05, 0.1$), agreement between the Simplified and General Models is encouraging at all but small non-dimensional radial distances ($\phi = 0.1, 0.2$). The discrepancy appears to begin at a small distance downstream from the entrance. The maximum difference between the two model predictions is approximately

10 percent. For larger annulus radius ratios, however, both models are in closer agreement. This result indicates that as the configuration tends to a parallel plate situation, the constant ratio of wall layer thickness assumption becomes more valid. This is consistent with flows through parallel plates in which $\delta_1/\delta_2 = 1$ for all axial locations.

The only direct comparison to date of analytical and experimental results for developing laminar annular flows to the author's knowledge is shown in Figure 4.15. The experimental values are those of Astill [5]. Overall agreement with both Models is quite good. The discrepancy near the inner wall (very small values of ϕ) may be due, to some extent, to difficulties associated with low velocity measurements as noted by Astill [5]. The radius ratio was 0.732 at $X = 0.2 \times 10^{-3}$.

(b) Wall Layer Growth

The predicted wall layer thickness growth in developing laminar annular flows is shown in Figure 4.16 to Figure 4.19. To the best of the author's knowledge, this is the first attempt at predicting wall layer thickness growth in laminar developing annular flows. The results of the outer wall layer for both models agree within 5 percent for the four radius ratios investigated.

For the inner wall layer, however, there exists a significant difference in the nature of the wall layer development between the two models. While a smooth uniform growth is predicted by the Simplified Model, the General Model results indicate that the inner wall layer

thickness grows, overshoots, and then decreases to the fully developed value within the developing region. Also, it was found that the axial position of the maximum inner wall layer thickness location shifts away from the inlet plane with increase in radius ratio (see Table 4.1).

α	X at $\delta_1 = \delta_{1\max}$	X at $\tau_1 = \tau_{1\min}$
0.05	0.0094	0.0055
0.10	0.0096	0.0067
0.50	0.0100	0.0095
0.75	0.0126	0.0112

Table 4.1 Axial Position at $\delta_1 = \delta_{1\max}$ and $\tau_1 = \tau_{1\min}$

The following may serve as a possible explanation for the inner wall layer thickness overshoot. Near the entrance where the fluid particles first meet the wall, viscous friction rapidly decelerates the flow to zero velocity at the wall. Wall layers are formed on each of the bounding surfaces along the duct, that on the outer wall developing faster than that on the inner wall. Also, the wall surface area exposed to the fluid is larger for the outer wall than for the inner wall. The outer wall layer, therefore, entrains more fluid than the inner wall layer. Consequently, the acceleration of the core flow is more strongly influenced by the wall layer on the outer wall than that on the inner wall.

The acceleration in the core resulting from the retardation at the outer wall may, indeed, act to speed up the flow in the inner wall layer adjacent to the core. This interaction produces complex velocity variations as can be seen by the curve for $\phi = 0.1$ in the velocity profile plots. These velocity variations cause the inner wall shear stress to 'undershoot' its fully developed value within the developing region. In fact, it was found that the minimum point on the $\phi = 0.1$ curve and the minimum inner wall shear stress value (given in Table 4.1) is at the same axial location. As a consequence of the 'undershoot' of the inner wall shear stress and in order to satisfy the continuity equation, an overshoot of inner wall layer thickness is formed.

It is worth reiterating that the predicted velocity profile curves agree very well with those of Sparrow and Lin [4]. Consequently, it would be reasonable to expect that the model of Sparrow and Lin [4] would have predicted the aforementioned undershoot of the inner wall shear stress.

The presence of irregularities in hydrodynamically developing flows has been reported in the literature. Wang and Longwell [51] in their numerical solution for parallel plates were the first to report that the velocity profiles have a local minimum at the centre line and symmetrically located maxima on either side of the centre line near the walls. Also, Friedman et al. [52] showed for the circular tube that the above velocity irregularities mentioned by Wang and Longwell [51] were

significant only for the case of exactly uniform entrance velocity profile (employed in the present study). Further, Burke and Berman [53] demonstrated for the pipe case that the velocity irregularities were not a mathematical oddity as they observed velocity irregularities in their experimental data.

Finally, the wall layer thickness plots computed from the results of Campbell and Slattery [54] and Gupta [55] for the pipe ($\alpha=0$) and parallel plates ($\alpha=1$) respectively are shown in Figure 4.16 to Figure 4.19 for comparison purposes.

(c) Core Velocity Variation

The predicted core velocity development is presented in Figure 4.20 to Figure 4.23 for the four radius ratios studied. Also shown are the results of Shah and Farnia [16] and wherever possible Heaton et al. [11].

The Simplified Model seems to underpredict, to some extent, the core velocity distribution. The results of the General Model, however, agree very well (within 2 percent) with those of Shah and Farnia [16] and Heaton et al. [11]. In addition, the General Model results agree best with the results of the finite difference solution of Shah and Farnia [16].

The initial development proposed by Heaton et al. [11] is steeper than that predicted by both the General Model and Shah and Farnia [16].

(d) Incremental Pressure Drop Number Variation

Wherever possible the findings of Sparrow and Lin [4] are compared with those of the Simplified and General Models for the incremental pressure drop number variation in the axial direction shown in Figure

4.24 to Figure 4.27. It can be seen that the agreement between the Simplified and General Models improves as the radius ratio decreases. The overall agreement between the three curves plotted is good.

(e) $f_{app} Re$ Variation

Shah [56] proposed the following correlation for predicting $f_{app} Re$ factors in the hydrodynamic entry region of circular (including the annulus) and non-circular ducts

$$f_{app} Re = \frac{3.44}{X^{0.5}} + \frac{[(fRe) + k(\infty)/(4X) - 3.44/X^{0.5}]}{1 + C X^{-2}} \quad (4.6)$$

where $k(\infty)$ and $f Re$ are for hydrodynamically fully developed flow and C is a constant depending on the duct geometry (see Table 4.2). As mentioned by Shah [56], the predicted $f_{app} Re$ factors obtained from Equation (4.6) agree within $\pm 2.4\%$ with the most accurate values in the literature for the above-mentioned geometries. To the author's knowledge, Equation (4.6) is the only correlation currently available which may be applied in the entire developing region of an annulus (in order to obtain $f_{app} Re$ factors). Also, Shah and London [57] reported that the results of Sparrow and Lin [4] and Coney and El-Shaarawi [18] are approximately 2% lower and 2-4% higher respectively than those of Shah and Farnia [16] whose results, in turn, agree with the $f_{app} Re$ factors of Equation (4.6) within an rms error of 2 percent. Consequently, the present results for $f_{app} Re$ are compared with those obtained from Equation (4.6) alone. Points obtained for $f_{app} Re$ from

Equation (4.6) and this investigation for both models are plotted in Figure 4.28 to Figure 4.31 from which it may be seen that the three results are almost identical.

α	$C \times 10^6$
0.05	50
0.10	43
0.50	32
0.75	30

Table 4.2 C Values for Different Radius-Ratio Annuli Extracted from Shah [56].

(f) Comparison with Experimental Results with Suction

Figure 4.32 shows the experimental values of Astill [5] in which suction was applied at the inner wall compared with the predicted velocity profile plots (without suction) at various X values for $\alpha = 0.732$. The measurement of Astill [5] indicated that the effect of suction at the inner wall is to decrease the inner wall layer thickness. This trend may be seen from the figures plotted.

4.2.2 Entry-region Turbulent Annular Flows

(a) Velocity Profiles

In Section 4.1.1, it was shown from the experimental investigations of Brighton and Jones [44], Rehme [45] and Lee and Park [28] that the velocity distribution in fully developed turbulent annular flows may be reasonably represented by a general power-law mean velocity profile.

This initial check on the assumed velocity profiles was useful in that it served to indicate the possible existence of a power-law mean velocity profile in the entry-region.

Figure 4.33 shows the variation of $\ln(u/U)$ with $\ln(y/\delta)$ for $\alpha = 0.344$ ($Re = 78800$) and $\alpha = 0.531$ ($Re = 142000$) derived from the experimental results of Okiishi and Serovy [1]. For each of the two radius ratios, a mean line was drawn to fit the experimental data points through the velocity data at the last measuring station (of Okiishi and Serovy [1]), i.e., at $X = 25$ and $X = 34.9$ respectively. Values of the wall layer thickness and core velocity were estimated from the mean velocity profile curve and values of u/U and y/δ were consequently obtained. The results were then plotted on a \ln - \ln scale (shown in Figure 4.33).

It may be seen from Figure 4.33 that a power-law profile reasonably represents the velocity distribution as the $1/n_1$ and $1/n_2$ values are approximately constant. It is estimated the uncertainty in the values of $1/n_1$ and $1/n_2$ to be within 10 percent. Table 4.3 shows the resulting exponent values (which were subsequently used as input data in the numerical study).

The velocity profile plots are presented in Figure 4.34 to Figure 4.36. Also shown are the results of Wilson and Medwell [24] for the same radius ratios (and Reynolds number). While the three predictions agree well with each other, one unexpected conclusion may be drawn from the curves, that is, the Simplified Model also appears to agree better than others in the inner wall layer. This may be seen in Figure 4.34 and Figure 4.35.

α	Re	$1/n_1$	$1/n_2$
0.344	78800	0.117	0.177
0.531	142000	0.121	0.128

Table 4.3 Experimental Power-Law Exponents Obtained from the Data of Okiishi and Serovy [1].

α	Re	$1/n_1$	$1/n_2$
0.1012	92800	0.049	0.174
"	157000	0.049	0.145
0.0239	315000	0.049	0.145
"	531000	0.049	0.133
0.1003	320000	0.089	0.148
"	451000	0.066	0.139

Table 4.4 Experimental Power-Law Exponents Taken From Paranjpe [2].

Also shown in Figure 4.35 is the curve obtained from the results using information at $\chi=3.81$ location as the initial values for $\alpha = 0.344$ ($Re = 78800$). The overall agreement between the four curves in Figure 4.35 is encouraging. The difference between the predictions of the Simplified or General Model and Wilson and Medwell [24] near the outer wall layer region for $\alpha = 0.531$ ($Re = 142000$) at $X = 5.33$ is partly due to uncertainties in the value of δ_2/D_h and hence $1/n_2$ used in the analysis. It is appropriate to mention that it is difficult to extract reliable values for δ_1/D_h and δ_2/D_h from experimental data.

To provide additional confidence to the numerical method, the analysis was reduced to the pipe case ($\alpha = 0$) and the resulting velocity profiles at different radial positions (measured from the pipe centre line) are shown in Figure 4.37 and Figure 4.38. Also shown is the core velocity distribution from the general pipe flow solution of Na and Lu [40] and the velocity data of the reliable experimental study of Barbin and Jones [36]. The agreement between the two previous works and the present study is encouraging (within 1 percent). The corresponding wall shear stress variation, shown in Figure 4.39, is likewise in concert with the two previously mentioned works. Not unexpectedly, agreement of the velocity profiles with the experimental data near the walls is not as good as that away from the walls, a consequence of a basic limitation of power-law velocity profiles.

As the experimental study of Barbin and Jones [36] indicated that the wall shear stress attained its fully developed value within 15 hydraulic

diameters, the fully developed shear stress was taken as the value of wall shear stress at the end of the entry-region, $X \approx 30$ (instead of the value obtained from Blasius formula).

Power-law exponents in fully developed turbulent annular flows were evaluated by Paranjpe [2] in his experimental study for $\alpha = 0.1003, 0.1012, 0.0239$ and $92800 < Re < 531000$. In all the previous relevant works discussed, the $1/n_1$ values were found to be approximately ≥ 0.1 . All except one $1/n_1$ value, however, obtained by Paranjpe [2] was less than 0.07 (see Table 4.4). In addition, it was observed that the $1/n_1$ values were obtained from his experimental data of u^+ and y^+ relatively far from the wall ($y^+ > 125$). Consequently, a smaller value of $1/n_1$ was found.

The experimental velocity profile data of Paranjpe [2] are compared with the predictions of the Simplified and General Models in Figure 4.40 to Figure 4.42 (using the values of Table 4.4). Only the results of three Reynolds number are presented ($\alpha = 0.1003$ ($Re = 320,000$ and $Re = 451,000$) and $\alpha = 0.0239$ ($Re = 531,000$)). In the outer wall layer (corresponds to small values of χ) both model predictions for $\alpha = 0.1003$ ($Re = 320,000$ and $Re = 451,000$) reasonably agree with the experimental data. For the annulus radius ratio of 0.0239, there appears to be some amount of uncertainty in measurement for $X = 7.4$ ($Re = 531,000$).

(b) Effect of Initial Conditions

There is no apparent way of obtaining the axial location where the turbulent wall layers start from the experimental results of Okiishi and Serovy [1] and Paranjpe [2] so the wall layers were assumed to start at the

inlet plane.

For the annulus with $\alpha = 0.344$ ($Re = 78800$), Figure 4.35 shows the predicted velocity distribution of the General Model with both the following boundary conditions: at $X=0$, $\delta_1/D_h=0$, $\delta_2/D_h=0$ and at $X=3.81$, $\delta_1/D_h=0.04$, $\delta_2/D_h=0.1$. The second of these boundary conditions was obtained by assuming that a laminar portion of wall layer exists up to the first measuring station in the experimental study of Okiishi and Serovy [1]. The difference between the resulting velocity profiles obtained for the aforementioned two initial conditions can be seen in Figure 4.35 to be negligible.

The prediction of the wall layer thickness using the two above initial conditions in the General Model is presented in Figure 4.43. While the results for the outer wall layer thickness remain approximately the same, that for the inner wall layer thickness show a significant difference.

In their pipe flow study, Na and Lu [35] used the following boundary conditions based on the experimental work of Barbin and Jones [36]: at $X=0.25$, $\delta/D_h=0.0055$. Solutions with both the initial conditions: $X=0$, $\delta/D_h=0$ and at $X=0.25$, $\delta/D_h=0.0055$ were obtained for the pipe case. (The approximate solution for the initial conditions: at $X=0$, $\delta/D_h=0$ was solved by the procedure described in Section 4.3). It was found, similar to the case for the annulus, that the effect on the pipe flow plots previously mentioned using these two different initial conditions was negligible. Figure 4.44 indicates the corresponding wall layer thickness plot. It was found that for $X \geq 2$, the two results agree within 2 percent with the agreement improving in the axial direction.

(c) Wall Layer Growth

The development of the wall layer thickness with axial distance is shown for the two annulus radius ratios (and corresponding Reynolds number) of Okiishi and Serovy [1] in Figure 4.43 and Figure 4.45. Reliable experimental values for comparison are unavailable.

The analysis of the General Model predicts for $\alpha=0.344$ ($Re=78800$), the development of the inner wall layer is faster than the outer wall layer within the entry region as shown in Figure 4.43. Also, the predicted growth of the inner wall layer thickness is strongly dependent on the initial condition unlike the case for the outer wall layer thickness.

The results of Figure 4.45, which show the wall layer thickness variation for $\alpha=0.531$ ($Re=142,000$), would tend to indicate that for a relatively large value of radius ratio, predictions of the Simplified and General Models are in close agreement. This fact is consistent with flows through parallel plates ($\alpha=1$) where $\delta_1/\delta_2=1$ for all axial positions.

The corresponding curves for the wall layer thickness obtained by using the power-law exponent values of Paranjpe [2] are presented in Figure 4.46 and Figure 4.47. Similar to the case of the velocity profile plots, only the results of two radius ratios are shown, i.e., $\alpha=0.1003$, ($Re=320,000$ and $Re=451,000$) and $\alpha=0.0239$ ($Re=531,000$). The initial variation of the wall layer thickness (with axial distance) is predicted by the General Model to be greater for the inner wall layer than the outer wall layer. The opposite effect, however, is the case from the Simplified Model predictions.

It can be seen from Figure 4.43 to Figure 4.47 that the length of the entry-region depends on both the radius ratio and Reynolds number,

its dependency on radius ratio being stronger than that on Reynolds number. Further, Figure 4.47 indicates that for a given annulus, the entry-length increases with a decrease in Reynolds number. The terminal points on all the curves represent the vanishing of potential core flow (i.e., the end of the entry-region).

(d) Core Velocity

Figure 4.48 shows the predicted core velocity variation for $\alpha = 0.344$ ($Re = 78800$) and $\alpha = 0.531$ ($Re = 142,000$) with the corresponding experimental data points of Okiishi and Serovy [1]. The agreement between the curves and the data is very good. Also, points of Wilson and Medwell [24] obtained from their analytical curve for the same radius ratio and Reynolds number are shown for comparison.

Also presented in Figure 4.48 is the analytical curve for $\alpha = 0.0653$ ($Re = 23000$) obtained from the present study. The power-law exponents were obtained from the fully developed velocity profile curve of Lee and Park [28]. Their experimental values (shown in Figure 4.48) are in very good agreement with the theoretical curve (within 1 percent).

The predicted curves using the power-law exponents of Paranjpe [2] are shown in Figure 4.49 and Figure 4.50. The U/V values obtained from the experimental study of Paranjpe [2] are high and appear to be incorrect. Consequently, his results are not shown in Figure 4.49 and Figure 4.50.

It is worth noting that despite the appreciable difference between the prediction of the Simplified and General Models for the inner wall layer thickness for the radius ratios discussed above, the core velocity prediction in all cases from both models agree well.

From inspecting Figure 4.48 to Figure 4.50, it may be concluded that the dependency of the core velocity variation on Reynolds number is greater than that on radius ratio. Also, the core velocity develops faster as the Reynolds number decreases.

(e) Pressure Gradient

The pressure gradient variation in the entry-region is presented in Figure 4.51 for the General and Simplified Models along with the prediction of Wilson and Medwell [24] for $\alpha = 0.531$ ($Re = 142000$). It can be seen that although all three predictions agree well, the curve of the Simplified Model is slightly better than that of Wilson and Medwell [24]. The comparison of the experimental data points with the curves, however, appear to be not too good.

Also shown in Figure 4.51 are the predicted curves for $\alpha = 0.1012$ ($Re = 92800$ and 157000) and the experimental results of Paranjpe [2]. It may be seen that the fit of the measurements with the analytical curves is good using the General Model. The same is not the case, however, with the curve obtained from the Simplified Model analysis. For comparison purposes, the experimental data points of Olson and Sparrow [21] for $\alpha = 0.5$ ($Re = 29500$) are shown. The wide scatter of data in Figure 4.51, undoubtedly, indicates the difficulty involved in obtaining accurate pressure gradient measurements for turbulent flows in the entry region of annular ducts. It is worth mentioning that the value of $\left(\frac{dp}{dx}\right)_{fd}$ was taken to be the value at the end of the entry region.

4.2.3 Entry-Region Turbulent Pipe Flows

In this section, a comparison is being made to see the effect on the results of using the Bernoulli's equation in the potential core region and the macroscopic mechanical energy balance over the whole flow area.

The results of the core velocity distribution from both the eddy viscosity models tested, that is, the Reichardt and Van Driest models, are presented in Figure 4.52. The results obtained from using the Bernoulli's equation and that from using the macroscopic energy balance are shown. It can be seen that each of the eddy viscosity models coupled with Bernoulli's equation yields predictions which are in very good agreement with the experimental results of Barbin and Jones [36]. The macroscopic energy balance predicts a very sharp increase in core velocity near the entrance. This may be due to the small pressure gradient variation which is predicted by the macroscopic energy balance equation as can be seen in Figure 4.53. With the small pressure gradient and in order to satisfy the momentum and continuity equations, the analysis predicts that the core velocity increases rapidly.

It was found that the effect on the plots of Figure 4.52 and Figure 4.53 of increasing the value of a_1 (in Equation 3.63) up to 1.01 was negligible. The upper limit of a_1 was taken as 1.01 since it is required that a value of a_1 close to unity be chosen in order to maintain an almost linear shear stress variation in the wall layer. In Figure 4.52 and Figure 4.53, only the results for $a_1 = 1.01$ using Reichardt

eddy viscosity model are shown. It is worth noting that the maximum difference between the curves is less than 0.5 percent.

4.3 Discussion of the Numerical Method

4.3.1 General

For both the laminar and turbulent annular flows studied, the initial conditions imposed on the resulting differential equations produced infinite slopes at the start. This posed a problem at the $x = 0$ location. An attempt was made to expand the equations about the $x = 0$ location using a Taylor series expansion in order to examine the behaviour near $x = 0$. Due to the very large number of algebraic terms present, however, it was found that this approach could not be employed. The methods outlined below were then used to solve the differential equations.

4.3.2 Simplified Model

The results of the Simplified Model reduced to a first order non-linear ordinary differential equation. The Simpson's integration scheme was used and the following procedure was adopted.

By definition the initial value of B_2 is unity. The integral was split up into two parts and the limits of integration were 1 to 1.01 and 1.01 to B_{2M} for the first and second parts respectively. Now, since $1/(\frac{dB_2}{dx})$ near the inlet plane is very small the contribution to X of the first part is very small compared to the second part of the integral and was consequently neglected in the numerical computations. Physically, this small contribution to X will only affect values of B_2 (and hence

δ_1 and δ_2) very near the inlet plane.

The number of steps between 1.01 and $B_{2_{fd}}$ was increased until convergence occurred (up to 5 decimal places) and was then found to be 200.

The entire procedure was then repeated for the entry-region turbulent annular flow problem.

4.3.3 General Model

Three and two first-order non-linear ordinary differential equations resulted from the analysis of laminar and turbulent annular developing flows respectively. The third equation in laminar flows came as a consequence of applying the macroscopic mechanical energy balance instead of the Bernoulli's equation (in the case of turbulent annular flows).

Similar to the Simplified Model, the boundary conditions on the differential equations resulted in infinite slopes at the inlet plane. The fifth-order Runge-Kutta integration technique was employed and the following method was used.

Equal values were assumed for the slopes of δ_1/D_h , δ_2/D_h and P at $X = 0$ and were put in the computer program for a given step size. The equal values of slopes were increased until the following criteria were met.

- (i) Slopes were positive for δ_1 and δ_2 near the inlet plane
- (ii) U/V is greater than unity and increases axially.

The entire procedure was repeated using different step sizes. Convergence (up to 5 decimal places) was found to occur at an h value

of 0.00001 and 0.0001 for laminar and turbulent annular flows respectively.

Finally, it was found that the effect of using different values for the slopes (instead of equal values) and changing the step-size within the integration routine on the resulting values for δ_1/D_h , δ_2/D_h , P , U/V , τ , etc. were negligible.

4.3.4 Pipe Flow Analysis Using Eddy Viscosity Model

Equation (3.60) and Equation (3.62) were solved for u^+ and y^+ by a fifth-order Runge-Kutta integration technique for a given value of δ^+ and h . The value of h was decreased until convergence occurred. Using the values of u^+ and y^+ (for the δ^+ value) in the first of Equation (3.58) and employing the Romberg integration R_0^+ was obtained. The Trapezoidal rule was then used in the second of Equation (3.58) to obtain X . This procedure was repeated for different values of δ^+ .

CHAPTER V

CONCLUSIONS AND RECOMMENDATIONS

From the present study, the following are the main conclusions.

- (a) For hydrodynamic developing laminar annular flows:
 - (i) The velocity distribution in the wall layers may be represented by an assumed velocity profile based only on fully developed flow information.
 - (ii) The inner wall shear stress undershoots its fully developed value within the developing region.
 - (iii) As a consequence of (ii), a non-asymptotic behaviour of the growth of the inner wall layer thickness is exhibited which is more significant for small values of the radius ratio.
 - (iv) The assumption of a constant ratio of wall layer thickness for all axial positions becomes more valid as the radius ratio increases.
 - (v) The present analysis is the simplest of all the methods currently available in the literature.
- (b) For hydrodynamic entry-region turbulent annular flows:
 - (i) The general power-law mean velocity profile reasonably approximates the velocity distribution in both the inner and outer wall layers within the entry-region.

- (ii) The use of the general power-law mean velocity profile coupled with the Ludwig and Tillman [27] friction coefficient yield results which are consistent with available experimental data.
 - (iii) The inner wall layer predictions of all methods available are not as good as the outer wall layer predictions. The results of the Simplified model, however, is slightly better than the rest.
 - (iv) The results of the General Model, on using different initial conditions in the Runge-Kutta integration routine, show significant differences in the prediction of the inner wall layer thickness.
 - (v) The core velocity growth is more dependent on Reynolds number than on radius ratio.
 - (vi) The present approach is the simplest of all methods found in the literature.
- (c) For entry-region turbulent pipe flows:
- (i) The use of a macroscopic energy balance over the whole flow area yields a smaller axial pressure gradient than using the Bernoulli's equation in the core region only.

The following recommendations for future work can be made:

- (i) Detailed measurements of velocity profiles for laminar flow in the hydrodynamic entrance region of concentric annuli should be undertaken to check the theory presented in this dissertation.

- (ii) In turbulent entry-region annular flows, a logarithmic velocity distribution within the wall layers may be used. The coefficients, generally, which depend on axial distance, may be taken to be approximately constant and equal to the fully developed value.
- (iii) Velocity and shear stress profiles for turbulent flow in the entry-region of concentric annuli should be measured and then compared with the theory postulated.
- (iv) Further attempts should be made to find alternate means of eliminating the pressure term in the momentum equation for developing turbulent pipe flows.

REFERENCES

1. Okiishi, T.H., and Serovy, G.K., "An Experimental Study of the Turbulent Flow Boundary-Layer Development in Smooth Annuli", *Journal of Basic Engineering*, pp. 823-836, (1967).
2. Paranjpe, S.C., "An Investigation of Developing and Developed Turbulent Flows Through Annuli", Ph.D. Dissertation, University of Windsor, Windsor, Ontario, Canada, (1973).
3. Sridhar, K., Nicol, A.A., and Padmanabha, A.V.A., "Settling Length for Turbulent Flow of Air in Smooth Annuli with Square-Edged and Bellmouth Entrances", *Journal of Applied Mechanics*, Paper No. 69-WA/APM 24 (1970).
4. Sparrow, E.M. and Lin, S.H., "The Developing Laminar Flow and Pressure Drop in the Entrance Region of Annular Ducts". *Journal of Basic Engineering*, pp. 827-834 (1964).
5. Astill, K.N., "Modes of Adiabatic Flow in the Entrance Region of an Annulus With An Inner Rotating Cylinder", Ph.D. Dissertation, Massachusetts Institute of Technology, Cambridge, Massachusetts, U.S.A. (1961).
6. Murakawa, K., "Theoretical Solutions of Heat Transfer in the Hydrodynamic Entrance Length of Double Pipes", *Bulletin of the Japan Society of Mechanical Engineers*, v3, n11, pp. 340-345 (1960).
7. Sugino, E., "Velocity Distribution and Pressure Drop in the Laminar Inlet of a Pipe With Annular Space", *Bulletin of the Japan Society of Mechanical Engineers*, v5 pp. 651-655 (1962).
8. Langhaar, H.L., "Steady Flow in the Transition Length of a Straight Tube", *Journal of Applied Mechanics*, v9, pp. A55-A58 (1942).
9. Chang, C.C. and Atabek, H.B., "Flow Between Two Co-axial Tubes Near the Entry", *Z. Angew. Math. Mech.*, v42 pp. 425-430 (1962).
10. Slezkin, N.A., "Dynamics of Viscous Incompressible Fluids", Gostekhzdat Press, Moscow, (1955) in Russian.

11. Heaton, H.S., Reynolds, W.C. and Kays, W.M., "Heat Transfer in Annular Passages: Simultaneous Development of Velocity and Temperature Fields in Laminar Flow". *International Journal of Heat and Mass Transfer*, v7, pp. 763-781 (1964).
12. Shumway, R.W. and McEligot, D.M., "Heated Laminar Gas Flow in Annuli with Temperature-dependent Transport Properties", *Nuclear Science and Engineering*, v46, pp. 394-407 (1971).
13. Lin, J., "Flow of a Bingham Fluid in the Entrance Region of an Annular Tube", M.S. Thesis, University of Wisconsin-Milwaukee (1974).
14. Roy, D.N., "Laminar Flow Near the Entry of Co-axial Tubes", *Applied Scientific Reserach, Section A*, v14, pp. 421-430 (1965).
15. Manohar, R., "An Exact Analysis of Laminar Flow in the Entrance Region of an Annular Pipe", *Z. Angew. Math. Mech.*, v45, pp. 171-176 (1965).
16. Shah, V.L. and Farnia, K., "Flow in the Entrance of Annular Tubes", *Computers and Fluids*, v2, pp. 285-294 (1974).
17. Patankar, S.V. and Spalding, D.B., "Heat and Mass Transfer in Boundary Layers", 2nd Edition. Intertext Books, London, (1970).
18. Coney, J.E.R. and El-Shaarawi, M.A.I., "Developing Laminar Radial Velocity Profiles and Pressure Drop in the Entrance Region of Concentric Annuli", *Nuclear Science and Engineering*, v57, pp. 169-174 (1975).
19. Fuller, R.E. and Samuels, M.R., "Simultaneous Development of the Velocity and Temperature Fields in the Entry Region of an Annulus", *Chemical Engineering Progress, Symposium Series*, n113, v67, pp. 71-77 (1971).
20. Rothfus, R.R., Monrad, C.C., Sikchi, K.G., and Heideger, W.J., "Isothermal Skin Friction in Flow Through Annular Sections", *Industrial and Engineering Chemistry*, v47, n5, pp. 913-918 (1955).
21. Olson, R.M. and Sparrow, E.M., "Measurements of Turbulent Flow Development in Tube and Annuli With Square and Rounded Entrances", *American Institute of Chemical Engineers Journal*, v9, pp. 766-770 (1963).

22. Nicol, A.A., Medwell, J.O. and Goel, R.K., "Settling Length for Turbulent Flow of Air in an Annulus", The Canadian Journal of Chemical Engineering, v45, pp. 97-99 (1967).
23. Quarmby, A., "An Experimental Study of Turbulent Flow Through Concentric Annuli", International Journal of Mechanical Sciences, v9, n4, p. 205 (1967).
24. Wilson, N.W. and Medwell, J.O., "An Analysis of the Developing Turbulent Hydrodynamic and Thermal Boundary Layers in an Internally Heated Annulus", Journal of Heat Transfer, Paper No. 70-MT-9 (1970).
25. Reichardt, H., "Complete Representation of Turbulent Velocity Distribution in Smooth Pipes", Z. Angew. Math.Mech. v31, p. 208 (1951).
26. Okiishi, T.H. and Bathie, W.W., "An Approximate Method for Predicting Annulus Inlet Turbulent Flow Development Characteristics", Journal of Basic Engineering, pp. 667-669 (1970).
27. Schlichting, H., "Boundary Layer Theory", Sixth Edition, McGraw Hill Book Company (1968).
28. Lee, Y. and Park, S.D., "Developing Turbulent Flow in Concentric Annuli: An Analytical and Experimental Study", Wärme- und Stoffübertragung, Bd 4, pp. 156-166 (1971).
29. Latzko, H., "Der Wärmeübergang an Einen Turbulenten Flüssigkeitsorder Gasstrom", Z. f.a. M.M., Bd I. Heft 4, p. 268 (1921).
30. Schiller, L., "Die Entwicklung Der Laminaren Geschwindigkeitsverteilung und ihre Bedeutung für Zähigkeitsmessungen" Z.f.a. M.M., Bd 2, Heft 2, p. 96.
31. Schiller, V.L., and Kirsten, H.J., "Die Entwicklung Der Geschwindigkeitsverteilung Bei Der Turbulenter Rohvstrommng", Z. Tech. Phys., v10, p. 268 (1929).
32. Deissler, R.G., "Analytical and Experimental Investigation of Adiabatic Turbulent Flow in Smooth Tubes", NACA, TN 2138, (1950).
33. Deissler, R.G., "Turbulent Heat Transfer and Friction in the Entrance Regions of Smooth Passages", Transactions of the A.S.M.E., pp. 1221-1233, (1955).

34. Ross, D., "Turbulent Flow in the Entrance Region of a Pipe", Transactions of the A.S.M.E., pp. 915-923 (1956).
35. Filippov, G.V., "On Turbulent Flow in the Entrance Length of a Straight Tube of Circular Cross-section", Soviet Physics - Technical Physics, v32, n8, pp. 1681-1686 (1958).
36. Barbin, A.R. and Jones, J.B., "Turbulent Flow in the Inlet Region of a Smooth Pipe", Journal of Basic Engineering, pp. 29-34 (1963).
37. Bowlus, D.A. and Brighton, J.A., "Incompressible Turbulent Flow in the Inlet Region of a Pipe", Journal of Basic Engineering, pp. 431-433 (1968).
38. Richman, J.W. and Azad, R.S., "Developing Turbulent Flow in Smooth Pipes", Applied Scientific Research, v28, pp. 419-440 (1973).
39. Van Driest, E.R., "On Turbulent Flow Near a Wall", Journal of Aeronautical Science, v23, pp. 1007-1011, and p. 1036 (1956).
40. Na, T.Y. and Lu, Y.P., "Turbulent Flow Development Characteristics in Channel Inlets", Applied Scientific Research, v27, pp. 425-439 (1973).
41. Wang, J.S. and Tullis, J.P., "Turbulent Flow in the Entry-region of a Rough Pipe", Journal of Fluids Engineering, pp. 62-68 (1974).
42. Walklate, P., Heikal, M.R. and Hatton, A.P., "Measurement and Prediction of Turbulence and Heat Transfer in the Entrance Region of a Pipe", Proceedings of the Institute of Mechanical Engineers, v190, n37 (1976).
43. Reichert, J.K. and Azad, R.S., "Nonasymptotic Behaviour of Developing Turbulent Pipe Flow", Canadian Journal of Physics, v54, pp. 268-278 (1976).
44. Brighton, J.A. and Jones, J.B., "Fully Developed Turbulent Flow in Annuli", Journal of Basic Engineering, pp. 835-844 (1964).
45. Rehme, K., "Turbulent Flow in Smooth Concentric Annuli with Small Radius Ratios", Journal of Fluid Mechanics, v64, part 2, pp. 263-287 (1974).

46. Kays, W.M. and Leung, E.Y., "Heat Transfer in Annular Passages - Hydrodynamically Developed Turbulent Flow with Arbitrarily Prescribed Heat Flux", International Journal of Heat and Mass Transfer, v6, pp. 537-557, (1963).
47. Rothfus, R.R., Sartory, W.K. and Kermode, R.I., "Flow in Concentric Annuli at High Reynolds Number", American Institute of Chemical Engineers Journal, v12, n6, pp. 1086-1091 (1966).
48. Clump, C.W. and Kwasnoski, D., "Turbulent Flow in Concentric Annuli", American Institute of Chemical Engineers Journal, v14, n1, pp. 164-168 (1968).
49. Doshi, M.P. and Gill, W.N., "Fully Developed Turbulent Flow in an Annulus: Radius of Maximum Velocity", Journal of Applied Mechanics, pp. 1090-1091 (1971).
50. Rothfus, R.R., Monrad, C.C., Sikchi, K.G. and Heideger, . "Isothermal Skin Friction in Flow Through Annular Sections", Industrial and Engineering Chemistry, v47, pp. 913 (1955).
51. Wang, Y.L. and Longwell, P.A., "Laminar Flow in the Inlet Section of Parallel Plates", American Institute of Chemical Engineers Journal, v10, pp. 323-329 (1964).
52. Friedmann, M., Gillis, J., and Liron, N., "Laminar Flow In a Pipe at Low and Moderate Reynolds Numbers", Applied Scientific Research, v19, pp. 426-438 (1968).
53. Burke, J.P. and Berman, N.S., "Entrance Flow Development in Circular Tubes at Small Axial Distances", American Society of Mechanical Engineers, paper 69-Wa/Fe-13 (1969).
54. Campbell, W.D. and Slattery, J.C., "Flow in the Entrance of a Tube", Journal of Basic Engineering, v85, pp. 41-46 (1963).
55. Gupta, R.C., "Flow Development in the Hydrodynamic Entrance Region of a Flat Duct", American Institute of Chemical Engineers Journal, v11, pp. 1149-1151 (1965).
56. Shah, R.K., "A Correlation for Laminar Hydrodynamic Entry Length Solutions for Circular and Non-circular Ducts", Journal of Fluids Engineering, v100, pp. 177-179, (1978).
57. Shah, R.K. and London, A.L., "Advances in Heat Transfer: Laminar Flow Forced Convection in Ducts", Academic Press (1978).

58. Goel, R.K., "An Experimental Determination of Settling Length for Turbulent Flow of Air in Annular Ducts", M.A.Sc. Thesis, University of Windsor, Windsor, Ontario, Canada (1966).
59. Padmanabha, A.V.A., "An Experimental Determination of Settling Length for Turbulent Flow of Air in Smooth Annuli with Square and Bellmouth Entrances", M.A.Sc. Thesis, University of Windsor, Windsor, Ontario, Canada (1968).
60. Paranjpe, S.C. and Sridhar, K., "Effects of Core Support and Core Curvature on Turbulent Flows Through Annuli", Transactions of the Canadian Society for Mechanical Engineering, v4, n3, pp. 137-143 (1976-1977).
61. Sissom, L.E. and Pitts, D.R., "Elements of Transport Phenomena", McGraw-Hill Book Company (1972).
62. Bird, R.B., Stewart, W.E. and Lightfoot, E.N., "Transport Phenomena", John Wiley & Sons, Inc. (1960).
63. Hildebrand, F.B., "Introduction to Numerical Analysis", McGraw-Hill Book Company, Inc., (1956).
64. Moursund, D.G. and Duris, C.S., "Elementary Theory and Application of Numerical Analysis", McGraw-Hill Book Company (1967).
65. Reddick, H.W. and Miller, F.H., "Advanced Mathematics for Engineers" John Wiley & Sons, Inc. (1962).
66. Nicol, A.A., Ivey, C.M. and Sridhar, K., "The Location of the Plane of Zero Shear in Annular Flow", Proceedings of the Third Canadian Congress of Applied Mechanics, pp. 581-582 (1971).

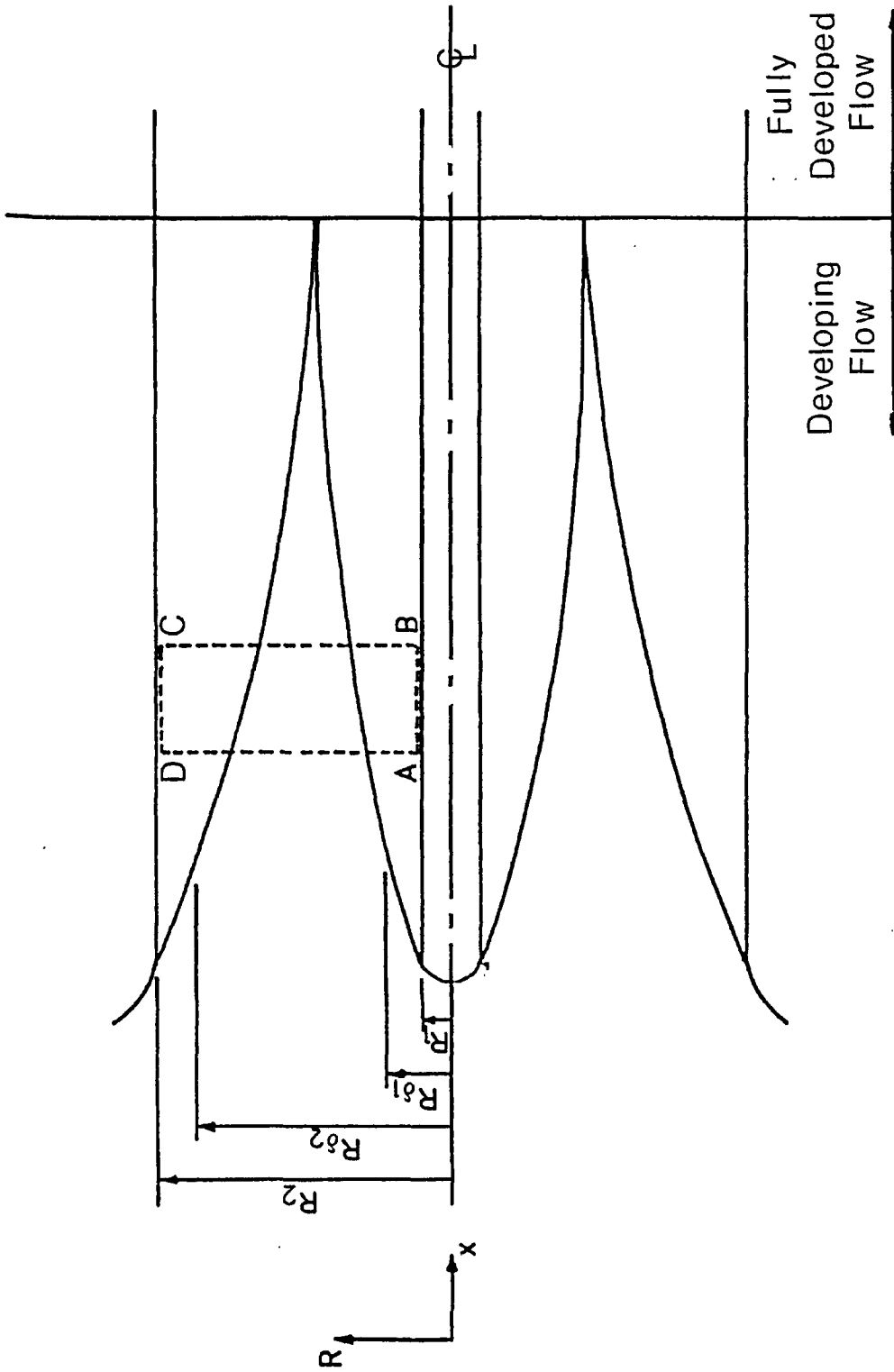


FIGURE 3.1 SCHEMATIC OF FLOW IN INLET REGION OF ANNULUS

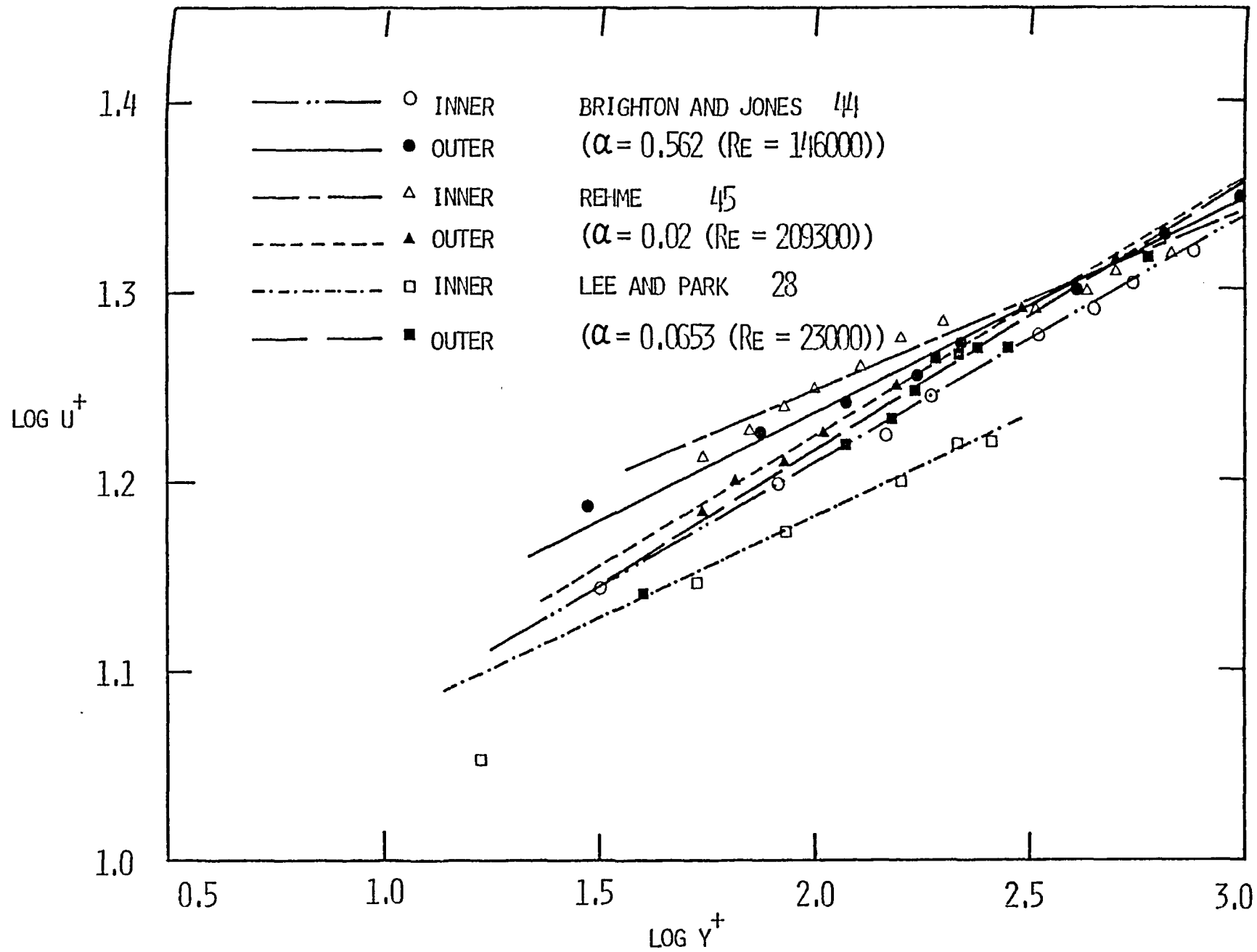


FIGURE 4.1 VELOCITY PROFILES IN FULLY DEVELOPED TURBULENT ANNULAR FLOWS

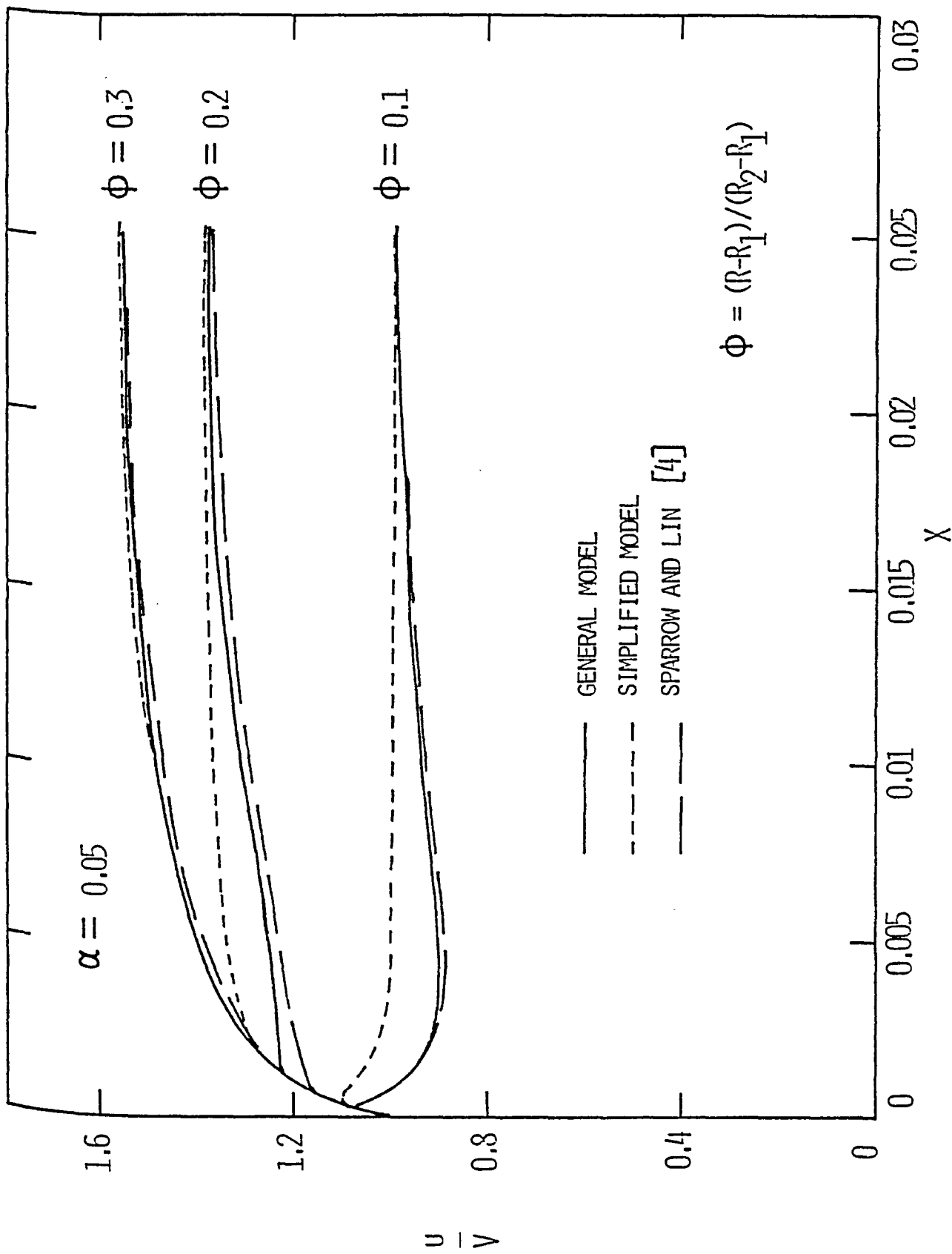


FIGURE 4.2 NON-DIMENSIONAL VELOCITY PROFILES
 ($\alpha = 0.05$; $\phi = 0.1, 0.2, 0.3$)

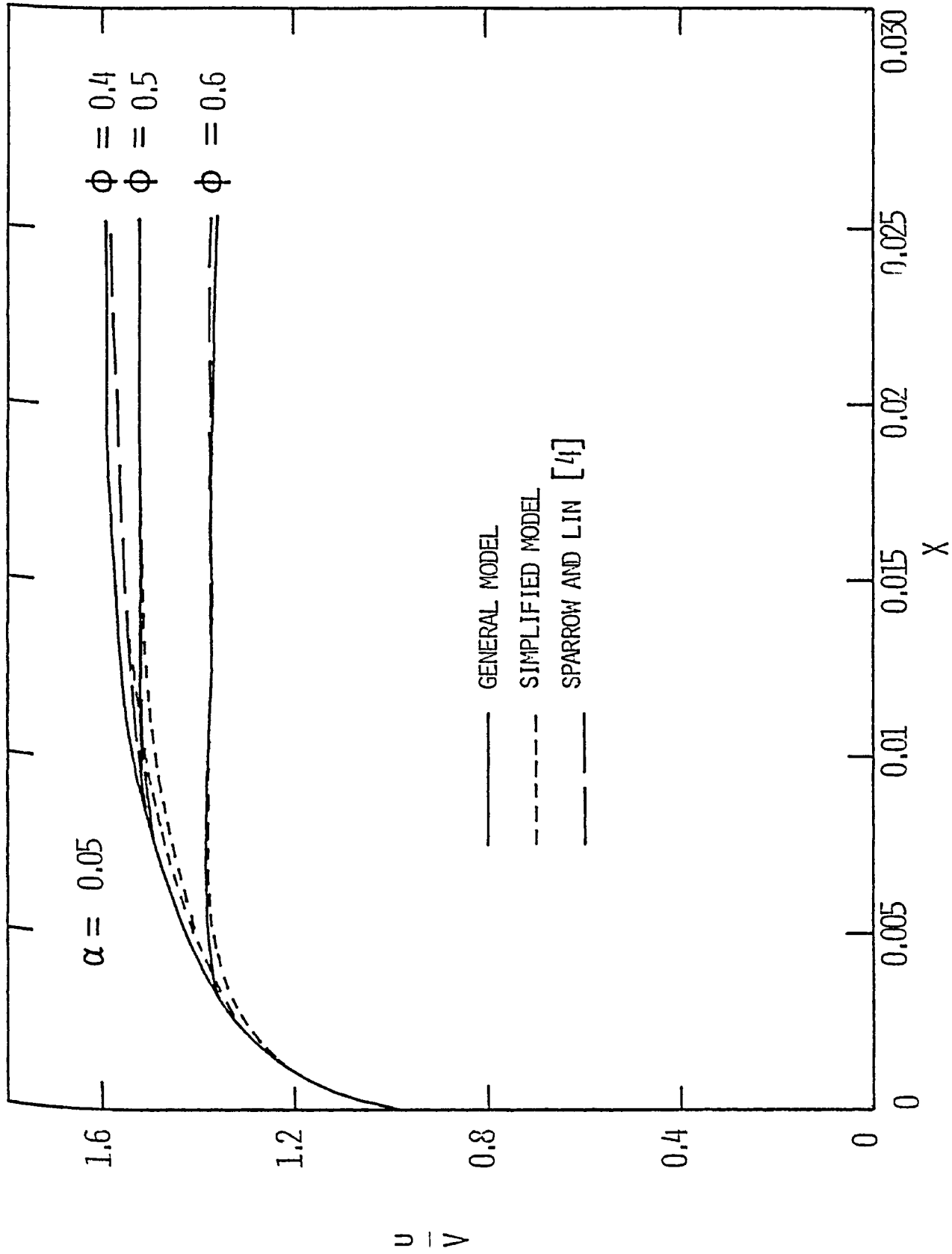


FIGURE 4.3 NON-DIMENSIONAL VELOCITY PROFILES
 ($\alpha = 0.05$; $\phi = 0.4, 0.5, 0.6$)

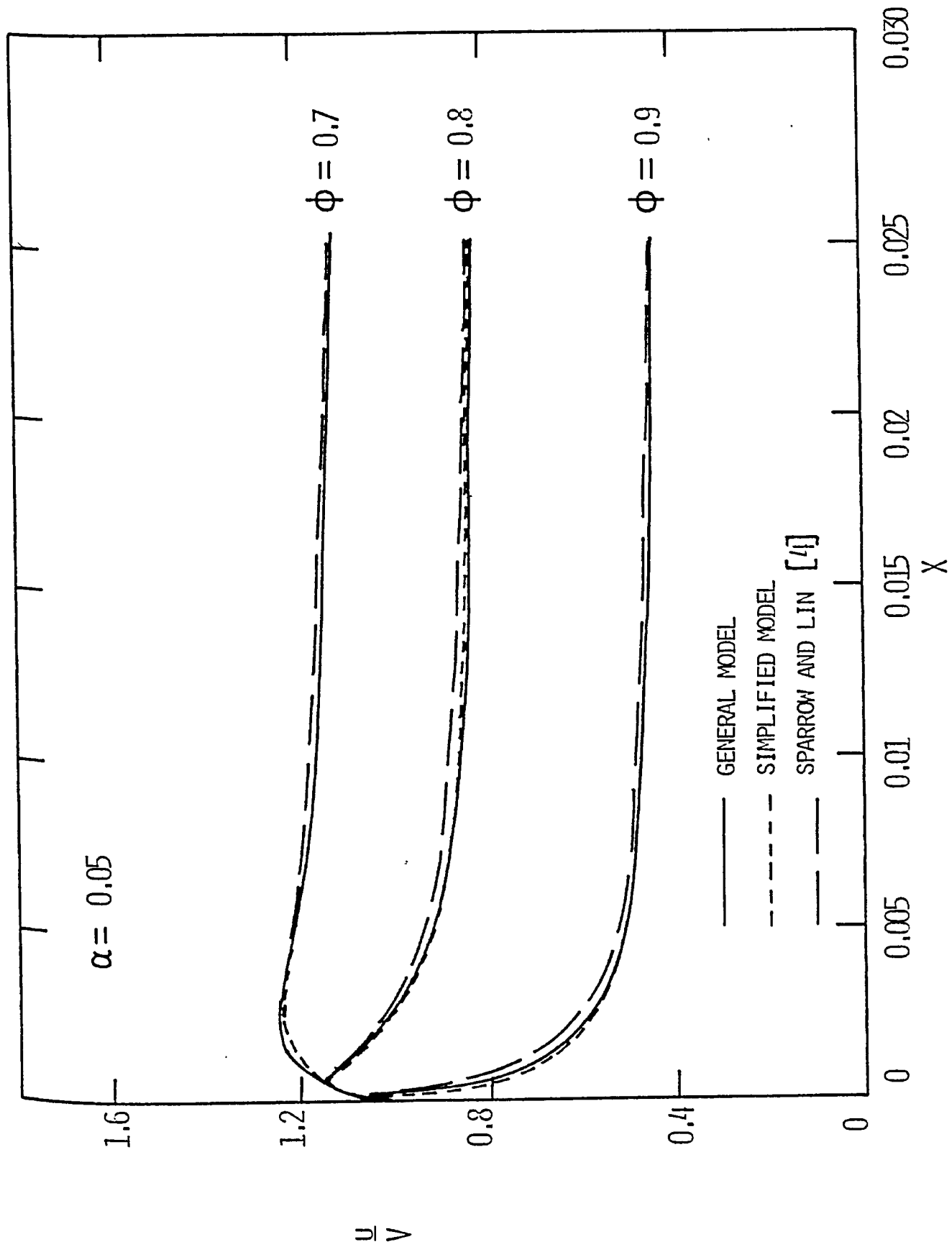


FIGURE 4.4 NON-DIMENSIONAL VELOCITY PROFILES
 ($\alpha = 0.05$; $\phi = 0.7, 0.8, 0.9$)

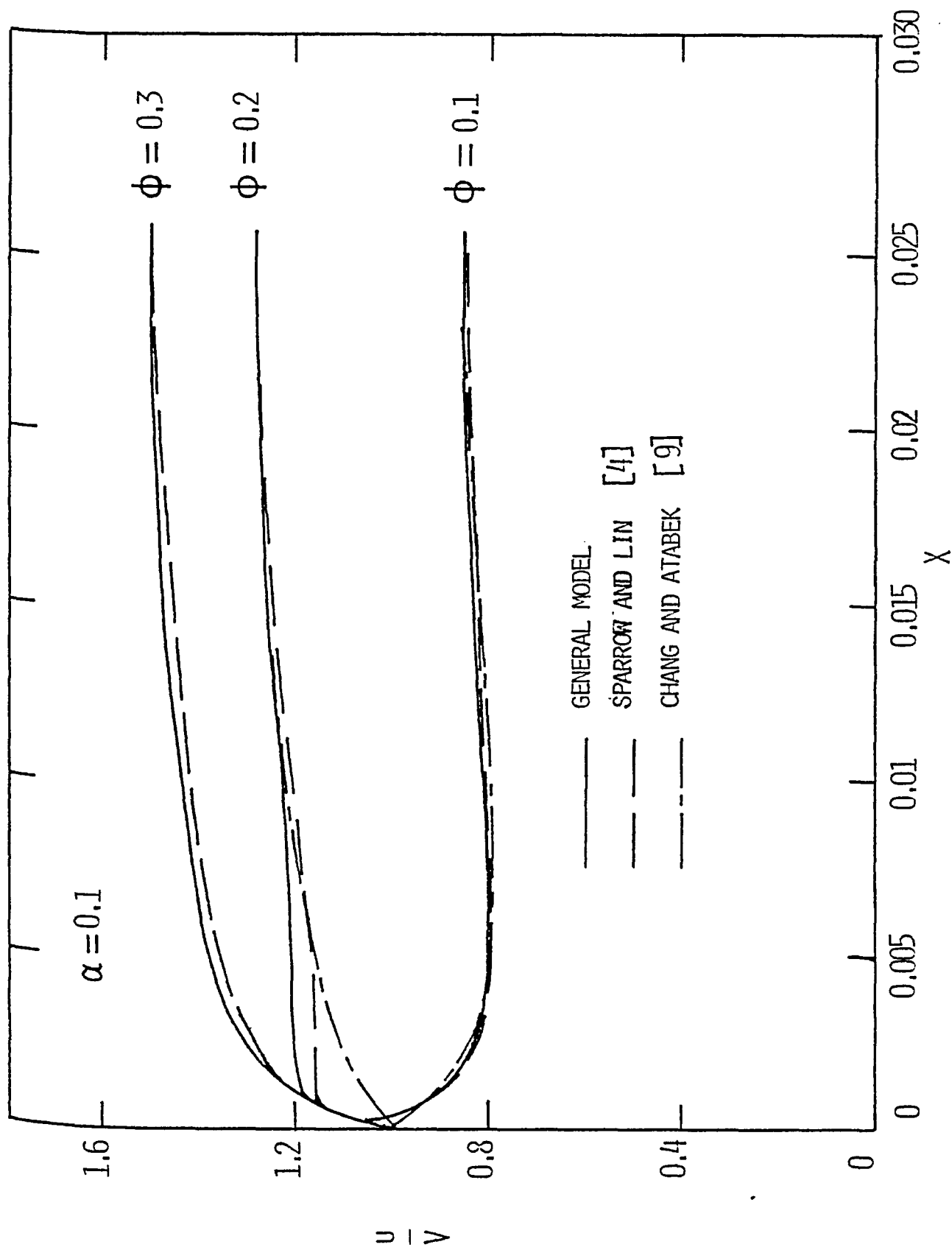


FIGURE 4.5 NON-DIMENSIONAL VELOCITY PROFILES
 ($\alpha = 0.1$; $\phi = 0.1, 0.2, 0.3$)

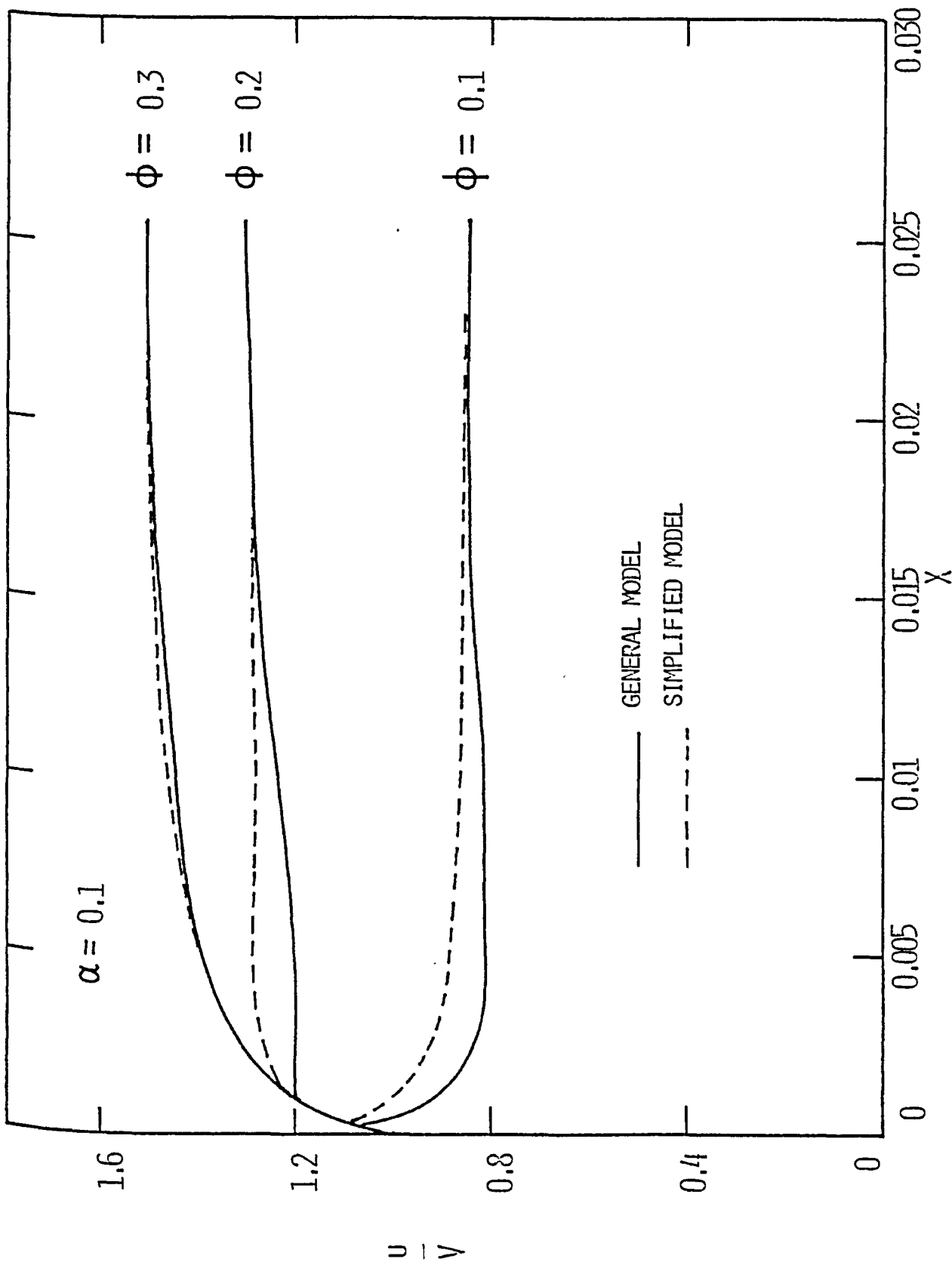


FIGURE 4.6 NON-DIMENSIONAL VELOCITY PROFILES
 ($\alpha = 0.1, \phi = 0.1, 0.2, 0.3$)

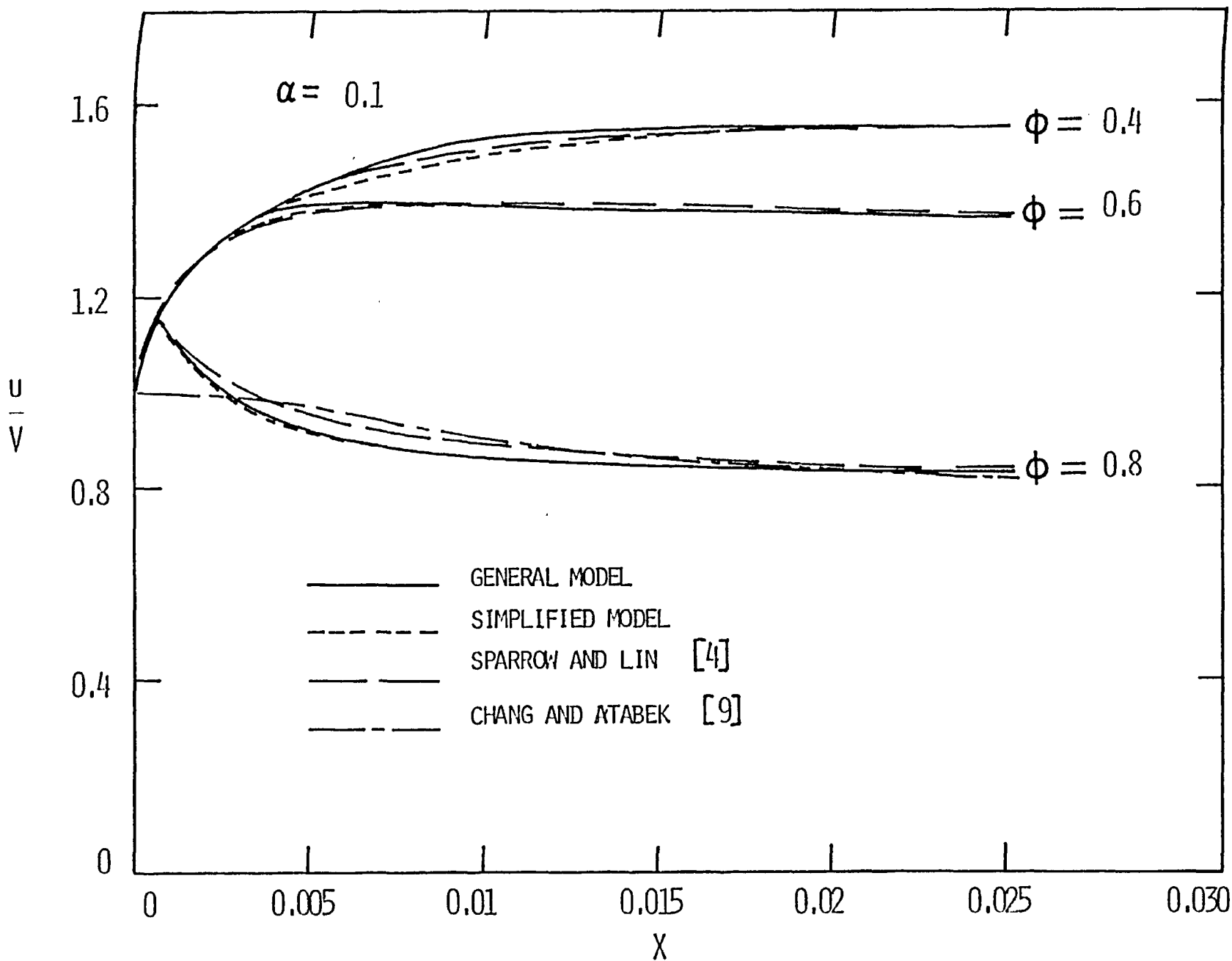


FIGURE 4.7 NON-DIMENSIONAL VELOCITY PROFILES
($\alpha = 0.1, \phi = 0.4, 0.6, 0.8$)

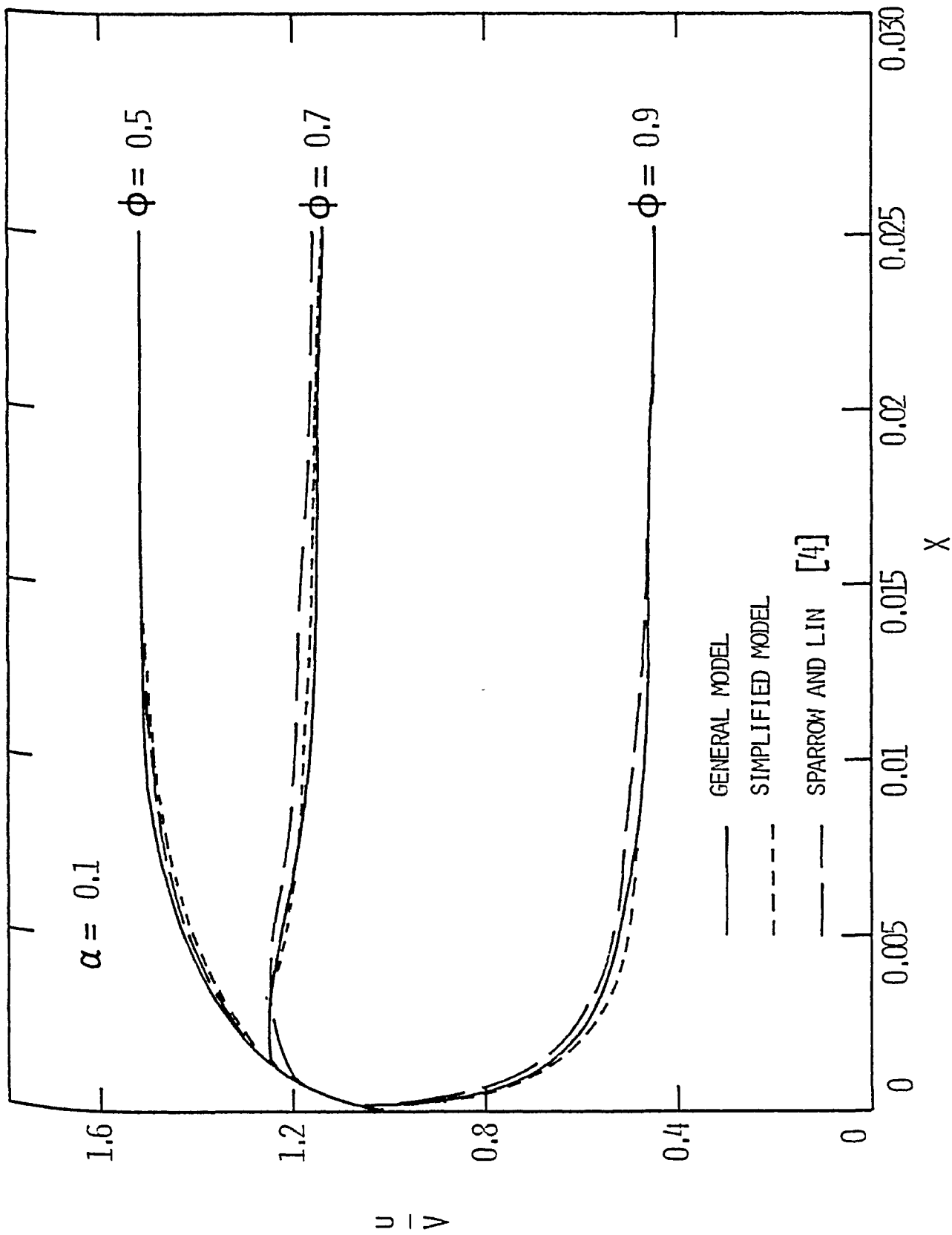


FIGURE 4.8 NON-DIMENSIONAL VELOCITY PROFILES
 ($\alpha = 0.1, \phi = 0.5, 0.7, 0.9$)

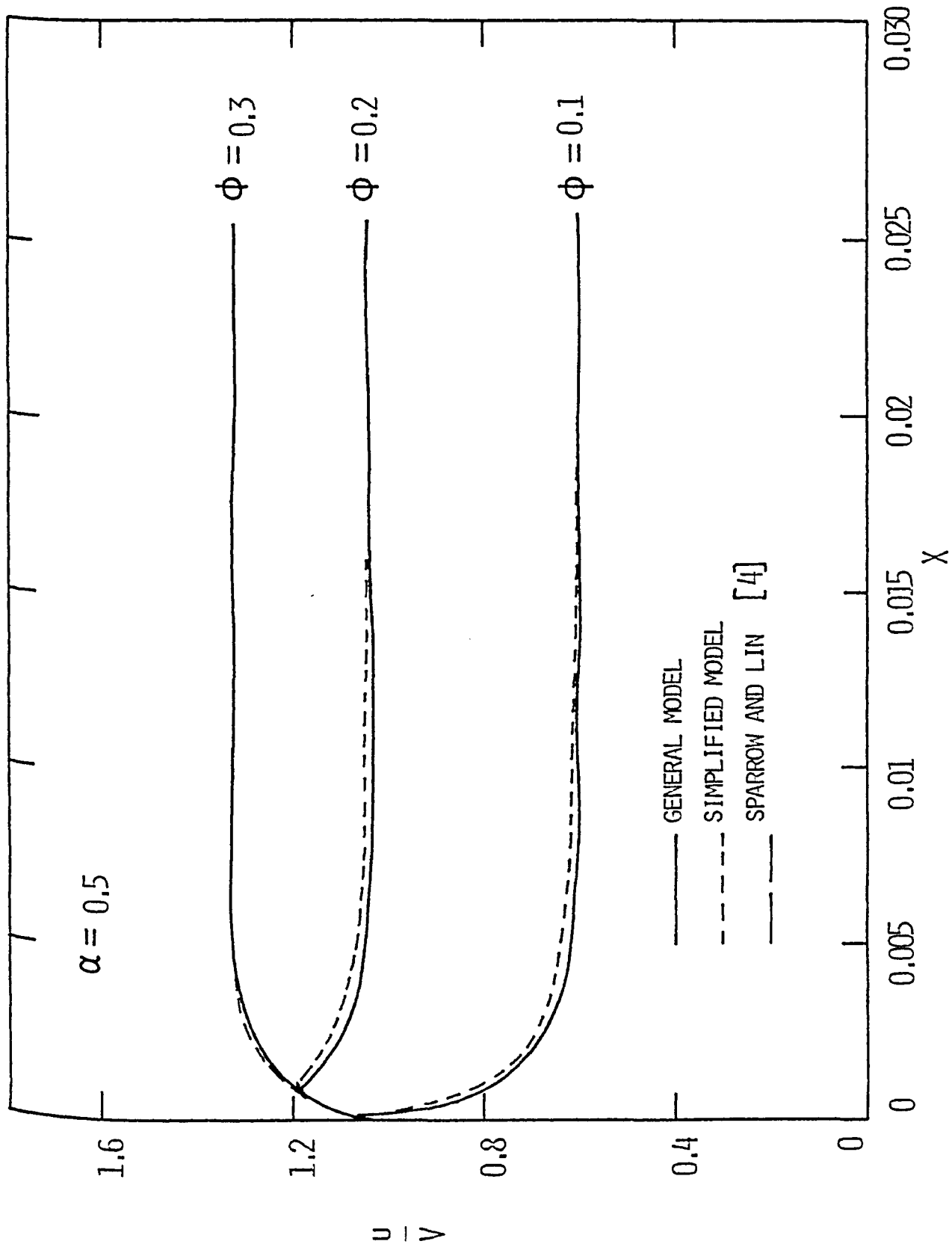


FIGURE 4.9 NON-DIMENSIONAL VELOCITY PROFILES
 ($\alpha = 0.1, \phi = 0.1, 0.2, 0.3$)

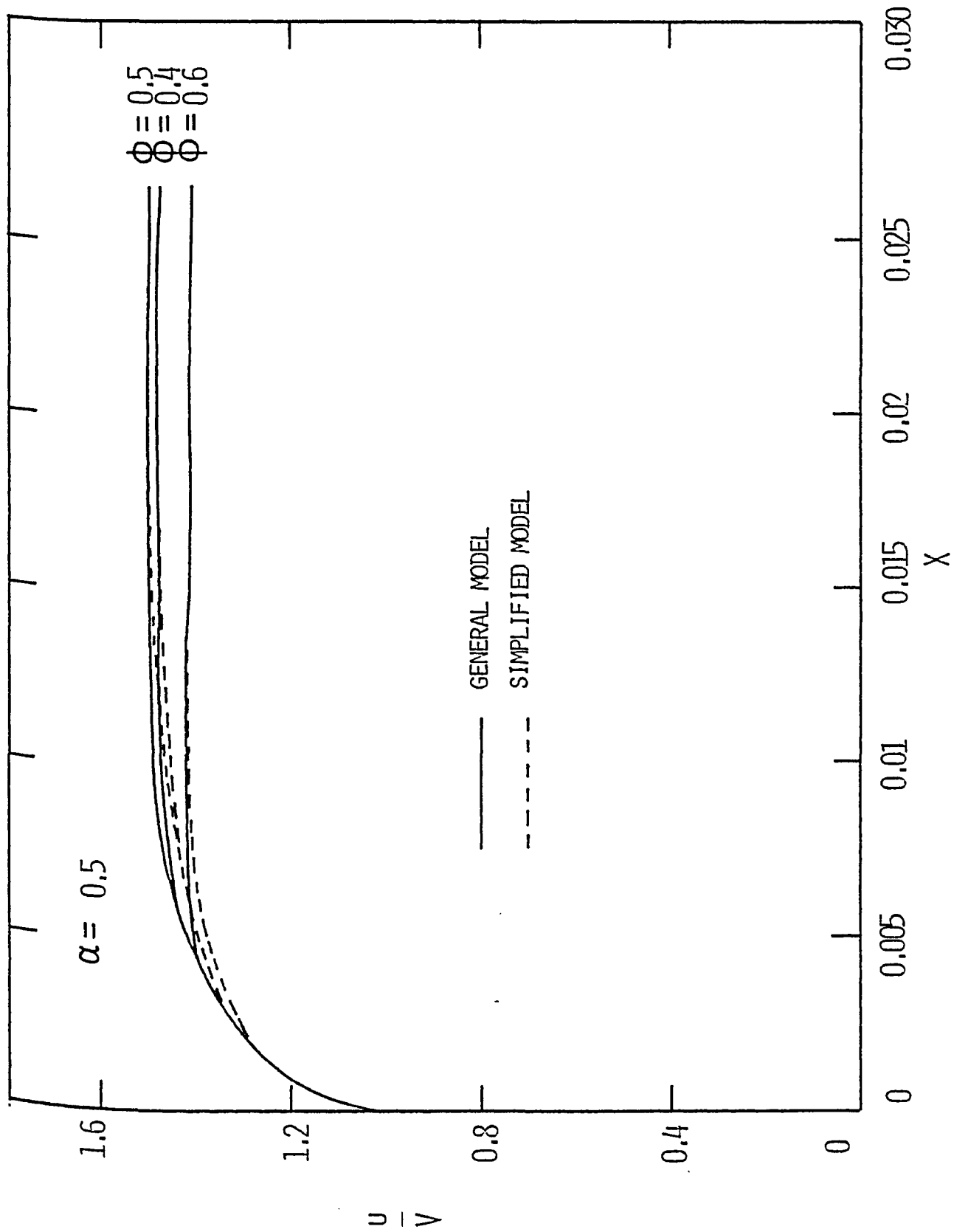


FIGURE 4.10 NON-DIMENSIONAL VELOCITY PROFILES
 ($\alpha = 0.5, \phi = 0.4, 0.5, 0.6$)

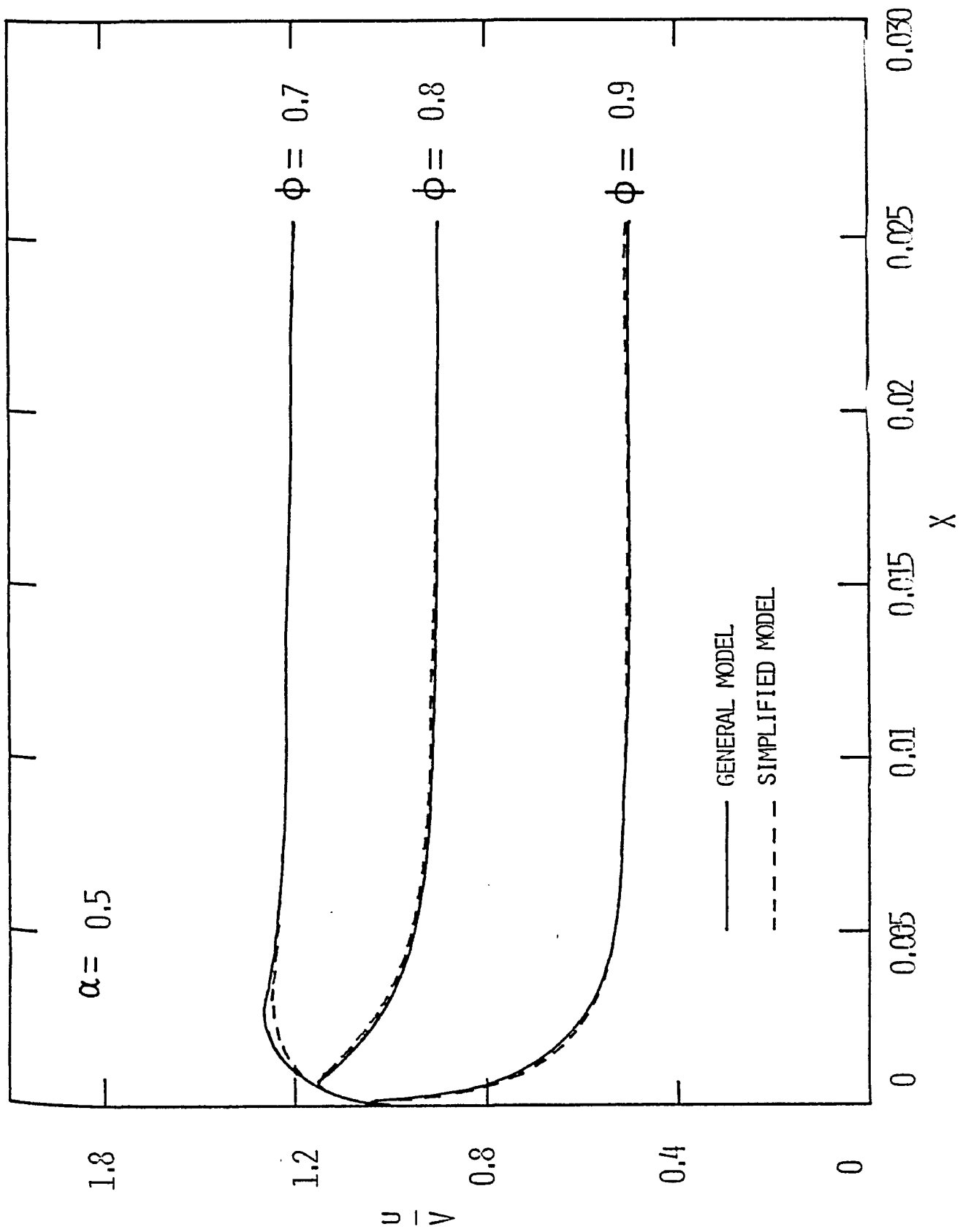


FIGURE 4.11 NON-DIMENSIONAL VELOCITY PROFILES
($\alpha = 0.5$; $\phi = 0.7, 0.8, 0.9$)

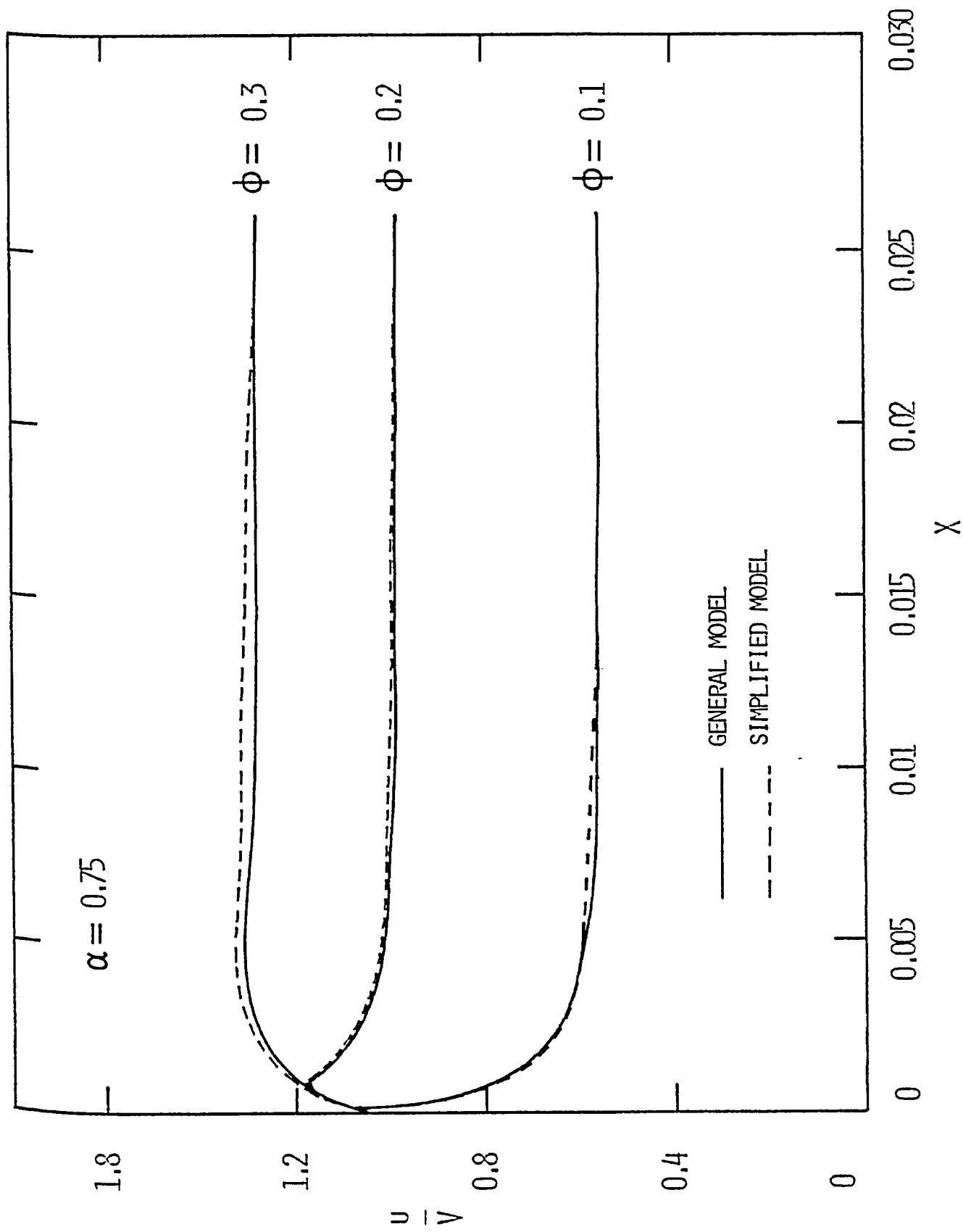


FIGURE 4.12 NON-DIMENSIONAL VELOCITY PROFILES
 ($\alpha = 0.75, \phi = 0.1, 0.2, 0.3$)

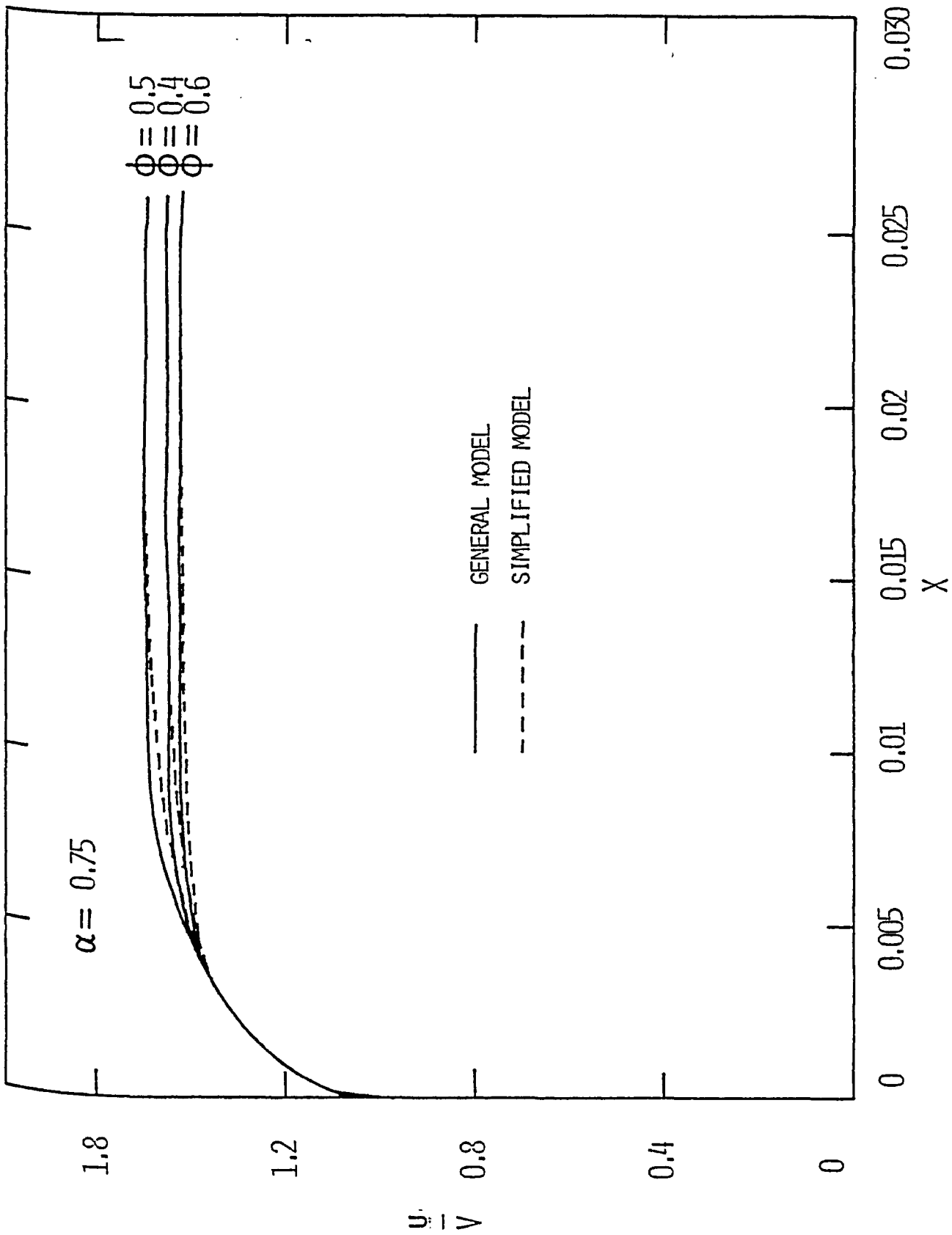


FIGURE 4.13 NON-DIMENSIONAL VELOCITY PROFILES
 ($\alpha = 0.75$, $\phi = 0.4, 0.5, 0.6$)

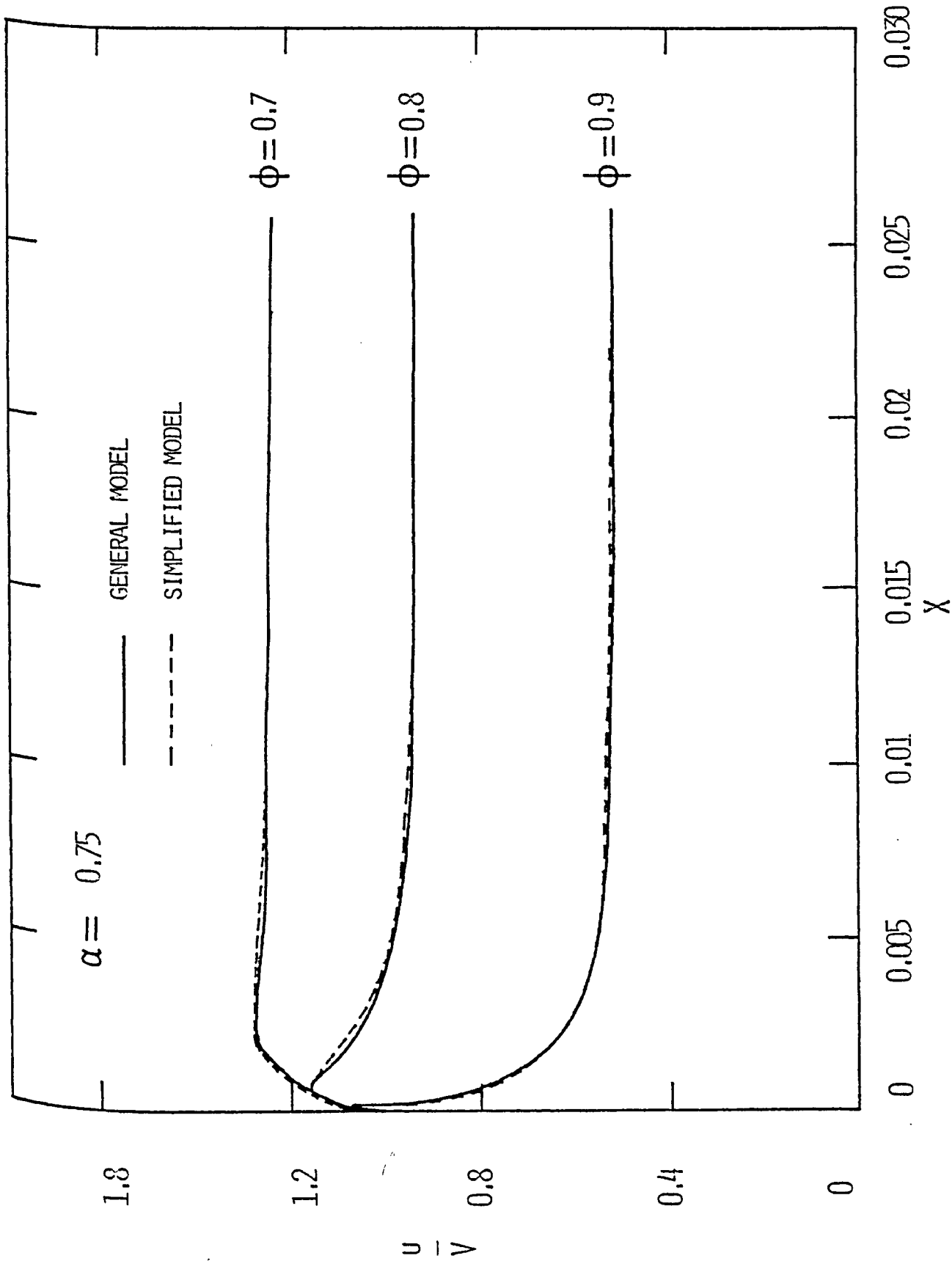


FIGURE 4.14 NON-DIMENSIONAL VELOCITY PROFILES
 ($\alpha = 0.75, \phi = 0.7, 0.8, 0.9$)

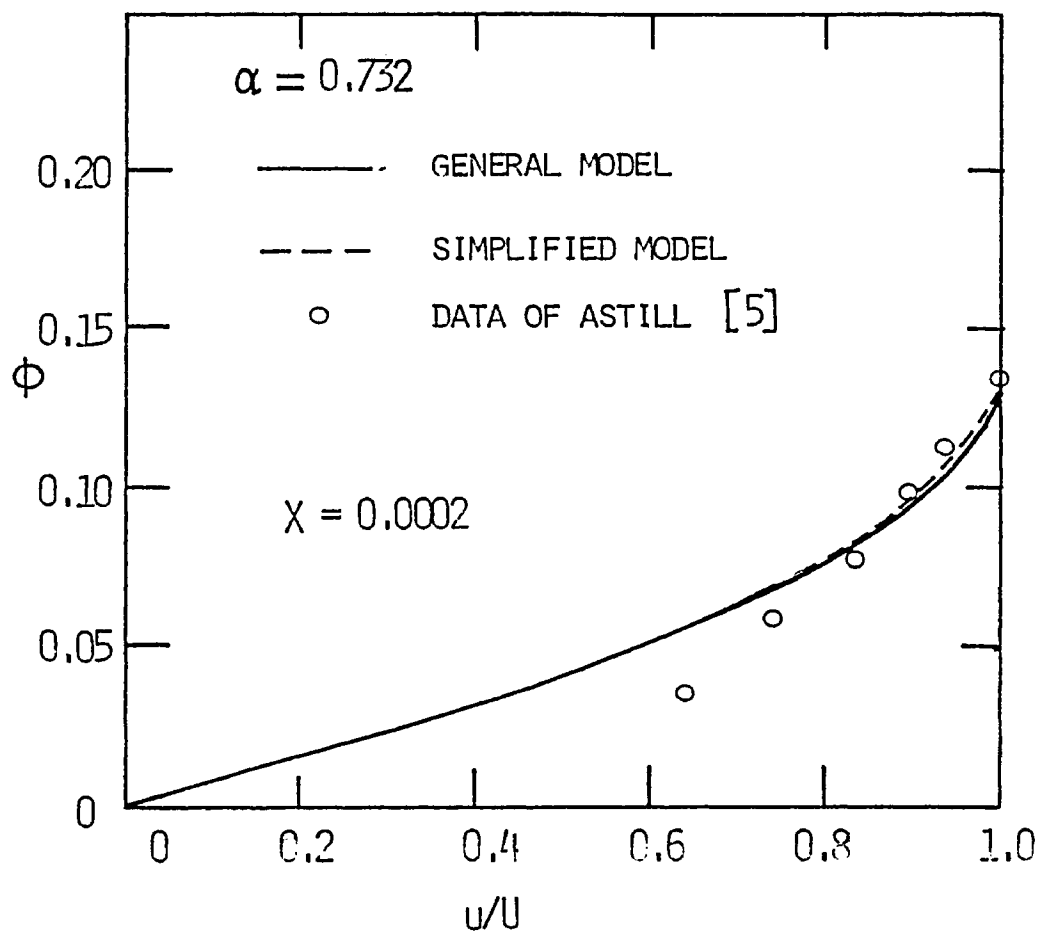


FIGURE 4.15 COMPARISON WITH EXPERIMENTAL RESULTS
($\alpha = 0.732$)

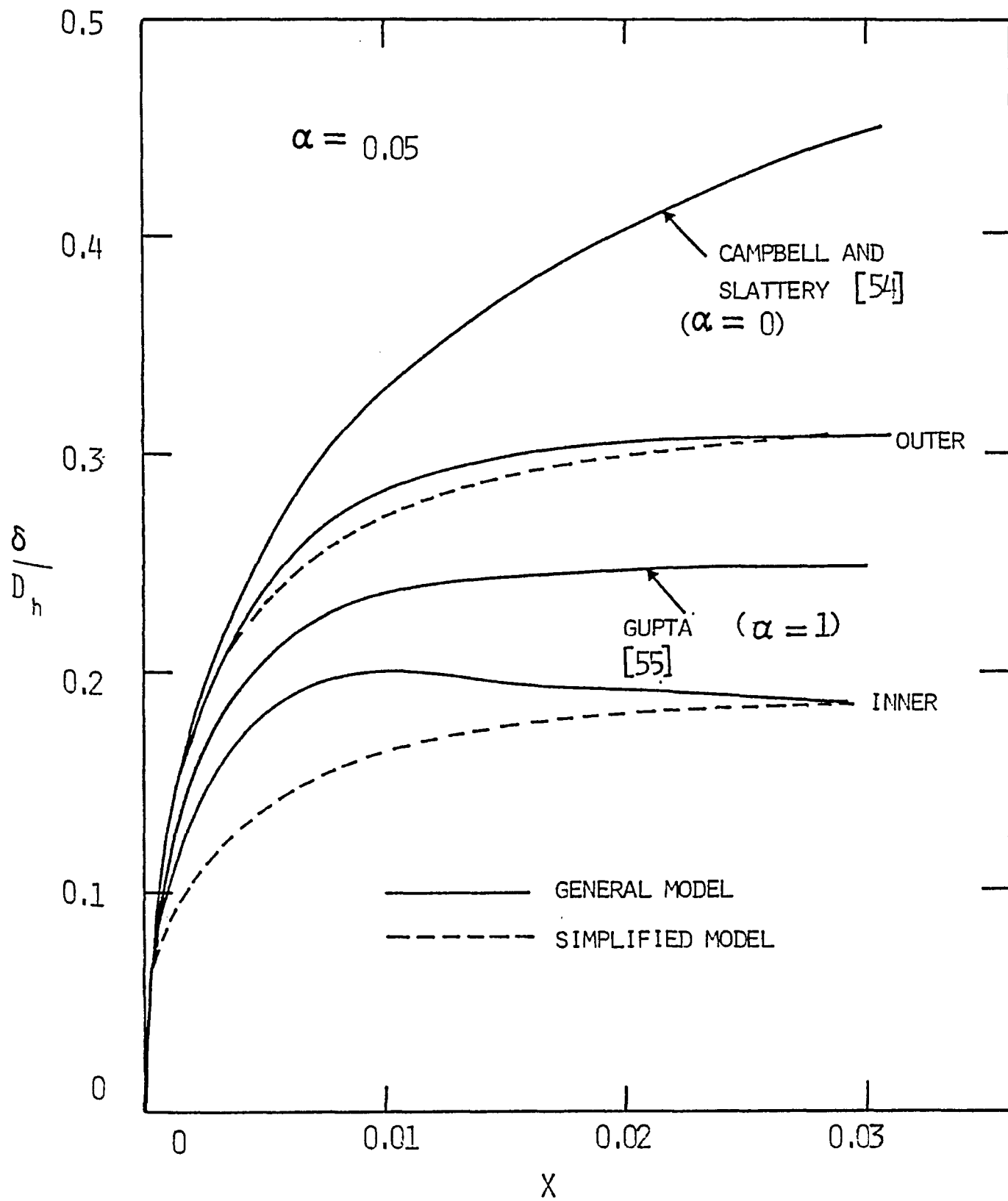


FIGURE 4.16 PREDICTED WALL LAYER GROWTH
($\alpha = 0.05$)

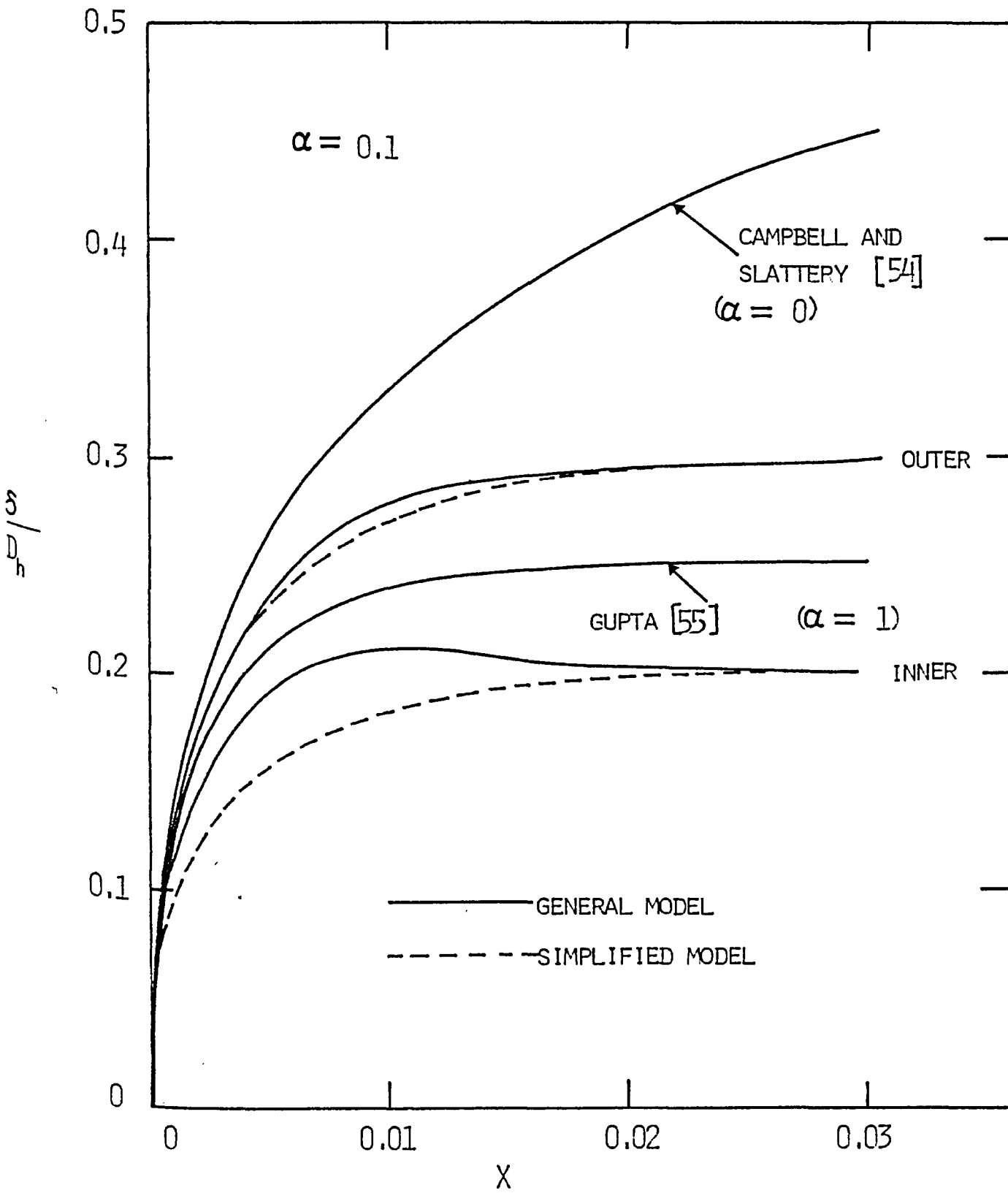


FIGURE 4.17 PREDICTED WALL LAYER GROWTH
($\alpha = 0.10$)

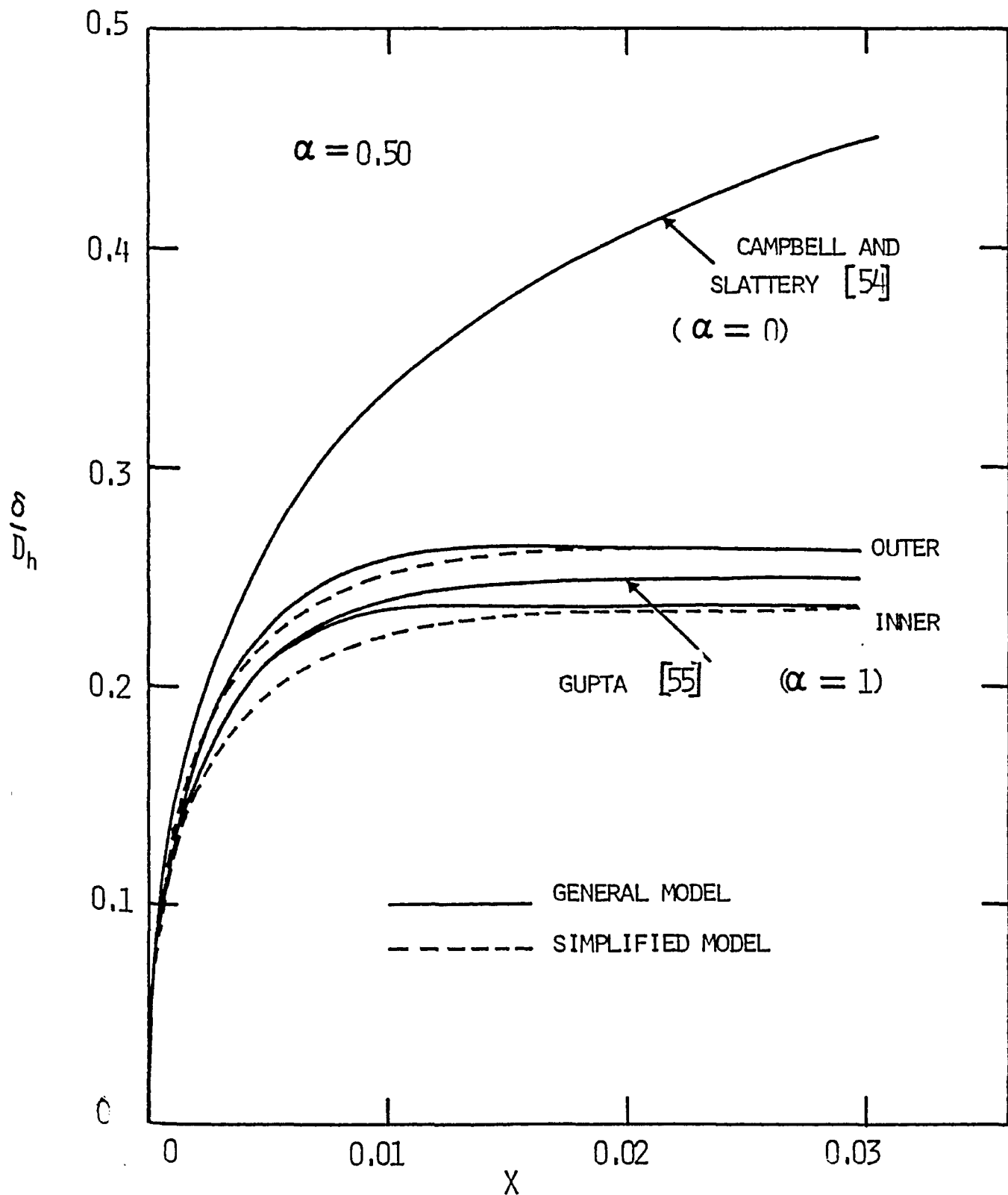


FIGURE 4.18 PREDICTED WALL LAYER GROWTH
($\alpha = 0.50$)

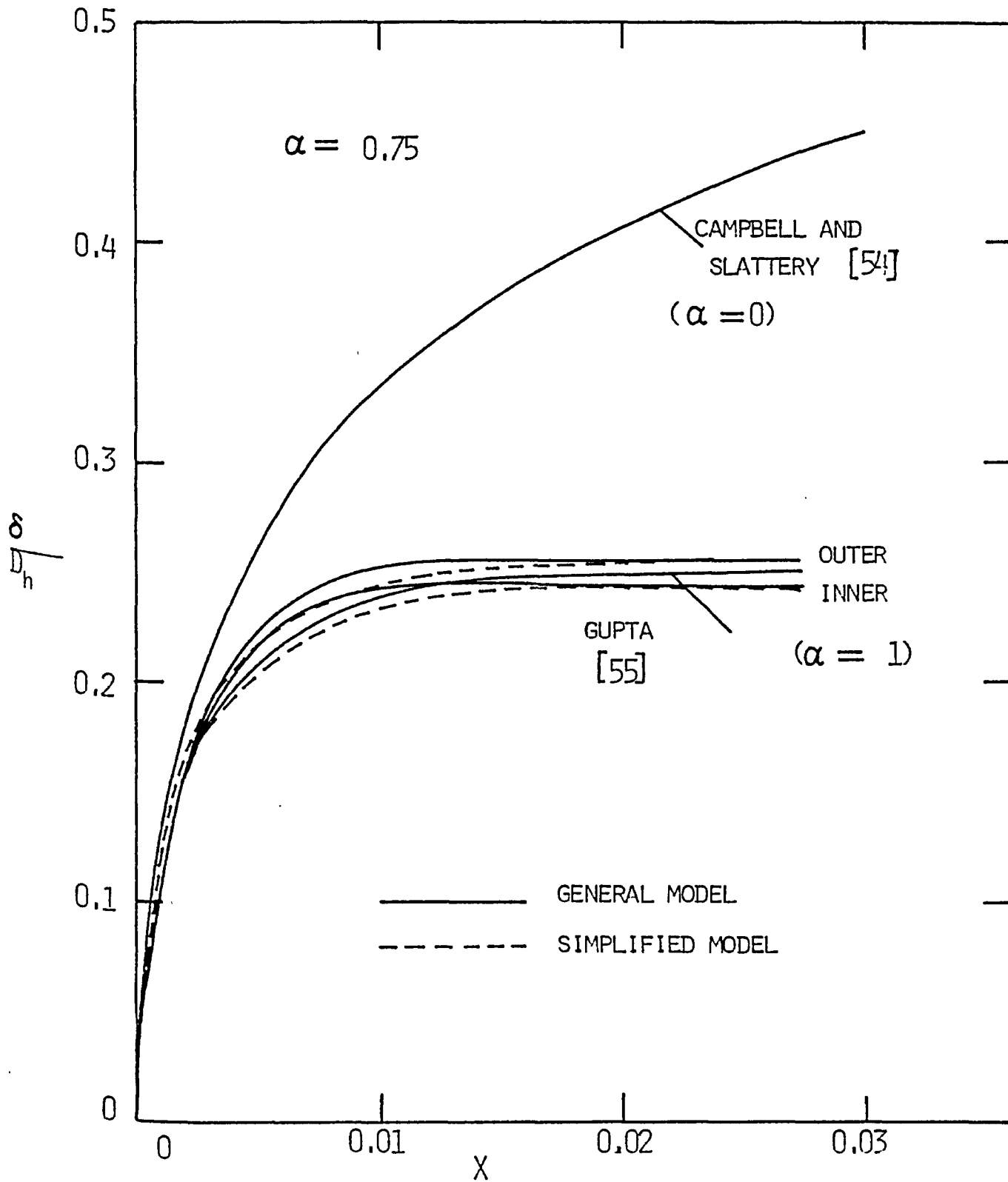


FIGURE 4.19 PREDICTED WALL LAYER GROWTH
($\alpha = 0.75$)

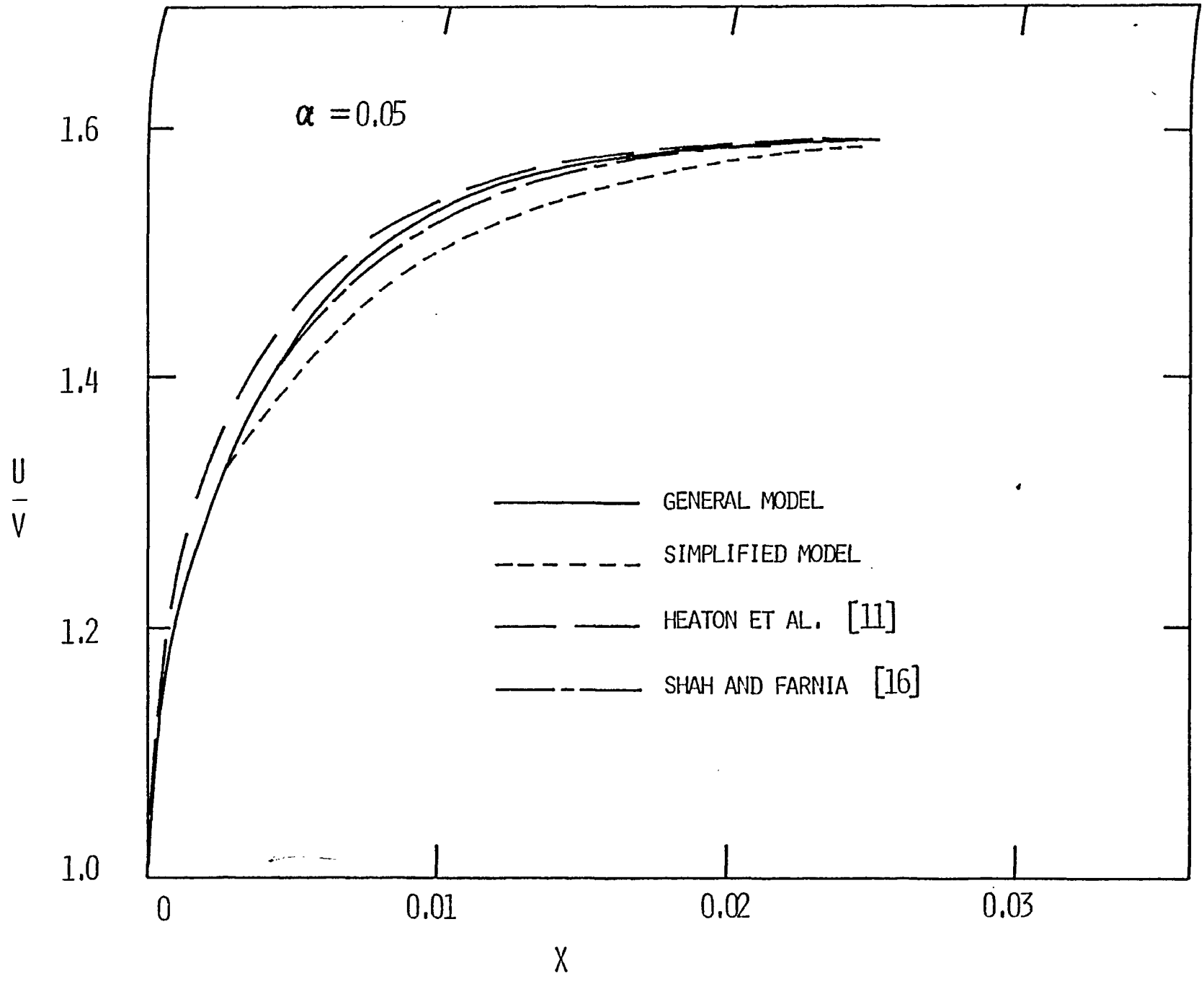


FIGURE 4.20 CORE VELOCITY VARIATION
($\alpha = 0.05$)

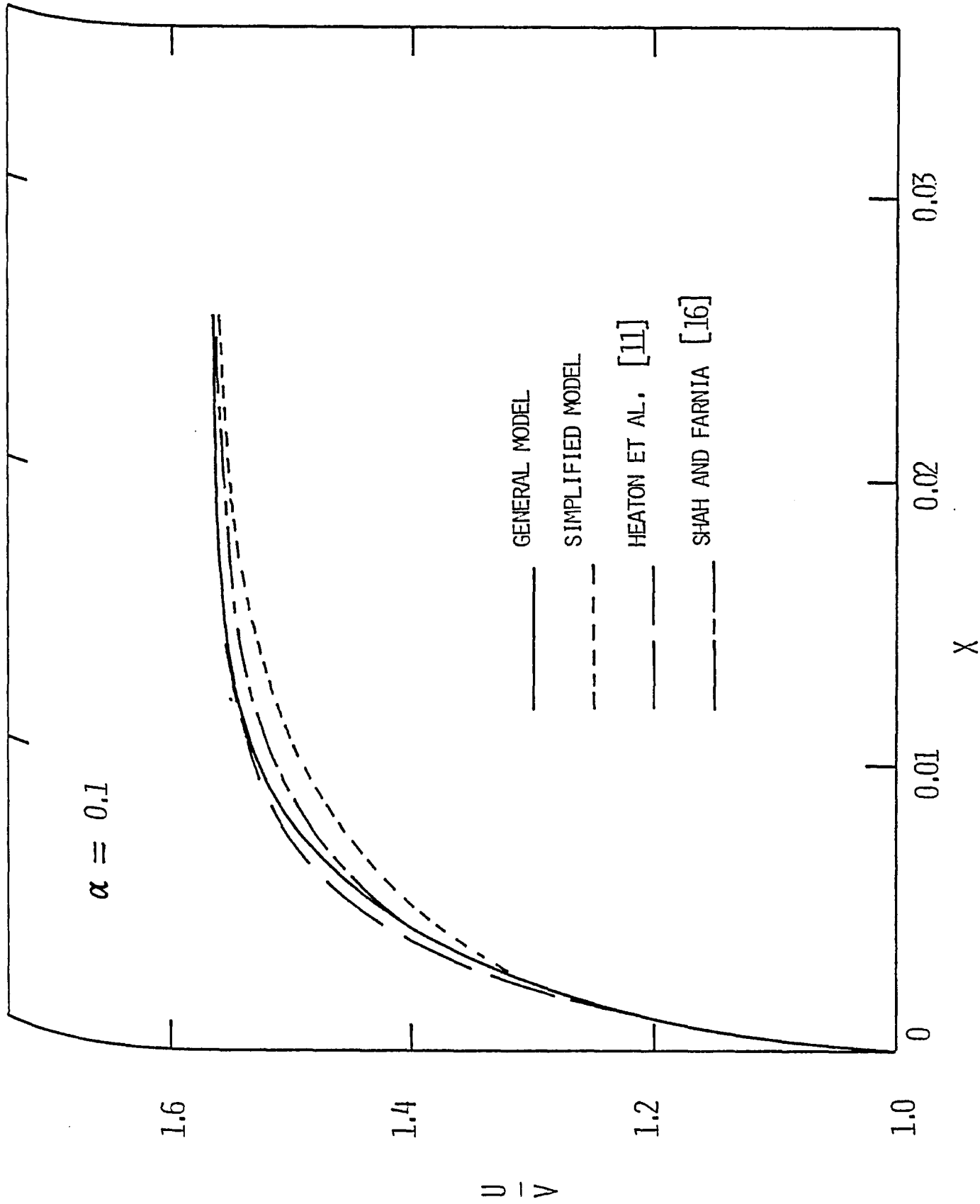


FIGURE 4.21 CORE VELOCITY VARIATION
($\alpha = 0.1$)

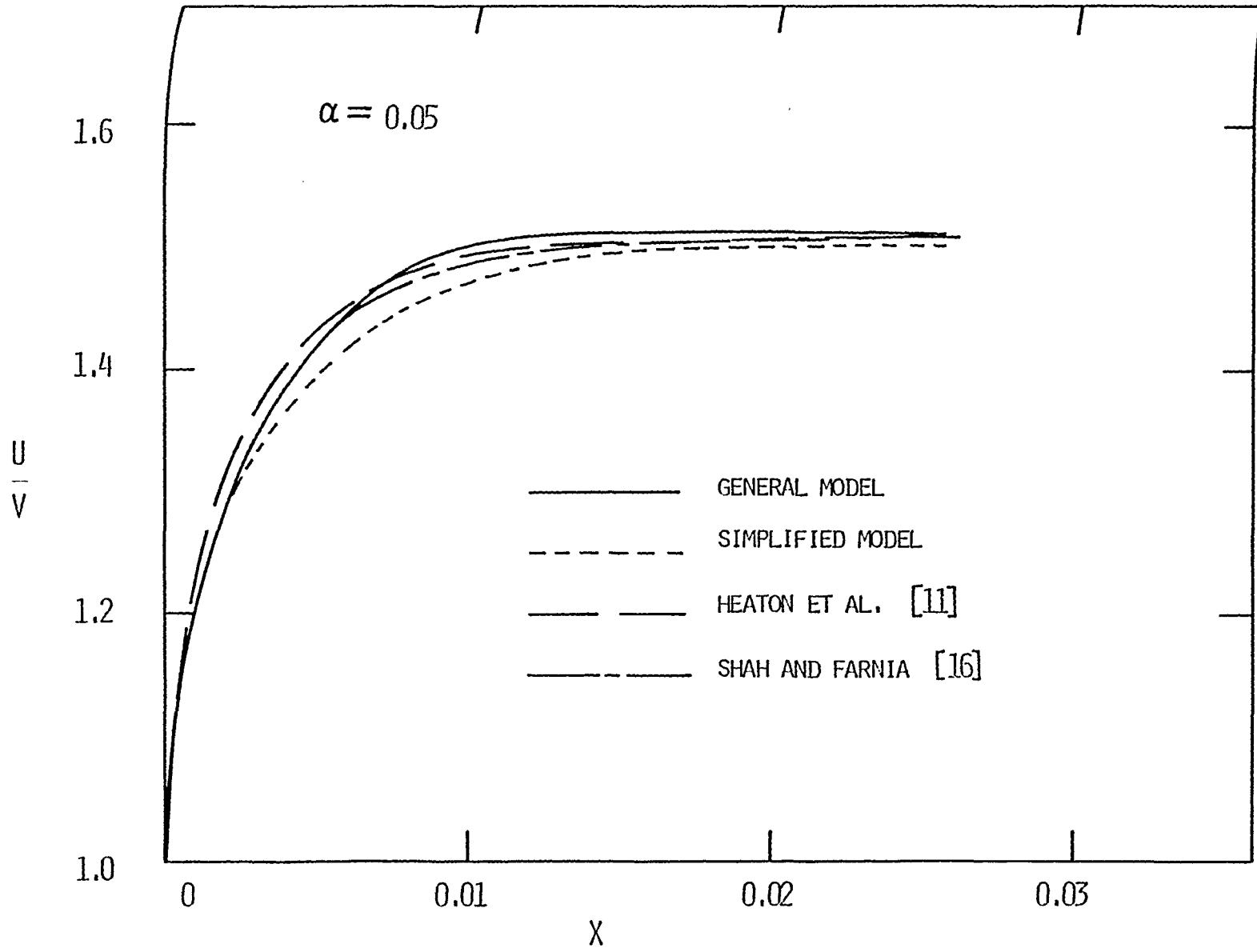


FIGURE 4.22 PREDICTED CORE VELOCITY VARIATION
($\alpha = 0.50$)

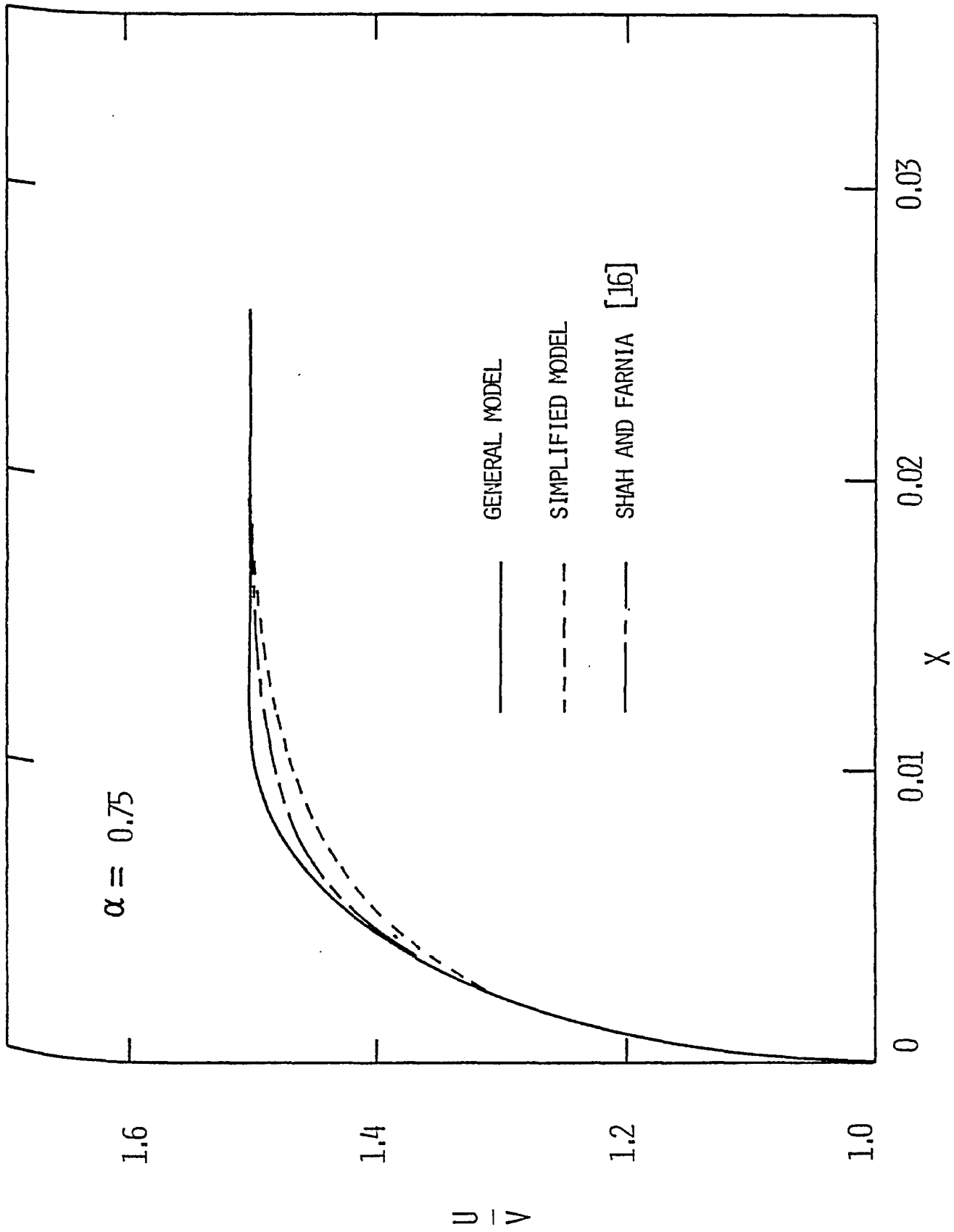


FIGURE 4.23 PREDICTED CORE VELOCITY VARIATION
($\alpha = 0.75$)

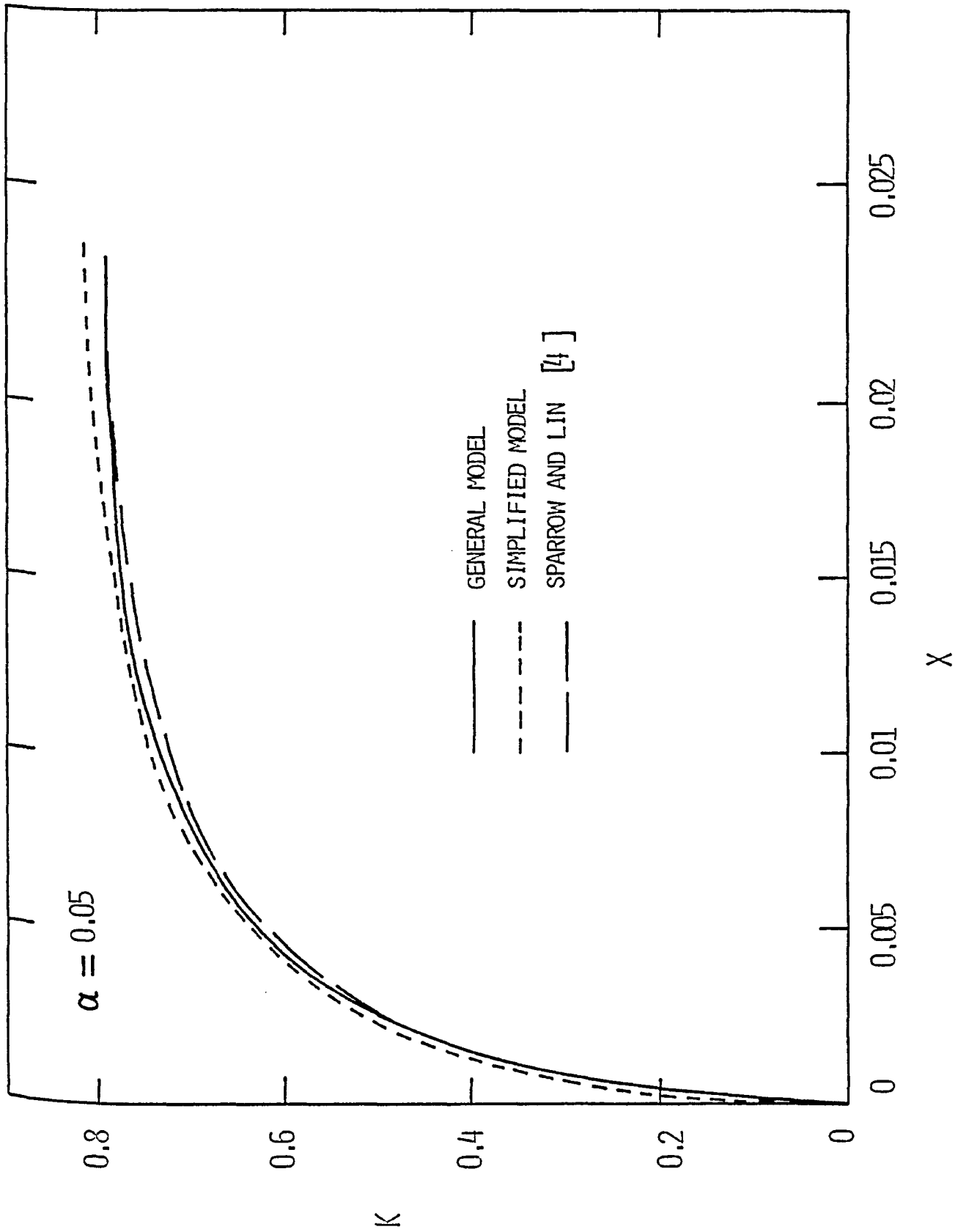


FIGURE 4.24 INCREMENTAL PRESSURE DROP NUMBER VARIATION
($\alpha = 0.05$)

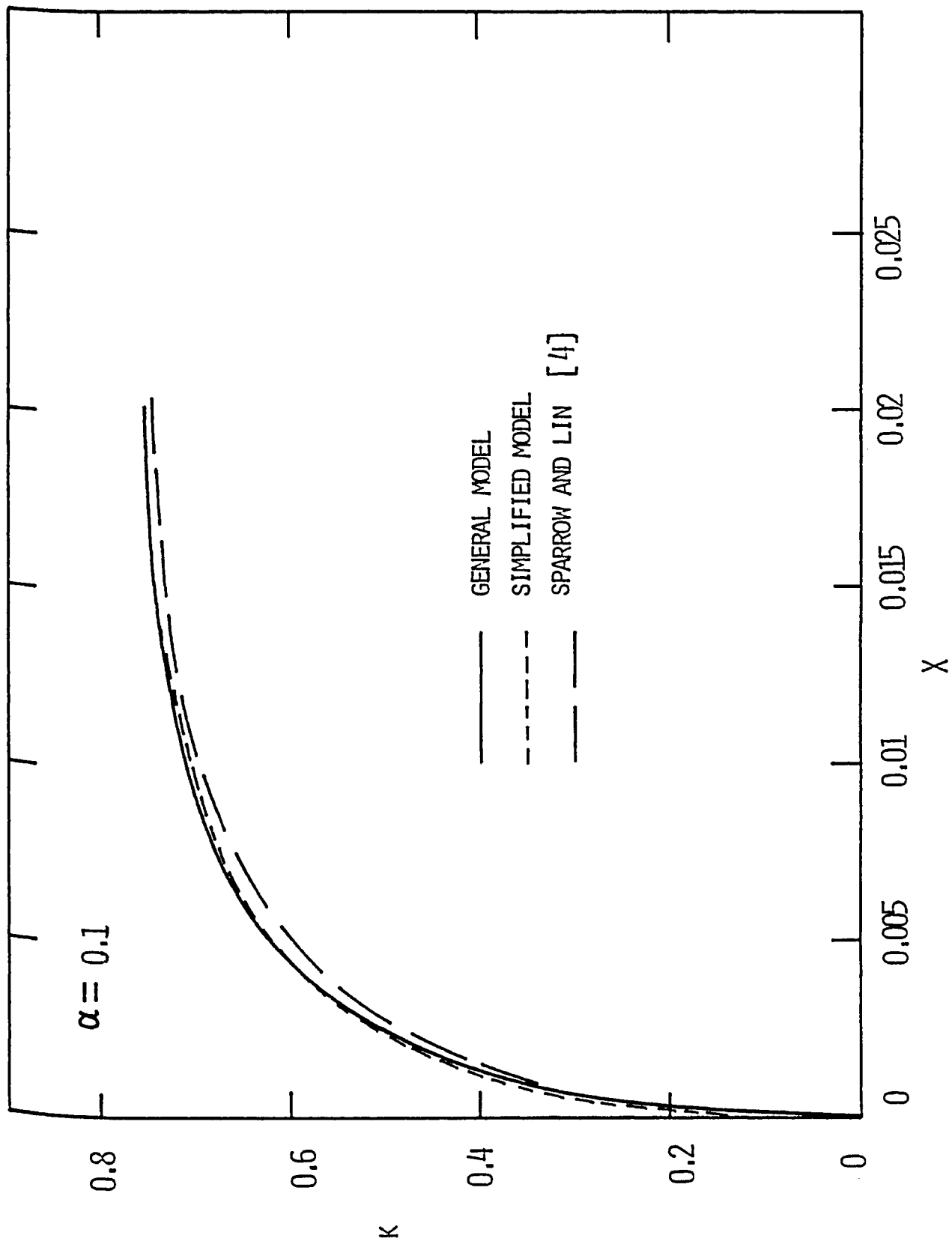


FIGURE 4.25 INCREMENTAL PRESSURE DROP NUMBER VARIATION
($\alpha = 0.10$)

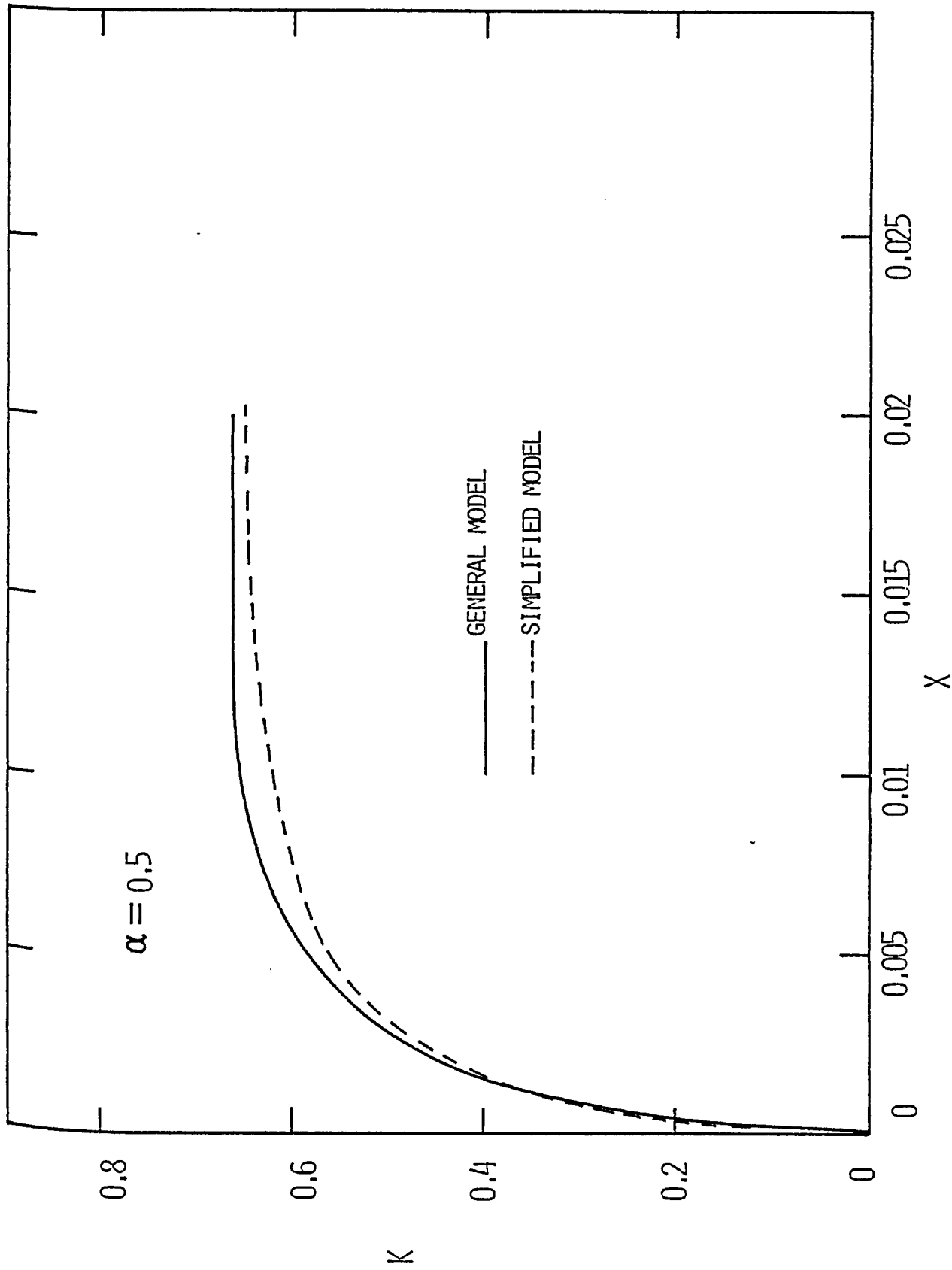


FIGURE 4.26 INCREMENTAL PRESSURE DROP NUMBER VARIATION
($\alpha = 0.50$)

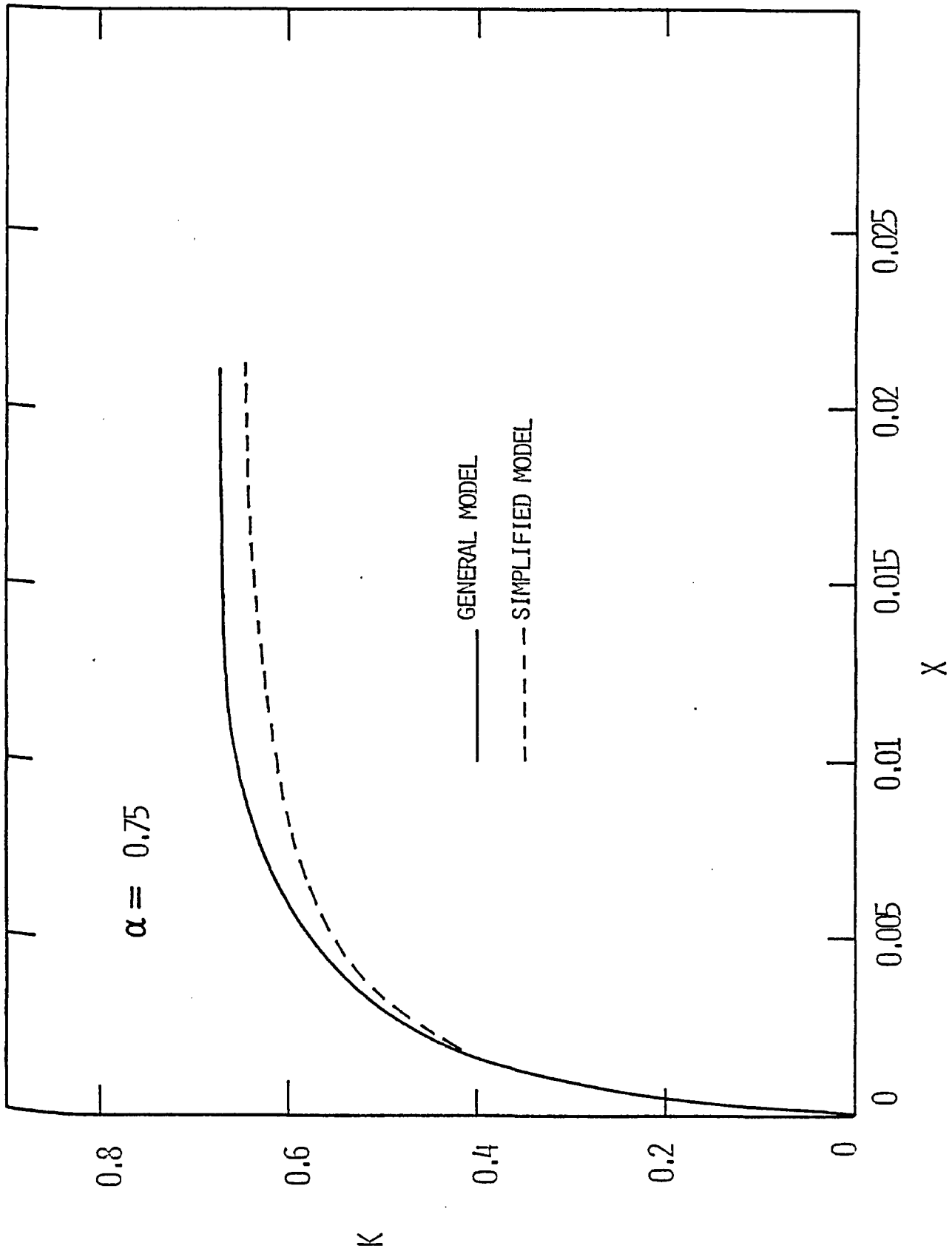


FIGURE 4.27 INCREMENTAL PRESSURE DROP NUMBER VARIATION
($\alpha = 0.75$)

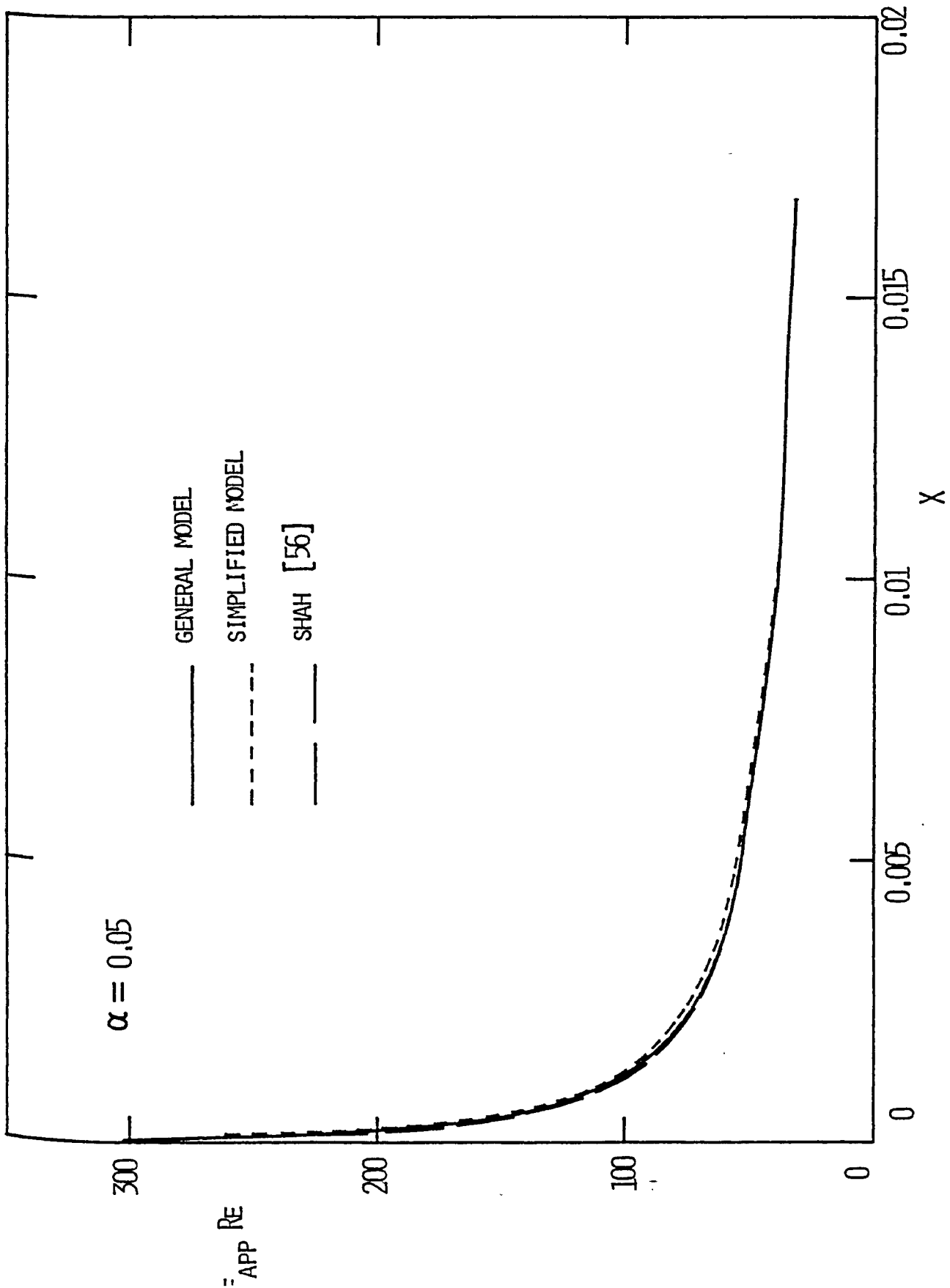


FIGURE 4.28 $F_{APP} RE$ VARIATION
($\alpha = 0.05$)

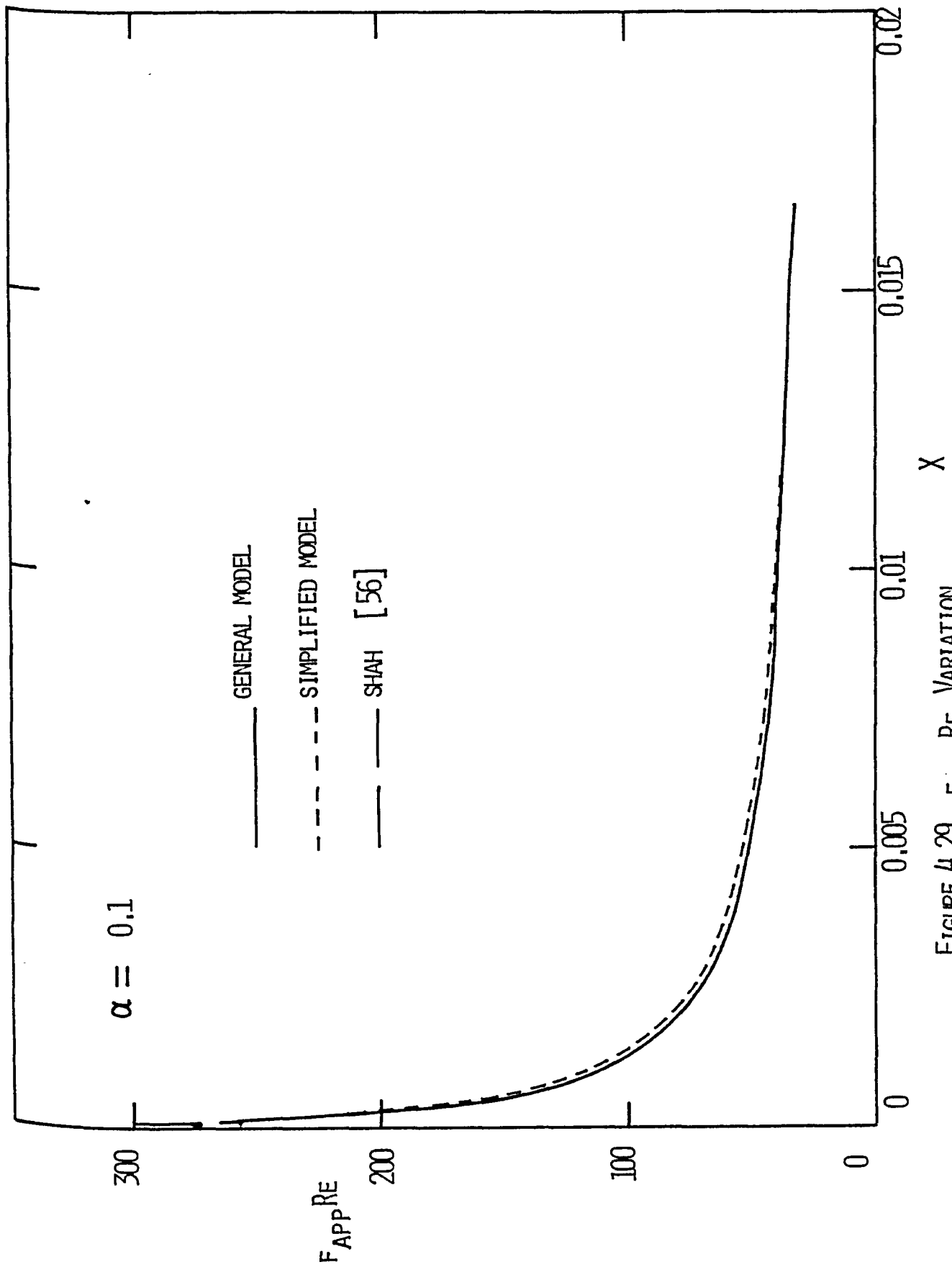


FIGURE 4.29 $F_{APP,RE}$ VARIATION
($\alpha = 0.1$)

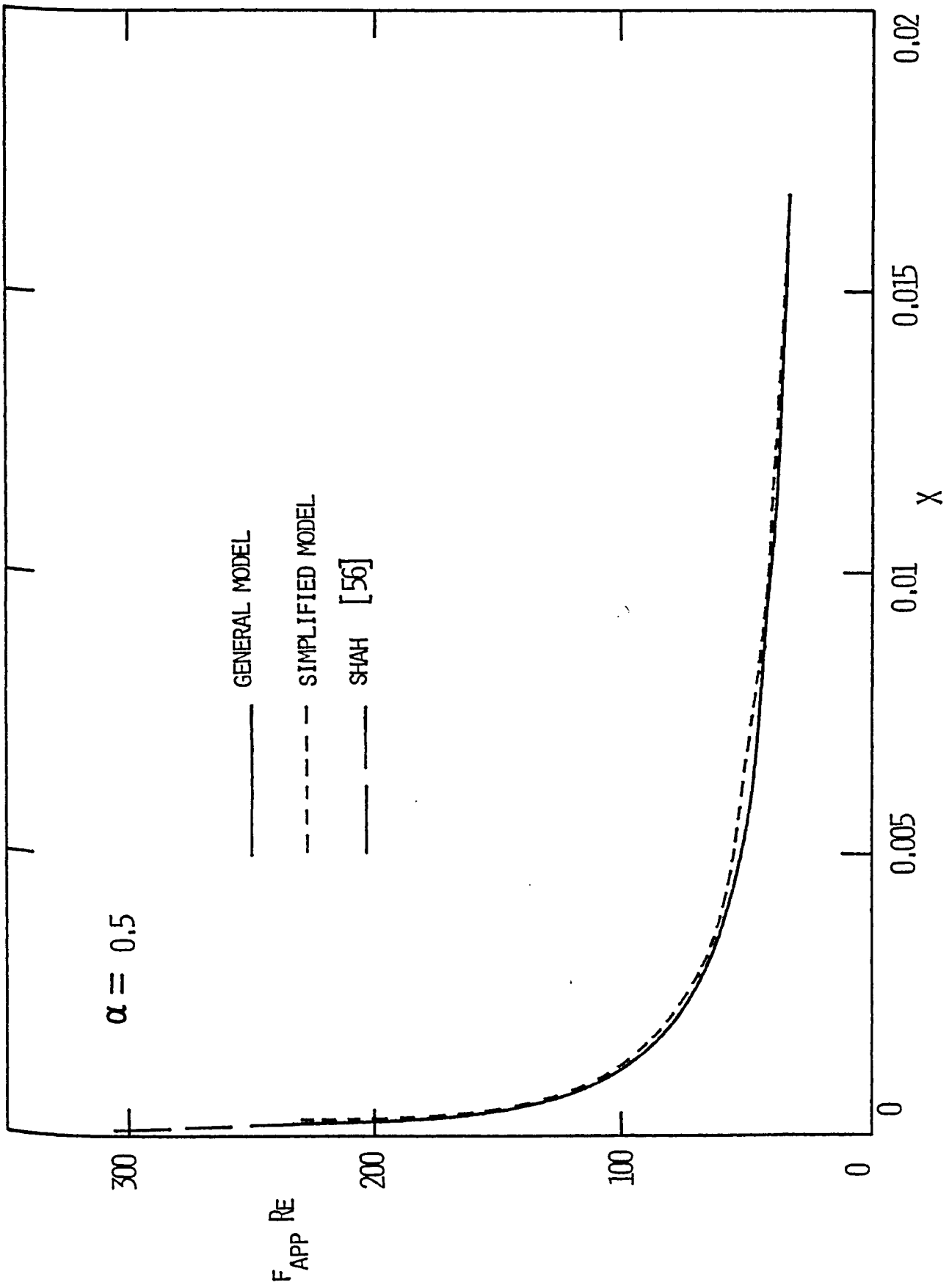


FIGURE 4.30 F_{APP} RE VARIATION
($\alpha = 0.5$)

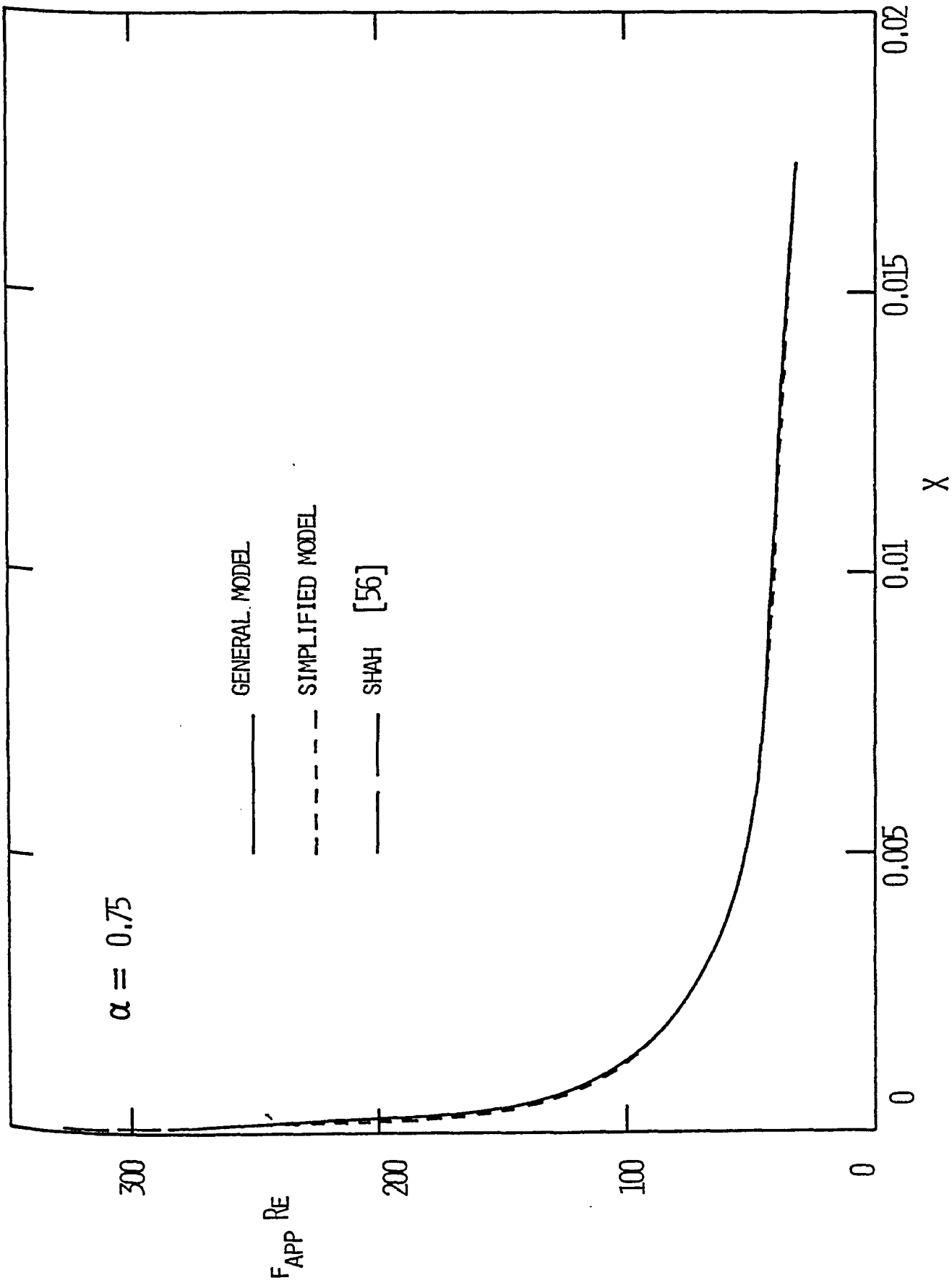


FIGURE 4.31 $F_{APP} RE$ VARIATION
($\alpha = 0.75$)

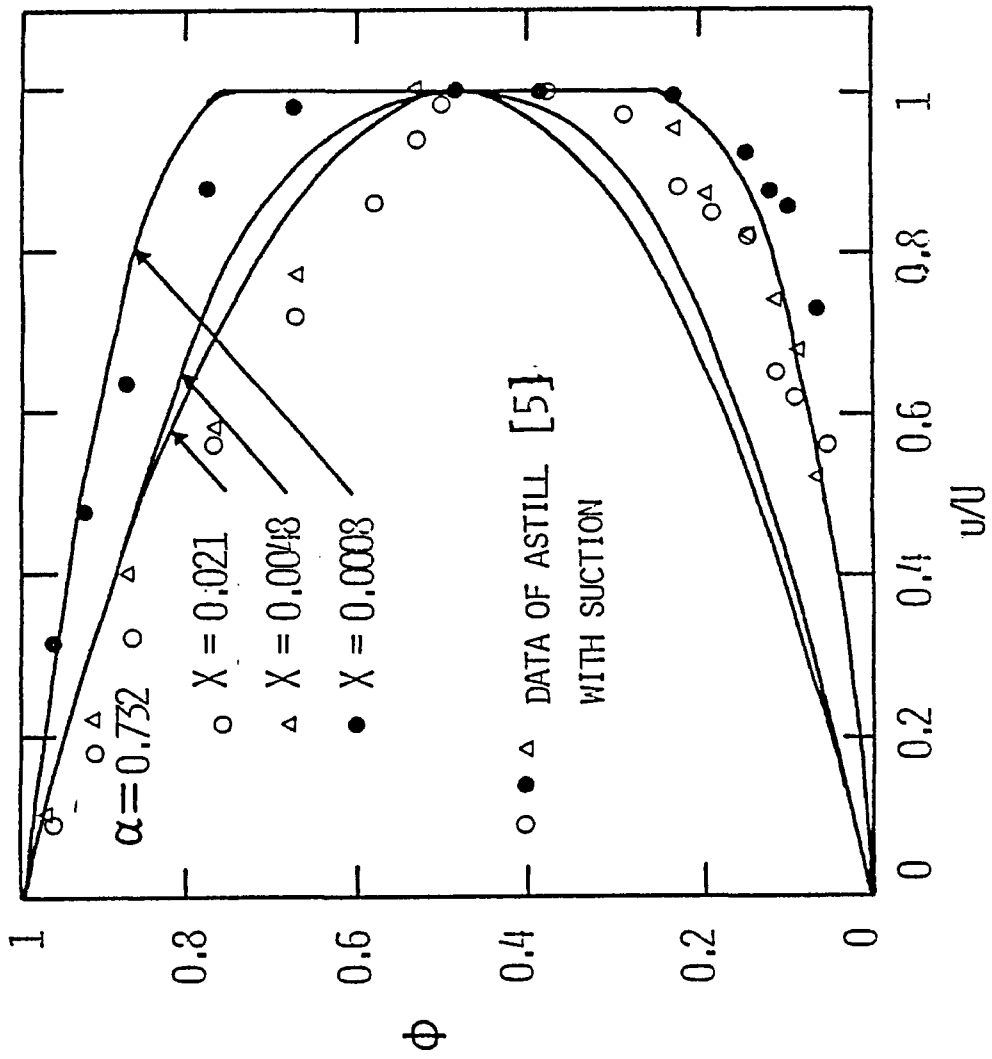


FIGURE 4.32 COMPARISON WITH EXPERIMENTAL DATA WITH SUCTION

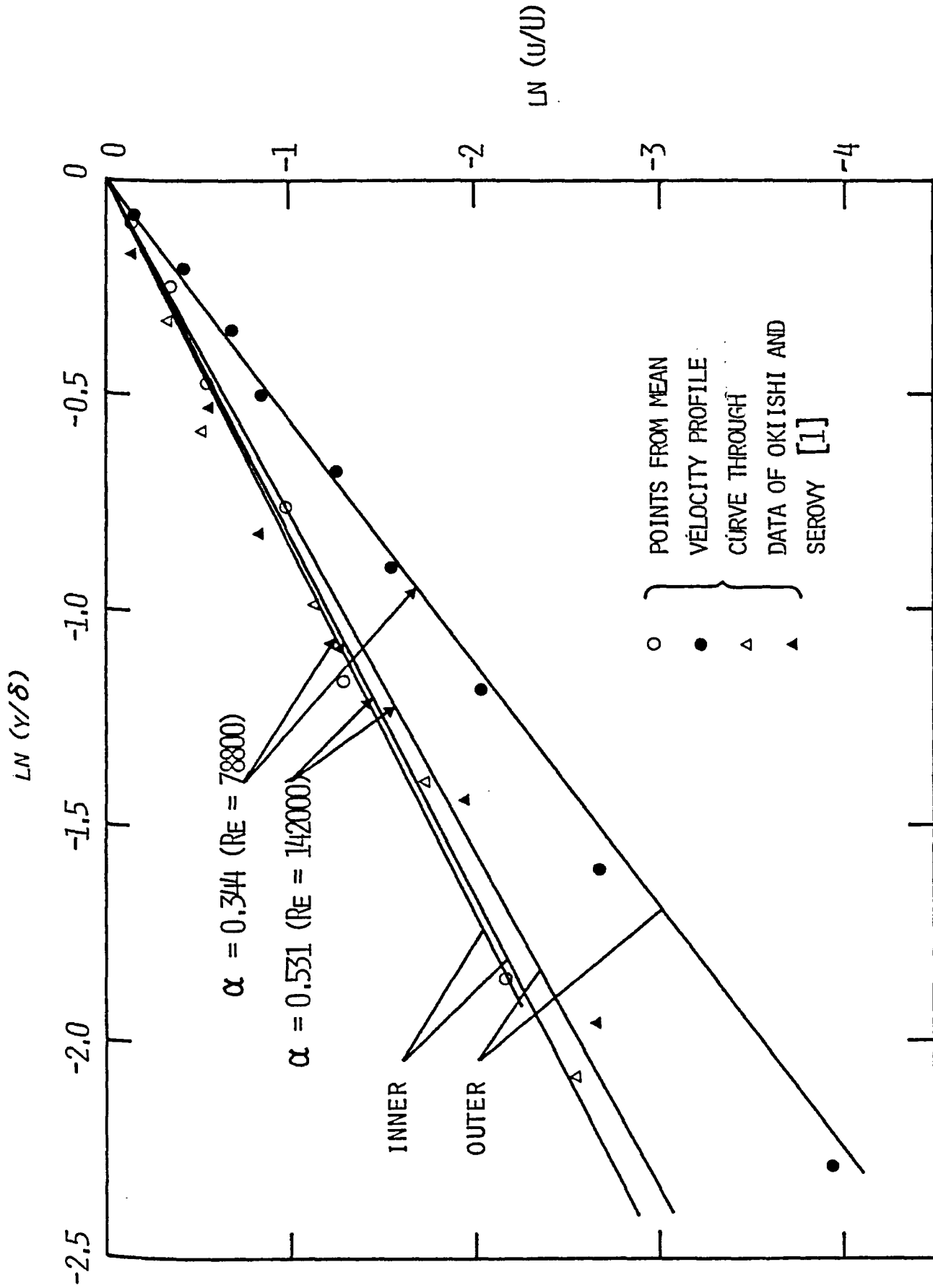


FIGURE 4.33 $\text{LN}(u/U)$ vs. $\text{LN}(y/\delta)$

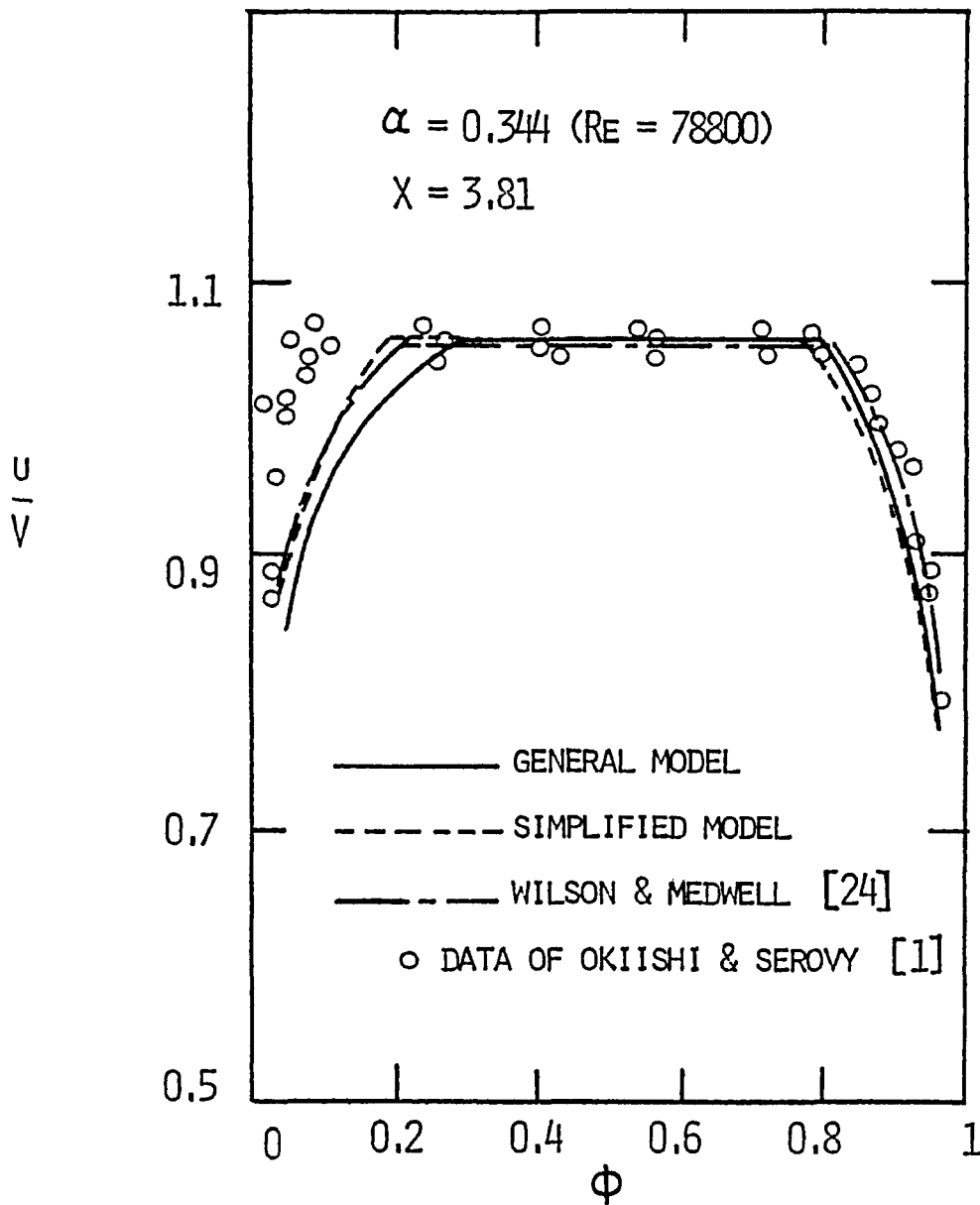


FIGURE 4.34 NON-DIMENSIONAL VELOCITY PROFILES
($\alpha = 0.344$ (RE = 78800); $X = 3.81$)

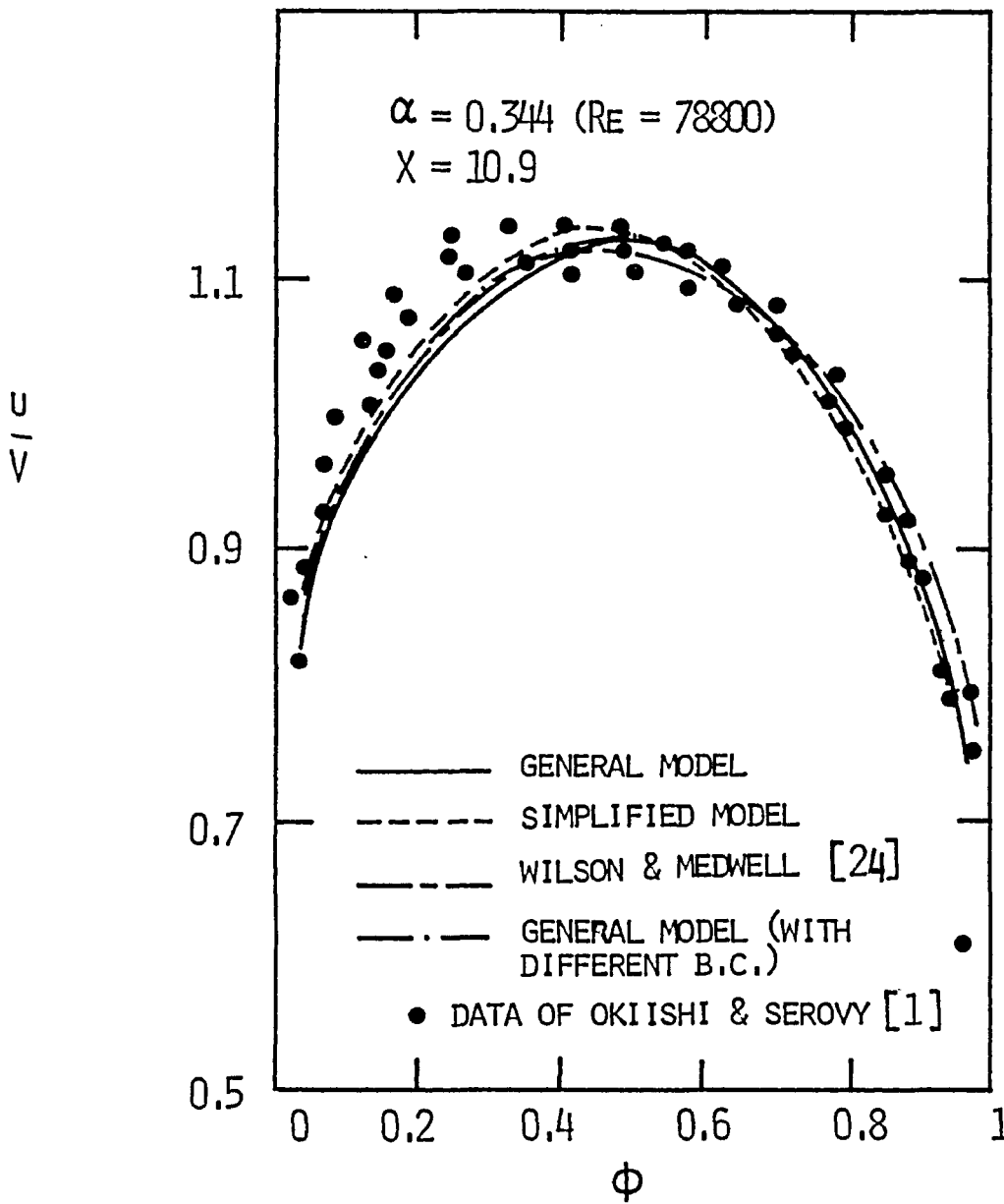


FIGURE 4.35 NON-DIMENSIONAL VELOCITY PROFILES
 ($\alpha = 0.344$ ($Re = 78800$); $X = 10.9$)

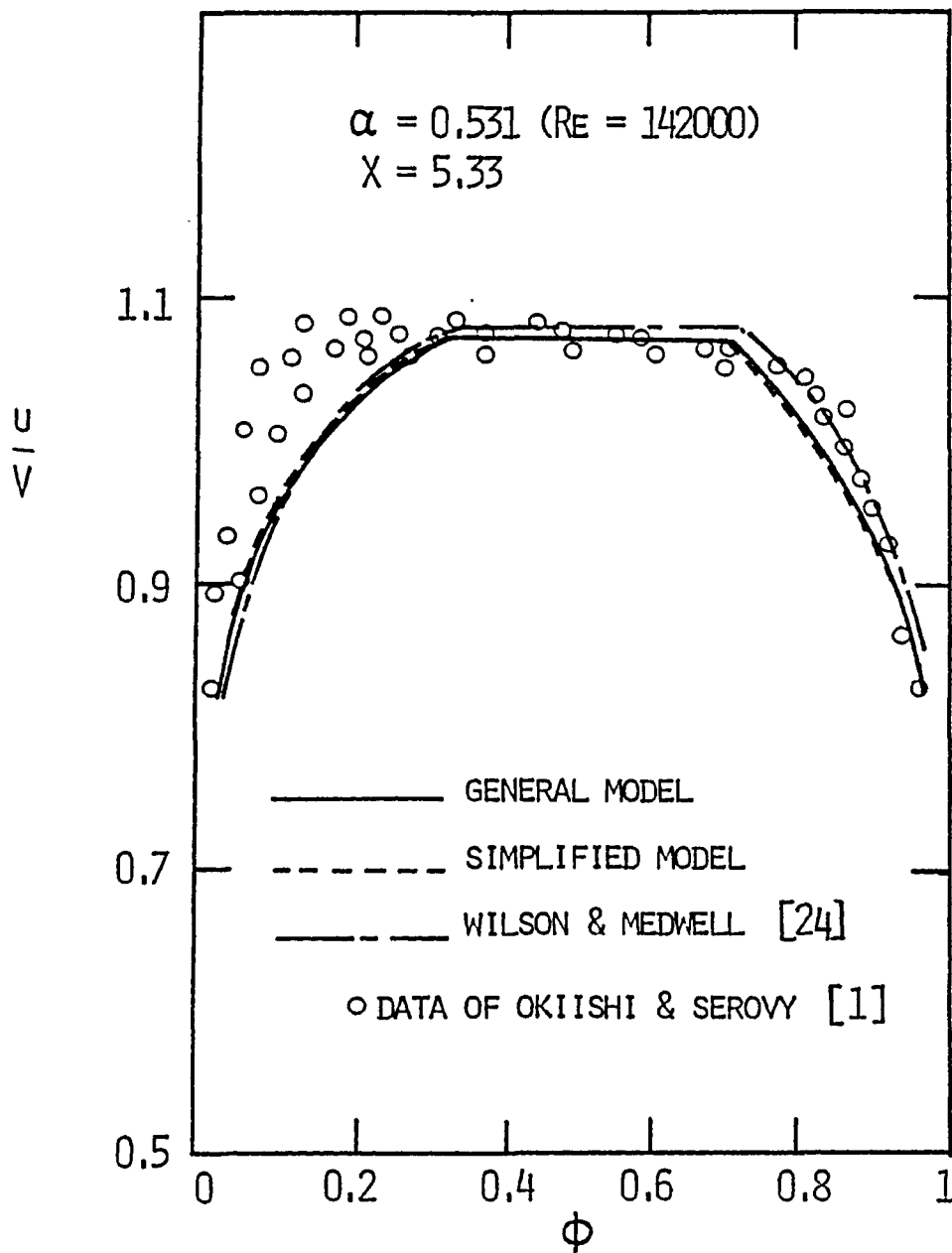


FIGURE 4.36 NON-DIMENSIONAL VELOCITY PROFILES
($\alpha = 0.531$ (Re = 142000))

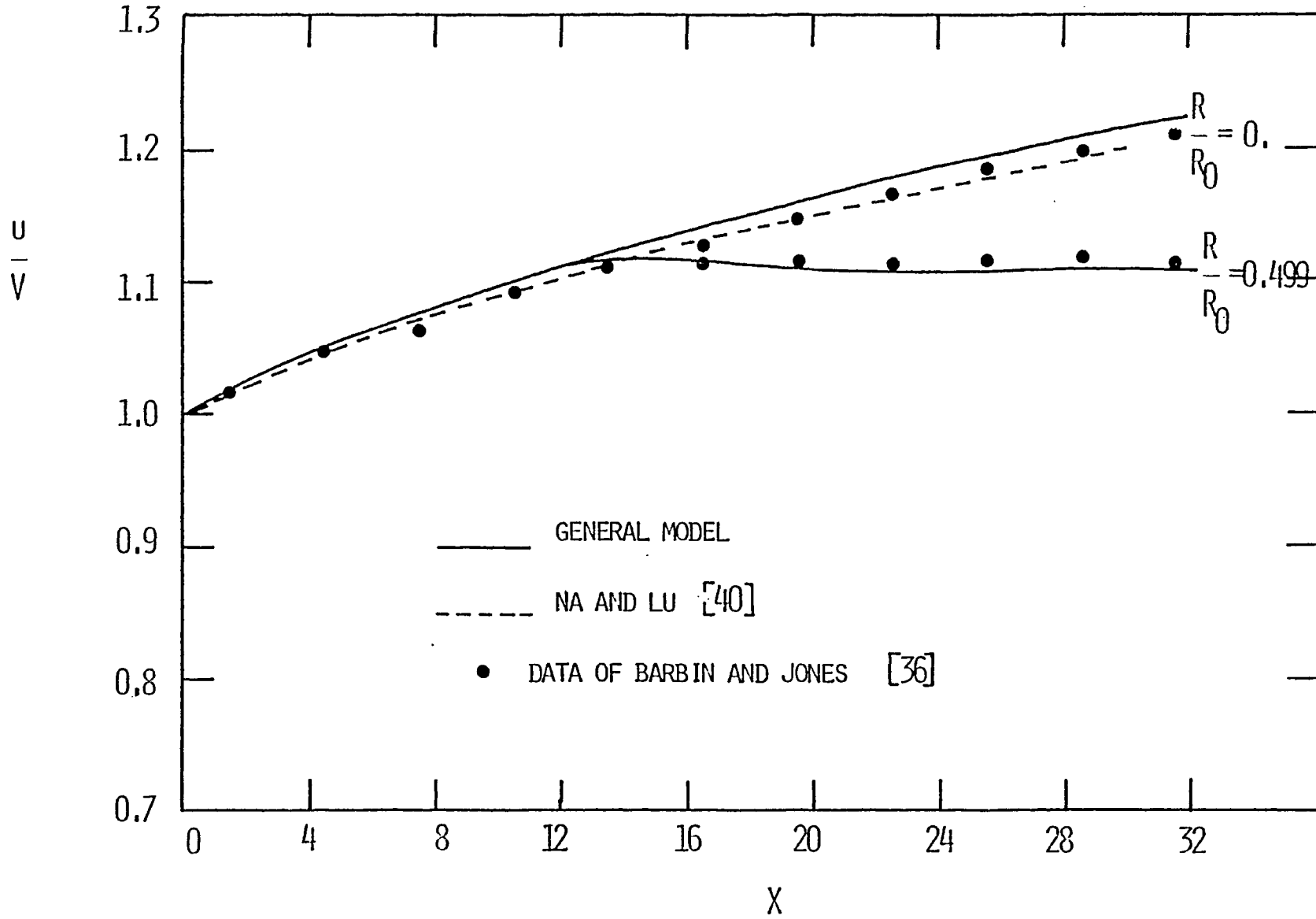


FIGURE 4.37 NON-DIMENSIONAL VELOCITY PROFILES
 ($\alpha = 0$ ($Re = 388000$); $R/R_0 = 0$ AND 0.499)

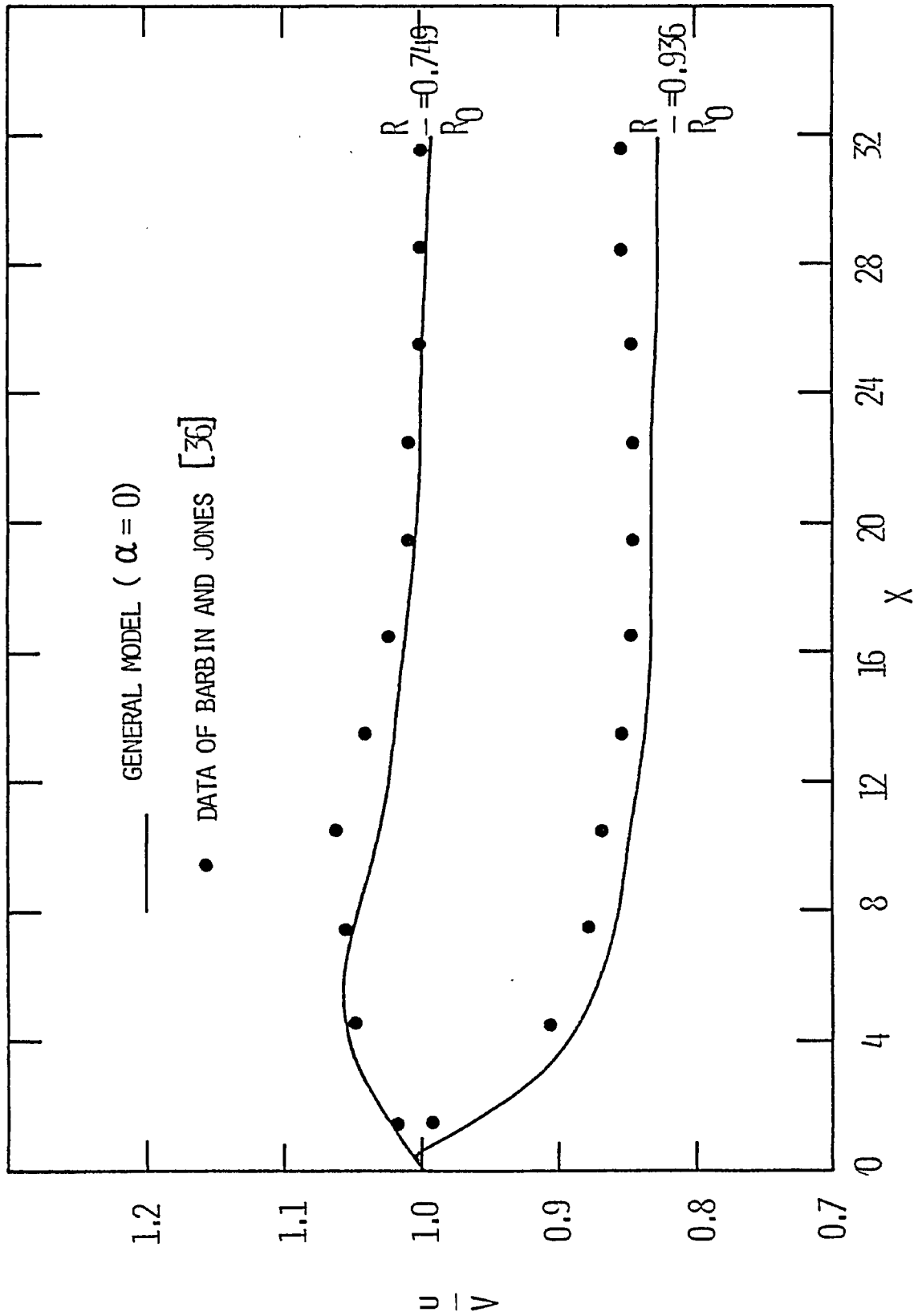


FIGURE 4.38 NON-DIMENSIONAL VELOCITY PROFILES
($\alpha = 0$ ($Re = 388000$); $R/R_0 = 0.749$ AND 0.936)

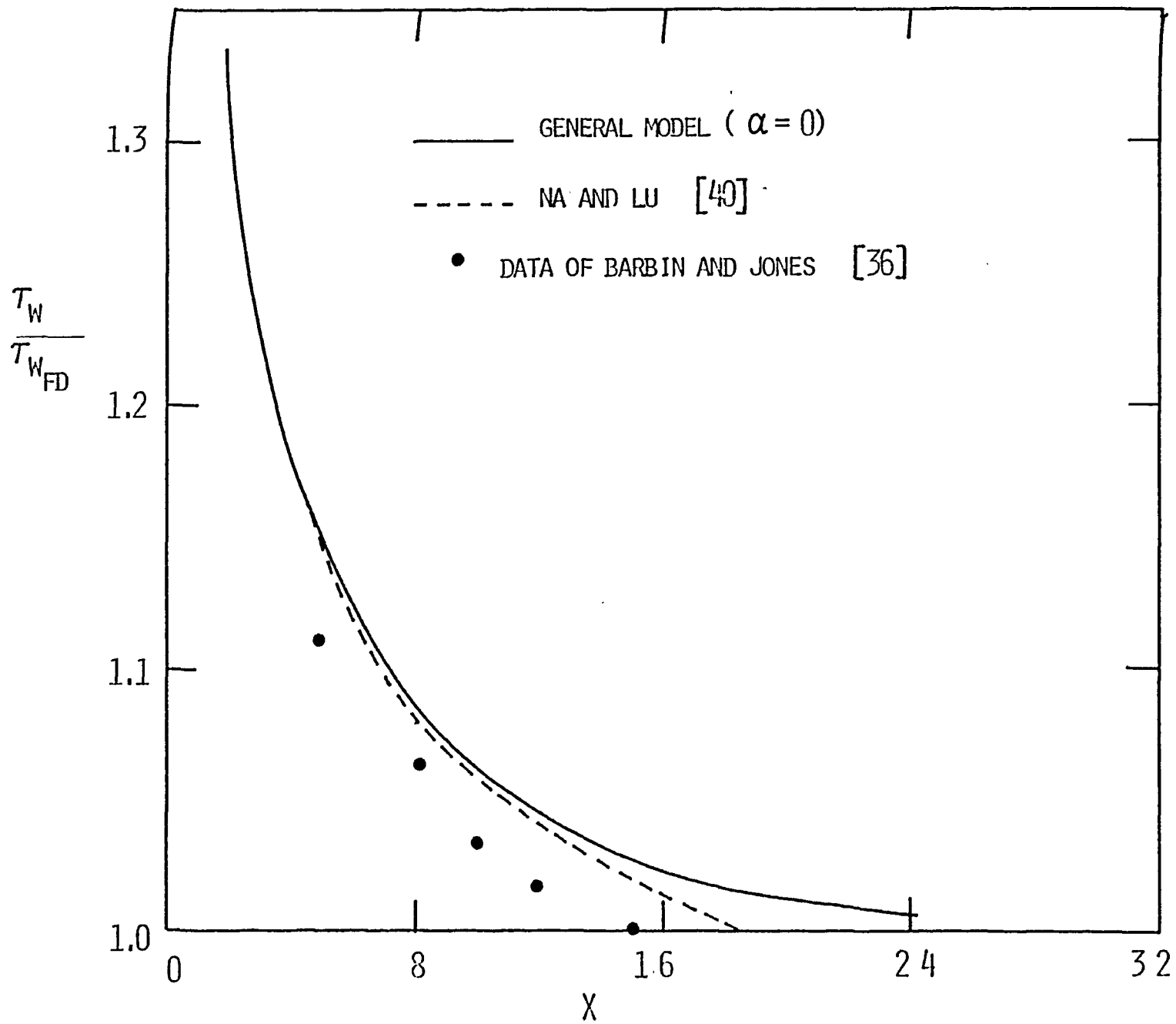


FIGURE 4.39 COMPARISON WITH PREDICTED SHEAR STRESS VARIATION
($\alpha = 0$ (PIPE); $RE = 388000$)

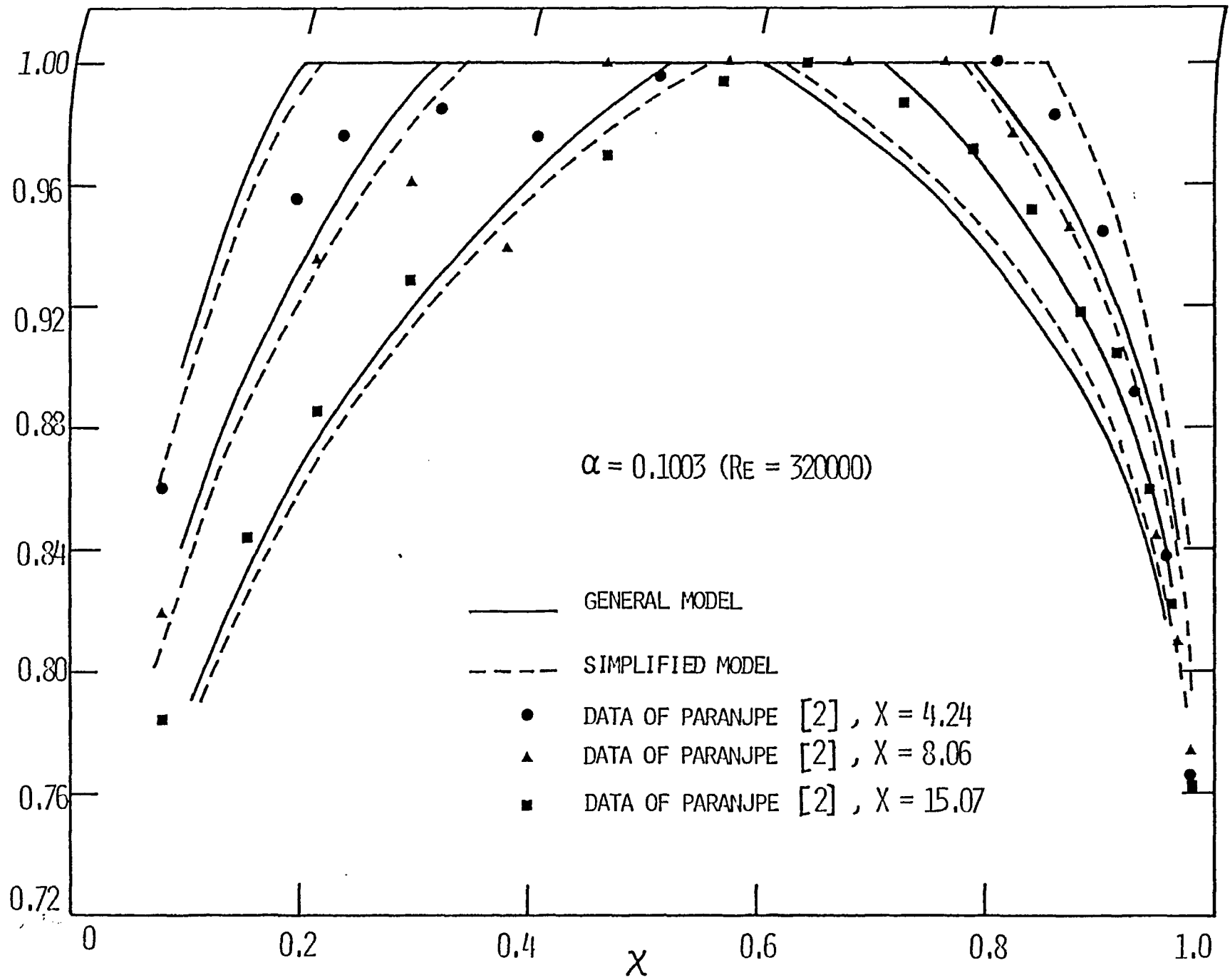


FIGURE 4.40 NON-DIMENSIONAL VELOCITY PROFILES
 ($\alpha = 0.1002 \text{ (Re} = 320000\text{)}$).

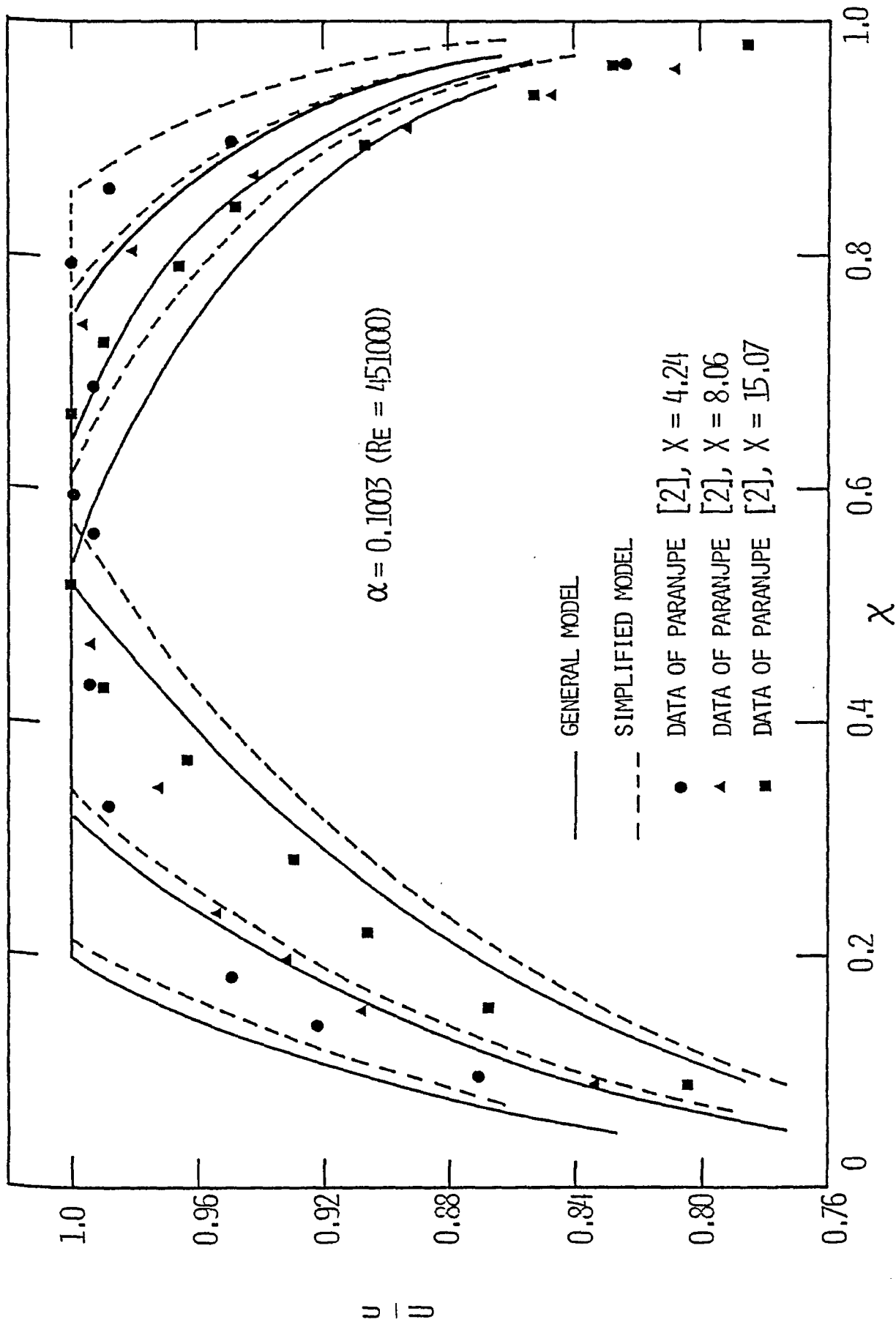


FIGURE 4.41 NON-DIMENSIONAL VELOCITY PROFILES
 ($\alpha = 0.1002 \text{ (Re} = 451000\text{)}$)

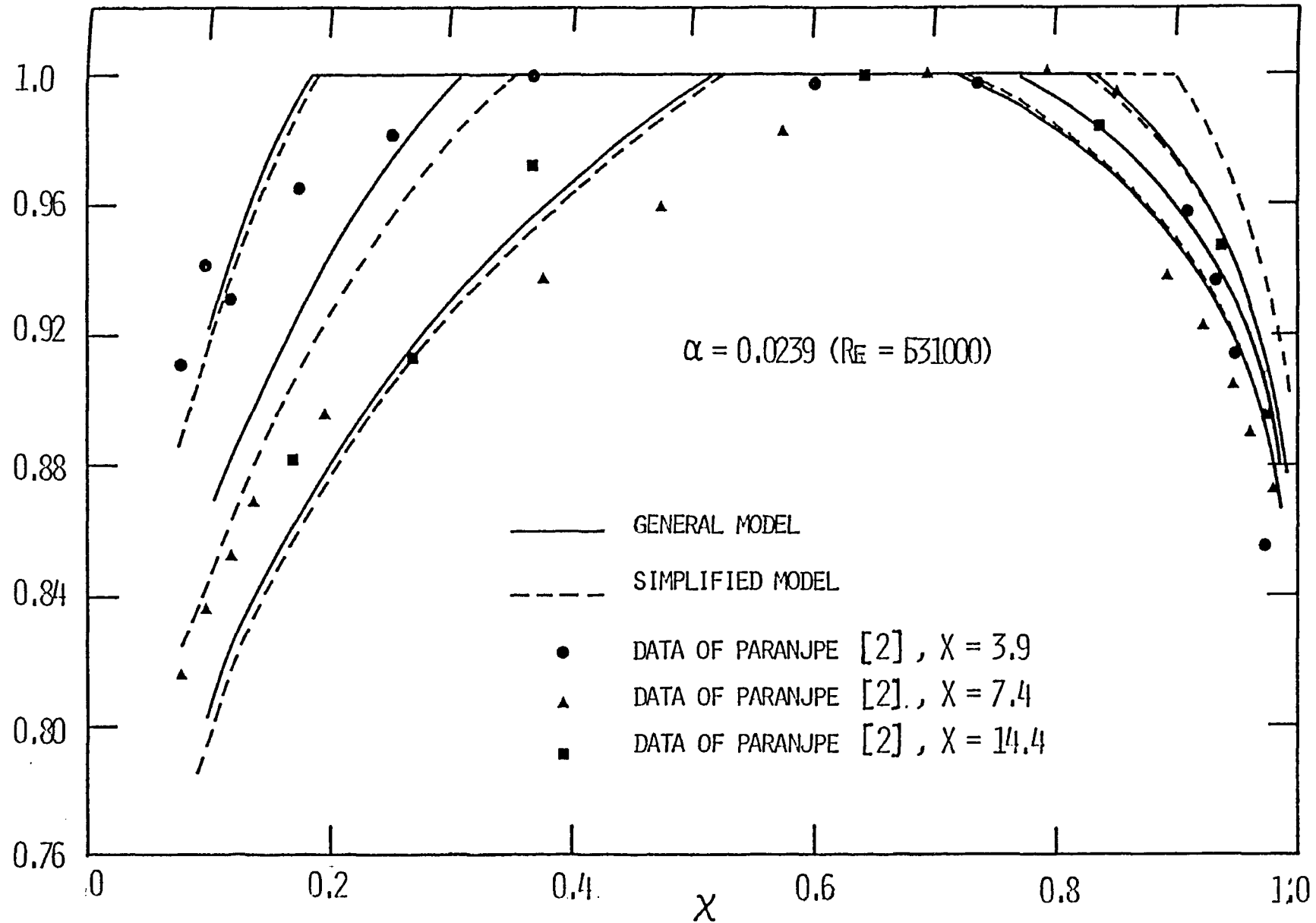


FIGURE 4.42 Non-DIMENSIONAL VELOCITY PROFILES
 ($\alpha = 0.0239 (Re = 531000)$)

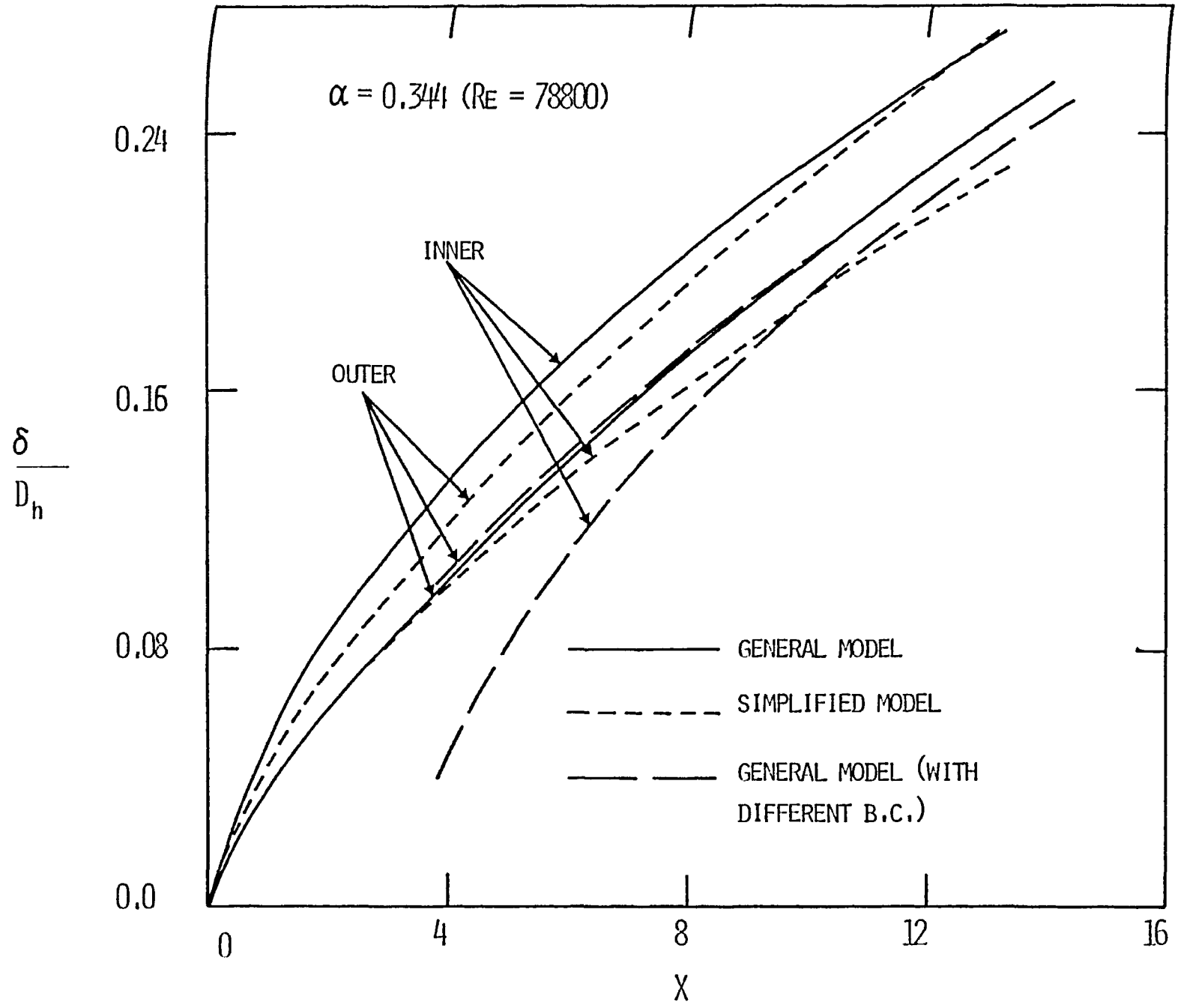


FIGURE 4.43 PREDICTED WALL LAYER GROWTH
($\alpha = 0.344$ ($Re = 78800$))

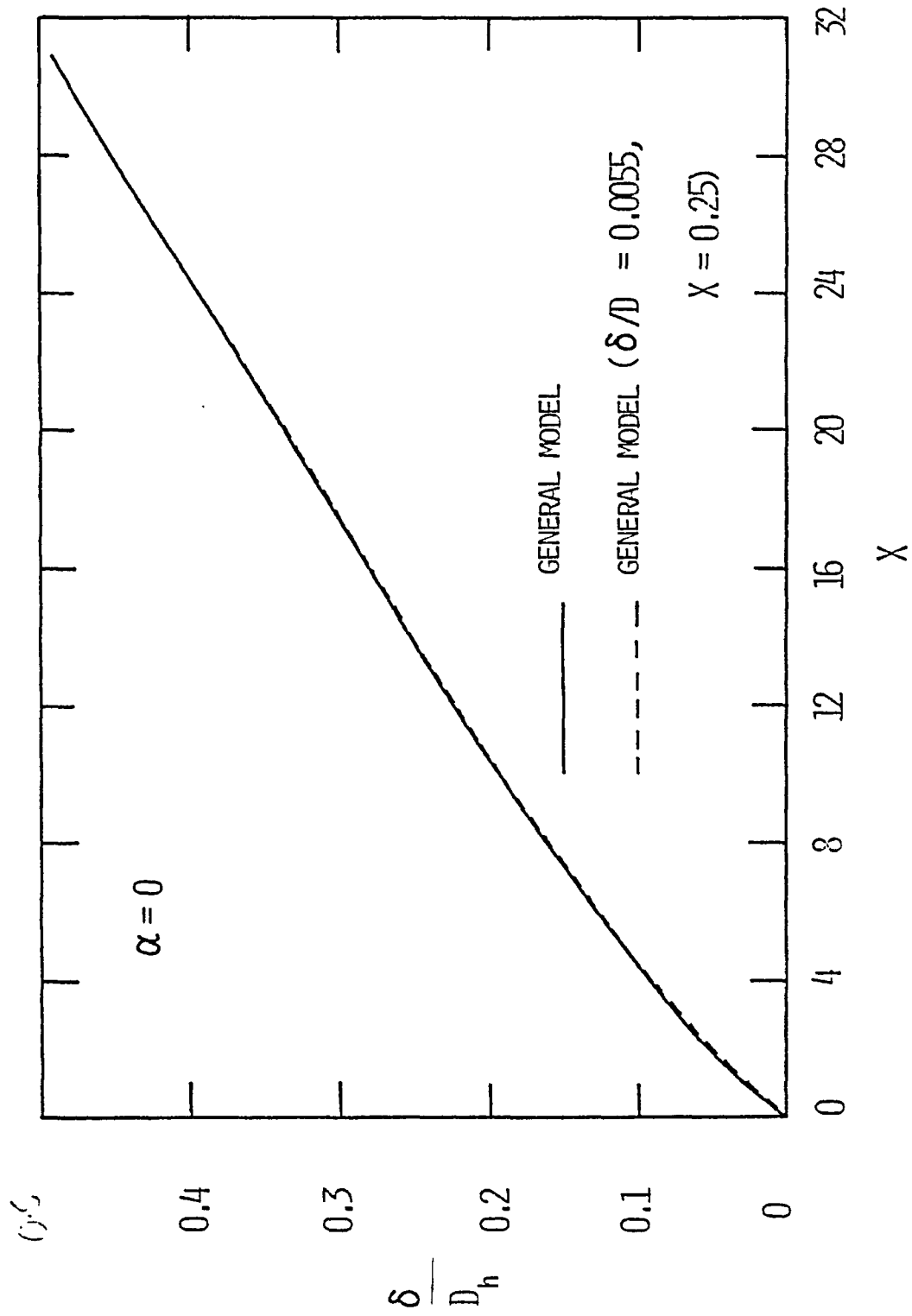


FIGURE 4.44 PREDICTED WALL LAYER GROWTH
($\alpha = 0$ (RE = 388000))

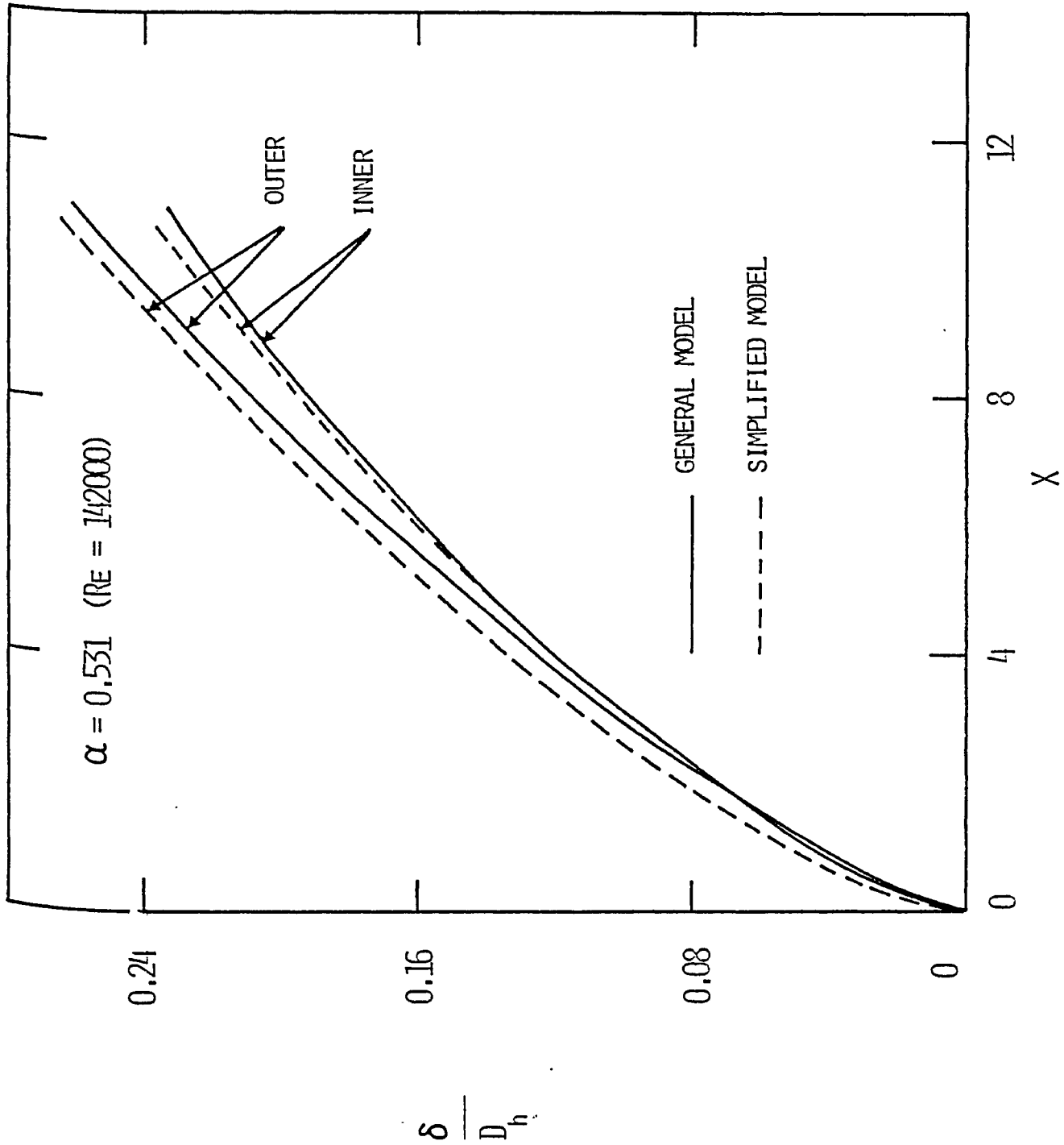


FIGURE 4.45 PREDICTED WALL LAYER GROWTH
($\alpha = 0.531$ (RE = 142000))

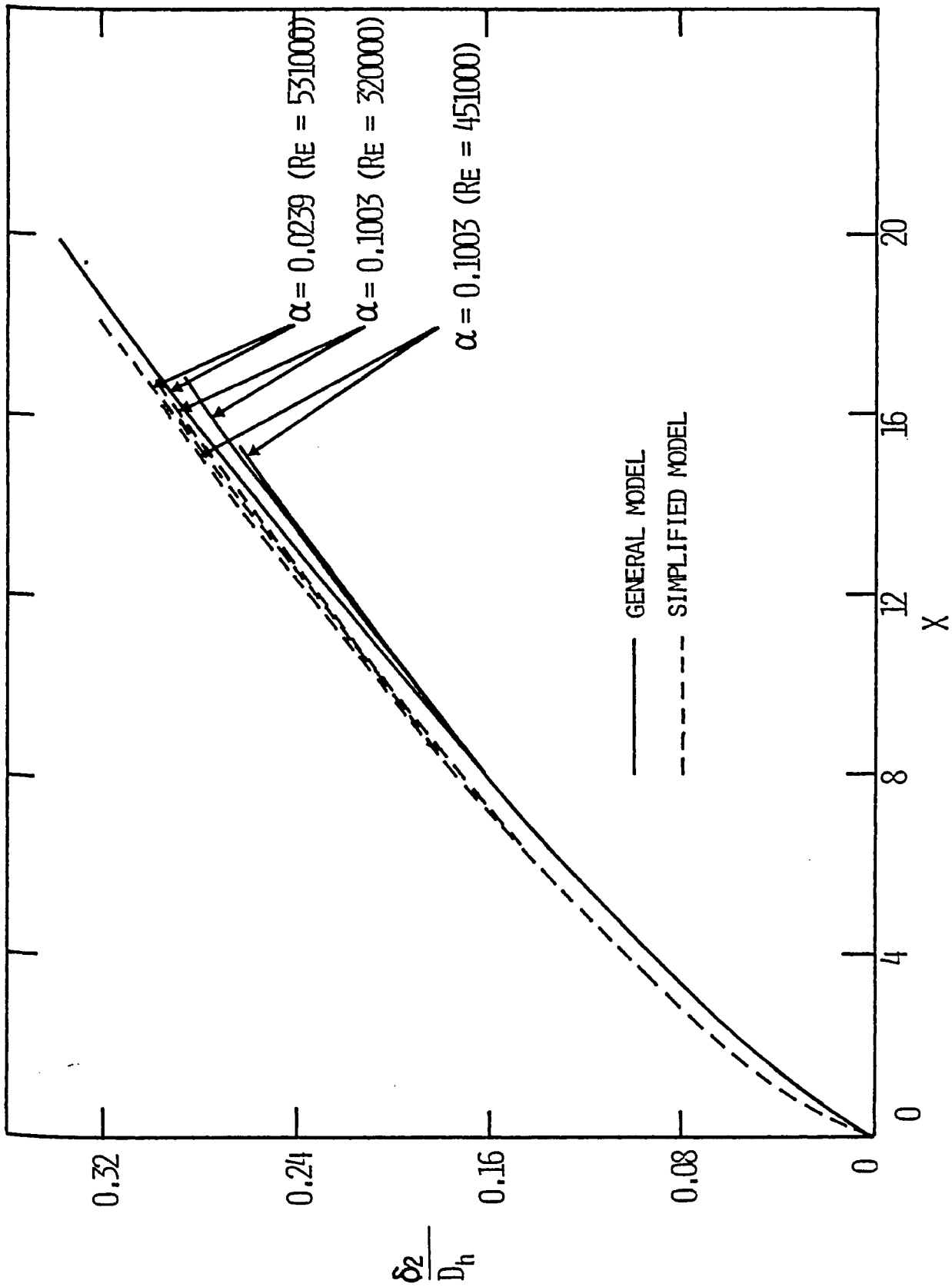


FIGURE 4.46 PREDICTED OUTER WALL LAYER GROWTH

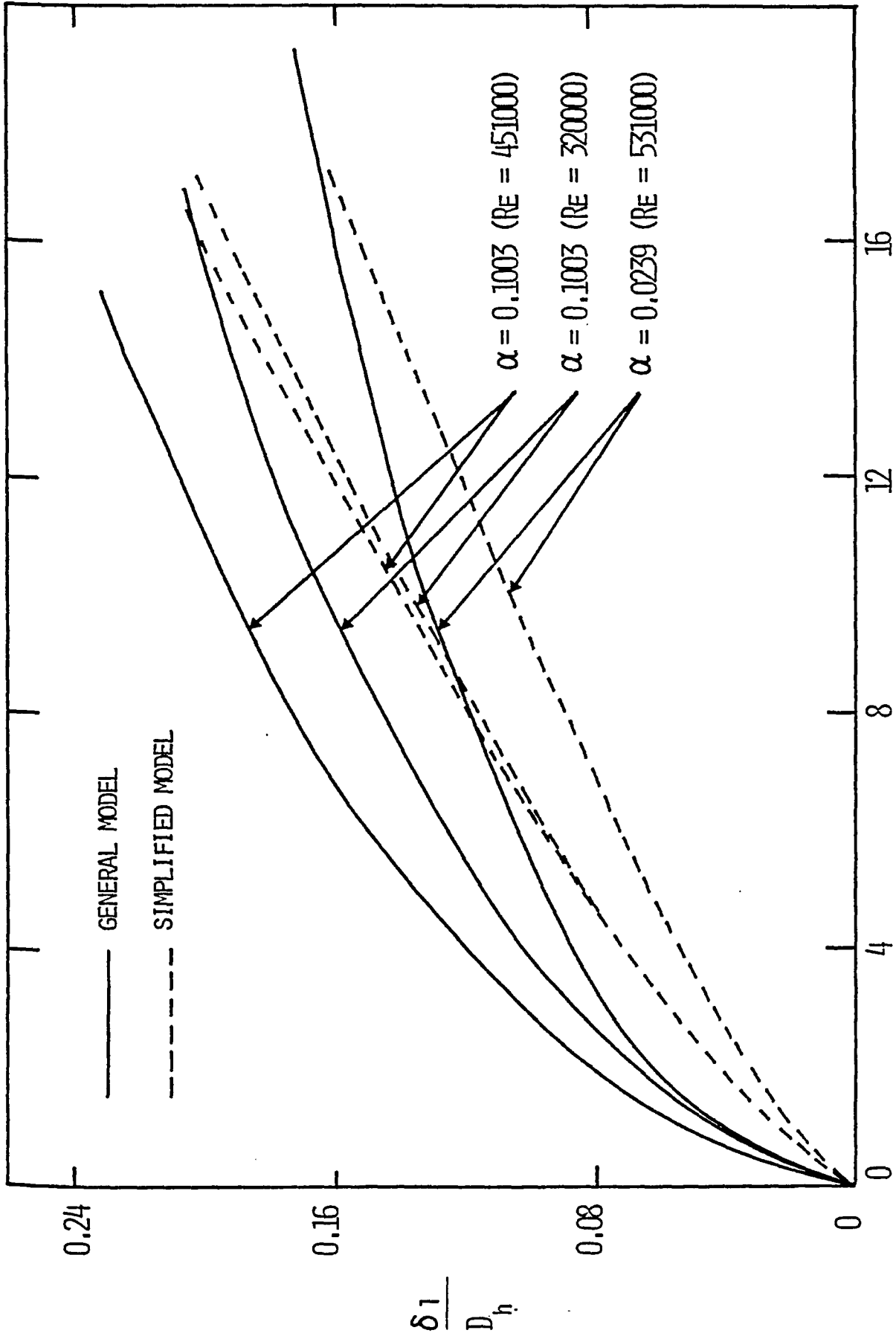


FIGURE 4.47 PREDICTED INNER WALL LAYER GROWTH

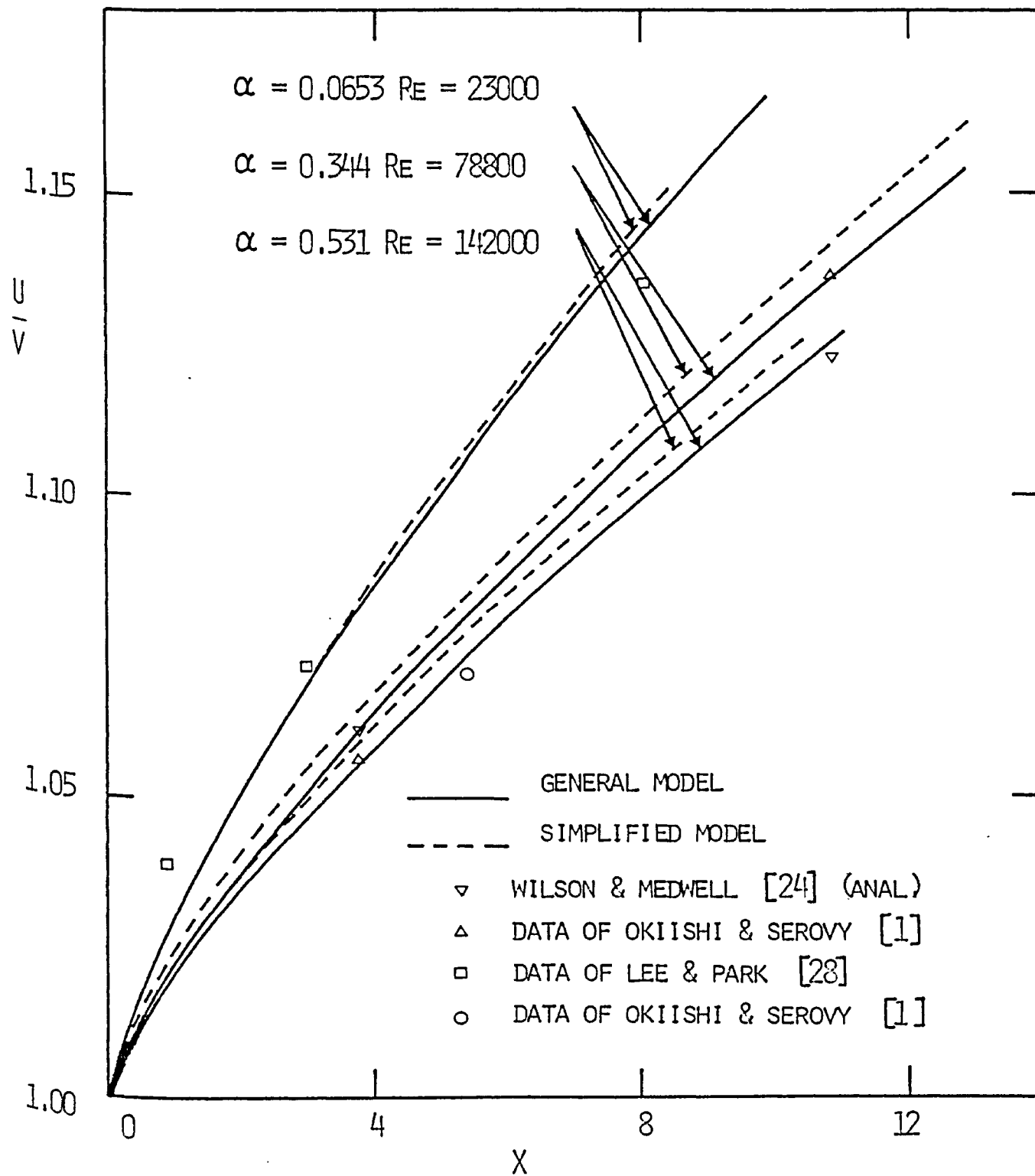


FIGURE 4.48 COMPARISON WITH PREDICTED CORE VELOCITY VARIATION

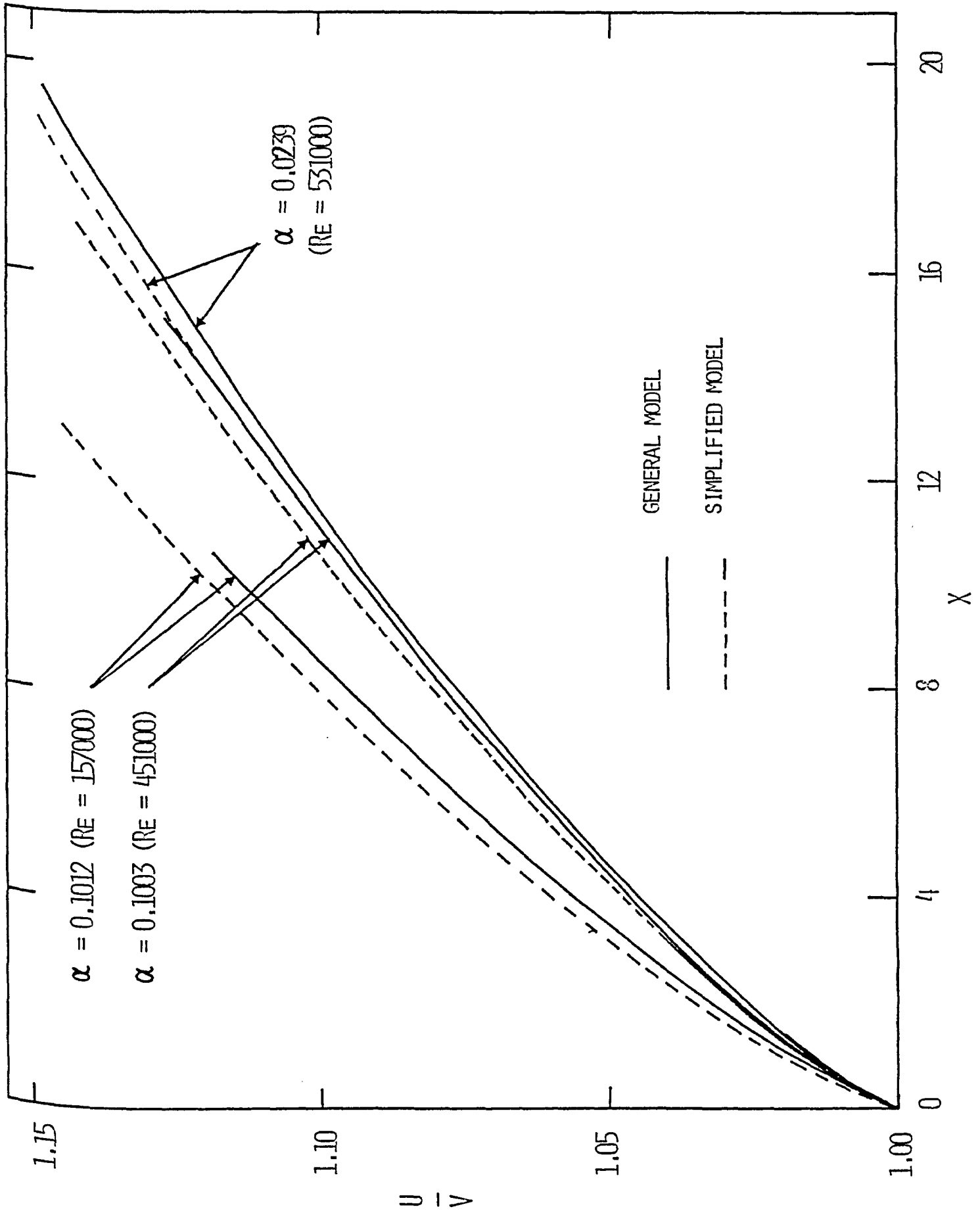


FIGURE 4.49 PREDICTED CORE VELOCITY VARIATION

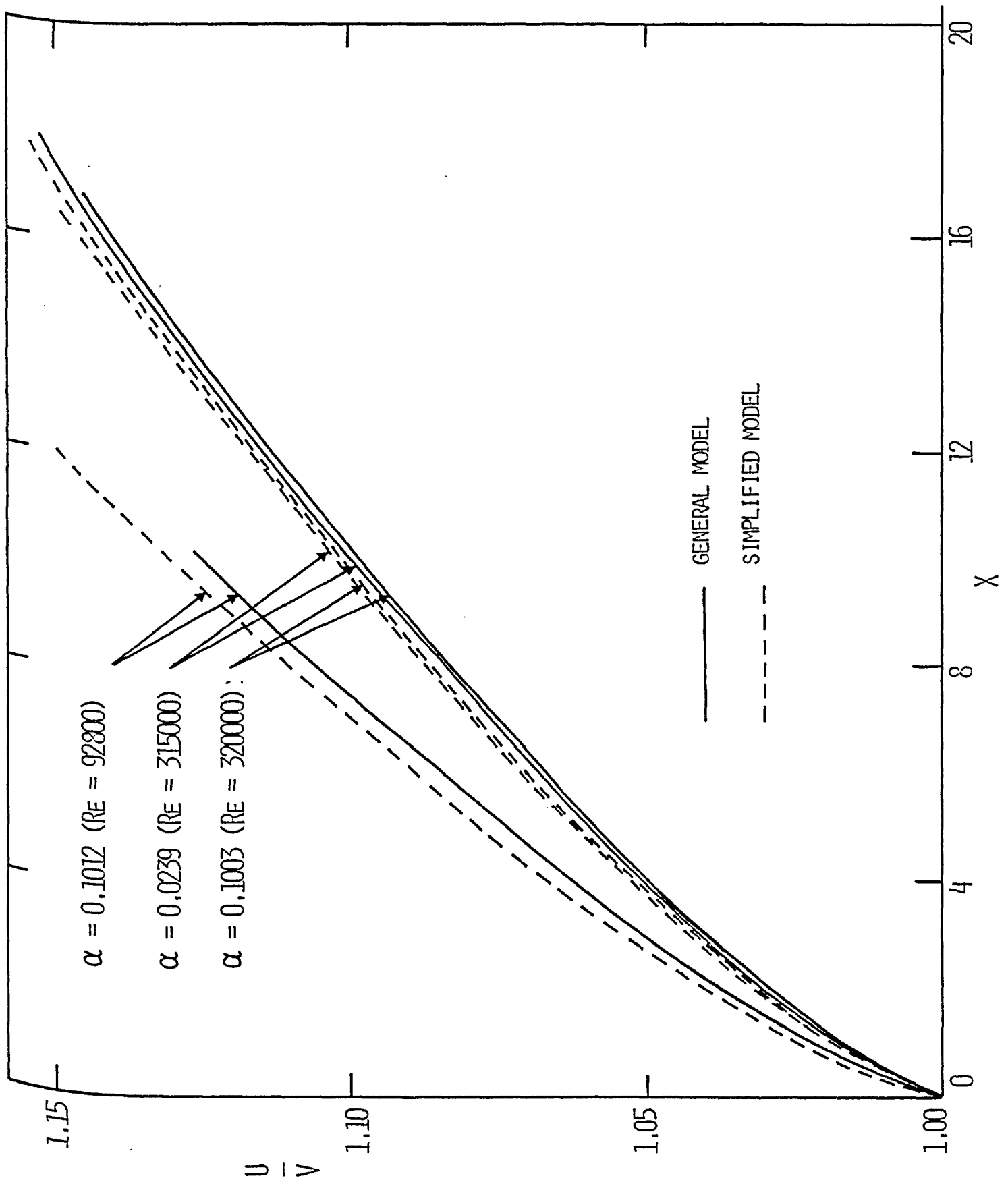


FIGURE 4.50 PREDICTED CORE VELOCITY VARIATION

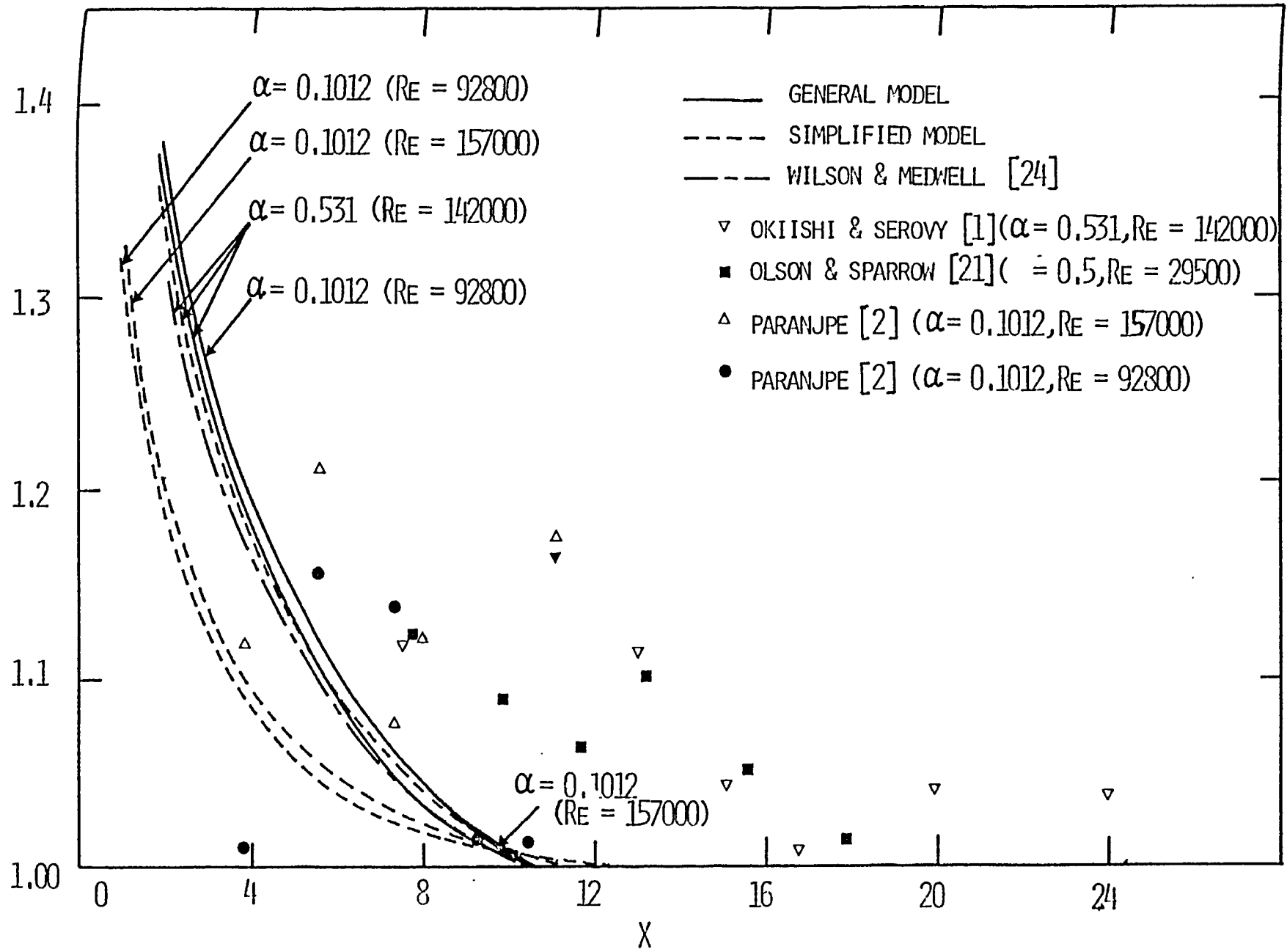


FIGURE 4.51 COMPARISON WITH PREDICTED PRESSURE GRADIENT VARIATION

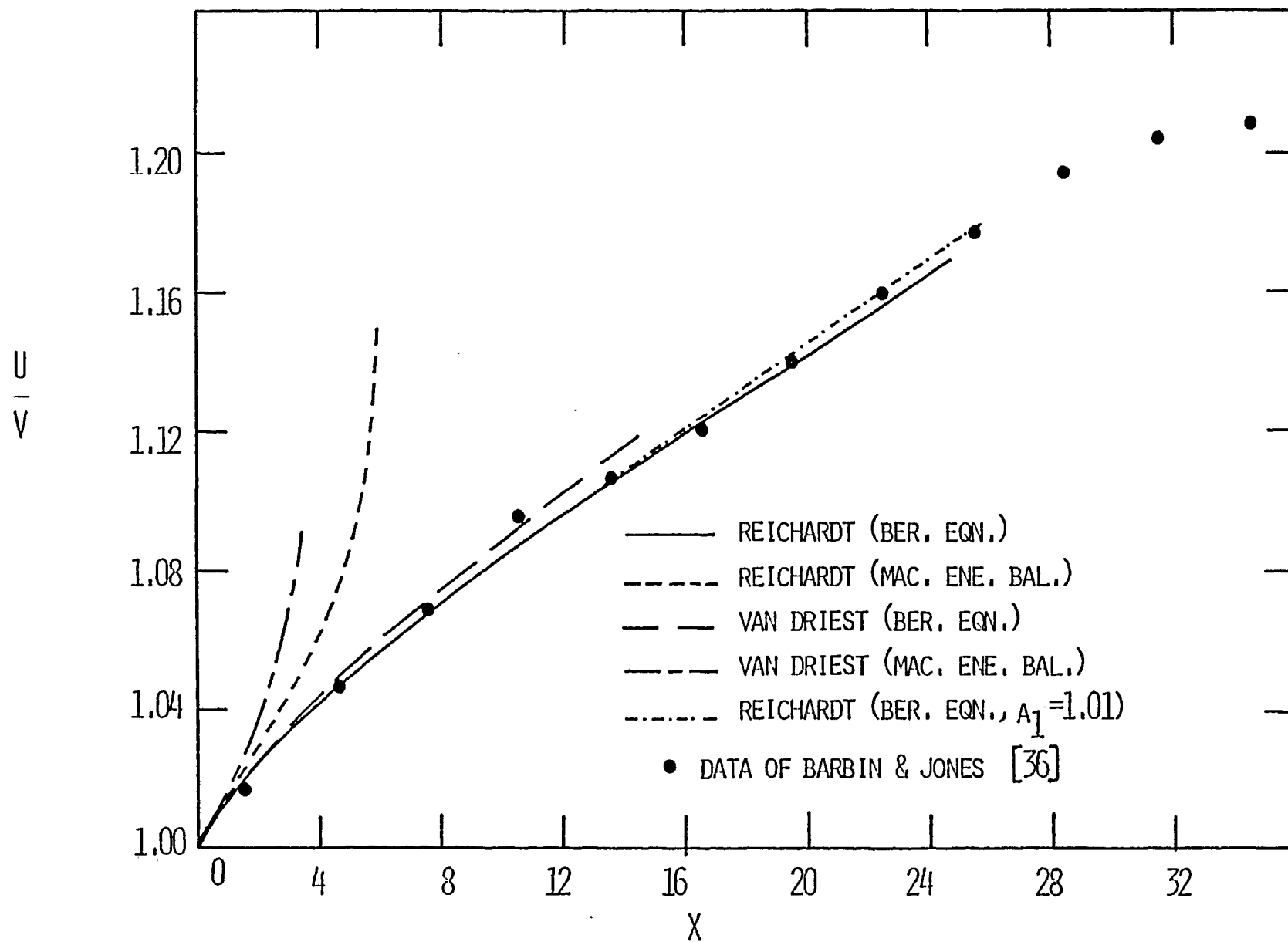


FIGURE 4.52 COMPARISON WITH PREDICTED CORE VELOCITY VARIATION
 ($\alpha = 0$ ($Re = 383000$))

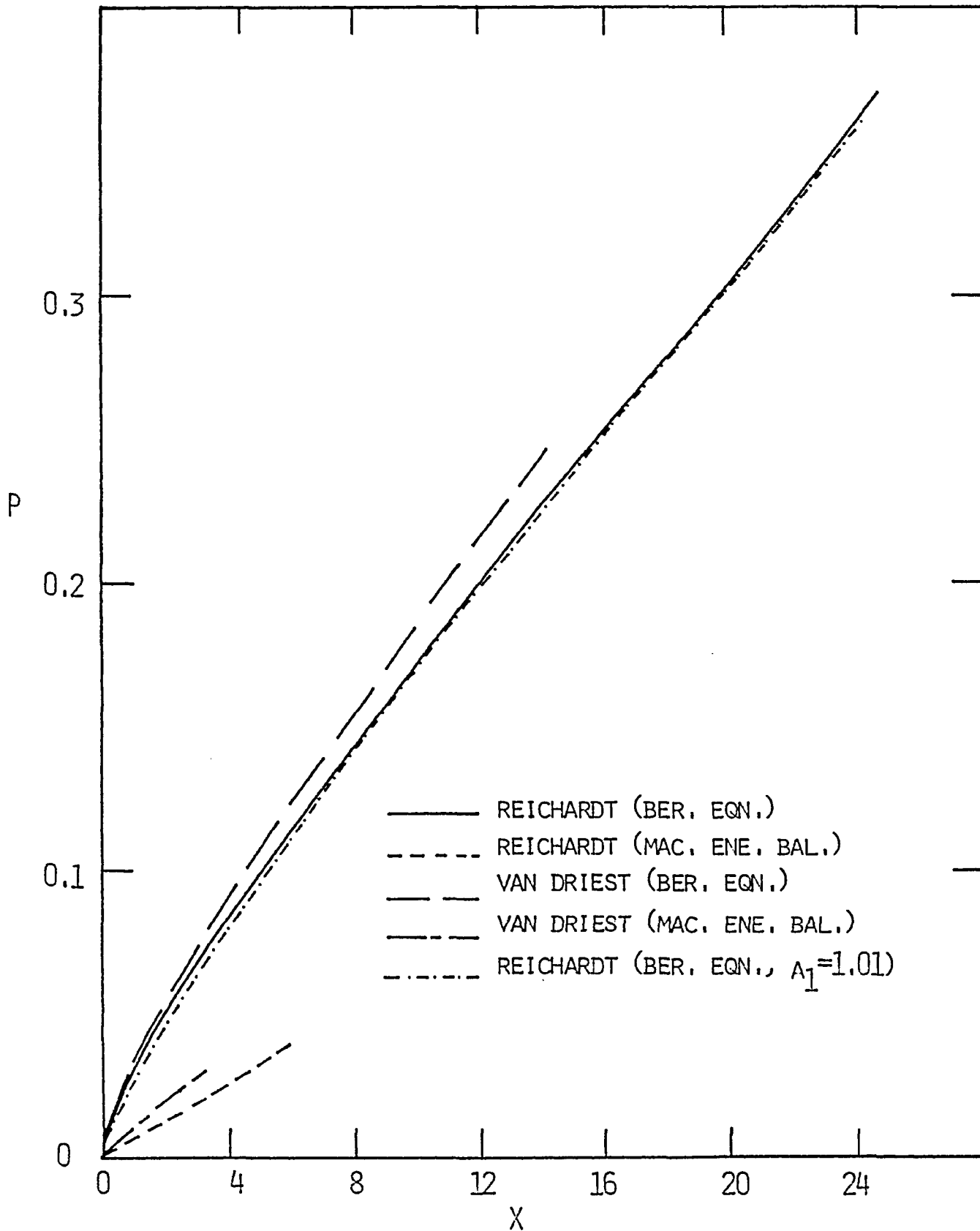


FIGURE 4.53 PRESSURE VARIATION
 ($\alpha = 0$ ($RE = 388000$))

APPENDIX A

DETAILS OF FORMULATIONS

A.1 Hydrodynamic developing laminar annular flows

(a) Simplified Model:

$$\begin{aligned}
& \rho d \left[\int_{R_1}^{R_2} u^2 2\pi R dR \right] = \\
& \pi \rho V^2 d \left[\frac{U^2}{V^2} \left\{ \frac{R_1^2}{B_1} \frac{\left[\frac{11}{6} - 3B_1 + \frac{3}{2}B_1^2 - \frac{B_1^3}{3} + \epsilon n B_1 \right]}{[1 - B_1 + \epsilon n B_1]^2} \right. \right. \\
& \left. \left. - \frac{R_2^2}{B_2} \frac{\left[\frac{11}{6} - 3B_2 + \frac{3}{2}B_2^2 - \frac{B_2^3}{3} + \epsilon n B_2 \right]}{[1 - B_2 + \epsilon n B_2]^2} \right\} \right] \\
& = \pi \rho V^2 d \left[A_{13}^2 \left\{ R_1^2 A_{12} - R_2^2 (A_{12})_{B_1=B_2} \right\} \right] \\
& = \pi \rho V^2 \left[A_{13}^2 d \left\{ R_1^2 A_{12} - R_2^2 (A_{12})_{B_1=B_2} \right\} + \right. \\
& \quad \left. 2 \left\{ R_1^2 A_{12} - R_2^2 (A_{12})_{B_1=B_2} \right\} A_{13} d (A_{13}) \right] \\
& = \pi \rho V^2 \left[A_{13}^2 R_1^2 A_{24} A_{12} dB_1 - A_{13}^2 R_2^2 (A_{24} A_{12})_{B_1=B_2} dB_2 \right. \\
& \quad \left. + 2 \left\{ R_1^2 A_{12} - R_2^2 (A_{12})_{B_1=B_2} \right\} A_{13}^2 (A_{22} dB_1 + A_{23} dB_2) \right]
\end{aligned}$$

$$\begin{aligned}
&= \pi \rho V^2 R_2^2 \left[\{ A_{13}^2 \alpha^2 A_{24} A_{12} + 2 A_{13}^2 [\alpha^2 A_{12} - (A_{12})_{B_1=B_2}] A_{22} \}^* \right. \\
&\quad \left. dB_1 + \{ -A_{13}^2 (A_{24} \cdot A_{12})_{B_1=B_2} + 2 A_{13}^2 * (\alpha^2 A_{12} - (A_{12})_{B_1=B_2})^* \right. \\
&\quad \left. A_{23} \} dB_2 \right]
\end{aligned}$$

$$\begin{aligned}
&= \pi \rho V^2 R_2^2 A_{13}^2 \left[\{ \alpha^2 A_{24} A_{12} + 2 [\alpha^2 A_{12} - (A_{12})_{B_1=B_2}] A_{22} \}^* \right. \\
&\quad \left. dB_1 + \{ - (A_{24} \cdot A_{12})_{B_1=B_2} + 2 (\alpha^2 A_{12} - (A_{12})_{B_1=B_2}) A_{23} \} dB_2 \right]
\end{aligned}$$

Also,

$$\begin{aligned}
&\pi \rho d \left[\int_{R_1}^{R_2} (u^3 - v^3) R dR \right] \\
&= \pi \rho d \left[\int_{R_1}^{R_2} u^3 R dR \right] - 0 \\
&= \pi \rho V^3 d \left[A_{13}^3 \frac{R_1^2}{2} A_{11} - A_{13}^3 \frac{R_2^2}{2} (A_{11})_{B_1=B_2} \right] \\
&= \pi \rho V^3 R_2^2 d \left[\frac{A_{13}^3}{2} \{ \alpha^2 A_{11} - (A_{11})_{B_1=B_2} \} \right] \\
&= \frac{\pi \rho V^3 R_2^2}{2} \left[A_{13}^3 \{ \alpha^2 A_{11} A_{21} dB_1 - (A_{11} A_{21})_{B_1=B_2} dB_2 \} \right. \\
&\quad \left. + 3 \{ \alpha^2 A_{11} - (A_{11})_{B_1=B_2} \} A_{13}^3 \{ A_{22} dB_1 + A_{23} dB_2 \} \right]
\end{aligned}$$

$$= \frac{\pi \rho V \alpha R_2^2}{2} A_{13}^3 [\{ \alpha^2 A_{11} A_{21} + 3 (\alpha^2 A_{11} - (A_{11})_{B_1=B_2}) A_{22} \}^* \\ dB_1 + \{ - (A_{11} A_{21})_{B_1=B_2} + 3 (\alpha^2 A_{11} - (A_{11})_{B_1=B_2}) A_{23} \} dB_2]$$

and

$$\left[\int_{R_1}^{R_2} \left(\frac{\partial u}{\partial R} \right)^2 R dR \right] dx = V^2 A_{13}^2 \left[\frac{A_{15}}{A_1^2} - \left(\frac{A_{15}}{A_1^2} \right)_{B_1=B_2} \right] dx$$

Using the above relations

$$V \{ \tau_{1w} 2\pi R_1 dx - \tau_{2w} 2\pi R_2 dx + \rho d \left[\int_{R_1}^{R_2} u^2 2\pi R dR \right] \} \\ = 2\mu \pi \left[\int_{R_1}^{R_2} \left(\frac{\partial u}{\partial R} \right)^2 R dR \right] dx + \pi \rho d \left[\int_{R_1}^{R_2} (u^3 - v^3) R dR \right]$$

may be written as

$$2V\mu \frac{U}{R_1} \frac{(B_1 - 1) 2\pi R_1 dx}{(1 - B_1 + \lambda n B_1)} \\ - 2V\mu \frac{U}{R_2} \frac{(B_2 - 1) 2\pi R_2 dx}{(1 - B_2 + \lambda n B_2)} \\ + \pi \rho V^3 R_2^2 A_{13}^2 [\{ \alpha^2 A_{24} A_{12} + 2 (\alpha^2 A_{12} - (A_{12})_{B_1=B_2}) A_{22} \} dB_1 \\ + \{ - (A_{24} A_{12})_{B_1=B_2} + 2 (\alpha^2 A_{12} - (A_{12})_{B_1=B_2}) A_{23} \} dB_2] \\ = 2\mu \pi V^2 A_{13}^2 \left[\frac{A_{15}}{A_1^2} - \left(\frac{A_{15}}{A_1^2} \right)_{B_1=B_2} \right] dx$$

$$+ \pi \rho V^3 \frac{R_2^2}{2} A_{13}^3 \left[\{\alpha^2 A_{11} A_{21} + 3 (\alpha^2 A_{11} - (A_{11})_{B_1=B_2}) A_{22}\} * \right. \\ \left. dB_1 + \{ (-A_{11} A_{21})_{B_1=B_2} + 3 (\alpha^2 A_{11} - (A_{11})_{B_1=B_2}) A_{23} \} dB_2 \right] \quad (A.1)$$

Dividing (A.1) by $\pi \rho V^3 D_h^2$ yields

$$4 \frac{(B_1-1)}{A_1} dx - 4 \frac{(B_2-1)}{(A_1)_{B_1=B_2}} dx + \left(\frac{1}{4} / (1-\alpha)^2 \right) A_{13} \left[\{-\alpha^2 A_{24} A_{12} + \right. \\ \left. 2 (\alpha^2 A_{12} - (A_{12})_{B_1=B_2}) A_{22}\} dB_1 + \{ (-A_{24} A_{12})_{B_1=B_2} + \right. \\ \left. 2 (\alpha^2 A_{12} - (A_{12})_{B_1=B_2}) A_{23}\} dB_2 \right] \\ = 2 A_{13} \left[\frac{A_{15}}{A_1^2} - \left(\frac{A_{15}}{A_1^2} \right)_{B_1=B_2} \right] dx + \frac{1}{2} A_{13}^2 \frac{1}{4(1-\alpha)^2} \left[\{\alpha^2 A_{11} A_{21} + \right. \\ \left. 3 (\alpha^2 A_{11} - (A_{11})_{B_1=B_2}) A_{22}\} dB_1 + \{ (-A_{11} A_{21})_{B_1=B_2} + \right. \\ \left. 3 (\alpha^2 A_{11} - (A_{11})_{B_1=B_2}) A_{23}\} dB_2 \right]$$

or

$$\left[\frac{4 (B_1-1)}{A_1} - \frac{4 (B_2-1)}{(A_1)_{B_1=B_2}} - 2 A_{13} \left\{ \frac{A_{15}}{A_1^2} - \left(\frac{A_{15}}{A_1^2} \right)_{B_1=B_2} \right\} \right] dx \\ = \frac{A_{13}}{8(1-\alpha)^2} \{ [\{\alpha^2 A_{11} A_{21} + 3 (\alpha^2 A_{11} - (A_{11})_{B_1=B_2}) A_{22}\} \}$$

$$\begin{aligned}
& - 2 \{ \alpha^2 A_{24} A_{12} + 2 (\alpha^2 A_{12} - (A_{12})_{B_1=B_2}) A_{22} \} dB_1 \\
& + [\{ (-A_{11} A_{21})_{B_1=B_2} + 3 (\alpha^2 A_{11} - (A_{11})_{B_1=B_2}) A_{23} \} \\
& - 2 \{ (-A_{24} A_{12})_{B_1=B_2} + 2 (\alpha^2 A_{12} - (A_{12})_{B_1=B_2}) A_{23} \}] * \\
& dB_2 \}
\end{aligned}$$

or

$$- 2 [A_{16} + A_{17}] 8 (1-\alpha)^2 dx = A_{13} \{ A_{25} dB_1 + A_{26} dB_2 \}$$

which may then be written as

$$8 (1-\alpha)^2 dx = I_1 dB_1 + I_2 dB_2.$$

(b) General Model:

Using the previous algebraic calculations, Equation (3.22) is:

$$\begin{aligned}
& \frac{-2 \mu V A_{13}}{R_1} \frac{(B_1-1)}{(A_1)} 2\pi R_1 dx + \frac{\pi R_1^2}{AV} \left(\frac{1}{B_1} - 1 \right) * \{ 2\mu\pi V^2 A_{13}^2 \\
& \left[\frac{A_{15}}{A_1^2} - \left(\frac{A_{15}}{A_1^2} \right)_{B_1=B_2} \right] \} dx
\end{aligned}$$

$$\begin{aligned}
& + \pi \rho V^3 \frac{R_2^2}{2} A_{13}^3 \left[\{ \alpha^2 A_{11} A_{21} + 3 (\alpha^2 A_{11} - (A_{11})_{B_1=B_2}) A_{22} \} * \right. \\
& dB_1 + \left. \{ (-A_{11} A_{21})_{B_1=B_2} + 3 (\alpha^2 A_{11} - (A_{11})_{B_1=B_2}) A_{23} \} dB_2 \right] \\
& = -\pi \rho V^2 A_{13} R_1^2 d \left[\frac{A_{13}}{B_1} \left\{ 1 + \frac{(1-B_1)^2}{2A_1} \right\} \right] + \rho \pi V^2 R_1^2 d \left[\frac{A_{13}^2}{B_1} * \right. \\
& \left. \left\{ 1 + \frac{A_4}{A_1^2} \right\} \right]
\end{aligned}$$

which may be written as

$$\begin{aligned}
& \left[-4 A_{13} \frac{(B_1-1)}{A_1} + \left(\frac{1}{B_1} - 1 \right) \frac{\alpha^2}{2(1-\alpha)^2} A_{13}^2 \left\{ \frac{A_{15}}{A_1^2} \right. \right. \\
& \left. \left. - \left(\frac{A_{15}}{A_1^2} \right)_{B_1=B_2} \right\} \right] dx \\
& + \frac{\alpha^2 A_{13}^3}{32(1-\alpha)^4} \left(\frac{1}{B_1} - 1 \right) \left[\{ \alpha^2 A_{11} A_{21} + 3 (\alpha^2 A_{11} - (A_{11})_{B_1=B_2}) * \right. \\
& \left. A_{22} \} dB_1 + \left\{ (-A_{11} A_{21})_{B_1=B_2} + 3 (\alpha^2 A_{11} - (A_{11})_{B_1=B_2}) * \right. \right. \\
& \left. \left. A_{23} \} dB_2 \right] \\
& = -\frac{A_{13} \alpha^2}{4(1-\alpha)^2} d \left[\frac{A_{13}}{B_1} \left\{ 1 + \frac{(1-B_1)^2}{2A_1} \right\} \right] + \frac{\alpha^2}{4(1-\alpha)^2} d \left[\frac{A_{13}^2}{B_1} * \right. \\
& \left. \left\{ 1 + \frac{A_4}{A_1^2} \right\} \right]
\end{aligned} \tag{A.2}$$

The R.H.S. of Equation (A.2) can be shown to be

$$\begin{aligned}
& - \frac{A_{13}\alpha^2}{4(1-\alpha)^2} \frac{A_{13}}{B_1} \left[\left\{ -0.5 \frac{(1-B_1)C_5^2}{B_1} + C_5 - \frac{1}{B_1} \left(1 + 0.5 \frac{(1-B_1)^2}{A_1} \right) \right. \right. \\
& + \left. \left. \left(1 + \frac{0.5(1-B_1)^2}{A_1} \right) A_{22} \right\} dB_1 + \left\{ 1 + 0.5 \frac{(1-B_1)^2}{A_1} A_{23} \right\} dB_2 \right] \\
& + \frac{\alpha^2}{4(1-\alpha)^2} \frac{A_{13}^2}{B_1} \left[\left\{ \frac{2A_4C_5}{B_1 A_1^2} + \frac{A_7}{A_1^2} - \frac{1}{B_1} \left(1 + \frac{A_4}{A_1^2} \right) + 2A_{22} \right. \right. \\
& \left. \left. \left(1 + \frac{A_4}{A_1^2} \right) \right\} dB_1 + \left\{ 2A_{23} \left(1 + \frac{A_4}{A_1^2} \right) \right\} dB_2 \right] \\
& = - \frac{A_{13}\alpha^2}{4(1-\alpha)^2} [A_{40} dB_1 + A_{41} dB_2] + \frac{\alpha^2 A_{13}}{4(1-\alpha)^2} [A_{42} dB_1 + A_{43} dB_2]
\end{aligned}$$

Substituting the above expression for the R.H.S. of Equation (A.2) we obtain:

$$\begin{aligned}
& \left[- \frac{4(B_1-1)}{A_1} + \left(\frac{1}{B_1} - 1 \right) \frac{\alpha^2}{2(1-\alpha)^2} A_{13} \left\{ \frac{A_{15}}{A_1^2} - \left(\frac{A_{15}}{A_1^2} \right)_{B_1=B_2} \right\} \right] dx \\
& = \frac{1}{4(1-\alpha)^2} \left\{ \left[-\alpha^2 A_{40} + \alpha^2 A_{42} - \frac{\alpha^2 A_{44} \left(\frac{1}{B_1} - 1 \right)}{8(1-\alpha)^2} \right] dB_1 \right.
\end{aligned}$$

$$+ \left[-\alpha^2 A_{41} + \alpha^2 A_{43} - \frac{\alpha^2 A_{45} \left(\frac{1}{B_1} - 1 \right)}{8(1-\alpha)^2} \right] dB_2 \} \quad (\text{A.3a})$$

Similarly it may be shown that Equation (3.23) reduces to

$$\frac{2\mu A_{13} V}{R_2} \frac{(B_2 - 1)}{(A_1)_{B_1=B_2}} 2\pi R_2 dx + \frac{\pi R_2^2}{AV} \left(1 - \frac{1}{B_2} \right)^*$$

$$\left\{ 2\mu\pi V^2 A_{13}^2 \left[\frac{A_{15}}{A_1^2} - \left(\frac{A_{15}}{A_1^2} \right)_{B_1=B_2} \right] dx \right.$$

$$\left. + \pi\rho V^3 \frac{R_2^2}{2} A_{13} [A_{44} dB_1 + A_{45} dB_2] \right\}$$

$$= -\rho\pi V^2 A_{13} R_2^2 [A_{49} dB_1 + A_{48} dB_2]$$

$$+ R_2^2 \rho\pi A_{13} V^2 [A_{50} dB_1 + A_{51} dB_2]$$

i.e.,

$$\frac{4A_{13} v (B_2 - 1)}{VD_h (A_1)_{B_1=B_2}} \frac{D_h^2}{R_2^2} d \left(\frac{x}{D_h} \right) + 2\pi \left(1 - \frac{1}{B_2} \right) \frac{v}{VD_h} *$$

$$A_{13}^2 \left(\frac{A_{15}}{A_1^2} - \left(\frac{A_{15}}{A_1^2} \right)_{B_1=B_2} \right) \frac{D_h^2}{A} d \left(\frac{x}{D_h} \right)$$

$$\begin{aligned}
&= - \left(1 - \frac{1}{B_2}\right) \frac{\pi R_2^2}{A} \frac{A_{13}}{2} [A_{44} dB_1 + A_{45} dB_2] \\
&\quad - A_{13} (A_{49} dB_1 + A_{48} dB_2) \\
&\quad + A_{13} (A_{50} dB_1 + A_{51} dB_2)
\end{aligned} \tag{A.2b}$$

or

$$\begin{aligned}
&[16 \frac{(B_2-1)}{(A_1)_{B_1=B_2}} (1-\alpha)^2 + 2 \left(1 - \frac{1}{B_2}\right) A_{13} \left(\frac{A_{15}}{A_1^2} - \left(\frac{A_{15}}{A_1^2}\right)_{B_1=B_2}\right) * \\
&\quad \left. 4 \frac{(1-\alpha)}{(1+\alpha)} \right] dX \\
&= \text{R.H.S. of Equation (A.2b)}
\end{aligned} \tag{A.3b}$$

Now from

$$B_1 = \frac{R_1^2}{R_{\delta_1}^2} \quad \text{and} \quad B_2 = \frac{R_2^2}{R_{\delta_2}^2}$$

it may be shown that

$$dB_1 = \frac{-2B_1 d(\delta_1/D_h)}{\left(\frac{\alpha}{2(1-\alpha)} + \frac{\delta_1}{D_h}\right)} = A_{56} d\left(\frac{\delta_1}{D_h}\right) \tag{A.4a}$$

$$dB_2 = \frac{2B_2 d(\delta_2/D_h)}{\left(\frac{1}{2(1-\alpha)} - \frac{\delta_2}{D_h}\right)} = B_{56} d\left(\frac{\delta_2}{D_h}\right) \quad (\text{A.4b})$$

Substituting Equations (A.4) in Equations (A.3a) and (A.3b) it can be seen that Equations (A.3a) and (A.3b) may be written, after some re-arrangement, as

$$F_1 \frac{d}{dx} (\delta_1/D_h) + F_2 \frac{d}{dx} (\delta_2/D_h) = F_3$$

$$F_4 \frac{d}{dx} (\delta_1/D_h) + F_5 \frac{d}{dx} (\delta_2/D_h) = F_6$$

From Equation (3.10), we may write

$$\begin{aligned} -AVdp &= 2\mu\pi V^2 A_{13} \left[\frac{A_{15}}{A_1^2} - \left(\frac{A_{15}}{A_1^2}\right)_{B_1=B_2} \right] dx \\ &+ \pi\rho V^3 \frac{R_2^2}{2} A_{13} [A_{44} dB_1 + A_{45} dB_2] \end{aligned} \quad (\text{A.5})$$

Dividing Equation (A.5) by $(-\frac{1}{2}\rho V^3 A)$

$$-\frac{dp}{\frac{1}{2}\rho V^2} = 16 \frac{(1-\alpha)}{(1+\alpha)} A_{13} \left[\frac{A_{15}}{A_1^2} - \left(\frac{A_{15}}{A_1^2}\right)_{B_1=B_2} \right] dx$$

$$+ \frac{1}{(1-\alpha)^2} A_{13} [A_{44} dB_1 + A_{45} dB_2] \quad (A.6)$$

Defining

$$P = \frac{p_i - p}{\frac{1}{2}\rho V^2} \Rightarrow dP = \frac{-dp}{\frac{1}{2}\rho V^2} \quad (A.7)$$

using Equations (A.7) and (A.4) in Equation (A.6), Equation (A.6) can be written as

$$\frac{dP}{dX} = F_7 \frac{d(\delta_1/D_h)}{dX} + F_8 \frac{d(\delta_2/D_h)}{dX} + F_9$$

$$R_{11} = 4(1-\alpha)^2$$

$$R_{12} = \alpha^2 / (8(1-\alpha)^2)$$

$$R_{13} = 1/G_1$$

$$R_{14} = 0.5 / (1-\alpha^2)$$

$$R_{15} = \frac{-2 \ln(\alpha)}{(1-\alpha^2)}$$

$$R_{16} = \frac{0.5}{(1-\alpha)}$$

$$R_{17} = \frac{0.5 \alpha}{(1-\alpha)}$$

$$C_1 = 1/B_1$$

$$C_2 = \ln(B_1)$$

$$A_1 = 1 - B_1 + \ln B_1$$

$$A_2 = \frac{5}{6} - B_1 + \frac{B_1^2}{2} - \frac{B_1^3}{3} + B_1 (B_1 - \ln B_1) \ln B_1$$

$$A_3 = \frac{7}{3} - 2B_1 - \frac{3}{4} B_1^2 + \frac{2}{3} B_1^3 - \frac{B_1^4}{4} + B_1 (3 - \frac{3}{2} B_1 + B_1^2) \ln B_1 \\ + B_1 (-\frac{3}{2} B_1 + \ln B_1) \ln^2 B_1$$

$$A_4 = \frac{11}{6} - 3B_1 + \frac{3}{2} B_1^2 - \frac{B_1^3}{3} + \ln B_1$$

$$C_3 = (-1 + B_1)/A_1$$

$$A_5 = (-1 + \frac{1}{B_1})/A_1$$

$$A_6 = \frac{1}{2} (1 - B_1^2) + B_1 \ln B_1$$

$$A_7 = -3 + 3B_1 - B_1^2 + \frac{1}{B_1}$$

$$A_8 = \alpha^2 (1 - B_1)^2 B_2 (A_1)_{B_1=B_2} - (1 - B_2)^2 B_1 A_1$$

$$A_9 = -(1 - B_1)^2 + 2(B_1 - 1) \ln B_1 - \ln^2 B_1$$

$$A_{10} = (1 - B_1)^3 + 3[(1 - B_1)^2 - B_1 \ln B_1] \ln B_1 + (3 + \ln B_1) \ln^2 B_1$$

$$A_{11} = [-B_1 + 3A_6/A_1 + 3A_2/A_1^2 + A_3/A_1^3]/B_1$$

$$A_{12} = A_4/(B_1 A_1^2)$$

$$A_{13} = [2(1 - \alpha^2) B_1 B_2 A_1 (A_1)_{B_1=B_2}]/A_8$$

$$A_{14} = \frac{\alpha^2}{2} A_{13} A_{11} + \frac{1}{2} A_{13} (A_{11})_{B_1=B_2} + \alpha^2 A_{12} - (A_{12})_{B_1=B_2}$$

$$A_{15} = (1 - B_1^2) + 4(B_1 - 1) - 2 \ln B_1$$

$$A_{16} = [-2(B_1 - 1) + (A_{13} A_{15}/A_1)]/A_1$$

$$A_{17} = [2(B_2 - 1) + A_{13} (-A_{15}/A_1)_{B_1=B_2}]/(A_1)_{B_1=B_2}$$

$$A_{18} = 3A_6 [(A_1/A_6) - A_5]/A_1$$

$$A_{19} = 3A_2 [(A_9/A_2) - 2A_5]/A_1^2$$

$$A_{20} = A_3 [(A_{10}/A_3) - 3A_5]/A_1^3$$

$$A_{21} = [(-1 + A_{18} + A_{19} + A_{20})/(A_{11}B_1) - 1/B_1]$$

$$A_{22} = \left[\frac{1}{B_1} + A_5 + \frac{2\alpha^2(1-B_1)^2 B_2 (A_1)_{B_1=B_2}}{A_8(1-B_1)} \right. \\ \left. + \frac{B_1(1-B_2)^2 A_1}{A_8} \left\{ \frac{1}{B_1} + A_5 \right\} \right]$$

$$A_{23} = \left[\frac{1}{B_2} + (A_5)_{B_1=B_2} - \frac{2B_1(1-B_2)^2 A_1}{A_8(1-B_2)} \right. \\ \left. - \frac{\alpha^2(1-B_1)^2 B_2 (A_1)_{B_1=B_2}}{A_8} \left\{ \frac{1}{B_2} + (A_5)_{B_1=B_2} \right\} \right]$$

$$A_{24} = (A_7/A_4) - \frac{1}{B_1} - 2A_5$$

$$A_{25} = [\alpha^2 A_{11} A_{21} + 3\{\alpha^2 A_{11} - (A_{11})_{B_1=B_2}\} A_{22}] \\ - 2[\alpha^2 A_{24} A_{12} + 2\{\alpha^2 A_{12} - (A_{12})_{B_1=B_2}\} A_{22}]$$

$$A_{26} = [- (A_{11} A_{21})_{B_1=B_2} + 3\{\alpha^2 A_{11} - (A_{11})_{B_1=B_2}\} A_{23}] \\ - 2[-(A_{24} A_{12})_{B_1=B_2} + 2\{\alpha^2 A_{12} - (A_{12})_{B_1=B_2}\} A_{23}]$$

$$I_1 = -A_{13} A_{25} / (A_{16} + A_{17})$$

$$I_2 = -A_{13} A_{26} / (A_{16} + A_{17})$$

$$C_4 = -2C_3 + \frac{\alpha^2}{(1-\alpha^2)} A_{13} (C_1 - 1) \left(\frac{A_{15}}{A_1} - \left(\frac{A_{15}}{A_1} \right)_{B_1=B_2} \right)$$

$$C_5 = 4(C_3)_{B_1=B_2} + \frac{2}{(1-\alpha^2)} (1-C_2) \left(\frac{A_{15}}{A_1} - \left(\frac{A_{15}}{A_1} \right)_{B_1=B_2} \right)$$

$$A_{27} = 1 + 0.5 \frac{(1-B_1)^2}{A_1}$$

$$A_{28} = A_{13} * C_1$$

$$A_{29} = 1 + \frac{A_4}{A_1^2}$$

$$A_{30} = \alpha^2 A_{11}$$

$$A_{31} = R_{12} / C_4$$

$$A_{40} = ((-0.5 (1-B_1) C_1 C_3 + 1) C_3 + (-C_1 + A_{22}) A_{27}) A_{28}$$

$$A_{41} = A_{27} A_{23} A_{28}$$

$$A_{42} = \left\{ \frac{(2A_4 C_3 C_1 + A_7)}{A_1^2} + (-C_1 + 2A_{22}) A_{29} \right\} A_{28}$$

$$A_{43} = 2A_{23} A_{29} A_{28}$$

$$A_{44} = A_{13}^2 \{A_{30} A_{21} + 3A_{22} (A_{30} - (A_{11})_{B_1=B_2})\}$$

$$A_{45} = A_{13}^2 \{(-A_{11} A_{21})_{B_1=B_2} + 3A_{23} (A_{30} - (A_{11})_{B_1=B_2})\}$$

$$A_{46} = (-A_{40} + A_{42} - R_{14} (C_1 - 1) A_{44}) A_{31}$$

$$A_{47} = (-A_{41} + A_{43} - R_{14} (C_1 - 1) A_{45}) A_{31}$$

$$A_{48} = \{(-0.5 (1 - B_2)(C_1 C_3)_{B_1=B_2} + 1)(C_3)_{B_1=B_2} + ((-C_1)_{B_1=B_2} + A_{23})(A_{27})_{B_1=B_2}\} A_{13} (C_1)_{B_1=B_2}$$

$$A_{49} = (A_{27})_{B_1=B_2} A_{22} A_{13} (C_1)_{B_1=B_2}$$

$$A_{50} = 2A_{22} (A_{29})_{B_1=B_2} A_{13} (C_1)_{B_1=B_2}$$

$$A_{51} = \left\{ \frac{(-2 (A_4 C_3 C_1)_{B_1=B_2} + A_7)}{(A_1^2)_{B_1=B_2}} + ((-C_1)_{B_1=B_2} + 2A_{23})(A_{29})_{B_1=B_2} \right\}$$

$$* A_{13} (C_1)_{B_1=B_2}$$

$$A_{52} = A_{44}$$

$$A_{53} = A_{45}$$

$$A_{54} = \frac{\{A_{49} - A_{50} - R_{14} (1 - (C_1)_{B_1=B_2}) A_{52}\} R_{13}}{C_5}$$

$$A_{55} = \frac{\{A_{48} - A_{51} - R_{14} (1 - (C_1)_{B_1=B_2}) A_{53}\} R_{13}}{C_5}$$

$$A_{56} = \frac{-2 B_1}{(R_{17} + (\delta_1/D_h))}$$

$$A_{57} = \frac{2 B_2}{(R_{16} - (\delta_2/D_h))}$$

$$F_1 = \frac{A_{56}}{4(1-\alpha)^2} \left[-\alpha^2 A_{40} + \alpha^2 A_{42} - \frac{\alpha^2 A_{44}}{8(1-\alpha)^2} \left(\frac{1}{B_1} - 1 \right) \right]$$

$$F_2 = \frac{A_{57}}{4(1-\alpha)^2} \left[-\alpha^2 A_{41} + \alpha^2 A_{43} - \frac{\alpha^2 A_{45}}{8(1-\alpha)^2} \left(\frac{1}{B_1} - 1 \right) \right]$$

$$F_3 = \frac{-4(B_1-1)}{A_1} + \left(\frac{1}{B_1} - 1 \right) \frac{\alpha^2}{2(1-\alpha)^2} A_{13} \left\{ \frac{A_{15}}{A_1^2} - \left(\frac{A_{15}}{A_1^2} \right)_{B_1=B_2} \right\}$$

$$F_4 = A_{56} \left[-A_{49} + A_{50} - \left(1 - \frac{1}{B_2} \right) \frac{1}{(1-\alpha^2)} \frac{A_{44}}{2} \right]$$

$$F_5 = A_{57} \left[-A_{48} + A_{51} - \left(1 - \frac{1}{B_2} \right) \frac{1}{(1-\alpha^2)} \frac{A_{45}}{2} \right]$$

$$F_6 = 16(1-\alpha)^2 \frac{(B_2-1)}{(A_1)_{B_1=B_2}} + \left(1 - \frac{1}{B_2} \right) 8 A_{13} \frac{(1-\alpha)}{(1+\alpha)} \left\{ \frac{A_{15}}{A_1^2} - \left(\frac{A_{15}}{A_1^2} \right)_{B_1=B_2} \right\}$$

$$F_7 = \frac{A_{13}}{(1-\alpha^2)} A_{44} A_{56}$$

$$F_8 = \frac{A_{13} A_{45} A_{57}}{(1-\alpha^2)}$$

$$F_9 = \frac{16(1-\alpha)}{(1+\alpha)} A_{13} \left[\frac{A_{15}}{A_1^2} - \left(\frac{A_{15}}{A_1^2} \right)_{B_1=B_2} \right]$$

A.2 Hydrodynamic developing turbulent annular flows.

(a) Simplified Model

$$\int_{R_1}^{R_2} u \, 2\pi R \, dR = \frac{2R_1^2}{S_1^2} \frac{(1-S_1)}{\left(\frac{1}{n_1} + 1\right)} \left[1 - \frac{(1-S_1)}{\left(\frac{1}{n_1} + 2\right)} \right] U$$

$$+ \frac{2R_2^2}{S_2^2} \frac{(S_2-1)}{\left(\frac{1}{n_2} + 1\right)} \left[1 - \frac{(1-S_2)}{\left(\frac{1}{n_2} + 2\right)} \right] U$$

$$+ \left(\frac{R_2^2}{S_2^2} - \frac{R_1^2}{S_1^2} \right) U = AV = \pi(R_2^2 - R_1^2)V$$

$$\therefore \frac{U}{V} = \frac{(1-\alpha^2)}{\left\{ \frac{2\alpha_1^2}{S_1^2} \frac{(1-S_1)}{\left(\frac{1}{n_1} + 1\right)} \left[1 - \frac{(1-S_1)}{\left(\frac{1}{n_1} + 2\right)} \right] + \frac{2}{S_2^2} \frac{(S_2-1)}{\left(\frac{1}{n_2} + 1\right)} \right.}$$

$$\left. \left[1 - \frac{(1-S_2)}{\left(\frac{1}{n_2} + 2\right)} \right] + \left(\frac{1}{S_2^2} - \frac{\alpha^2}{S_1^2} \right) \right\}}$$

$$= (1-\alpha^2)/E_0 \tag{A.8}$$

Differentiating Equation (A.8)

$$d\left(\frac{U}{V}\right) = - \frac{(1-\alpha^2)}{E_0^2} d(E_0)$$

Now, it can be shown that

$$\begin{aligned}
d(E_0) &= \frac{2\alpha^2}{S_1^3} dS_1 \left[\frac{1}{\left(\frac{1}{n_1} + 1\right)} (S_1^{-2}) + \frac{2(1-S_1)}{\left(\frac{1}{n_1} + 1\right)\left(\frac{1}{n_2} + 2\right)} + 1 \right] \\
&\quad - \frac{2dS_2}{S_2^3} \left[\frac{1}{\left(\frac{1}{n_2} + 1\right)} (S_2^{-2}) + \frac{2(1-S_2)}{\left(\frac{1}{n_2} + 1\right)\left(\frac{1}{n_2} + 2\right)} + 1 \right] \\
&= E_1 dS_1 + E_2 dS_2
\end{aligned} \tag{A.9}$$

$$\begin{aligned}
\therefore d\left(\frac{U}{V}\right) &= - \frac{(1-\alpha^2)}{E_0} (E_1 dS_1 + E_2 dS_2) \\
&= - \frac{U}{V} [E_1 dS_1 + E_2 dS_2]
\end{aligned} \tag{A.10}$$

$$\begin{aligned}
\int_{R_1}^{R_2} u^2 2\pi R dR &= U^2 R_2^2 \pi E_3 \\
&= \frac{2\pi R_1^2}{S_1^2} U^2 \frac{(1-S_1)}{\left(\frac{2}{n_1} + 1\right)} \left[1 - \frac{(1-S_1)}{\left(\frac{2}{n_1} + 2\right)} \right] \\
&\quad + \pi U^2 \left(\frac{R_2^2}{S_2^2} - \frac{R_1^2}{S_1^2} \right) + 2\pi \frac{R_2^2}{S_2^2} U^2 \frac{(S_2-1)}{\left(\frac{2}{n_2} + 1\right)} \\
&\quad * \left[1 - \frac{(1-S_2)}{\left(\frac{2}{n_2} + 2\right)} \right]
\end{aligned}$$

$$d\left[\int_{R_1}^{R_2} u^2 2\pi R dR \right] = R_2^2 \pi U^2 d E_3 + E_3 \pi R_2^2 2U dU$$

$$\begin{aligned}
&= \frac{2\alpha^2 dS_1}{S_1^3} \left[\frac{(S_1-2)}{\left(\frac{2}{n_1} + 1\right)} + \frac{2(1-S_1)}{\left(\frac{2}{n_1} + 1\right)\left(\frac{2}{n_1} + 2\right)} + 1 \right] \\
* \pi U^2 R^2 - \frac{2dS_2}{S_2^3} U^2 &\left[\frac{(S_2-2)}{\left(\frac{2}{n_1} + 1\right)} + \frac{2(1-S_2)}{\left(\frac{2}{n_2} + 1\right)\left(\frac{2}{n_2} + 2\right)} + 1 \right] R_2^2 \pi \\
&- E_3 \pi R_2^2 2U^2 [E_1 dS_1 + E_2 dS_2] \\
&= (E_4 dS_1 + E_5 dS_2) U^2 R_2^2 \pi \tag{A.11}
\end{aligned}$$

Introducing Equations (A.10) and (A.11) in Equation (3.37) and dividing by $\pi V^2 D_h^2 \rho$

$$\begin{aligned}
-0.123*10^{-0.678H_1} \left(\frac{u\delta_1^{**}}{v}\right)^{-0.268} \frac{U^2}{V^2} \frac{2R_1}{D_h} d\left(\frac{x}{D_h}\right) \\
-0.123*10^{-0.678H_2} \left(\frac{u\delta_2^{**}}{v}\right)^{-0.268} \frac{U^2}{V^2} \frac{2R_2}{D_h} d\left(\frac{x}{D_h}\right) \\
- \frac{U}{V} \frac{(R_2^2 - R_1^2)(1-\alpha^2)}{D_h^2 E_0} (E_1 dS_1 + E_2 dS_2) \\
= \frac{U^2}{V^2} \frac{R_2^2}{D_h^2} (E_4 dS_1 + E_5 dS_2) \tag{A.12}
\end{aligned}$$

Equation (A.12) may be written as

$$T_1 dS_1 + T_2 dS_2 = T_3 dx$$

(b) General Model

Equation (A.10) is

$$d \left(\frac{U}{V} \right) = - \frac{(1-\alpha^2)}{E_0} (E_1 dS_1 + E_2 dS_2) \quad (\text{A.10})$$

$$\begin{aligned} & d \left[\int_{R_1}^{R_2} u_1^2 2\pi R dR \right] U \\ &= U d \left[2\pi U \frac{R_1^2 (1-S_1)}{S_1^2 \left(\frac{1}{n_1} + 1 \right)} \left\{ 1 - \frac{(1-S_1)}{\left(\frac{1}{n_1} + 2 \right)} \right\} \right] \\ &= \frac{V^2 U 2\pi R_1^2 \alpha^2}{V \left(\frac{1}{n_1} + 1 \right)} d \left[\frac{(1-S_1)}{S_1^2} \frac{U}{V} \left\{ 1 - \frac{(1-S_1)}{\left(\frac{1}{n_1} + 2 \right)} \right\} \right] \\ &= \frac{(1-\alpha^2)}{E_0} \frac{2\pi R_1^2 \alpha^2 V^2}{\left(\frac{1}{n_1} + 1 \right)} \left\{ \frac{U}{V} \left[\frac{(S_1-2)}{S_1^3} + \frac{2}{\left(\frac{1}{n_1} + 2 \right)} \frac{(1-S_1)}{S_1^3} \right] dS_1 \right. \\ &\quad \left. + \frac{(1-S_1)}{S_1^2} \left[1 - \frac{(1-S_1)}{\left(\frac{1}{n_1} + 2 \right)} \right] d \left(\frac{U}{V} \right) \right\} \\ &= \frac{(1-\alpha^2)}{E_0} \frac{2\pi R_1^2 \alpha^2 V^2}{\left(\frac{1}{n_1} + 1 \right)} \{ E_{10} dS_1 + E_{11} dS_2 \} \quad (\text{A.13}) \end{aligned}$$

$$d \left[\int_{R_1}^{R_2} u_1^2 2\pi R dR \right]$$

$$\begin{aligned}
&= \frac{V^2 2\pi R_2^2 \alpha^2}{\left(\frac{2}{n_1} + 1\right)} d \left[\frac{(1-S_1) U^2}{S_1^2 V^2} \left\{ 1 - \frac{(1-S_1)}{\left(\frac{2}{n_1} + 2\right)} \right\} \right] \\
&= \frac{2\pi R_2^2 \alpha^2 V^2}{\left(\frac{2}{n_1} + 1\right)} \left\{ \frac{U^2}{V^2} \left[\frac{(S_1-2)}{S_1^3} dS_1 + \frac{2}{\left(\frac{2}{n_1} + 1\right)} \frac{(1-S_1)}{S_1^3} dS_1 \right] \right. \\
&\quad \left. + \frac{(1-S_1)}{S_1^2} \left[1 - \frac{(1-S_1)}{\left(\frac{2}{n_1} + 2\right)} \right] 2 \frac{U}{V} d \left(\frac{U}{V} \right) \right\} \\
&= \frac{2\pi R_2^2 \alpha^2 V^2}{\left(\frac{2}{n_1} + 1\right)} \frac{(1-\alpha^2)}{E_0} \left\{ \frac{(1-\alpha^2)}{S_1^3 E_0} \left[(S_1-2) + \frac{2(1-S_1)}{\left(\frac{2}{n_1} + 2\right)} \right] dS_1 \right. \\
&\quad \left. - 2 \frac{(1-S_1)}{S_1^2} \left[1 - \frac{(1-S_1)}{\left(\frac{2}{n_1} + 2\right)} \right] \frac{(1-\alpha^2)}{E_0} (E_1 dS_1 + E_2 dS_2) \right\} \\
&= \frac{2\pi R_2^2 \alpha^2 V^2}{\left(\frac{2}{n_1} + 1\right)} \frac{(1-\alpha^2)}{E_0} \{ E_{12} dS_1 + E_{13} dS_2 \} \tag{A.14}
\end{aligned}$$

Similarly

$$\begin{aligned}
&d \left[\int_{R_{\delta_2}}^{R_2} u_2 2\pi R dR \right] U \\
&= U d \left[2\pi U \frac{R_2^2}{S_2^2} \frac{(S_2-1)}{\left(\frac{1}{n_2} + 1\right)} \left\{ 1 - \frac{(1-S_2)}{\left(\frac{1}{n_2} + 2\right)} \right\} \right]
\end{aligned}$$

$$\begin{aligned}
&= \frac{2\pi R_2^2 V^2}{\left(\frac{1}{n_2} + 1\right)} \frac{U}{V} d \left[\frac{U (S_2 - 1)}{V S_2^2} \left\{ 1 - \frac{(1 - S_2)}{\left(\frac{1}{n_2} + 2\right)} \right\} \right] \\
&= \frac{2\pi R_2^2 V^2}{\left(\frac{1}{n_2} + 1\right)} \frac{U}{V} \left\{ -\frac{U}{V} \left[\frac{(S_2 - 2)}{S_2^3} + \frac{2}{\left(\frac{1}{n_2} + 2\right)} \frac{(1 - S_2)}{S_2^3} \right] dS_2 \right. \\
&\quad \left. - \frac{(S_2 - 1)}{S_2^2} \left[1 - \frac{(1 - S_2)}{\left(\frac{1}{n_2} + 2\right)} \right] \frac{(1 - \alpha^2)}{E_0} (E_1 dS_1 + E_2 dS_2) \right\} \\
&= \frac{2\pi R_2^2 V^2}{\left(\frac{1}{n_2} + 1\right)} \frac{U}{V} \{E_{14} dS_1 + E_{15} dS_2\} \tag{A.15}
\end{aligned}$$

Also,

$$\begin{aligned}
d \left[\int_{R_{\delta_2}}^{R_2} u_2^2 2\pi R dR \right] &= V^2 \frac{2\pi R_2^2}{\left(\frac{2}{n_2} + 1\right)} d \left[\frac{(S_2 - 1)}{S_2^2} \frac{U^2}{V^2} \left\{ 1 - \frac{(1 - S_2)}{\left(\frac{2}{n_2} + 2\right)} \right\} \right] \\
&= \frac{(1 - \alpha^2)}{E_0} \frac{2\pi R_2^2 V^2}{\left(\frac{2}{n_2} + 1\right)} \left\{ \frac{-(1 - \alpha^2)}{S_2^3 E_0} \left[(S_2 - 2) + \frac{2(1 - S_2)}{\left(\frac{2}{n_2} + 2\right)} \right] dS_2 \right. \\
&\quad \left. - \frac{2(S_2 - 1)}{S_2^3} \left[1 - \frac{(1 - S_2)}{\left(\frac{2}{n_2} + 2\right)} \right] \frac{(1 - \alpha^2)}{E_0} (E_1 dS_1 + E_2 dS_2) \right\} \\
&= \frac{V^2 2\pi R_2^2}{\left(\frac{2}{n_2} + 1\right)} \frac{(1 - \alpha^2)}{E_0} \{E_{16} dS_1 + E_{17} dS_2\} \tag{A.16}
\end{aligned}$$

Dividing Equations (3.45) and (3.46) by $\rho V^2 \pi D_h^2$ and using Equations

(A.13) to (A.16), we obtain

$$\begin{aligned}
 & -0.123 \cdot 10^{-0.678 H_1} \left(\frac{U \delta_1^{**}}{v} \right)^{-0.268} \left(\frac{U}{V} \right)^2 \frac{R_1}{D_h} d \left(\frac{x}{D_h} \right) \\
 & + \alpha^2 \frac{R_2^2}{D_h^2} \left(\frac{1}{S_1^2} - 1 \right) \left\{ - \frac{(1-\alpha^2)^2}{E_0^2} (E_1 dS_1 + E_2 dS_2) \right\} \\
 & = \frac{-(1-\alpha^2)}{E_0} \frac{2R_2^2}{D_h^2} \frac{\alpha^2}{\left(\frac{1}{n_1} + 1 \right)} [E_{10} dS_1 + E_{11} dS_2] \\
 & + 2 \frac{R_2^2}{D_h^2} \frac{\alpha^2}{\left(\frac{2}{n_1} + 1 \right)} \frac{(1-\alpha^2)}{E_0} [E_{12} dS_1 + E_{13} dS_2] \tag{A.17}
 \end{aligned}$$

and

$$\begin{aligned}
 & -0.123 \cdot 10^{-0.678 H_2} \left(\frac{U \delta_2^{**}}{v} \right)^{-0.268} \frac{U^2}{V^2} \frac{2R_2}{D_h} d \left(\frac{x}{D_h} \right) \\
 & + \frac{R_2^2}{D_h^2} \left(1 - \frac{1}{S_2^2} \right) \frac{U}{V} d \left(\frac{U}{V} \right) = \frac{-2R_2^2}{D_h^2} \frac{1}{\left(\frac{1}{n_2} + 1 \right)} \frac{U}{V} [E_{14} dS_1 + E_{15} dS_2] \\
 & + \frac{2R_2^2}{D_h^2} \frac{(1-\alpha^2)}{E_0} \frac{1}{\left(\frac{2}{n_2} + 1 \right)} [E_{16} dS_1 + E_{17} dS_2] \tag{A.18}
 \end{aligned}$$

Also,

$$\begin{aligned}
S_1 = \frac{R_1}{R_{\delta_1}} &\Rightarrow dS_1 = \frac{-R_1}{R_{\delta_1} R_{\delta_1}} d\delta_1 = \frac{-S_1 d(S_1/D_h)}{(R_1 + \delta_1)/D_h} \\
&= \frac{-S_1 d(\delta_1/D_h)}{\left(\frac{\alpha}{2(1-\alpha)} + \frac{\delta_1}{D_h}\right)} \\
&= E_{18} d(\delta_1/D_h)
\end{aligned} \tag{A.19 a}$$

$$\begin{aligned}
S_2 = \frac{R_2}{R_{\delta_2}} &\Rightarrow dS_2 = \frac{R_2}{R_{\delta_2}} \frac{1}{R_{\delta_2}} d(\delta_2) \\
&= \frac{S_2 d(\delta_2/D_h)}{(R_2 - \delta_2)/D_h} \\
&= \frac{S_2 d(\delta_2/D_h)}{\frac{1}{\left(\frac{\alpha}{2(1-\alpha)} - \frac{S_2}{D_h}\right)}} \\
&= E_{19} d(\delta_2/D_h)
\end{aligned} \tag{A.19 b}$$

Using Equations (A.10) and (A.19) in Equations (A.17) and (A.18), Equations (A.17) and (A.18) may be written as

$$\begin{aligned}
G_1 \frac{d}{dx} (\delta_1/D_h) + G_2 \frac{d}{dx} (\delta_2/D_h) &= G_3 \\
G_4 \frac{d}{dx} (\delta_1/D_h) + G_5 \frac{d}{dx} (\delta_2/D_h) &= G_6
\end{aligned} \tag{3.48}$$

$$E_0 = \frac{2\alpha^2}{S_1^2} \frac{(1-S_1)}{\left(\frac{1}{n_1} + 1\right)} \left[1 - \frac{(1-S_1)}{\left(\frac{1}{n_2} + 2\right)} \right] + \frac{2}{S_2^2} \frac{(S_2-1)}{\left(\frac{1}{n_2} + 1\right)}$$

$$* \left[1 - \frac{(1-S_2)}{\left(\frac{1}{n_2} + 2\right)} \right] + \left(\frac{1}{S_2^2} - \frac{\alpha^2}{S_1^2} \right)$$

$$E_1 = \frac{2\alpha^2}{S_1^3} \left[\frac{1}{\left(\frac{1}{n_1} + 1\right)} (S_1-2) + \frac{2(1-S_1)}{\left(\frac{1}{n_1} + 1\right)\left(\frac{1}{n_1} + 2\right)} + 1 \right]$$

$$E_2 = \frac{-2}{S_2^3} \left[\frac{1}{\left(\frac{1}{n_2} + 1\right)} (S_2-2) + \frac{2(1-S_2)}{\left(\frac{1}{n_2} + 1\right)\left(\frac{1}{n_2} + 2\right)} + 1 \right]$$

$$E_3 = \frac{2\alpha^2(1-S_1)}{S_1^2\left(\frac{2}{n_1} + 1\right)} \left[1 - \frac{(1-S_1)}{\left(\frac{2}{n_2} + 2\right)} \right] + \left(\frac{1}{S_2^2} - \frac{\alpha^2}{S_1^2} \right)$$

$$\frac{+2(S_2-1)}{S_2^2\left(\frac{2}{n_2} + 1\right)} \left[1 - \frac{(1-S_2)}{\left(\frac{2}{n_2} + 2\right)} \right]$$

$$E_4 = \frac{2\alpha^2}{S_1^3} \left[\frac{(S_1-2)}{\left(\frac{2}{n_1} + 1\right)} + \frac{2(1-S_1)}{\left(\frac{2}{n_1} + 1\right)\left(\frac{2}{n_1} + 2\right)} + 1 \right] - 2 E_3 E_1$$

$$E_5 = \frac{-2}{S_2^3} \left[\frac{(S_2-2)}{\left(\frac{2}{n_2} + 1\right)} + \frac{2(1-S_2)}{\left(\frac{2}{n_2} + 1\right)\left(\frac{2}{n_2} + 2\right)} + 1 \right] - 2 E_3 E_2$$

$$T_1 = \frac{1}{4(1-\alpha)} \frac{(1+\alpha)E_4}{E_0} + \frac{(1+\alpha)^2 E_1}{4E_0}$$

$$T_2 = \frac{1}{4(1-\alpha)} \frac{(1+\alpha)E_5}{E_0} + \frac{(1+\alpha)^2 E_2}{4E_0}$$

$$E_6 = \frac{\alpha}{2(1-\alpha)} \frac{(1-S_1)}{S_1^2} \left\{ \frac{1}{\left(\frac{1}{n_1} + 1\right)} \left[1 - \frac{(1-S_1)}{\left(\frac{1}{n_1} + 2\right)} \right] \right. \\ \left. - \frac{1}{\left(\frac{2}{n_1} + 1\right)} \left[1 - \frac{(1-S_1)}{\left(\frac{2}{n_1} + 2\right)} \right] \right\}$$

$$E_7 = \frac{1}{2(1-\alpha)} \frac{(S_2-1)}{S_2^2} \left\{ \frac{1}{\left(\frac{1}{n_2} + 1\right)} \left[1 + \frac{(S_2-1)}{\left(\frac{1}{n_2} + 2\right)} \right] \right. \\ \left. - \frac{1}{\left(\frac{2}{n_2} + 1\right)} \left[1 + \frac{(S_2-1)}{\left(\frac{2}{n_2} + 2\right)} \right] \right\}$$

$$E_8 = \left\{ \frac{(1+S_1)}{2} - \frac{1}{\left(\frac{1}{n_1} + 1\right)} \left[1 - \frac{(1-S_1)}{\left(\frac{1}{n_1} + 2\right)} \right] \right\}$$

$$\left\{ \frac{1}{\left(\frac{1}{n_1} + 1\right)} \left[1 - \frac{(1-S_1)}{\left(\frac{1}{n_1} + 2\right)} \right] - \frac{1}{\left(\frac{2}{n_1} + 1\right)} \left[1 - \frac{(1-S_1)}{\left(\frac{2}{n_1} + 2\right)} \right] \right\}$$

$$E_9 = \left\{ \frac{(S_2+1)}{2} - \frac{1}{\left(\frac{1}{n_2} + 1\right)} \left[1 + \frac{(S_2-1)}{\left(\frac{1}{n_2} + 2\right)} \right] \right\}$$

$$\left\{ \frac{1}{\left(\frac{1}{n_2} + 1\right)} \left[1 + \frac{(S_2-1)}{\left(\frac{1}{n_2} + 2\right)} \right] - \frac{1}{\left(\frac{2}{n_2} + 1\right)} \left[1 + \frac{(S_2-1)}{\left(\frac{2}{n_2} + 2\right)} \right] \right\}$$

$$T_3 = -0.123 \cdot 10^{-0.678 E_8} \left(\frac{(1-\alpha^2)}{E_0} \operatorname{Re} E_6 \right)^{-0.268} *$$

$$\frac{(1-\alpha^2)}{E_0} \frac{\alpha}{1-\alpha} - 0.123 \cdot 10^{-0.678 E_9} \left(\frac{(1-\alpha^2)}{E_0} \operatorname{Re} E_7 \right)^{-0.268}$$

$$* \frac{(1-\alpha^2)}{E_0} \frac{1}{(1-\alpha)}$$

$$E_{10} = \frac{(1-\alpha^2)}{S_1^3 E_0} \left[(S_1-2) + \frac{2(1-S_1)}{\left(\frac{1}{n_1} + 2\right)} \right] - \frac{(1-S_1)}{S_1^2} \left[1 - \frac{(1-S_1)}{\left(\frac{1}{n_1} + 2\right)} \right] \frac{(1-\alpha^2)}{E_0} E_1$$

$$E_{11} = \frac{-(1-\alpha^2)}{E_0} \frac{(1-S_1)}{S_1^2} \left\{ 1 - \frac{(1-S_1)}{\left(\frac{1}{n_1} + 2\right)} \right\} E_2$$

$$E_{12} = \frac{(1-\alpha^2)}{S_1^3 E_0} \left[(S_1-2) + \frac{2(1-S_1)}{\left(\frac{2}{n_1} + 2\right)} \right] \frac{-2(1-S_1)}{S_1^2} \frac{(1-\alpha^2)}{E_0}$$

$$\left[1 - \frac{(1-S_1)}{\left(\frac{2}{n_1} + 2\right)} \right] E_1$$

$$E_{13} = \frac{-2(1-S_1)}{S_1^2} \left\{ 1 - \frac{(1-S_1)}{\left(\frac{2}{n_1} + 2\right)} \right\} \frac{(1-\alpha^2)}{E_0} E_2$$

$$E_{14} = \frac{-(S_2-1)}{S_2^2} \left\{ 1 - \frac{(1-S_2)}{\left(\frac{1}{n_2} + 2\right)} \right\} \frac{(1-\alpha^2)}{E_0} E_1$$

$$E_{15} = \frac{-(1-\alpha^2)}{S_2^3 E_0} \left[(S_2-2) + \frac{2(1-S_2)}{\left(\frac{1}{n_2} + 2\right)} \right] - \frac{(S_2-1)}{S_2^2} \left[1 - \frac{(1-S_2)}{\left(\frac{1}{n_2} + 2\right)} \right] \frac{(1-\alpha^2)}{E_0} E_2$$

$$E_{16} = \frac{-2(S_2-1)}{S_2^3} \left\{ 1 - \frac{(1-S_2)}{\left(\frac{2}{n_2} + 2\right)} \right\} \frac{(1-\alpha^2)}{E_0} E_1$$

$$E_{17} = \frac{-(1-\alpha^2)}{S_2^3 E_0} \left\{ (S_2-2) + \frac{2(1-S_2)}{\left(\frac{2}{n_2} + 2\right)} \right\} - \frac{2(S_2-1)}{S_2^3} \left\{ 1 - \frac{(1-S_2)}{\left(\frac{2}{n_2} + 2\right)} \right\} \frac{(1-\alpha^2)}{E_0} E_2$$

$$E_{18} = -S_1 / \left(\frac{\alpha}{2(1-\alpha)} + \frac{\delta_1}{D_h} \right)$$

$$E_{19} = S_2 / \left(\frac{1}{2(1-\alpha)} - \frac{\delta_2}{D_h} \right)$$

$$G_1 = \left[\frac{2\alpha^2}{4(1-\alpha)^2} \frac{E_{12}}{\left(\frac{2}{n_1} + 1\right)} - \frac{2\alpha^2}{4(1-\alpha)^2} \frac{E_{10}}{\left(\frac{1}{n_1} + 1\right)} + \frac{\alpha^2}{4(1-\alpha)^2} \left(\frac{1}{S_2^2} - 1 \right) \frac{(1-\alpha^2)}{E_0} E_1 \right] E_{18}$$

$$G_2 = \left[\frac{2E_{13}}{\left(\frac{2}{n_1} + 1\right)} - \frac{2E_{11}}{\left(\frac{1}{n_1} + 1\right)} + \left(\frac{1}{S_2^2} - 1 \right) \frac{(1-\alpha^2)}{E_0} E_2 \right] \frac{\alpha^2 E_{19}}{4(1-\alpha)^2}$$

$$G_3 = -0.123 \cdot 10^{-0.678 E_8} \left(\frac{(1-\alpha^2)}{E_0} \operatorname{Re} E_6 \right)^{-0.268} * \frac{\alpha(1+\alpha)}{E_0}$$

$$G_4 = \left[\frac{2}{4(1-\alpha)^2} \frac{E_{16}}{\left(\frac{2}{n_2} + 1\right)} \frac{-2}{4(1-\alpha)^2} \frac{E_{14}}{\left(\frac{1}{n_2} + 1\right)} + \frac{(1-\alpha^2)}{E_0} \frac{E_1}{4(1-\alpha)^2} * \left(1 - \frac{1}{S_2^2} \right) \right] \frac{E_{18}}{4(1-\alpha)^2}$$

$$G_5 = \left[\frac{2E_{17}}{\left(\frac{2}{n_2} + 1\right)} - \frac{2E_{15}}{\left(\frac{1}{n_2} + 1\right)} + \frac{(1-\alpha^2)}{E_0} E_2 \left(1 - \frac{1}{S_2^2} \right) \right] \frac{E_{19}}{4(1-\alpha)^2}$$

$$G_6 = -0.123 \cdot 10^{-0.678 E_9} \left(\frac{(1-\alpha^2)}{E_0} \operatorname{Re} E_7 \right)^{-0.268} * \frac{(1+\alpha)}{E_0}$$

A.3 Entry-region Pipe Flows

Equations (3.56) and (3.57) are non-dimensionalizing as follows:

$$\delta^+ = \frac{\delta u^*}{\nu}, \quad R_0^+ = R_0 \frac{u^*}{\nu}, \quad X = \frac{x}{D}$$

$$u^+ = \frac{u}{u^*}, \quad y^+ = y \frac{u^*}{\nu}$$

We have

$$\begin{aligned} dp = & \frac{2\pi}{\pi R_0^2 V} \left[\frac{1}{2} \rho d \left\{ \int_{R_0^+}^0 u^{+3} u^{*3} R_0 \left(1 - \frac{y^+}{R_0^+}\right) dy^+ \frac{\nu}{u^*} \right\} \right. \\ & \left. - dx \tau_w \int_{\delta^+}^0 \left(1 - \frac{y^+}{\delta^+}\right) \frac{du^+}{dy^+} \frac{\tau_w}{\mu} R_0 \left(1 - \frac{y^+}{R_0^+}\right) dy^+ \frac{\nu}{u^*} \right] \end{aligned}$$

which can be written as

$$\begin{aligned} \frac{dp}{\rho V^2} = & \frac{2}{Re} d \left[\frac{u^{*2}}{V^2} \int_{R_0^+}^0 u^{+3} \left(1 - \frac{y^+}{R_0^+}\right) dy^+ \right] \\ & - 4 dX \frac{u^{*3}}{V^3} \left[\int_{\delta^+}^0 \left(1 - \frac{y^+}{\delta^+}\right) \frac{du^+}{dy^+} \left(1 - \frac{y^+}{R_0^+}\right) dy^+ \right] \end{aligned} \quad (A.20)$$

Also

$$\int_0^{R_0} u \, 2\pi R dR = \int_0^{R_0-\delta} u \, 2\pi R dR + \int_{R_0-\delta}^{R_0} u \, 2\pi R dR = AV$$

$$\begin{aligned}
&= \pi R_0^2 V \\
&= \pi U (R_0 - \delta)^2 - \int_{\delta}^0 u \, 2\pi (R_0 - y) \, dy = \pi R_0^2 V \\
&= \pi U R_0^2 \left(1 - \frac{\delta^+}{R_0^+}\right)^2 - 2\pi \int_{\delta^+}^0 u^+ u^* R_0 \left(1 - \frac{y^+}{R_0^+}\right) \, dy^+ \frac{v}{u^*} \\
&= \pi R_0^2 V \tag{A.21}
\end{aligned}$$

Dividing Equation (A.21) by $\pi R_0 v$, we obtain

$$\begin{aligned}
&u_{\max}^+ R_0^+ \left(1 - \frac{\delta^+}{R_0^+}\right)^2 \\
&- 2 \int_{\delta^+}^0 u^+ \left(1 - \frac{y^+}{R_0^+}\right) \, dy^+ = \frac{R_0 V}{v} = \frac{2R_0 V}{v} \cdot \frac{1}{2} = \frac{1}{2} \text{Re}
\end{aligned}$$

or

$$- u_{\max}^+ \frac{R_0^+}{2} \left(1 - \frac{\delta^+}{R_0^+}\right)^2 + \int_{\delta^+}^0 u^+ \left(1 - \frac{y^+}{R_0^+}\right) \, dy^+ = -\frac{1}{4} \text{Re}$$

or

$$\int_{\delta^+}^0 u^+ \left(1 - \frac{y^+}{R_0^+}\right) \, dy^+ = -\frac{1}{4} \text{Re} + u_{\max}^+ \frac{R_0^+}{2} \left(1 - \frac{\delta^+}{R_0^+}\right)^2$$

Equation (3.57) can be written as

$$\begin{aligned}
& \frac{\delta^+}{R_0^+} \left(2 - \frac{\delta^+}{R_0^+} \right) \frac{2}{V} \left[-\frac{1}{2} \rho d \left\{ \int_0^{R_0^+} u^{+3} u^{*3} R^+ \frac{v}{u^*} \frac{v}{u^*} dR^+ \right\} \right. \\
& - 2R_0^+ \frac{v}{u^*} dX \int_0^{R_0^+} \left(1 - \frac{y^+}{\delta^+} \right) \tau_w \frac{du^+}{dy^+} \frac{\tau_w}{\mu} dR^+ \frac{v}{u^*} \\
& + 2R_0^+ \frac{v}{u^*} \tau_w 2R_0^+ \frac{v}{u^*} dX = 2 \rho u_{\max}^+ u^* d \left[\int_0^{\delta^+} u^+ u^* \left(1 - \frac{y^+}{R_0^+} \right) \right. \\
& \left. R_0^+ \frac{v}{u^*} y^+ \frac{v}{u^*} dy^+ \right] - 2 \rho d \left[\int_0^{\delta^+} u^{+2} u^{*2} \left(1 - \frac{y^+}{R_0^+} \right) R_0^+ \frac{v}{u^*} \right. \\
& \left. \frac{v}{u^*} dy^+ \right]
\end{aligned}$$

which may be written, on rearranging, as Equation (3.58).

APPENDIX B
COMPUTER PROGRAMS

```

3JOB  *ATFIV XXXXXXXXXXXX ANAND
C     THIS PROGRAM PREDICTS FLOW CHARACTERISTICS FOR HYDRODYNAMIC
C     DEVELOPING LAMINAR FLOW THROUGH A CONCENTRIC ANNULUS
C     SIMPLIFIED MODEL
C     THE RATIO OF WALL LAYER THICKNESS IS ASSUMED TO BE A CONSTANT
C     VALUE FOR ALL AXIAL POSITIONS AND EQUAL TO THE VALUE FOR FULLY
C     DEVELOPED FLOW
      IMPLICIT REAL*8 (A-H,O-Z)
      DIMENSION B88(200),FFF(200),Y(200),AC(200),AD(200),TI(200),TJ(200)
      DIMENSION U(200),V(200),YA(200),ZA(200)
      DIMENSION XAG(40),FA(40),DA(40),BA(40),Z(200),CA(40)
      DIMENSION P(40),TIA(40),TOA(40),OPA(50),UA(40),PK(40),UI(40,11),YA
      LG(40),RAB(40,11),ALC(40),ALD(40),ALX(40)
      REAL P1(40),TIA1(40),TJA1(40),OPA1(40),UA1(40),FA1(40),BA1(40),DA1
      I(40),CA1(40),XAG1(40),ALDA(40),ALCA(40),ALXA(40)
      R=0.5
      FM=-2.0000*DLG(R)/(1.0000-R*R)
      R99=DSORT((1.0000-R*R)/(-2.0000*DLG(R)))
      R98=(R99-R)/(1.-R99)*1./R
      AM=1.0001
      N=199
      NN=N+1
      AN=N
      AK1=(FM-AM)/AN
      IAK1=AK1*10.0**6.0
      IFM=FM*10.0**6.0
      IAM=AM*10.0**6.0
      K=0
      DO 7 L=IAM,IFM,IAK1
      F=L
      F=F/1000000.0000
      B=1.0000/(R98+1.0000-R98/F**0.5000)**2.0000
      A1=1.0000/B
      A2=1.0000/F
      A4=DLG(F)
      A3=DLG(B)
      A11=1.0000-B+A3
      A12=0.5000-0.5000*B*B+B*A3
      A13=5.0000/6.0000-B+0.5000*B*B-B**3.0000/3.0000+B*B*A3-B*A3*A3
      A14=7.0000/3.0000-2.0000*B-0.75000*B*B+2.0000*B*B**3.0000/3.0000-B**
      4.0000/4.0000+B*A3*(3.0000-1.5000*B*B*B)-1.5000*B*B*A3*A3+B*A3**3
      A15=1.0000-F+A4
      A16=0.5000-0.5000*F*F+F*A4
      A17=5.0000/6.0000-F+0.5000*F*F-F**3.0000/3.0000+F*F*A4-F*A4*A4
      A18=7.0000/3.0000-2.0000*F-0.75000*F*F+2.0000*F*F**3.0000/3.0000-F**
      4.0000/4.0000+F*A4*(3.0000-1.5000*F*F*F)-1.5* F*F*A4*A4+F*A4**3
      A19=A1*(-B+3.0000*A12/A11+3.0000*A13/(A11*A11)+A14/(A11**3))
      A20=A2*(-F+3.0000*A16/A15+3.0000*A17/(A15*A15)+A18/(A15**3))
      A21=11.0000/6.0000-3.0000*B+1.5000*B*B-B**3.0000/3.0000+A3
      A22=A21/(8*A11*A11)
      A23=11.0000/6.0000-3.0000*F+1.5000*F*F-F**3.0000/3.0000+A4
      A24=A23/(F*A15*A15)
      A25=R*R*(1.0000-B)**2.0000*F*A15
      A26=B*(F-1.0000)**2.0000*A11
      A27=2.0000*(1.0000-R*R)*B*F*A11*A15/(A25-A26)
      A28=-R*R*A19*A27/2.0000+ A27*A20/2.+R*R*A22-A24
      A29=1.0000-B*B+4.0000*(B-1.0000)-2.0000*A3
      A30=(-2.0000*(B-1.0000)+A27*A29/A11)/A11
      A31=1.0000-F*F+4.0000*(F-1.0000)-2.0000*A4
      A32=(2.0000*(F-1.0000)-A27*A31/A15)/A15
      A33=(-1.0000+A1)/A11
      A34=3.0000*A12/A11*(A11/A12-A33)
      A35=-1.0000+2.0000*B-B*B+2.0000*(B-1.0000)*A3-A3*A3
      A36=3.0000*A13/(A11*A11)*(A35/A13-2.0000*A33)
      A37=1.0000-3.0000*B+3.0000*B*B-B**3.0000+3.0000*A3*(1.0000-2.0000*
      2B+B*B-B*A3)+A3*A3*(3.0000+A3)
      A38=A14/A11**3*(A37/A11+-3.0000*A33)
      A39=A1*(1.-1.0000+A34+A36+A38)/A19-1.0000)
      A40=A25-A26
      A41=A1+A33+2.0000*A25/((1.0000-B)*A40)+A26/A40*(A1+A33)
      A42=(-1.0000+A2)/A15
      A43=A2+A42-2.0000*A26/((1.0000-F)*A40)-A25/A40*(A2+A42)
      A44=3.0000*A16/A15*(A15/A16-A42)
      A45=-1.0000+2.0000*F-F*F+2.0000*(F-1.0000)*A4-A4*A4
      A46=3.0000*A17/(A15*A15)*(A45/A17-2.0000*A42)
      A47=1.0000-3.0000*F+3.0000*F*F-F**3.0000+3.0000*A4*(1.0000-2.0000*
      2F+F*F-F*A4)+A4*A4*(3.0000+A4)
      A48=A18/A15**3*(A47/A18-3.0000*A42)
      A49=A2*(1.-1.0000+A44+A46+A48)/A20-1.0000)
      A50=-3.0000+3.0000*B-B*B+A1

```

```

A51=A50/A21-A1-2.0000*A33
A52=-3.0000+3.0000*F-F*F+A2
A53=A52/A23-A2-2.0000*A42
A54=-R*R*A19*A27*(A39+A+1)/2.0000+A20*A27*A41/2.0000+R*R*A51*A22
A55=-R*R*A19*A27*A43/2.0000+A27*A20*A49/2.0000+A20*A27*A+3/2.0000-
JA53*A24
A56=-R98*(B/F)**1.5000
A57=A27*(A54+2.0000*A28*A41)*A56+(A55+2.0000*A28*A43)/(A30+A32)
A58=A57/(B.0000*(1.0000-R)**2.0000)
A59=(R*A*A51*A22+2.0000*R*R*A22*A41-2.0000*A24*A41)*A56
A60=2.0000*R*R*A22*A43-A53*A24-2.0000*A24*A43
A61=(B-1.0000)/A11-(F-1.0000)/A15
A62=A27*A27*(A59+A60)
A63=A57
A64=-A62/A63-2.0000*A27*A61
A65=-A64*A63/(1.0000-R*R)*2.0000
A66=8.0000*(1.0000-R)*A64/(1.0000+R)
K=K+1
Y(K)=A58
YA(K)=A65
DP(K)=A66
BBB(K)=B
FFF(K)=F
AD(K)=(1.0000/B**0.5000-1.0000)/(2.0000*(R-1.0000))*(-R)
AC(K)=(1.0000-1.0000/F**0.5000)*R/(2.0000*(R-1.0000))*(-R)
U(K)=A27
PRINT 75, BBB(K), FFF(K), AD(K), AC(K), Y(K), U(K)
75 FORMAT (1H, 6D14.0)
BET1=A27*A27*(R*R*A21/(B*A11*A11)-A23/(F*A15*A15))/(1.-R*R)
ALP1=A27**3*(R*R*A19-A20)/(1.-R*R)
BETC=(ALP1+2.)/3.
7 CONTINUE
A93=(1.0000-BBB(K)+DLG(BBB(K)))/(BBB(K)-1.0000)*U(K)
A94=(1.0000-FFF(K)+DLG(FFF(K)))/(FFF(K)-1.0000)*U(K)
DO 80 I=1,K
A96=1.0000-BBB(I)+DLG(BBB(I))
A97=1.0000-FFF(I)+DLG(FFF(I))
TI(I)=(BBB(I)-1.0000)*U(I)*A93/A96
TO(I)=(FFF(I)-1.0000)*U(I)*A94/A97
PRINT 81, FFF(I), BBB(I), TI(I), TC(I)
81 FORMAT (1H, 4D14.6)
80 CONTINUE
JA1=0
JA2=0
DO 101 NK1=10, NN, 10
AA1=0.0000
BB1=0.0000
JA1=JA1+1
KB1=2*JA1-1
NK11=NK1-1
Z(1)=Y(1)
Z(NK1)=Y(NK1)
ZA(1)=YA(1)
ZA(NK1)=YA(NK1)
DO 103 J11=2, NK11, 2
Z(J11)=4.0000*Y(J11)
ZA(J11)=YA(J11)*4.
103 CONTINUE
DO 104 J12=3, NK11, 2
Z(J12)=2.0000*Y(J12)
ZA(J12)=YA(J12)*2.
104 CONTINUE
DO 102 J1=1, NK1
AA1=Z(J1)+AA1
BB1=ZA(J1)+BB1
KA1=J1
102 CONTINUE
XAG(KB1)=AA1*AK1/3.0000
P(KB1)=BB1*AK1/3.
FA(KB1)=FFF(KA1)
BA(KB1)=BBB(KA1)
DA(KB1)=AD(KA1)
CA(KB1)=AC(KA1)
TIA(KB1)=TI(KA1)
TUA(KB1)=TU(KA1)
OPA(KB1)=OP(KA1)
UA(KB1)=U(KA1)
JB1=JA1
101 CONTINUE
DO 201 NK2=10, NN, 10

```

```

AA2=0.0000
BB2=0.0000
JA2=JA2+1
KB2=2*JA2
NK21=NK2-1
Z(1)=Y(1)
Z(NK2)=Y(NK2)
ZA(1)=YA(1)
ZA(NK2)=YA(NK2)
DO 203 J21=2,NK21,2
Z(J21)=4.0000*Y(J21)
ZA(J21)=4.*YA(J21)
203 CONTINUE
DO 204 J22=3,NK21,2
Z(J22)=2.0000*Y(J22)
ZA(J22)=2.*YA(J22)
204 CONTINUE
DO 202 J2=1,NK2
AA2=Z(J2)+AA2
BB2=ZA(J2)+BB2
KA2=J2
202 CONTINUE
XAG(KB2)=AA2*AK1/3.0000
P(KB2)=BB2*AK1/3.
FA(KB2)=FFF(KA2)
BA(KB2)=BBB(KA2)
DA(KB2)=AD(KA2)
CA(KB2)=AC(KA2)
TIA(KB2)=TI(KA2)
TOA(KB2)=TU(KA2)
OPA(KB2)=OP(KA2)
UA(KB2)=U(KA2)
JB2=JA2
201 CONTINUE
JC=JB1+JB2
ARI0=64.0000*(1.0000-R)**2.0000/(1.0000+R*R+(1.0000-R*R)/DLOG(R))
DO 300 J3=1,JC
PK(J3)=P(J3)-ARI0*XAG(J3)
ALX(J3)=DLOG(XAG(J3))
ALD(J3)=DLOG(DA(J3))
ALC(J3)=DLOG(CA(J3))
YAG(J3)=XAG(J3)*4.0000
PRINT 310,FA(J3),BA(J3),DA(J3),CA(J3),XAG(J3),PK(J3),YAG(J3)
310 FORMAT (1H,7D14.6)
300 CONTINUE
DO 301 J3=1,JC
PRINT 320,FA(J3),BA(J3),P(J3),TIA(J3),TOA(J3),OPA(J3),UA(J3),XAG(J
13),PK(J3)
320 FORMAT (1H,9D14.6)
301 CONTINUE
JC=JC-1
DO 801 J=1,JC
DO 800 I=5,100.5
H1=I
RA=R+(1.-R)*H1*0.01
RAA=H1*0.01
RA1=R+2.0000*DA(J)*(1.0000-R)
RA2=1.0000-2.0000*CA(J)*(1.0000-R)
IF(RA.GE.R.AND.RA.LE.RA1) U1=(RA*RA-R*R-2.*RA1*RA1*DLOG(RA/R))
1*UA(J)/|RA1*RA1-R*R-2.*RA1*RA1*DLOG(RA1/R)|
IF(RA.GE.RA1.AND.RA.LE.RA2) J1=UA(J)
IF(RA.GE.RA2.AND.RA.LE.1.0000) U1=(RA*RA-1.0000-2.0000
2*RA2*RA2*DLOG(RA))*UA(J)/(RA2*RA2-1.0000-2.0000*RA2*RA2*DLOG(RA2))
PRINT 805,RAA,U1,YAG(J),XAG(J)
805 FORMAT (1H,4D14.6)
800 CONTINUE
801 CONTINUE
STOP
END

```

SENTRY

```

$JOB      *ATFIV  XXXXXXXXXXXX SEERAJ
C        THIS PROGRAM PREDICTS FLOW CHARACTERISTICS FOR HYDRODYNAMIC
C        DEVELOPING LAMINAR FLOW THROUGH A CONCENTRIC ANNULUS
C        GENERAL MODEL
C        THE ASSUMPTION OF A CONSTANT RATIO OF WALL LAYER THICKNESS FOR ALL
C        AXIAL LOCATIONS WAS RELAXED IN THIS FLOW MODEL
C        IMPLICIT REAL*8 (A-H,O-*)
C        EXTERNAL VECTOR
C        REAL*8 Y(25),*(25),DY(25)
C        REAL*8 BA(500),FA(500),UA(500),XAG(500)
C        COMMON B,F,CS,DS
C        COMMON R,G1,G2,G3,G4,FM,FM2,FM3
C        COMMON A13,*,1,*,2,*,3
C        COMMON A1,B1,A4,B4,A11,B11
C        DO 14 K=1,5
C        GO TO (1,2,3,4,5),K
1        CONTINUE
C        R=0.05
C        WC=0.000050
C        WF=21.567
C        WK=0.830
C        GO TO 10
2        CONTINUE
C        R=0.5000
C        WC=0.000032
C        WF=23.813
C        WK=0.688
C        GO TO 10
3        CONTINUE
C        R=0.732
C        WC=0.000030
C        WF=22.967
C        WK=0.678
C        GO TO 10
4        CONTINUE
C        R=0.75
C        WC=0.000030
C        WF=22.967
C        WK=0.678
C        GO TO 10
5        CONTINUE
C        R=0.1
C        WC=0.000043
C        WF=22.343
C        WK=0.784
C        GO TO 10
10       CONTINUE
C        G1=4.0000*(1.0000-R)**2.0000
C        G2=R*R/(2.0000*G1)
C        G3=1.0000/G1
C        G4=0.5000/(1.0000-R*R)
C        FM=-2.0000*OLCG(R)/(1.0000-R*R)
C        FM2=0.5000/(1.0000-R)
C        FM3=R*FM2
C        N1=10
C        N=3
C        NN=200
C        ANN=200.
C        NN1=500
C        BD1=0.5*(1./FM**0.5-R)/(1.-R)
C        BD2=0.5*(1.-1./FM**0.5)/(1.-R)
C        J=2800
C        W1=J
C        W2=J
C        W3=J
C        AB=0.
C        X=AB
C        Y(1)=AB
C        Y(2)=AB
C        Y(3)=AB
C        Z1=0.00001
C        DO 11 I=1,NN1
C        START OF RUNGE-KUTTA INTEGRATION ROUTINE
C        CALL RKSES(X,Y,DY,Z1,N,VECTOR)
C        AY=Y(1)+Y(2)
C        FAP1=Y(3)/(4.*X)
C        FAP2=3.44/X**0.5+(WK/(4.*X)+WF-3.44/X**0.5)/(1.+WC/X**2.)
C        BA(I)=B
C        FA(I)=F
C        UA(I)=A13

```

```

XAG(1)=X
T1=A13*CS
T2=A13*OS
RR=Y(1)/Y(2)
N2=1
251 *WRITE(6,251) Y(1),Y(2),Y(3),X,RR,A13,FAP1,FAP2,T1,T2
FORMAT(1H,10D12.5)
BET1=A13*A13*(R*R*A4/(B*A1*A1)-B4/(F*B1*B1))/(1.-R*R)
ALP1=A13**3*(R*R*A11-B11)/(1.-R*R)
BETC=(ALP1+2.)/3.
16 *WRITE(6,16) BET1,ALP1,BETC
FORMAT(1H,3D14.6)
IF (N2 .GE. 100) ZI=0.0001
11 CONTINUE
15 CONTINUE
12 CONTINUE
DO 22 I1=5,100.5
DO 23 I2=1.9
A11=I1
A12=A11*0.01
R2=A12*(1.-R)+R
D1=R/BA(I2)**0.5
D2=1./FA(I2)**0.5
IF (R2 .LT. D1) U1=UA(I2)*BA(I2)*((R2/R)**2.-1.-2.*DLOG(R2/R)/BA(I
U2))/(1.-BA(I2)+DLOG(BA(I2)))
IF (R2 .GE. D1 .AND. R2 .LE. D2) U1=UA(I2)
IF (R2 .GT. D2) U1=FA(I2)*UA(I2)*((R2**2.-1.-2.*DLOG(R2)/FA(I2))/(1
1.-FA(I2)+DLOG(FA(I2)))
XA=4.*(1.-R)**2.*XAG(I2)
*WRITE(6,24)R2,XAG(I2),U1,XA,A12
23 CONTINUE
24 FORMAT(1H,5D14.6)
DO 230 I2=N1,N2,N1
A11=I1
A12=A11*0.01
R2=A12*(1.-R)+R
D1=R/BA(I2)**0.5
D2=1./FA(I2)**0.5
IF (R2 .LT. D1) U1=UA(I2)*BA(I2)*((R2/R)**2.-1.-2.*DLOG(R2/R)/BA(I
U2))/(1.-BA(I2)+DLOG(BA(I2)))
IF (R2 .GE. D1 .AND. R2 .LE. C2) U1=UA(I2)
IF (R2 .GT. D2) U1=FA(I2)*UA(I2)*((R2**2.-1.-2.*DLOG(R2)/FA(I2))/(1
1.-FA(I2)+DLOG(FA(I2)))
XA=4.*(1.-R)**2.*XAG(I2)
*WRITE(6,240) R2,XAG(I2),U1,XA,A12
240 FORMAT(1H,5D14.6)
230 CONTINUE
22 CONTINUE
PRINT 25
25 FORMAT('1')
14 CONTINUE
STOP
END

SUBROUTINE VECTOR (X,Y,*N)
IMPLICIT REAL*8 (A-H,O-* )
REAL*8 X,Y(25),*(25)
COMMON B,F,CS,OS
COMMON R,G1,G2,G3,G4,FM,FM2,FM3
COMMON A1,B1,A4,B4,A11,B11
B=FM3*FM3/(FM3+Y(1))**2
F=FM2*FM2/(FM2+Y(2))**2
IF (X .EQ. 0.) *(1)=*1
IF (X .EQ. 0.) *(2)=*2
IF (X .EQ. 0.) *(3)=*3
IF (X .EQ. 0.) GO TO 1
C1=1.0000/B
C2=1.0000/F
C3=DLOG(B)
C4=DLOG(F)
A1=1.0000-B+C3
B1=1.0000-F+C4
A2=5.0000/0.0000-B+B*B/2.0000-B**3.0000/3.0000+B*(B-C3)*C3
B2=5.0000/0.0000-F+F*F/2.0000-F**3.0000/3.0000+F*(F-C4)*C4
A3=7.0000/3.0000-2.0000*B-0.75*B*B+2.0000*B**3.0000/3.0000-B**4.00
100/4.0000+B*(3.0000-1.5000*B+B*B)*C3+B*(-1.5000*B+C3)*C3*C3
B3=7.0000/3.0000-2.0000*F-0.75*F*F+2.0000*F**3.0000/3.0000-F**4.00
100/4.0000+F*(3.0000-1.5000*F+F*F)*C4+F*(-1.5000*F+C4)*C4*C4
A4=11.0000/0.0000-3.0000*B+1.5000*B*B-B**3.0000/3.0000+C3

```

```

B4=11.0000/6.0000-3.0000*F+1.5000*F*F-F**3.0000/3.0000+C3
C5=(-1.0000+B1)/A1
D5=(-1.0000+F)/B1
A5=(-1.0000+1.0000/B1)/A1
B5=(-1.0000+1.0000/F)/B1
A6=0.5000*(1.0000-B*B)+B*C3
B6=0.5000*(1.0000-F*F)+F*C4
A8=R*R*(1.0000-B)**2 *F*B1-(F-1.0000)**2 *B=A1
A11=(-B+3.0000*A6/A1+3.0000*A2/(A1*A1)+A3/(A1**3))/B
B11=(-F+3.0000*B6/B1+3.0000*B2/(B1*B1)+B3/(B1**3))/F
A13=(2.0000*(1.0000-R*R)*B*F*A1*B1)/A8
A15=(1.0000-B*B)+4.0000*(B-1.0000)-2.0000*C3
B15=(1.0000-F*F)+4.0000*(F-1.0000)-2.0000*C4
E1=-2.0000*C5+R*R*A13*(C1-1.0000)*(A15/(A1*A1)-B15/(B1*B1))/(1.000
10-R*R)
F1=4.0000*D5+2.0000*(1.0000-C2)*A13*(A15/(A1*A1)-B15/(B1*B1))/(1.0
1000-R*R)
A7=-3.0000+3.0000*B-B*B+C1
B7=-3.0000+3.0000*F-F*F+C2
A9=-1.0000-B)**2 +2.0000*(B-1.0000)*C3-C3*C3
B9=-1.0000-F)**2 +2.0000*(F-1.0000)*C4-C4*C4
A10=(1.0000-B)**3 +3.0000*(1.0000-B)**2 -B*C3)*C3+(3.0000
1+C3)*C3*C3
B10=(1.0000-F)**3 +3.0000*((F-1.0000)**2 -F*C4)*C4+(3.0000
1+C4)*C4*C4
A18=3.0000*A6*(A1/A6-A5)/A1
B18=3.0000*B6*(B1/B6-B5)/B1
A19=3.0000*A2*(A9/A2-2.0000*A5)/(A1*A1)
B19=3.0000*B2*(B9/B2-2.0000*B5)/(B1*B1)
A20=A3*(A10/A3-3.0000*A5)/(A1**3)
B20=B3*(B10/B3-3.0000*B5)/(B1**3)
A21=((1.0000+A18+A19+A20)/(A11*B1)-C1)
B21=((1.0000+B18+B19+B20)/(B11*B1)-C2)
A22=C1+A5+2.0000*R*R*(1.0000-B)**2 *F*B1/(A3*(1.0000-B))+B*(F-
11.0000)**2 *A1*(C1+A5)/A8
A23=C2+B5-2.0000*B*(F-1.0000)**2 *A1/(A8*(1.0000-F))-R*R*(1.00
100-B)**2 *F*B1*(C2+B5)/A8
A27=1.0000+0.5000*(1.0000-B)**2 /A1
B27=1.0000+0.5000*(F-1.0000)**2 /B1
A28=A13*C1
B28=A13*C2
A29=1.0000+A/(A1*A1)
B29=1.0000+B/(B1*B1)
A30=R*R*A11
A31=G2/F1
B31=G3/F1
A40=((0.5000*(1.0000-B)*C1*C5+1.0000)*C5+(-C1+A22)*A27)*A28
A41=A27*A23*A28
A42=((2.0000*A4*C5*C1+A7)/(A1*A1)+(-C1+2.0000*A22)*A29)*A28
A43=2.0000*A23*A29*A28
A44=A13*A13*(A30*A21+3.0000*A22*(A30-B11))
A45=A13*A13*(-(B11*B21)+3.0000*A23*(A30-B11))
A46=(-A40+A42-G4*(C1-1.0000)*A44)*A31
A47=(-A41+A43-G4*(C1-1.0000)*A45)*A31
A48=((0.5000*(1.0000-F)*C2*D5+1.0000)*D5+(-C2+A23)*B27)*B28
A49=B27*A22*B28
A50=2.0000*A22*B29*B28
A51=((2.0000*B4*D5*C2+B7)/(B1*B1)+(-C2+2.0000*A23)*B29)*B28
A52=A44
A53=A45
A54=(A49-A50-G4*(1.0000-C2)*A52)*B31
A55=(A48-A51-G4*(1.0000-C2)*A53)*B31
A56=-2.0000*B/(F*M3+Y(1))
B56=2.*F/(F*M2-Y(2))
A57=A56*A46
A58=B56*A47
A59=A56*A54
A60=B56*A55
A61=A57*A60-A58*A59
*(1)=(A60-A58)/A61
*(2)=(A57-A59)/A61
*(3)=A13*(A44*A56*(1)+A45*B56*(2))/(1.-R*R)+16.*(1.-R)*A13*A13*
1(A15/(A1*A1)-B15/(B1*B1))/(1.+R)
CCNT INLE
RETURN
END

```

SENTRY

```

$JOB      *ATFIV XXXXXXXXXX ANAND
C        THIS PROGRAM PREDICTS FLOW CHARACTERISTICS FOR HYDRODYNAMIC
C        ENTRY-REGION TURBULENT FLOW THROUGH A CONCENTRIC ANNULUS
C        SIMPLIFIED MODEL
C        THE RATIO OF *ALL LAYER THICKNESS IS ASSUMED TO BE A CONSTANT
C        VALUE FOR ALL AXIAL POSITIONS AND EQUAL TO THE VALUE FOR FULLY
C        DEVELOPED FLOW
          IMPLICIT REAL*8 (A-H,O-Z)
          DIMENSION DBB(200),FFF(200),Y(200),AC(200),AD(200),U(300)
          DIMENSION XAG(40),FA(40),BA(40),DA(40),CA(40),Z(200)
          DIMENSION UA(40)
          DIMENSION U2(15)
          DIMENSION T1(200),TO(200),T13(40),TO3(40)
          DIMENSION HI(200),HO(200),H1(40),HO1(40)
          REAL XAG1(40),DA1(40),UA1(40)
          DO 14 K9=1,2
          GO TO (1,2) ,K9
1        CONTINUE
          R=0.0653
          RE=23000.
          VN1=0.107
          VN2=0.14
          GO TO 10
2        CONTINUE
          R=0.531
          RE=142000.
          VN1=0.121
          VN2=0.129
          GO TO 10
10       CONTINUE
          C1=16.0000
          C2=11.0000
          AF1=0.00362000
          FM=DSORT(-2.0000*DL0G(R)/(1.0000-R*R))
          FM1=2.0000*(1.0000-R)
          N=199
          NN=N+1
          AN=N
          AM=1.01000
          AK1=(FM-AM)/AN
          IAK1=AK1*10.00*6.0
          IFM=FM*10.00*6.0
          IAM=AM*10.00*6.0
          K=0
          AN1=VN1+1.0000
          AN2=VN1+2.0000
          AN3=2.0000*VN1+1.0000
          AN4=2.0000*VN1+2.0000
          AN5=VN2+1.0000
          AN6=VN2+2.0000
          AN7=2.0000*VN2+1.0000
          AN8=2.0000*VN2+2.0000
          AM1=-2.0000/(1.0000+1.0000/VN1)
          AM2=-2.0000/(1.0000+1.0000/VN2)
          AV1=AM1/VN1
          AV2=AM2/VN2
          R90=(-R+1.0000/FM)/(1.0000-1.0000/FM)
          BM=FM*R
          AL1=0.5000-1.0000/(AN1*AN2)
          AL2=0.5000-(1.0000-1.0000/AN2)/AN1
          AL3=1.0000/(AN1*AN2)-1.0000/(AN3*AN4)
          AL4=(1.0000-1.0000/AN2)/AN1-(1.0000-1.0000/AN4)/AN3
          AL5=0.5000-(1.0000/(AN5*AN6))
          AL6=0.5000-(1.0000-1.0000/AN6)/AN5
          AL7=1.0000/(AN5*AN6)-1.0000/(AN7*AN8)
          AL8=(1.0000-1.0000/AN6)/AN5-(1.0000-1.0000/AN8)/AN7
          AL9=(AL1*BM+AL2)*(AL7*FM+AL8)/(AL3*BM+AL4)*(AL5*FM+AL6)
          DO 7 L=IAM,IFM,IAK1
          F=L
          F=F/1000000.0000
          B=1.0000/(R90*(1.0000-1.0000/F)/R+1.0000)
          A1=2.0000*(1.0000-B)/(B*B)
          A2=2.0000*(F-1.0000)/(F*F)
          A3=(1.0000-R)**AM1
          A4=(1.0000-R)**AM2
          A5=C1**AV1
          A7=RE**AM1
          A8=C2**AV2
          A10=RE**AM2
          A11=R**R*A1/AN3-R*R*(1.0000-B)*A1/(AN3*AN4)+1.0000/(F*F)-R*R/(B*B)+

```

```

A2/AN7+(F-1.0000)*A2/(AN7*AN8)
A12=R*R*(F-1.0000)*A1/AN1-R*R*(F-1.0000)*A1/(AN1*AN2)+1.0000/(F*F)-R*R/(B*B)+
A2/AN5+(F-1.0000)*A2/(AN5*AN6)
A13=(1.0000-R*R)/A12
A6=A13*(AM1+1.0000)
A9=A13*(AM2+1.0000)
A14=-A5*A6*A7*(1.0000-B)**AM1*(R/B)**AM1
A15=4.0000*R*(1.0000-R)/(2.0000**AM1*A3)
A17=-A8*A9*A10*(F-1.0000)**AM2*(1.0000/F)**AM2
A18=4.0000*(1.0000-R)/(2.0000**AM2*A4)
A20=2.0000*(1.0000-R*R)/A12
A21=R*R*(B-2.0000)/AN3+2.0000*R*R*(1.0000-B)/(AN3*AN4)+R*R
A22=(2.0000-F)/AN7+2.0000*(F-1.0000)/(AN7*AN8)-1.0000
A23=A20*A21/B**3.0000
A24=A20*A22/F**3.0000
A25=2.0000*A13*(-2.0000*A11+1.0000-R*R)/A12
A26=R*R*(B-2.0000)/AN1+2.0000*R*R*(1.0000-B)/(AN1*AN2)+R*R
A27=A25*A26/B**3.0000
A28=(2.0000-F)/AN5+2.0000*(F-1.0000)/(AN5*AN6)-1.0000
A29=A25*A28/F**3.0000
A31=(R*(1.0000-B)-R90*B)/(R*F+R90*(F-1.0000))
A32=(A23+A27)*A31+A24+A29
K=K+1
A34=2.0000*(1.0000-R)
AD(K)=R*(1.0000/B-1.0000)/A34
AC(K)=(1.0000-1.0000/F)/A34
U(K)=A13
BBB(K)=B
FFF(K)=F
A35=1.0000-B
A36=(1.0000-A35/AN2)/AN1
A37=(1.0000-A35/AN4)/AN3
A38=((1.0000+B)/2.0000-A36)/(A36-A37)
A39=A35*(A36-A37)/B
A40=RE*A39*R/(B*2.0000*(1.0000-R))
A41=F-1.0000
A42=(1.0000+A41/AN6)/AN5
A43=(1.0000+A41/AN8)/AN7
A44=((F+1.0000)/2.0000-A42)/(A42-A43)
A45=A41*(A42-A43)/F
A46=RE*A45/(F*2.0000*(1.0000-R))
TI1=-A14/(A13*A3*2.0000**AM1)
TI2=0.123000*10.0000**(-0.678000*A38)*A40**(-0.268000)
TO1=-A17/(A13*A4*2.0000**AM2)
TO2=0.123000*10.0000**(-0.678000*A44)*A46**(-0.268000)
A16=TI2*A13*4.0000*R*(R-1.0000)
A19=TO2*A13*4.0000*(R-1.0000)
A30=A16+A19
A33=A32/A30
Y(K)=A33
TI(K)=TI2
TO(K)=TO2
HI(K)=A38
HO(K)=A44
TOI=R*A35*((1.0000+B)/2.0000-A36)/(2.0000*B**2.0000*(1.0000-R))
TDC=(F-1.0000)*((F+1.0000)/2.0000-A42)/(2.0000*F**2.0000*(1.0000
1-R))
THI=A39*R/(2.0000*B*(1.0000-R))
TMO=A45/(2.0000*F*(1.0000-R))
7 CCNTINUE
JA1=0
JA2=0
DO 101 NK1= 10,NN,10
AA1=0.0000
BB1=0.0000
JA1=JA1+1
KB1=2*JA1-1
NK11=NK1-1
Z(1)=Y(1)
Z(NK1)=Y(NK1)
DO 103 J11=2,NK11,2
Z(J11)=4.0000*Y(J11)
103 CCNTINUE
DO 104 J12=3,NK11,2
Z(J12)=2.0000*Y(J12)
104 CCNTINUE
DO 102 J1=1,NK1
AA1=Z(J1)+AA1
KA1=J1
102 CCNTINUE

```

```

XAG(KB1)=AA1*AK1/3.0000
FA(KB1)=FFF(KA1)
BA(KB1)=888(KA1)
DA(KB1)=AD(KA1)
CA(KB1)=AC(KA1)
UA(KB1)=U(KA1)
TI3(KB1)=TI(KA1)
TO3(KB1)=TO(KA1)
HI1(KB1)=HI(KA1)
HO1(KB1)=HO(KA1)
JB1=JA1
101 CONTINUE
DC 201 NK2=16.NN.10
AA2=0.0000
BB2=0.0000
JA2=JA2+1
KB2=2*JA2
NK21=NK2-1
Z(1)=Y(1)
Z(NK2)=Y(NK2)
DO 203 J21=2.NK21.2
Z(J21)=4.0000*Y(J21)
203 CONTINUE
DO 204 J22=3.NK21.2
Z(J22)=2.0000*Y(J22)
204 CONTINUE
DO 202 J2=1.NK2
AA2=Z(J2)+AA2
KA2=J2
202 CONTINUE
XAG(KB2)=AA2*AK1/3.0000
FA(KB2)=FFF(KA2)
BA(KB2)=888(KA2)
DA(KB2)=AD(KA2)
CA(KB2)=AC(KA2)
UA(KB2)=U(KA2)
TI3(KB2)=TI(KA2)
TO3(KB2)=TO(KA2)
HI1(KB2)=HI(KA2)
HO1(KB2)=HO(KA2)
JB2=JA2
201 CONTINUE
JC=JB1+JB2
F10=UA(JC)*UA(JC)*TI3(JC)*2.0000
F20=JA(JC)*UA(JC)*TO3(JC)*2.0000
F30=F10*R+F20
DO 300 J3=1.JC
F1=UA(J3)*UA(J3)*TI3(J3)*2.0000
F2=UA(J3)*JA(J3)*TO3(J3)*2.0000
TIF=(UA(J3)/UA(JC))*2.0000*TI3(J3)/TI3(JC)
TOF=(UA(J3)/UA(JC))*2.0000*TO3(J3)/TO3(JC)
F15=(F1*R+F2)/F30
960 PRINT 960,UA(J3),DA(J3), XAG(J3),F1,F2,TIF,TOF,F15
300 FORMAT (1H .8D14.6,/)
CONTINUE
DO 500 J=1.JC
XAG1(J)=XAG(J)
DA1(J)=DA(J)
UA1(J)=UA(J)
500 CONTINUE
DC 22 I2=2.JC.2
DC 23 I1=5.95.5
A11=I1
A12=A11*0.01
R2=1.-A12*(1.-R)
DR1=R/(BA(I2))
DR2=1./FA(I2)
R20=(1.-DR2)/(1.-R)
R21=(1.-DR1)/(1.-R)
IF (R2 .LT. DR1) U1=((R2-R)/(R*(1./BA(I2)-1.)))*VN1
IF (R2 .GE. DR1 .AND. R2 .LE. DR2) U1=1.
IF (R2 .GT. DR2) U1=((1.-R2)/(1.-1./FA(I2)))*VN2
U1=U1*UA(I2)
WRITE (6,24) R2,XAG(I2),U1,A12,F20,R21
24 FORMAT (1H .8D14.6)
23 CONTINUE
22 CONTINUE
14 CONTINUE
STOP
END

```

```

SJOB  WATFIV XXXXXXXXXXXX ANAND
C     THIS PROGRAM PREDICTS FLOW CHARACTERISTICS FOR HYDRODYNAMIC
C     ENTRY-REGION TURBULENT FLOW THROUGH A CONCENTRIC ANNULUS
C     GENERAL MODEL
C     THE ASSUMPTION OF A CONSTANT RATIO OF WALL LAYER THICKNESS FOR ALL
C     AXIAL LOCATIONS WAS RELAXED IN THIS FLOW MODEL
      IMPLICIT REAL*8 (A-H,O-W)
      EXTERNAL VECTOR
      REAL*8 Y(25),W(25),OY(25)
      REAL*8 BA(1000),FA(1000),JA(1000),XAG(1000)
      COMMON R,R1,R3,AN1,AN2,AN3,AN4,AN5,AN6,AN7,AN8
      COMMON B,F,C1,BE11,BE21,RE,W1,W2,W3
      DO 14 K=1,2
      NN=1000
      J1=5
      J2=5
      ZJ=2,
      W1=100,
      W2=100,
1     GO TO (1,2,3,4,5,6,7,8),K
      CONTINUE
      R=0.344
      RE=78800,
      VN1=0.1176471
      VN2=0.1777778
      X=1.081
      Y(1)=0.0233
      Y(2)=0.0233
2     GO TO 10
      CCNTINUE
      R=0.531
      RE=142000,
      VN1=0.121
      VN2=0.129
3     GO TO 10
      CONTINUE
      R=0.1003
      RE=320000,
      VN1=0.089
      VN2=0.148
      X=0.6752
      Y(1)=0.00992
      Y(2)=0.00992
4     GO TO 10
      CONTINUE
      R=0.1012
      RE=157000,
      VN1=0.049
      VN2=0.145
      X=1.081
      Y(1)=0.0179
      Y(2)=0.0179
5     GO TO 10
      CONTINUE
      R=0.0239
      RE=531000,
      VN1=0.049
      VN2=0.133
      X=0.6223
      Y(1)=0.0074
      Y(2)=0.0074
6     GO TO 10
      CCNTINUE
      R=0.433
      RE=23000,
      VN1=0.2147
      VN2=0.2477
      GO TO 10
7     CCNTINUE
      R=0.1003
      RE=451000,
      VN1=0.066
      VN2=0.139
      X=0.6752
      Y(1)=0.00835
      Y(2)=0.00835
      GO TO 10
8     CONTINUE
      R=0.0653
      RE=23000,

```

```

VN1=0.121
VN2=0.137
GO TO 10
10 CONTINUE
R1=R/(2.*(1.-R))
R3=1./(2.*(1.-R1))
AN1=1./(VN1+1.)
AN2=1./(VN1+2.)
AN3=1./(2.*VN1+1.)
AN4=1./(2.*VN1+2.)
AN5=1./(VN2+1.)
AN6=1./(VN2+2.)
AN7=1./(2.*VN2+1.)
AN8=1./(2.*VN2+2.)
N=2
AB=0.
X=AB
Y(1)=AB
Y(2)=AB
N1=10
ZI=0.00001
DO 11 I=1,NN
C START OF RUNGE-KUTTA INTEGRATION ROUTINE
CALL RKSES(X,Y,DY,ZI,N,VECTOR)
BA(I)=B
FA(I)=F
UA(I)=C1
AY=UA(I)**2-1.
AZ=Y(1)+Y(2)
XAG(I)=X
T1=BE11
T2=BE21
RR=Y(1)/Y(2)
N2=1
*WRITE (6,251) Y(1),Y(2),Y(3),X,RR,UA(I),T1,T2,AY
251 FORMAT(1H ,9D14.6)
IF (AZ .GE. 0.5) GO TO 12
IF (ZI .GE. 0.03) ZI=Z1
IF (ZI .GE. 0.03) GO TO 11
IF (N2 .EQ. J1) ZI=ZI*ZJ
IF (N2 .EQ. J1) J1=J1+J2
11 CONTINUE
12 CONTINUE
DO 22 I2=N1,N2,N1
DO 23 I1=S.95.5
AI1=I1
AI2=AI1*0.01
R2=1.-AI2*(1.-R)
DR1=R/(BA(I2))
DR2=1./FA(I2)
R20=(1.-DR2)/(1.-R)
R2I=(1.-DR1)/(1.-R)
IF (R2 .LT. DR1) U1=((R2-R)/(R*(1./BA(I2)-1.)))*VN1
IF (R2 .GE. DR1 .AND. R2 .LE. DR2) U1=1.
IF (R2 .GT. DR2) U1=((1.-R2)/(1.-1./FA(I2)))*VN2
*WRITE (6,24) R2,XAG(I2),U1,AI2,R20,R2I
24 FORMAT(1H ,6D14.6)
23 CONTINUE
22 CONTINUE
14 CONTINUE
STOP
END

SUBROUTINE VECTOR(X,Y,w,N)
IMPLICIT REAL*8 (A-H,C-W)
REAL*8 X,Y(25),w(25)
COMMON R,R1,R3,AN1,AN2,AN3,AN4,AN5,AN6,AN7,AN8
COMMON B,F,C1,BE11,BE21,RE,w1,w2,w3
B=R1/(R1+Y(1))
F=R3/(R3-Y(2))
IF (Y(1) .EQ. 0.) w(1)=w1
IF (Y(2) .EQ. 0.) w(2)=w2
IF (Y(1) .EQ. 0.) GO TO 7
A50=AN1*(1.-(1.-B)*AN2)
A51=AN3*(1.-(1.-B)*AN4)
B50=AN5*(1.+(F-1.)*AN6)
B51=AN7*(1.+(F-1.)*AN8)
H1=((1.+B)/2.-A50)/(A50-A51)
H2=((F+1.)/2.-B50)/(B50-B51)
DIS=R1*(1.-B)*(A50-A51)/(B*B)

```

```

DOOS=R3*(F-1.)*(850-851)/(F*F)
A1=2.*R*R*(1.-B)*A50/(B*B)+2.*(F-1.)*850/(F*F)+1./(F*F)-R*R/(B*B)
C1=(1.-R*R)/A1
DMI=(C1*RE*DOIS)**0.268
DMO=(C1*RE*DOOS)**0.268
1 CONTINUE
G1=2.*R*R*(AN1*(B-2.+2.*(1.-B)*AN2)+1.)*(-1./R1)/B
G2=2.*(AN5*(F-2.+2.*(1.-F)*AN6)+1.)*(1./R3)/F
G2=-G2
G20=R1*R1*(1./(B*B)-1.)*C1*(-C1/A1)
BE12=G20*G1
BE13=G20*G2
C10=(1.-B)/(B*B)
C11=(F-1.)/(F*F)
C3=C10*(1.-(1.-B)*AN2)
C4=C10*(1.-(1.-B)*AN4)
C5=C11*(1.+(F-1.)*AN6)
C6=C11*(1.+(F-1.)*AN8)
C12=(-1./R1)/B
C13=(1./R3)/F
G3=(B-2.+2.*(1.-B)*AN2)*C12
G4=(B-2.+2.*(1.-B)*AN4)*C12
G5=(2.-F+2.*(F-1.)*AN6)*C13
G6=(2.-F+2.*(F-1.)*AN8)*C13
BE11=-0.123*10.**(-0.678*H1) *2.*R1*C1*C1/DMI
BE21=-0.123*10.**(-0.678*H2) *2.*R3*C1*C1/DMO
BE14=2.*R1*R1*C1*C1*((-G3*AN1+G4*AN3)-(-C3*AN1+2.*C4*AN3)*G1/A1)
BE15=2.*R1*R1*C1*C1*((-C3*AN1+2.*C4*AN3)*G2/A1)
BO22=-R3*R3*(1.-1./(F*F))*C1*C1*1./A1
BE22=BO22*G1
BE23=BO22*G2
BE24=2.*C1*C1*R3*R3*(-G1)*(-C5*AN5+2.*C6*AN7)/A1
BE25=2.*C1*C1*R3*R3*((-G5*AN5+G6*AN7)-(-C5*AN5+2.*C6*AN7)*G2/A1)
AL11=BE14-BE12
AL12=BE15-BE13
AL13=BE11
AL21=BE24-BE22
AL22=BE25-BE23
AL23=BE21
A60=AL22*AL11-AL12*AL21
W(1)=(AL13*AL22-AL23*AL12)/(A60)
W(2)=(AL13*AL21-AL23*AL11)/(-A60)
7 CONTINUE
WRITE(6,2) W(1),W(2),B,F
2 FORMAT(1H ,4D14.6)
RETURN
END
SENTRY

```

```

$JOB      *ATFIV   XXXXXXXXXXXX ANAND
C        THIS PROGRAM PREDICTS FLUX CHARACTERISTICS FOR TURBULENT FLOW IN THE
C        ENTRY-REGION OF PIPES
          IMPLICIT REAL*8 (A-M,C-W)
          REAL*8 AL1(275),AL2(275),AL3(275),BX(275),UP(275),AY(275),AZ(275),
          *BY(275),BZ(275),U1(275),U2(275),U3(275)
          REAL*8 UC1(275),AL4(275)
          REAL*8 Y(25),X(25),OY(25)
          REAL*8 UPM(1)
          EXTERNAL VECTOR
          EXTERNAL RMBRGD
          COMMON D,DO,EK
          COMMON DO2
          COMMON VN1
          DO2=2.5
          EK=0.36
          DO=42.
          VN1=1.
          J1=0
          RE=338000.
          XX=0.
          PD1=0.
          PD2=0.
          K1=0
          RK=14000.
          DO 1 J=50,100000.50
          K1=K1+1
          AIN=200.
          AK=1.
          N=1
          O=J
          NN=200
          ANN=NN
          AB=0.
          Y(1)=AB
          X=AB/O
          AX=AB/O
          ZI=(1.-AX)/ANN
          DO 2 I=1,NN
C        START OF RUNGE-KUTTA INTEGRATION ROUTINE
          CALL RKSES (X,Y,OY,ZI,N,VECTOR)
          UPM(1)=Y(1)
          CX=X
          UP(1)=Y(1)
          BX(1)=X
2         CONTINUE
16        CONTINUE
          I=0
          6         CALL RMBRGD (AX,CX ,7,1,ANS,B,FX)
          O1=B*O/DO
          IF (O1.GE. 173.) DE=0.
          IF (O1.GE. 173.) GO TO 11
          DE=DEXP(-O1)
          11        CONTINUE
          IF (DE .EQ. 1.) R3=0
          IF (DE .EQ. 1.) GO TO 18
C        AN EDDY VISCOSITY MODEL IS ASSUMED
          R3 =O*(1.-B)**VN1/(1.+EK*O*(1.- (1.-B)**2)*(1.+DO2*(1.-B)**2)*(1.-
18        IDE)/6.)
          CCNTINUE
          F1=RE/4.-UPM(1)*RK/2.
          FX=-O*B*(1.-B*O/(2.*RK))*R3
          IF (I) 7,7,6
          7         CONTINUE
          F2=ANS/F1
          F2=F2*100.
          DR=O/RK
          UC=2.*UPM(1)*RK/RE
          *WRITE (6,8) O,RK,F2,UPM(1),DR,UC
          3         FORMAT (1H ,6014.6)
          IF (F2 .GT. 100.0.OR. F2 .LT. 99.9)GO TO 5
          GO TO 10
          5         CCNTINUE
          IF ( AK .GE. 2.) GO TO 51
          IF (F2 .GT. 100.0.OR. F2 .LE. 0.) GO TO 51
          RK=RK-AIN
          GO TO 30
          51        CONTINUE
          IF (F2 .GT. 100.0.OR. F2 .LE. 0.) RK=RK+AIN/(2.**AK)
          IF (F2 .GT. 100.0.OR. F2 .LE. 0.) GO TO 52

```

```

IF (F2 .LT. 99.9) RK=RK-AIN/(2.**AK)
52 CONTINUE
AK=AK+1.
50 CONTINUE
GO TO 16
10 CONTINUE
IF (D .GE. RK) GO TO 15
J1=J1+1
AY(1)=0.
BY(1)=0.
I=0
22 CALL RMBRGD (AX,CX,6,I,BNS,C,GX)
D3=C*O/OD
IF (D3 .GE. 173.) DF=0.
IF (D3 .GE. 173.) GO TO 20
DF=DEXP(-D3)
20 CONTINUE
IF (DF .EQ. 1.) R5=D
IF (DF .EQ. 1.) GO TO 23
R5 =D*(1.-C)**VN1/(1.+EK*D*(1.-(1.-C)**2)*(1.+DD2*(1.-C)**2)*(1.-
10F)/6.)
23 CONTINUE
GX=(1.-C)*(1.-C*DR)*R5
IF (I) 21,21,22
21 CONTINUE
AL=(2.*O*(2.-DR)*BNS/RE+1.)*2.*RK*RK
AL1(J1)=(RK/RE)**3*BNS
AL2(J1)=UP(NN)*RK/AL
AL3(J1)=-1./AL
AL4(J1)=-DR*(2.-DR)/(RE*AL)
DO 36 I=1,NN
I1=I+1
C1=1.-BX(I)*DR
AY(I1)=UP(I)*UP(I)*C1
BY(I1)=UP(I)**3*C1
36 CONTINUE
I2=I1-1
AZ(I1)=AY(I1)
AZ(I1)=AY(I1)
BZ(I1)=BY(I1)
BZ(I1)=BY(I1)
DO 37 K=2,12,2
AZ(K)=4.*AY(K)
BZ(K)=4.*BY(K)
37 CONTINUE
I3=I2-1
DO 38 L=3,13,2
AZ(L)=2.*AY(L)
BZ(L)=2.*BY(L)
38 CONTINUE
BB1=0.
AA1=0.
DO 19 M=1,11
AA1=AA1+AZ(M)
BB1=BB1+BZ(M)
19 CONTINUE
V1=UP(NN)*(D*(1.-0.5*DR)-RK/2.)
U1(J1)=RE/4.+V1
U2(J1)=D*RK*AA1*Z1/3.
U3(J1)=RK*RK*(UP(NN)**2*V1-D*BB1*Z1/3.)
UC1(J1)=UC*UC
IF (J1 .EQ. 1) GO TO 100
J2=J1-1
U11=U1(J2+1)-U1(J2)
U12=U2(J2+1)-U2(J2)
U13=U3(J2+1)-U3(J2)
A14=AL1(J2+1)+AL1(J2)
A15=AL2(J2+1)+AL2(J2)
A16=AL3(J2+1)+AL3(J2)
A17=AL4(J2+1)+AL4(J2)
DP1=-UC1(J2+1)+UC1(J2)
PD1=PD1+DP1
OX=0.5*(A15*U11+A16*U12+A17*U13)
XX=XX+OX
DP2=16.*U13/(RE**2)*1./RE+32.*A14*OX
PO2=PO2+DP2
25 *RITE(6,25) J1(J2),U2(J2),U3(J2),AL1(J2),AL2(J2),AL3(J2),AL4(J2)
100 FORMAT (1H ,7D1+.6)
CONTINUE
*RITE (6,24) D,RK,UC,XX,UPM(1),PC1,PD2

```

```

24  FORMAT(1H .7D14.6./)
1   CONTINUE
15  CONTINUE
    STOP
    END

SUBROUTINE VECTOR (X,Y,*,N)
IMPLICIT REAL*8 (A-H,C-Z)
REAL *8 W(25),Y(25),JY(25)
COMMON D,DD,EK
COMMON DD2
COMMON VN1
DD2=X*0/DD
IF (D2.GE. 173.) DE=C.
IF (D2.GE. 173.) GO TO 12
DE=DEXP(-D2)
12  CONTINUE
IF (X .EQ. 0.) W(1)=0
IF (X .EQ. 0.) GO TO 17
W(1)=D*(1.-X)**VN1/((1.+EK*D*(1.-(-X)**2))*(1.+DD2*(1.-X)**2)*(1.-
17  IDE)/6.)
CONTINUE
RETURN
END

SUBROUTINE RMBRGD(A,B,ICFD,I,ANS,X,FX):REAL*8A,B,ANS,X,FX,T(21),H,F,00
*A,C,RN,U,D,F:I=1+1:GOTO(1,2,3,4),I:1:CONTINUE:H=B-A:X=A:RETURN:000
2  FA=FX:X=B:RETURN:3:T(1)=(FA+FX)*0.500:RN=1.000:LP1=1:12:L=LP1:LP1=000
*L+1:IF(L.GT.(ORD))GOTO7:U=0.000:C=H/(2.000*RN):K=2.000*RN-1.000:J=-000
*1:13:J=J+2:IF(J.GT.K)GUTC9:8:C=J:I=3:X=A+0*C:RETURN:4:U=U+FX:GOTO1000
*3:9:T(LP1)=(U/RN+T(L))*0.500:F=1.000:0014J=1.L:K=LP1-J:F=4.000*F:000
14 T(K)=T(K+1)+(T(K+1)-T(K))/(F-1.000):RN=2.000*RN:GOTO12:7:ANS=T(1)*000
*H:I=0:RETURN:END

```

3ENTRY

VITA AUCTORIS

- 1953 Born at Hague, West Coast Demerara, Guyana, on March 7.
- 1969 Completed G.C.E. 'O' Levels Examinations at Queen's College, Georgetown, Guyana.
- 1971 Completed G.C.E. 'A' Levels Examinations at Queen's College, Georgetown, Guyana.
- 1974 Received the Degree of Bachelor of Science in Mechanical Engineering from University College London, University of London, London, England.
- 1974 Joined the Department of Mechanical Engineering, Faculty of Technology, University of Guyana as an Instructor. Also joined Government Technical Institute, Georgetown, Guyana as Part-Time Lecturer.
- 1980 Currently a candidate for the Degree of Doctor of Philosophy in Mechanical Engineering at the University of Windsor, Windsor, Ontario, Canada.